Morphology, Wear and Corrosion Behaviour of HVOF Cermet Coatings Sprayed on Inner Cylindrical Surfaces

Teză destinată obţinerii
titlului ştiinţific de doctor inginer
la
Universitatea "Politehnica" din Timişoara
în domeniul ŞTIINŢA ŞI INGINERIA MATERIALELOR
de către

Ing. Ioan Florin Secoşan

Conducător ştiinţific:	prof.univ.dr.ing. Viorel-Aurel Şerban
	prof.univ.dr.ing. Waltraut Brandl
Referenţi ştiinţifici:	prof.univ.dr.ing. Doina Frunzăverde
	prof.univ.dr.ing. Ioan Vida-Simiti
	prof.univ.dr.ing. Ion Mitelea

Ziua susţinerii tezei: 25.04.2012

BUPT

Foreward

The present thesis was elaborated during my activities at the Politehnica University of Timişoara, Romania in cooperation with the Westfälische Hochschule Gelsenkirchen, Germany as well as with the company Thermico GmbH&Co, having as purpose the development of new HVOF coatings suitable for inner surfaces.

This scientific work gives a comprehensive description of thermal sprayed surface protective coatings on inner diameters (ID), their behaviour and potential uses in tribological and anti-corrosion applications. The ID-deposition techniques, tribological and corrosion mechanisms, characterization and properties evaluation methods of the coatings are discussed.

In this context, I would like to express my sincere gratitude to my scientific supervisors, Prof. Dr.-Eng. Waltraut Brandl from the Westfälische Hochschule Gelsenkirchen, Germany for her knowledge and for allowing me great freedom in this research and also to Prof. Dr.-Eng. Viorel-Aurel Şerban from Politehnica University of Timişoara, Romania for his guidance and encouragement throughout the achievement of my PhD thesis.

My honest gratitude also to Dr.-Eng. Gabriela Mărginean from the Westfälische Hochschule Gelsenkirchen, Germany, for her invaluable suggestions and unwavering support during the experimental investigations and for guiding the microscopical and structural characterization.

I wish to acknowledge the production of the HVOF-sprayed cermet coatings by general manager Dipl.-Eng. Götz Matthäus from Thermico GmbH company and by Dipl.-Eng. Johannes Wolf and of course by all the other employees. Likewise, I would like to pay my sincere thanks to RS Rittel GmbH and Siebtechnik GmbH companies for manufacturing the parts necessary for the construction of the "cylinder on ring" wear tester.

Acknowledgements to my friend and colleague Eng. Dragoş Pascal for his cheerful way of confronting problems and for making the long working hours a bit more enjoyable.

I want to thank my family, especially my wife Adina, for the patience and moral support during the hardest moments encountered in these last years.

And last but not least, I appreciate the help from my colleagues Dr.-Eng. Ion-Dragoş Uţu, Dipl.-Eng. Carsten Strübbe and Dr.-Eng. Călin Pogan.

Timişoara, aprilie 2012   Ioan Florin Secoşan

Summary,

The present thesis deals with one of the most current topics in the field of thermal spraying, namely the deposition of wear and corrosion protective cermet coatings on inner cylindrical surfaces using the High Velocity Oxygen Fuel process. Until recently this deposition method was applied only for outer surfaces because of the dimensions and geometries of existing spraying guns, which required a distance from the nozzle to the substrate surface of several hundred millimeters (~300). At that time, plasma spraying using miniature guns was recognized as a good method of coating inner surfaces, but the resulted coatings presented a high degree of porosity due to the extreme process temperature (~12000°C), thus leading to the dramatically degradation of the powdery material. Therefore, appeared the increasing need to develop a new HVOF system which will eliminate as far as possible these drawbacks and allow the deposition of cermet coatings in order to overhaul parts, and/or protect new components with small inner diameters. In this respect, the following thesis focuses on a study of the morphology, wear and corrosion behaviour of cermet coatings deposited on inner surfaces using the new HVOF system. Based on this study, process limitations were drawn regarding some constrains that arise in such circumstances (d$_{min}$, residues extraction, substrate temperature etc). Also, using several types of powders, ultimately, the optimum compromise between wear resistance, corrosion resistance and deposition efficiency was determined. It can be said that this work was dealing with questions that are essential for a good performance of HVOF thermal spraying coatings for inner surface components. All these pieces of information and results have to be documented in such a way that they can be used as a knowledge base for the future.

Rezumat,

Teza abordează una dintre cele mai de actualitate topici în domeniul pulverizării termice şi anume, depunerea de straturi cermet antiuzare şi anticoroziune pe suprafeţe interioare utilizând procedeul de pulverizare cu flacără de mare viteză HVOF. Până nu de mult această metodă de depunere era utilizată doar pentru suprafeţe exterioare datorită gabaritelor/geometriilor pistoalelor de pulverizare existente care necesitau o distanţă de la duză la suprafaţa de acoperit (substrat) de câteva sute de milimetri (~300mm). La acea vreme pulverizare cu plasmă utilizând pistoale miniaturale era recunoscută ca o bună metodă de acoperire a suprafeţelor interioare, dar totodată straturile obţinute prezentau un grad ridicat de porozitate din cauza temperaturilor înalte de proces (~12000°C) conducând în mod dramatic la fenomenul de degradare a materialului pulverulent. Prin urmare, a apărut cerinţa din ce în ce mai mare de dezvoltare a unui nou sistem HVOF de acoperire care să înlăture pe cât posibil acest neajuns şi să permită în acelaşi timp depunerea de straturi cermet în vederea recondiţionării pieselor şi/sau protejarea componentelor noi fabricate cu o astfel de formă geometrică. În acest sens, prezenta teză şi-a propus un studiu al morfologiei şi comportamentului la uzare şi coroziune a straturilor cermet depuse cu ajutorul noului sistem HVOF pe suprafeţe cilindrice interioare. Pe baza acestuia s-au putut trasa anumite limitări de proces având în vedere constrângerile ce apar în astfel de condiţii (d$_{min}$, evacuarea rezidurilor, temperatura substratului, etc). De asemenea, folosind mai multe tipuri de materiale pulverulente, în final s-a putut stabili compromisul optim între rezistenta la uzare, coroziune precum şi eficienta de depunere.

În baza acestor investigaţii se evidenţiază faptul că această lucrare ştiinţifică s-a confruntat cu întrebări esenţiale legate de performanţele straturilor depuse termic prin procedeul HVOF pe suprafaţate cilindrice interioare. Toate aceste informaţii şi rezultate trebuiesc documentate astfel încât să poată fi folosite ca o bază de cunoştinţe pentru aplicaţii şi cercetări viitoare.

Content

Chapter III EXPERIMENTAL PLAN AND METHODOLOGY

Chapter IV RESULTS AND DISCUSSION

Chapter V CONCLUSIONS, ORIGINAL CONTRIBUTIONS AND OUTLOOK

Acronyms/Abbreviations

HVOF	High-velocity oxygen fuel
OD	Outside diameter
ID	Internal diameter
hcp	Hexagonal close-packed
fcc	Face cubic-centred
Orth	Orthorhombic
D-gun	Detonation-gun spraying
TS	Thermal spraying
AS	Arc spraying
HVAF	High-velocity air fuel
CGSM	Cold-gas spraying method
VPS	Vacuum plasma spraying
CAPS	Controlled-atmosphere plasma spraying
IPS	Inert plasma spraying
SPS	Shrouded plasma spraying
GS-HVOF	Gas-shrouded HVOF
UPS	Underwater plasma spraying
LPPS	Low-pressure plasma spraying
FS	Flame spraying
HPPS	High-power plasma spraying
WPS	Water-stabilized plasma spraying
SM-gun	Sulzer Metco-gun
ChamPro	Controlled atmosphere plasma spray
SM-DJ®gun	Sulzer Metco-Diamond Jet® Gas-Fuel HVOF Spray Gun
TBC	Thermal barrier coating
SCC	Stress corrosion cracking
AES	Auger Electron Spectroscopy
POD	Pin-on-disc
LENS®	Laser engineered net shaping
SPS	Spark plasma sintering
PVD	Physical vapour deposition
HCAT	Hard Chrome Alternatives Team
FT	Force Transducer
SM	Stereo microscope
SEM	Scanning electron microscopy
EDS	Energy dispersive spectrometry
XRD	X-ray diffraction
SE	Secondary electrons
BSE	Backscattered electrons
DC	Direct current
SCE	Saturated calomel electrode
HP	High pressure
CJS	Carbide jet system

Symbols

T	Temperature
RT	Room temperature
F_N or w	Normal load (different authors)
F	Friction force
v	Velocity
t	Time
K_L	Linear wear rate
K_V	Volumetric wear rate
K_W	Gravimetric wear rate
K_E	Energetic wear rate
β	Coefficient of abrasion resistance
L	Sliding distance
μ or f	Coefficient of friction (different authors)
A'	Abrasion factor
g	Gramm
V or W_V	Worn volume (different authors)
s	Sliding distance
K	Wear rate
Δm	Mass difference
ρ	Material density
f_0	Initial friction coefficient
f_{max}	Maximum friction coefficient
f_{final}	Friction coefficient at the end of test
f_{spring}	Spring flexibility
δ	Secondary electron yield
Ra	Surface roughness
ω	Angular velocity
E_{corr}	Corrosion potential
E_{appl}	Applied potential
E_{pit}	Pitting potential
i	Current density
i_{corr}	Corrosion current density
d_{002}	Lattice constant

List of figures

List of tables

Trade names

D-gun[®]   Detonation spray technigue, used by Praxair ST, Appeleton, WI, USA

Super D-gun[®]   Spray technique (futher development of D-gun), used by Praxair ST, Appleton, WI, USA

Sonarc   Spray technique (combination of AS and HVOF), developed at the University Dortmund, Germany, Steffens and Nasssenstein 1996

SPS   Shrouded plasma spraying, developed by Okada and Maruo in1968 and by Jackson in 1969. This method has a shielding nozzle attached to the anode of the plasma tourch, in close contact with the substrate, which enables the plasma forming gases to be evacuated

GS-HVOF   Gas-shrouded HVOF, has been developed over the past several years. By using an extension nozzle at the exit of a commercial HVOF spray gun, GS-HVOF is capable of controlling the oxidation of sprayed materials during flight as well as achieving higher velocity of sprayed particles

UPS   Underwater plasma spraying was initiated by Waldie and Harris in 1983 at the Heriot Watt University and further developed by Lugschrider and Bugel in 1988 at the Technical University of Achen, Germany. This technique makes possible off-shore and underwater coatings deposition using a typical arc plasma torch with slightly higher working gas flow rates and much lower spraying distance

ID A60   Internal single-cathode plasma spraying burner developed by Thermico Company, Dortmund, Germany, 2006

ID Axial III   Internal three-cathode plasma gun developed by Thermico Company, Dortmund, Germany, 2006

Praxair
SG-guns   Internal plasma spray extension guns developed by Praxair Company

SM-F series
Gun   Internal plasma spray guns developed by Sulzer Metco Company

ID-CoolFlow   Internal High-velocity oxygen fuel burners developed in the last years by the Thermico Company

Termika 3   Patented portable HVOF set Termika-3 with ID spraying, A.Termica Ltd., Israel

HVOF-P2000   High velocity powder gun developed by the Metatherm Verschleiß-schutz GmbH company, Bexbach, Germany

SM-DJ guns   HVOF-Diamond Jet[®] Guns with DJT series extension modules developed by Sulzer Metco Company

Chapter I

INTRODUCTION

1.1 Background and Motivation

Thermal spraying, especially high velocity oxygen fuel (HVOF) is a versatile method for coatings depositing, which has been used to enhance the product lifetimes under severe conditions and also rebuilding dimensions and repairing worn components. During the spraying process, molten or semi molten particles impact on the substrate to form a laminar coating composed of many layers, called splats. As engineering applications become ever more demanding, the requirements for composite coatings that both protect the substrate, to retain its mechanical strength, but also to enhance the resistance of the substrate to wear and corrosion are increasing [1]. Besides of the variety of surface engineering techniques, HVOF thermal spraying has been applied successfully to deposit composite coatings with high density, superior bond strength and relatively low decarburization due to the high velocity and "low" particle temperatures induced in the deposition process.

The HVOF sprayed WC-based cermet coatings shown attractive characteristics, which make them superior to other iron base coatings concerning the wear and corrosion properties. These coatings are employed as wear resistance materials in a wide variety of applications, some of which require resistance to both corrosion and wear simultaneously. They have been successfully used as internal sealing faces of gate valves to overcome tribological and tribo-corrosion issues associated with leakage and jamming. Moreover, HVOF thermal spraying has become the method of choice to replace hard chromium plating on outside diameters (ODs) for commercial and military aircraft. It is now used for landing gear pistons and axle journals, hydraulic rods, engine shaft journals, and numerous other external surface applications on wear components [2]. Carbide based cermet coatings are also widely used against wear and corrosion in gas and oil industries. Their wear resistance have demonstrated to be higher than that of electroplated chromium, and also lower manufacturing costs can be achieved [3].

The tribological performance of such HVOF coatings depends mostly on the chemical composition, the nature of phases and their distribution, the porosity, the microhardness and on the residual stresses induced in the coating system. Moreover, there is substantial evidence that thermally sprayed coatings with a nanostructured carbide feedstock powder exhibit enhanced wear resistance compared to those sprayed with conventional powders.

Besides of the wear performance, in some applications corrosive environments are severe and corrosion resistance is the most important aspect for the performance of the coating. Corrosion behaviour of thermally sprayed coatings has been widely studied, during the past years. These coatings can be used either for new constructions or for repair of worn equipment components. Corroded and worn out surfaces are coated in order to achieve the original tolerances and also to obtain similar or better wear and corrosion performance of the equipment. The most common cases are pump and paper industry, in which there are moderate concentrations of chloride present in the environment. Chlorides can concentrate in

some parts of the equipment making the conditions very challenging for the corrosion resistant coatings [4].

Selection of the coating materials (especially the metallic binder type) should be chosen based on the knowledge of the environment in order to exhibit both wear and corrosion resistance, when exposed to severe conditions. Many publications are in this respect available, but a lot of them are in contradiction. It was found that using Ni instead of Co as a binder material or alloying Ni into Co binder phase leads to a higher corrosion resistance [5]. Cr alloying to Co as in the WC-CoCr coating does not offer enough passivity and extensive carbide matrix interface attack occurs in neutral chloride solution [5-8]. In contrast both WC-CrNi and Cr_3C_2-CrNi coatings seems to exhibit lower corrosion rates. Some other researchers [4] reported that the Cr_3C_2-25CrNi cermet coating exhibits high corrosion rate in comparison with the WC-10Co4Cr coating. However, as it can be seen, these results differ from each other, mainly due to the different spraying parameters and different testing conditions. This makes selection of such investigations very difficult unless relevant tests and obtaining processes are conducted to match exactly one to another. Only in this case the corrosion or wear behaviour of such coatings can be compared as close as possible.

Based on the main challenge of this work namely, HVOF spraying on inner cylindrical surfaces, no information is nowadays available in the literature regarding the wear and corrosion behaviour of coatings deposited under ID conditions. However, HVOF was a line-of-sight spray technology that cannot be used for many non-line-of-sight geometries such as internal diameters (IDs). HVOF guns were quite large and require a standoff (distance from gun to surface) of several hundreds of millimetres. Consequently, there was a need for an ID coating technology that can be used to renew internal diameters and is environmentally acceptable. Lower cost, better performance and faster turnaround time are additional drivers for change. For these reasons the interest in ID-HVOF coatings has increased in the recent years. This is due to the potential improvement of the particles grain size down to nanometric scale having a direct influence onto the spraying distance, which allows small inner diameters to be coated (the finer the powder the shorter the standoff). Besides of this, new developed ID-HVOF guns are now available onto the market. In this domain of thermal spraying, only some final reports are available regarding the deposition of coatings on inner surfaces. They investigated the deposition of coatings using miniature plasma spraying guns that could replace hard chromium on internal surfaces, where conventional thermal spraying technologies could not be used. At that time, it was reported that HVOF is becoming accepted as the best alternative to replace the hard chrome plating on outside diameters (ODs), but cannot coat IDs less than 280 mm because of the flame standoff. As was mentioned before, new HVOF guns and also very fine powders are now available, which makes the ID HVOF commercially viable for coating inner surfaces down to a diameter of 80 mm. However, numerous common results have been reported showing that WC nanocomposites are far more sensitive to carbide degradation than the standard microsized powders traditionally used.

Using nanopowders in plasma ID-spray (high process temperature) dramatically increases the degradation of the coating depositions and makes the process much less reliable. In contrast, the HVOF spraying process required less thermal energy and the floating time of the powders in the flame is very short. Under these conditions, it may be assumed that, the possibility of the WC decomposition is very

low and thus, no significant deterioration with respect of the mechanical properties of the coating will occur.

Moreover, the significant advantage of ID HVOF spraying process is the possibility to coat IDs by using fine powder materials which cannot be processed by the plasma spray technology. Therefore, the performances of the ID coatings will be somewhat above that of plasma sprayed ones. It was already demonstrated that under normal conditions (OD coatings), the HVOF coatings exhibits higher adhesion strength and hardness, lower porosity than the plasma deposited coatings.

It needs to be mentioned that, technically, ID HVOF spraying technique is not as mature as the conventional HVOF spraying (ODs coatings). The latter has been studied and developed during a long period of time, since the 80's. The spraying parameters are very different for the two processes. Moreover, working in a closed atmosphere it is difficult to control the spraying conditions, especially the overspray (powder that does not adhere to the substrate). This powder can easily be trapped in the spraying region and can settle on the surface, becoming incorporated into the coatings. In the case of conventional HVOF, the overspray powder can be easily swept away by the cooling air jets (open atmosphere). All these factors can contribute to the scatter in tribological and corrosion properties. Therefore, deposition and afterwards testing of these coatings at relevant service conditions is advisable to determine the range of wear rates, friction or corrosion mechanisms.

The present work was undertaken to investigate and to compare in various test conditions, the coating properties especially the wear and corrosion behaviour of ID-HVOF coatings for possible applications of spraying inner surfaces of cylinder housing (e.g. landing gear actuator inner cylinder).

The need to select or design new surfaces for future equipment as well as to minimize the operating costs and extend the life of existing machinery has led to demands for a much better understanding of surface degradation processes particularly when tribological components are operating in corrosive environments.

1.2 Purpose

The properties of HVOF cermet coatings obtained under ID conditions such as their morphology as well as the wear and corrosion behaviour are still barely known. As it was mentioned before, no available information of such type of investigations were found. The goal of this PhD thesis is to explore the production of ID HVOF cermet coatings sprayed on non-line-of-sight geometries such as inner surfaces of cylindrical pieces.

Considering the present knowledge about cermet coatings, this work aims to further investigation of the morphology, wear and corrosion resistance of WC-Co-Cr and WC-Cr_3C_2-Ni coatings deposited using three different granulometric fractions (fine, medium, coarse) of powder for each chemical composition. The coated specimens produced under ID conditions are subjected to several types of tests. As a result of these examinations relevant information regarding the areas where these coatings could be applied with favourable outcomes are expected.

In this direction, a new ID HVOF gun is used for the inner deposition process of coatings onto all the specimens investigated in this research work. For that, a special sample holder which permits the simulation of inner spraying conditions has to be designed and manufactured. Concerning that, this is a new HVOF process, a first step of parameters optimisation is required in order to obtain low porosity coatings. The morphology of these coatings is investigated by means of phase

transformation (XRD-measurements) as well as microstructure characterization (SEM/EDS-analysis) and microhardness measurements (HV0.3).

In order to accomplish the main aim of this work, a special wear tester has to be constructed, because presently there is no available equipment to perform the wear test on inner surfaces. Moreover, the conception of this tester is fundamental because of the different spraying parameters and conditions in OD- and ID spraying (temperature of the substrate, energy content of the flame, powder grain size etc).
One should take into consideration that through the wear tester design, pair specimens of the investigated coatings could be brought into sliding contact (rubbing against each other). This opportunity to test materials obtained under the same HVOF spraying process will be a significant advantage that allows the optimal tribopairs selection. It is also desired to overcome the usual point contact between the two sliding tribopair (see pin on disc tests) in order to avoid a premature wear of the counterbody during the sliding wear test, considering that the specimen to be tested is the ring inner surface and not the counterbody (e.g. ball's material). Therefore, it is expected, that the new wear testing arrangement allows a "line-surface" contact between the tested specimens, which will lead to a closer simulation of the service conditions and the premature wear of the static partner should be diminished. Besides of this task, this tribometer needs to be also very flexible (e.g. various loads, velocities, different environments), considering that for this work, the sliding wear tests will be performed under two different conditions, dry and wet respectively.

Another important goal is the assessment of the corrosion behaviour of the coatings obtained under the same ID conditions by applying the electrochemical corrosion measurements using a three electrode system.
All the above mentioned tests are able to facilitate to establishment of the investigated materials (chemical compositions, granulometric fraction) which offers the best compromise regarding the deposition efficiency, the wear and the corrosion resistance.

Accordingly, the thesis has been structured into the following chapters: **chapter 1** represents the background and motivation; **chapter 2** displays theoretical aspects regarding the properties of cermet materials, current trends in thermal spraying processes as well as an overview of the tribological and corrosion behaviour of cermet coatings; **chapter 3** presents the experimental program concerning the coating and substrate materials, deposition and investigation methods; **chapter 4** is dedicated to the characterization of as-sprayed coatings and also to the results and discussions of the proposed investigations and **chapter 5** points out the general conclusions and original contributions of the present work.

Chapter II

STATE OF THE ART

2.1 Theoretical aspects regarding cermet materials

2.1.1 Introduction

CerMet is an acronym derived from CERamic-METall which is used world wide to designate a heterogeneous combination of metal(s) or alloy(s) with one or more ceramic phases in which the latter constitutes approximately 15 to 85% by volume [9]. The cermets are commonly produced using powder metallurgy techniques where metal and ceramic powders are mixed, pressed and sintered at high temperatures to form dense compacts [10].

Typically, but not exclusively, a ceramic is a metallic oxide, boride, carbide, or a mixture or compound of such materials [11]. In contrast to composite laminates, the combination of metal and non-metal in cermets occurs on a microscale. The non-metallic phase is usually not fibrous, but consists of more or less equiaxed fine grains that are well dispersed in and bonded to the metal matrix. The bond between the nonmetallic phase and the metal matrix makes important contributions to the cermet; it is strongly affected by the phase relations: solubilities, and wetting properties that exist in the relationship between the ceramic and metallic components.

The basic objective of cermet materials is to incorporate the desirable qualities and suppress the undesirable properties by combining the metal and ceramic components on an intimate scale. The most outstanding example of the desirable properties obtained from combining metal and ceramic materials involves the hard-metal types made from cemented carbides [9-12].

2.1.2 Types of cermet materials

Cermets can be classified according to their hard refractory component, the ceramic phase. In this system, the principal categories of cermets are determined by the presence of the following components:

carbides, nitrides, oxides, borides, and also carbonitrides

and the metallic binder phase can consist of a variety of elements, alone or in combination, such as:

cobalt, nickel, iron, chromium and molybdenum

Ceramic phase

Metallic binder
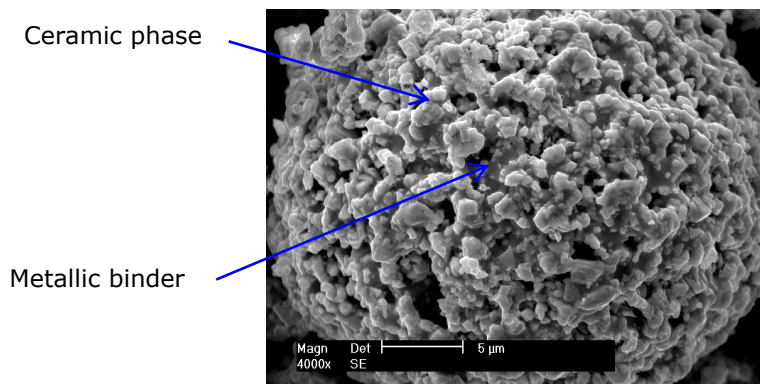
Figure 2.1 Example of cermet material (powder)

The ductile phase can also contain other metals, such as stainless steel, superalloys, titanium, zirconium, or some of the lower-melting copper or aluminium alloys [13]. The metallic bond for each cermet is selected in order to produce the desired structure and properties for the specific application. The iron group metals and their alloys dominate in the cemented tungsten carbide class of hard metals; nickel and, to a lesser extent, cobalt and iron possess a desirable combination of relatively high hardness and good ductility. However, the binder for a cermet material can also be chosen from the group of more reactive metals, such as titanium or zirconium, or it can be selected from series of refractory metals that includes chromium, niobium, and molybdenum.

Carbide-based cermets (cemented-carbide) are by far the largest category of cermets, even if the term is used in its narrower sense and excludes the broad field of cemented-carbide cutting tools and wear parts based on tungsten carbide (WC). Since the inception of cermet technology, the dominant concept has been that of a material based on TiC as the primary hard and refractory constituent, with the bonding provided by any of a variety of lower-melting ductile metals or alloys (much the same as those used for cemented tungsten carbides). The TiC cermets have found use in tools and wear resistance applications, in selected high-stress, high-temperature systems, and in corrosive environments. Cermets based on SiC and B_4C, which generally are classified as metal-matrix composites, have gained considerable industrial significance in wear and corrosion resistance, or antifriction, applications; they are also used in nuclear reactor applications. Cermets with chromium carbide (Cr_3C_2) base have been used for variety of corrosion resistance applications and as gage blocks; however, they have apparently lost much of their industrial usage.

Nitride-based cermets constitute a special class of tool materials. Titanium nitride (TiN) and especially cubic boron nitride (CBN) produce excellent cutting materials if they are combined with a hard binder metal. Titanium nitride and zirconium nitride (ZrN) bonded with their respective metallic elements have been developed for special heat- and corrosion-resistant purposes.

Oxide-based cermets constitute a category that includes uranium dioxid (UO_2) or thorium dioxide (ThO_2), which are used as blanket material in liquid metal cooled

fast breeder reactors (LMFBR) and as fuel elements in nuclear reactors; Al_2O_3 and other highly refractory oxides, used for components in liquid-metal manipulation (for example pouring spouts) and general furnace parts; and SiO_2 used as a minor constituent in friction elements. Combinations of Al_2O_3 with TiC are suitable for hot-machining tools. Besides of these oxides there are also known titanium dioxide (TiO_2), zirconium dioxide (ZrO_2) and chromium oxide (Cr_2O_3) which are used in a wide range of applications.

Boride-based cermets have a boride of one of the transition metals as the dominant phase. These cermets provide excellent high-temperature corrosion resistance to attack by active metals, such as aluminium in the molten or vapour state. A combination of ZrB_2 and SiC is resistant to erosion caused by the propulsion gases of chemical rockets [12].

Carbonitride-based cermets can be produced with or without additions of various other carbides (of which Mo_2C is the most important); they are bonded with the common cemented-carbide binders. At present, these materials are the primary cermets for tool applications. Their enhanced strength, which makes them suitable for high-speed cutting tools, is based on a greatly improved bond between the hard carbide grains and the binder metal. The improved bond is a consequence of a miscibility gap in the quaternary TiC, TiN, MoC, and MoN system that results in so-called spinodal decomposition into two isostructural phases with inherently better wettability to the binder [14].
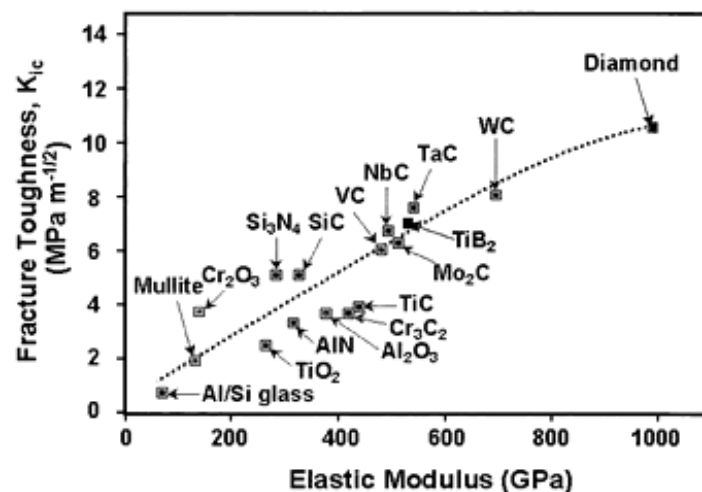
Figure 2.2 Fracture toughness vs. elastic modulus of some cermets types [17]

The fracture toughness vs. elastic modulus plot (Fig. 2.2) is referred to the paper presented in the Gareth Thomas Symposium on Microstrucutre Design of Advanced Materials, 2002, Columbus Ohio, entitled "Microstructure Design of Composite Materials: WC-Co Cermets and their Novel Architectures" by K.S. Ravichandran and Z. Fang, Univ of Utah. The figure shows that of all the ceramics, tungsten carbide (WC) has exceptional fracture toughness srivalling that of diamond but with greater chemical stability.

The cermets, as mentioned earlier, are commonly produced using powder metallurgy techniques in which both ceramic and metallic components are in form of dense compact powder, see figure 2.1. All the cermet powder types offer an interesting alternative to produce a protective layer on a steel structure due to the excellent wear, corrosion and thermal resistance of both ceramic and metallic materials [15]. Cermet powder types to be used depend a lot on the application and the planned spray system. Table 2.1 shows a variety of application and examples of powder materials. The first three applications such as:

- wear protection
- corrosion protection
- thermal protection

are especially important for power-generation components. It is evident that every specific application requires a specific powder.

Table 2.1 Powder types and functions (Compiled based on [16])

Material			
CuNiIn WC-Co WC-CoCr Al_2O_3-TiO_2 Cr_2O_3 AlSi-Polyester TiC SiC B_4C CBN-W	MCrAlY NiCr Mo TiC SiC B_4C Cr_3C_2 TiN ZrN	ZrO_2-Y_2O_3 ZrO_2-MgO TiN ZrN SiO_2	Al_2O_3 $YBa_2Cu_2O_7$ WCu
Coating requirements			
Wear resistance Good bonding Good cohesion Homogeneous Low porosity High hardness	Corrosion resistance Low porosity Good bonding Same heat expansion as the substrate	Thermal conductivity Thermal stability Good mechanical properties	Good electrical insolating Low porosity No microcracks No oxides
Wear protection	**Corrosion protection**	**Thermal functions**	**Electrical functions**
Abrasion Sliding Erosion Fretting	Atmospheric corrosion Intermediate corrosion Oxidation Sulfidation	Thermal Insulation Reflection Absorption	Isolation Conductivity High temperature supercondition

2.1.3 Tungsten carbides

Tungsten carbide (WC), known as well as cemented carbide belongs to a class of hard, wear-resistant materials in which the hard carbide particles are bound together, or cemented, by a soft and ductile metal binder, usually cobalt or nickel. The first cemented carbide was produced in Germany in the early 1920s and consisted of tungsten carbide (WC) with a cobalt binder (Widia = "like diamond")

[17]. Tungsten carbide was first synthesized by the French chemist Henri Moissan in the 1890s [18]. In the W-C system, two carbides are mainly found: WC which directly decomposes at 2800 °C, and W_2C, which melts at 2700 °C [19, 20].
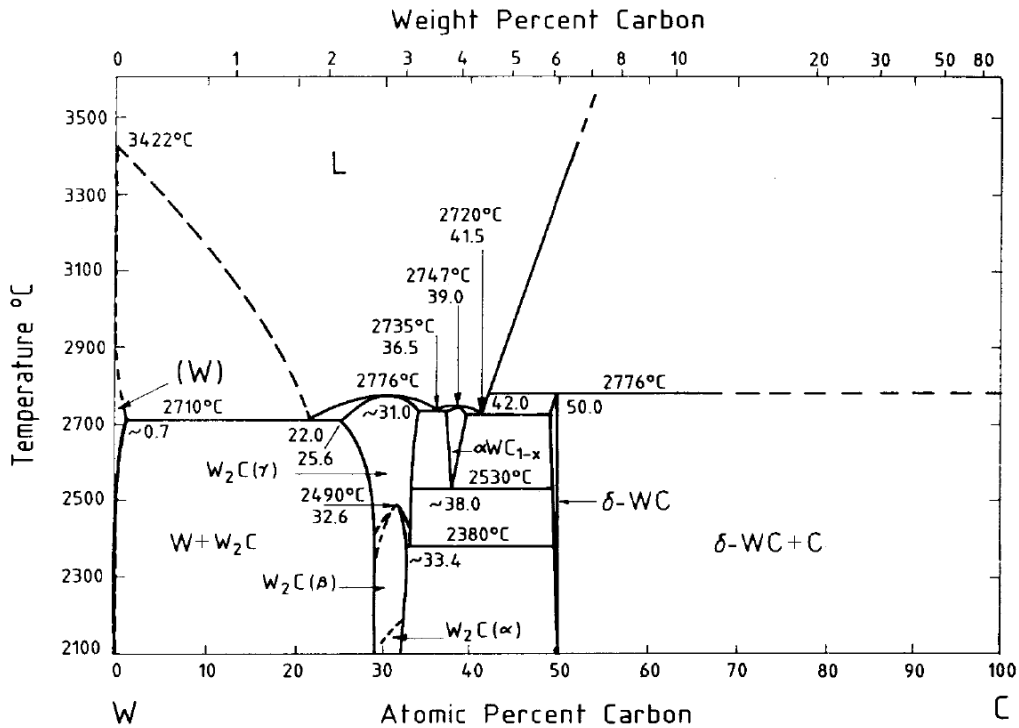
Figure 2.3 W-C phase diagram [21]

In the tungsten-rich part of the binary W-C equilibrium diagram (Fig. 2.3), three W-C stoichiometries have been found: hexagonal W_2C denoted in W_2C (α), W_2C (β) respectively W_2C (γ), hexagonal WC and the cubic sub-carbide $αWC_{1-x}$ crystallizing in the NaCl type structure. W_2C exhibits a comparatively wide homogeneity range of 25.5 to 34 at.% C at 2715 °C. This phase originates from a eutectoidal reaction between elemental W and δ-WC at 1250 °C and melts congruently with the W solid solution at 1715 ±5 °C and with $α-WC_{1-x}$ at approximately 2758 °C. Phases of W_2C stoichiometry are obtained as intermediate products during WC production. The $αWC_{1-x}$-phase results from an eutectoidal reaction between W_2C (γ) and δ-WC at 2535 °C and melts at approximately 2785 °C. The technically important δ-WC is the only binary phase stable at room temperature and has almost no solid solubility up to 2384 °C but may become carbon deficient between this temperature and its incongruent melting point. The monocarbide, WC, has a simple hexagonal crystal structure with two atoms per unit cell and a c/a ratio of 0.976. Unfortunately, the cast pure WC is quite impractical because the stoichiometric compound WC, with 6.13 weight percent carbon, does not melt congruently; it decomposes to a fragile mixture of W2C, WC and graphite upon cooling. However, at lower carbon contents, mixtures of WC and W2C are formed on cooling, which melt at a relatively moderate

temperature, around 2750 °C, and result in a cast product which is very hard, although by nature quite brittle [22].

In the field of thermal spraying, some authors have found that a high flame spraying temperature produces a dense coating, but it can causes also the decomposition of WC to W_2C even metallic W, the preferential evaporation of C and the formation of brittle Co-W-C phase [23-26]. These additional phases are detrimental to hardness, toughness and wear resistance. The decarburization and WC decomposition are much pronounced for the WC-Co coatings produced from extra fine powder because of the greater surface area of these nano-sized WC particles, and therefore, the potential benefits offered by nanocomposites have not been fulfilled [23-25].

Table 2.2 Properties of metal carbides as hard phases [27-30]

Hard-carbide phase	WC	W_2C	Cr_3C_2	TiC
Crystallography	hcp	hcp[b]	orth	fcc
Hardness (HV 50)	2200	2000	1400	3000
Melting point [°C]	2870[a]	2700	1800[a]	3100
Theoreical density [g/cm^3]	15.7	17.2	6.6	4.9
Modulus of elasticity [GPa]	696	444	373	450
Coefficient of thermal expansion [µm/m*K]	5.2	1.2	10.3	7.7
Poisson´s ratio*	0.24	0.28	-	0.17-0.25

[a] not congruently melting, dissociation temperature
[b] at: T < 1520 K, hexagonal close-packed thermally unstable; 1520 K < T < 2350 K, orthorhombic; 2350 K < T < 2700 K, hexagonal close-packed
* the Poisson´s ratios of thermal sprayed ceramic coatings range from 0.20 to 0.30

Tungsten carbides have enjoyed a steady expansion over the past nine decades. Over the years, the basic WC-Co material has been modified to produce a variety of cemented carbides containing WC-TiC, WC-CoCr, WC-Cr_3C_2-Ni, WC-TiC-TaC, WC-TiC-(Ta, Nb)C etc.. that covers a wide range of applications, including metal cutting, mining, construction, rock drilling, metal forming, structural components, and wear parts. A remarkable feature of tungsten carbide cermets is that they can be tailored to provide different combinations of wear and corrosion resistance by controlling the amount of Co or Ni and WC grain size. Carbide grain sizes from 0.5 to 5 µm are commonly used [31].

In the last years, laboratory tests conducted by Sandvik Hard Materials Company expose some statistical results (see figures 2.4 and 2.5) about the main mechanical properties such as: hardness, toughness, wear and corrosion behaviour of tungsten carbide. The graphs show that hardness increases with decreasing grain size and binder content. Unfortunately, this will always be at the expense of reduced toughness. In truly abrasive applications, hardness is a good measure of wear resistance.

(a)   (b)
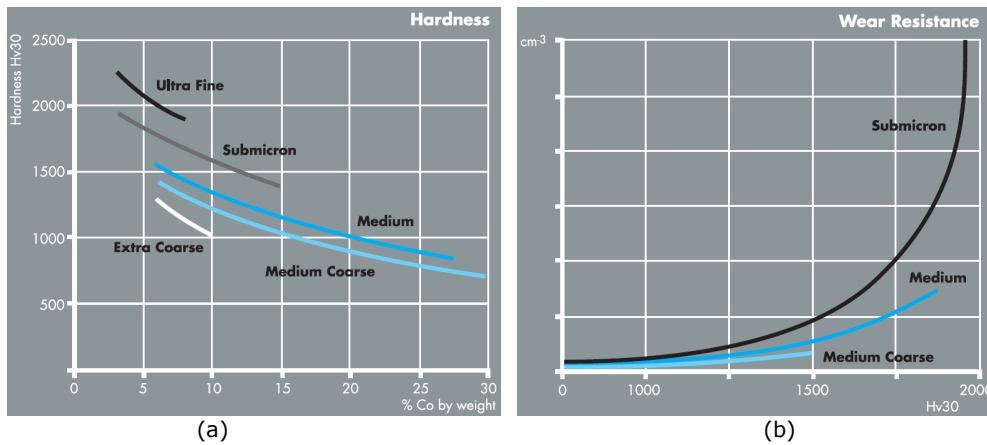
Figure 2.4 Hardness as a function of the Co content for various WC grain sizes (a); Wear resistance as a function of hardness (ASTM B611-85) (b) [32]. Reproduced by permission of Sandvik AB, Sweden

(a)   (b)
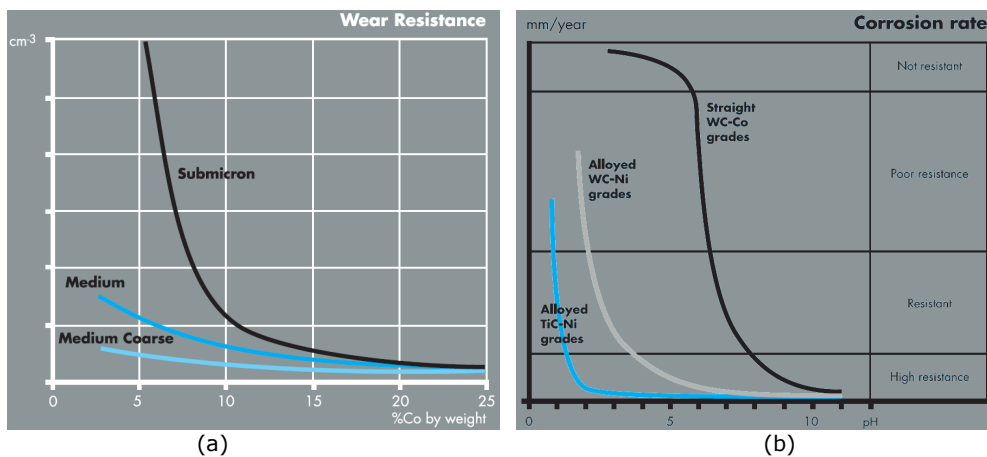
Figure 2.5 Wear resistance as a function of the Co content with different WC grain sizes according to the ASTM B611-85 test method (a); Corrosion rate as a function of the pH value for different types of cemented carbide (b) [32]. Reproduced by permission of Sandvik AB, Sweden

As illustrated, straight WC-Co coatings are corrosion resistant down to pH 7. The highest corrosion resistance is obtained for the TiC-Ni coatings, which are resistant down to pH1. However, compared with the straight WC-Co coatings, they have low strength and inferior thermal conductivity and thus they are used only when corrosion resistance requirements are high. In most corrosion-wear situations, optimum choices are the WC-Ni grades, which are resistant down to pH 3-4. These grades retain WC as the hard phase, and substitute Co for Ni; thus they exhibit mechanical and thermal properties similar to the WC-Co coatings [32].

2.2 Thermal spraying

2.2.1 Overview

Thermal spraying was mentioned for the first time in patent "Powder metal and wire-flame spraying" applied by Dr. Max Ulrich Schoop in 1909, Switzerland. He came to realize that a stream of molten particles colliding with each other can form a coating. At first the lead and tin wires molten in the flame produced by burning acetylene in oxygen were used as coating materials. Only some time after that, powders started to be used. M. U. Schoop also patented the wire arc spraying process in 1911 by which the deposition of a greater number of metal coatings was made possible [33]. After a few years he sold the rights of his "Scoop Process" to a German company called Metallizator. This company has made the process available throughout Europe and the USA by the early 1920's [34].

Thermal spraying is defined according the European standard DIN EN 657:2005 [35] as follows: "Thermal spraying is a process in which surfacing materials are heated to the plastic or molten state, inside or outside of the spraying gun/torch, and then propelled on to a prepared surface; the substrate remains unmelted".
In thermal spraying the material is in the form of powder, wire, cord or rod and is fed into the flame produced by a spray gun, where it melts and the formed droplets are accelerated towards the substrate to be coated (see figure 2.6). The thermal and kinetic energy of the flame can be produced either with burning mixtures of fuel gas and oxygen, or by using an electrical power source [36].
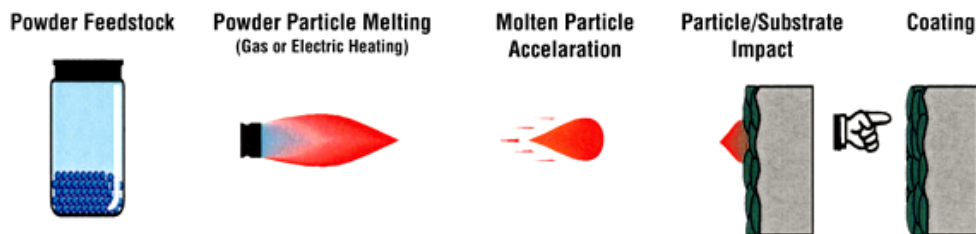
Figure 2.6 Thermal spray coating process [http://www.tungsten-powder.com]

Based on the energy carriers, thermal spray processes can be divided into a few main groups according to DIN EN 657 from 2005, see the figure 2.7:
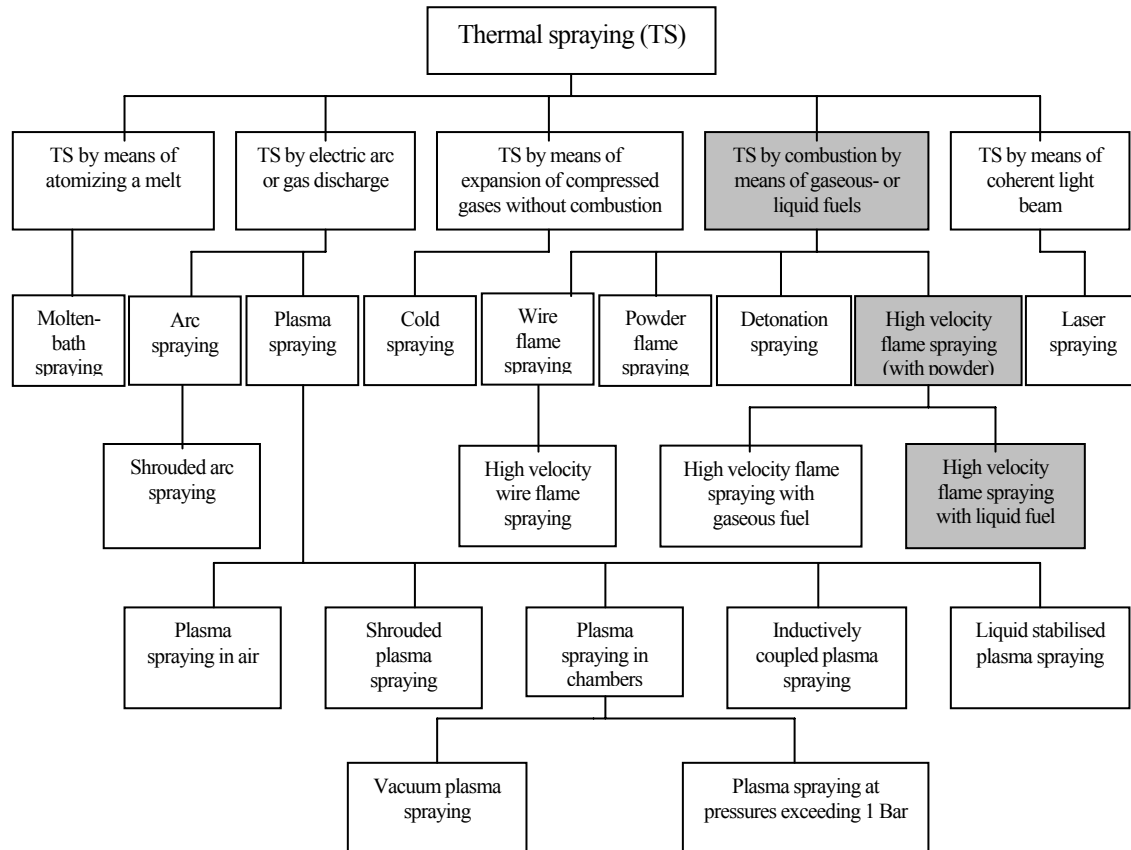
Figure 2.7 Overview of thermal-spray processes according to DIN EN 657 [35]

In thermal spraying the coating is built up from the lamellas formed by rapid solidification of the melted or semi-melted droplets attached to the substrate. A typical structure of the coating is a pancake-like lamellar structure, where the flattening degree and adhesion between the lamellas, together with the coating material itself, define the main properties of the coating [37]. Coatings can be generated if the particles can plastically deform at impact with the substrate, which may only happen if they are molten or solid and are sufficiently rapid [38]. The adhesion and porosity of the coating is mainly defined by the particle melting behavior and the velocity when attaching to the surface (see figure 2.8).
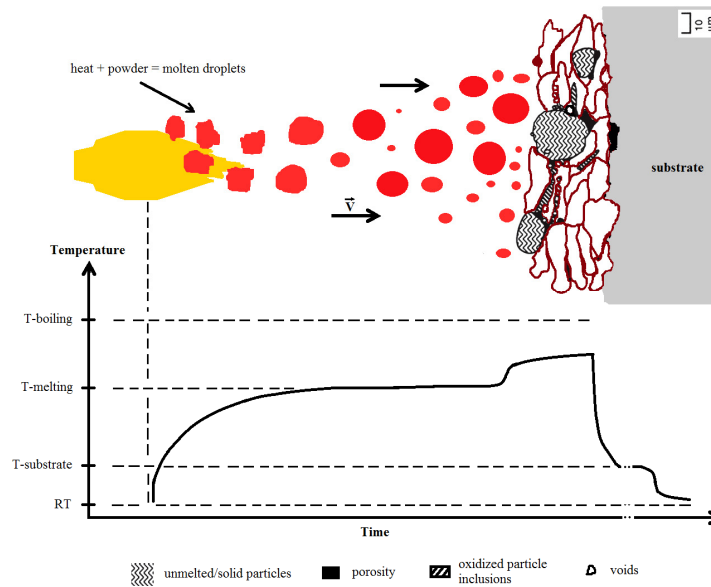
Figure 2.8 Basics of thermal spraying showing the heating and acceleration of the particles in the heat bath (e.g. flame) and impact at the surface, including the temperature versus time evolution. Compiled based on [16]

In addition, due to the fast cooling rate of the particles, some special features, such as residual stresses and metastable phases can be observed in thermally sprayed coatings [36; 39-40]. Such coatings are often applied to improve corrosion, wear resistance and thermal oxidation. Therefore, low porosity and good adhesion are desired properties for the coating. High velocity processes especially HVOF (High velocity oxy-fuel) spraying is the most potential method for producing a well adherent coating with low porosity. In HVOF spraying heat is produced by burning mixtures of oxygen, hydrogen and fuel gas or liquid. Due to the special nozzle design, a jet with supersonic speed is produced.

Another commonly used method is APS (Atmospheric plasma spraying), where the energy is based on the plasma produced by ionizing an inert gas, typically a mixture of argon and hydrogen or helium, between the anode and the cathode in the spray gun. Due to the high energetic ionized plasma, the temperature of the plasma flame is very high. The main difference between HVOF and APS is the relationship between the kinetic and thermal energy of the process described by the particle velocity and the flame temperature. Typical ranges of these parameters for each of the process are given in table 2.3.

Table 2.3 Characteristic features of HVOF and APS processes. [36, 41].

Spraying method	Particle velocity [m/s]	Flame temperature
HVOF	500-800	~ 3000°C
APS	150-400	~ 8000-12000 K

The ability to produce dense coatings with low amount of phase transformations and oxidation is the main feature of the HVOF process. This is due to the short dwelling time of the particles in a relatively "cold" flame (~3000°C) in comparison with the APS flame temperature (~10000 K). The HVOF process is widely used to produce cermets and metal coatings, but also has demonstrated an ability to deposit dense ceramic coatings [36, 42-45]. The use of thermal spray coatings has traditionally been based on extending the life time of the component. However, thermal spray coatings have increasingly been considered "prime reliant" and such coatings are already being included in the design of the systems [46]. This requires considerable enhancement of the reliability and reproducibility of the coatings. Thermal spraying is a very complex process and includes a big number of parameters. A better understanding of the relationship between these parameters and their effect on the coating properties must be obtained in order to apply thermal sprayed coatings to "prime reliant" applications [36]. Thermal spraying is an effective and low cost method to apply thick coatings to change surface properties of the component [47].

2.2.2 Characteristics of thermally sprayed coatings

The relative importance given to different properties depends on a number of factors, such as a coating´s level of development, e.g. the need for further optimisation, and the intended application. A coating in full production for a number of years may be subjected to less rigorous testing than one which is newly introduced. Indeed, in that case the emphasis moves towards non-destructive methods. The relative importance of each coating property to be characterized and evaluated is thus usually different depending on whether the coating to be studied is intended for production or for research and development. The emphasis in the former case is on quality control and repeatability, whereas the latter is aimed towards the evaluation of specific properties and the way in which they are influenced by process variables [48]. The most important properties of coatings intended for production or development use can be ranked as shown in the following table:

Table 2.4 Ranking of the most important properties for engineering coatings [48]

In production	Research and development
1. adhesion 2. thickness 3. surface finish 4. corrosion resistance 5. friction/wear performance 6. hardness 7. porosity 8. composition 9. internal stress 10. structure/morphology	1. friction/wear performance 2. composition 3. adhesion 4. corrosion resistance 5. internal stress 6. surface finish 7. structure/morphology 8. thickness 9. porosity 10. fracture toughness

Once a particular coating has been optimised and is put into routine production the primary need is for effective process control, following the adage that "good quality should be built in rather than poor quality tested out".

Hardness, density, and porosity. Thermal spray coatings are often used because of their high degree of hardness and density. Their hardness and erosion resistance make them especially valuable in high-wear applications. The hardness and density of thermal spray coatings are typically lower than for the feedstock material from which the coatings were formed. The porosity degree of conventionally thermally sprayed coatings is between 0.025% and 50%, and can be caused by: low impact energy (unmelted particles / low velocity), shadowing effects (unmelted particles / spray angle), shrinkage and stress relieving effects. It can be detrimental in coatings with respect to: surface finish, strength, hardness, corrosion resistance and wear characteristics.

In the case of thermal sprayed coatings, the hardness, density and porosity of the coating depend on the thermal spray material, type of thermal spraying equipment, and the spraying parameters. In general, the higher the particle velocity is, the harder and denser are the coatings [49, 50]. The most common hardness measures used for coatings are the Vickers or the Knoop microhardness, typically using loads of between 10g and 500g. The nature of the basic test, involving the measurement of the dimensions of an indentation left after the removal of an indentor, also introduces some subjectivity to the reading. Nevertheless hardness is one of the simplest properties to measure and it is widely used as a ranking parameter when comparing coatings, without having to carry out special specimen preparation [48].
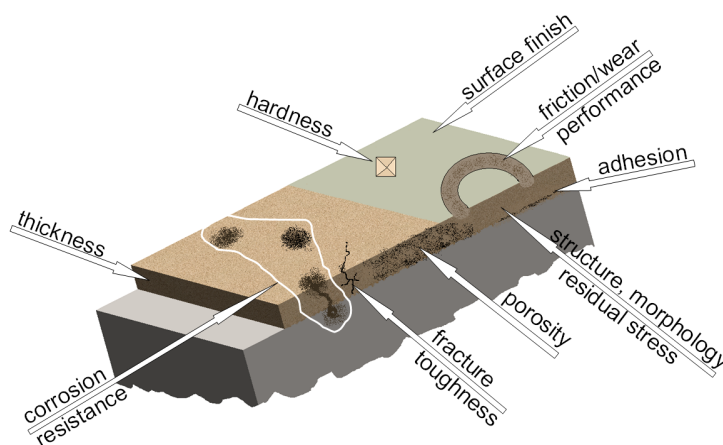
Figure 2.9 Engineering coating properties

Corrosion resistance. Thermal coatings are applied as "sacrificial" or as a barrier component in order to protect the underlying substrate from corrosion. Besides of the selection from thermal spray corrosion resistant coating, the key to sustainable corrosion protection is lower surface porosity, optimal coating thickness and perfect isolation of the base metal. Any exposed metal prone to corrosive attack will disassociate from the parent metal, taking the coating with it. Metallic thermal spray coatings may be either anodic or cathodic to the underlying metal substrate. Because corrosion occurs at the anode, anodic coatings will corrode in corrosive environments and the cathode will not. Anticorrosive coating systems are generally designed such that the coating material is anodic to the substrate metal. Anodic coatings will corrode or sacrifice to protect the substrate [49]. More details about this property will be discussed in section 2.5 (Corrosion of thermal spray coatings).

Wear performance. Wear behaviour of the coating can be influenced by:
- the contact conditions, which includes parameters such as load, speed, geometry, temperature, environment etc;
- the contacting materials, which includes parameters such as the physical and chemical properties of the coating and the counterface;
- the coating microstructure, which includes parameters such as grain size, density and porosity. These are influenced by the material or materials used as well as by the spraying method.
- the composite coating/substrate system that includes parameters as: coating thickness, coating hardness, elasticity, surface roughness as well as thermal and chemical compatibility, including adhesion, of the coating and substrate. For more details see section 2.4 (tribological behaviour of thermally sprayed coatings).

Thickness. This, apparently simple, property has an important role, especially in tribological applications. There is a complex interplay between effects such as the intrinsic stress within a coating, the hardness of the coating, the substrate and the adhesion which must be optimized, essentially by the appropriate choice of thickness [48]. From the economical point of view, the thickness of the coating has a direct influence on the process costs, the higher the thickness is the higher the cost are. It is always good to have a close relation between the technical (e.g. coating thickness) and economical demands. The thickness of a thin layer on a surface can be measured by a large variety of different methods, such as: optical, removal, electromagnetic, scattering or X-ray fluorescence method.

Fracture toughness. Thermal sprayed coatings or in general coatings have poor strength, ductility and impact properties. These properties tend to be dictated by the "weakest link in the chain" which in coatings tends to be the particle or grain boundaries and coating/substrate interface. Coatings are limited to the load they can carry, and thus require a substrate for support; even then, coatings are poor when point loaded. Effective bond strength is reduced and can be destroyed by increasing levels of internal stress. This in turn effects coating thickness limits. Coatings on external diameters can be built up to greater thickness than that on internal diameters [50].

Adhesion. It has been argued that this is the most important coating property, since if it is inadequate all functionality of the surface may be lost. The ability of a coating to remain attached to the substrate under the required operating conditions is clearly vital [48].There are a lot of factors which can effect the bonding (adhesion) and subsequent the build up of the coating as follows: cleanliness, surface area, substrate topography or profile, temperature (thermal energy), time (reaction rates and cooling rates), velocity (kinetic energy), physical and chemical reactions, mechanical properties of the substrate. Cleaning and grit blasting are important for substrate preparation. This provides a more chemically and physically active surface needed for good adhesion. The surface area is increased which will increase the coating bond strength and the rough surface profile will promote an optimal mechanical keying. Besides of that, increase in thermal and kinetic energy increases the chances of good metallurgical bonding; (temperature, velocity, enthalpy, mass, density and specific heat content etc..). Thermal spray materials like molybdenum, tungsten carbide, and aluminum/metal composites produce so called "self bonding" coatings. These materials have comparatively high bond strengths (increased metallurgical or diffusion bonding) and can easily bond to clean

polished substrates [50]. Special coatings, used for wear resistance, that are applied by thermal spray processes with high kinetic energy, such as HVOF can have tensile adhesions of greater than 34,000 kPa as measured by ASTM C633 "Standard Test Method for Adhesion or Cohesive Strength of Flame-Sprayed Coatings". Most coatings used for infrastructure applications have adhesion values comparable to paint coatings. Typical field- and shop-applied zinc, aluminum, and zinc-aluminum alloy coatings will have adhesion ranging from 5440 to 13,600 kPa as measured by ASTM D4541 "Standard Test Method for Pull-Off Strength of Coatings Using Portable Adhesion Testers [49].

Morphology. The various thermal spray materials and also the spraying methods produce coatings structures or morphologies which are specific to themselves. The morphology of as-sprayed coatings produced by each method can be very different, for example a WC-Co coating produced by HVOF would be different to a MCrAlY coating by APS, see figure 2.10.
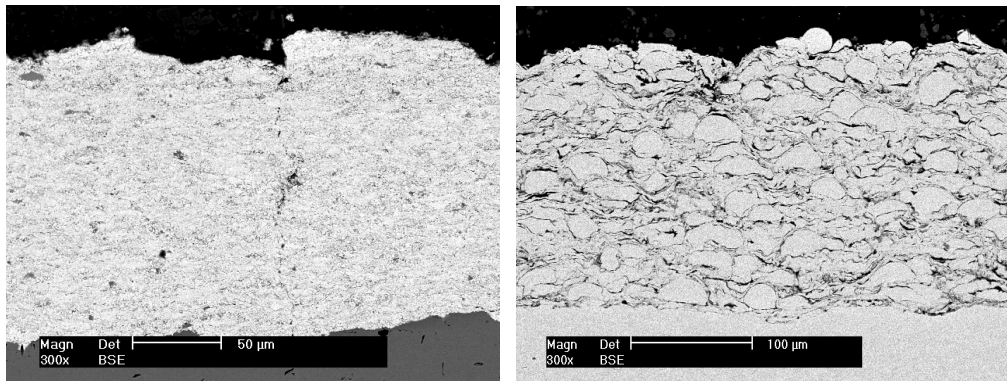
Figure 2.10 Typical coating morphology of WC-Co coating (left) and APS MCrAlY coating (right)

In practice the differences which we see between different coatings are largely determined by distinct morphology concerning the grain structure, grain boundary effects, splat flattening, interlamellar adhesion as well as residual stresses.

The molten or semi-molten state processes typically produce coatings with splat-like features whose boundaries tend to be parallel rather than perpendicular on the substrate surface. Coatings properties such as hardness, elastic modulus and residual stress are all influenced by the morphology, as indeed is the corrosion and wear response. [48, 51, 36]

As a conclusion, after all the discussions about the characteristics of thermal spray coatings, it was made a new ranking of the most important properties for engineering coatings, as follow:

1. Adhesion
2. Porosity which has direct influence onto: surface finish, strength, hardness, corrosion and wear performance
3. Fracture toughness
4. Structure/morphology
5. Thickness.

It can also be said that some coatings properties are related to each other. For example, porosity is an important coating feature that strongly influences the other coating properties. For hardface or wear-resistant coatings, porosity lowers coating hardness and contributes to poor surface finishes, thus decreasing wear resistance. Porosity in wear coatings can also lead to the generation of coating fragments that break away and become abrasive cutting agents, increasing the wear rates of the coating. It creates also poor coating cohesion and allows higher wear and corrosion rates. Porosity is generally associated with a higher number of unmelted or resolidified particles that become trapped in the coating. Poor splat or particle cohesion leads to premature coating cracking, delamination, or spalling [52]. Open porosity can interconnect to the coating interface, enabling corroding or oxidizing elements to attack the base material.
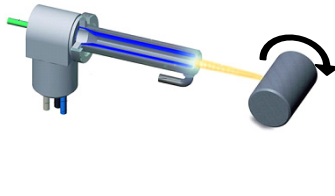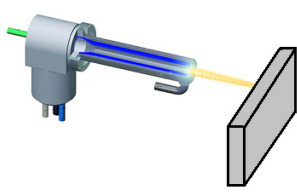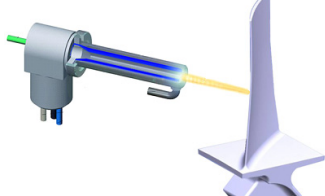
2.2.3 Costs of thermal spraying process

Every coating process is a sequence of operations and quality-assurance steps: surface preparation, coating and surface finish. Every step can be charged with a value in Euro. This value depends on the actual piece, the specific equipment, personnel, overhead, deposition efficiency, time, consumables cost, tooling etc.

In value-added steps the longest times are the coating cycle and the heat treatment. In both cases expensive equipment is involved. Therefore this equipment never should be idle and the manipulation times for the component which needs to be coated and the torch have to be optimized.

In quality assurance the laboratory investigations in the metallography requires also specific costs. On the other hand, metallography is a destructive method that has to be minimized by a thorough process control.

Table 2.5 Cost as a function of shape pattern [16, 53]

Rotative coating - highest yield	Traverse coating of simple surfaces – reduced yield	Traverse coating of complex surfaces – extremely reduced yield
The spray spot is always on the surface of the substrate	The spray spot leaves the surface, slows down, jumps the offfset and accelerates again	The effective time spent on the substrate becomes rather short
Cost/m^2 = 100%	Cost/m^2 = 140 - 200%	Cost/m^2 = 300 - 500%

A further important factor is the yield of process. In thermal spraying for some components such as power plants the yield is expected to be at 100%. Therefore, a statement cannot be made saying, this coating process is less costly than another one. This statement can only be made on comparable basis that is, e. g. identical raw material cost, identical labour cost, and new equipment. It is more reliable for comparison to look at coating process time, deposition efficiency, overspray removal, equipment usage etc. in order to determine the spraying costs. The

difference in cost is manly due to different deposition efficiencies of each scenario. Tabel 2.5 shows the influence of part geometry on costs. [16]

The conclusion is that the spray time is a key factor regarding the costs; it depends on size and shape of the spray pattern. For most manufacturers, total production cost, rather than coating cost alone, is the most important issue, while for most users; lifecycle cost (or cost of ownership) is the critical issue.

2.2.4 Classification of thermal spray techniques as a function of technical demand

Thermal-spray equipments are usually classified according to the energy source needed to heat and accelerate the particles (see section 2.2.1). In the European standards EN 657 as well as in the equivalent international standard ISO 14917 the different systems are described. Given the principal subject of this work, resulted from a technical demand, namely internal coatings, another clasification of spray thechniques was made.

Besides of the energy source, thermal-spray equipment can also be classified following technical and economical demands related to the sprayed coatings [52]. These demands generate the axes around which new techniques are being developed. These axes are related to the techniques characterized by the following:
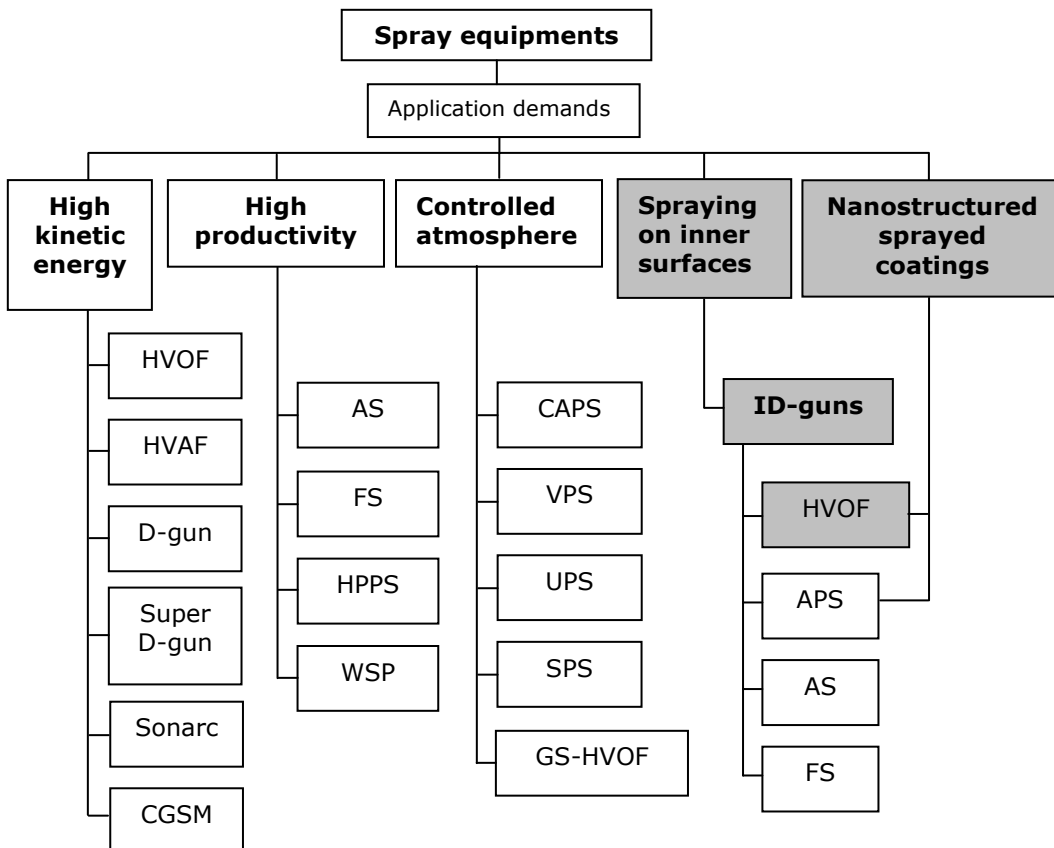
Figure 2.11 Thermal spraying techniques used for different application

2.2.4.1 High kinetic energy

High kinetic energy of sprayed particles, being in contact with high velocity flames but having a relatively low temperature. The "time in flight" is short and the impact of the spraying particles on the substrate occurs without their complete melting. Examples of this family of techniques are high-velocity oxygen fuel (HVOF) spraying, high-velocity air fuel (HVAF) spraying, D-gun, Super D-gun, Sonarc or cold-gas spraying method (CGSM). All these techniques are adapted to spray materials of relatively low melting point, which can modify their chemical composition at spraying, such as, carbides which decarburize or melt incongruently, forming the phases less interesting form the point of view of future applications.

2.2.4.2 Controlled atmosphere

The atmosphere modifies the chemical composition of the jet or its physical properties, such as, level of turbulence or the mean free path of the species. Examples of such techniques are vacuum plasma spraying (VPS), controlled-atmosphere plasma spraying (CAPS), inert plasma spraying (IPS), underwater plasma spraying (UPS), gas-shrouded HVOF spraying (GS-HVOF) [54], and shrouded plasma spraying (SPS). These types of techniques are adapted to spray materials that oxidize easily, for example titanium und tantal or alloys that oxidize when spraying in an air atmosphere, such as, NiAl, or MCrAlY.

2.2.4.3 High productivity

High productivity techniques, with high output of sprayed material, between 6-60Kg/h, involve more voluminous flames or jets. This kind of techniques are, flame spraying (FS) and arc spraying (AS), which are used mainly to spray metals (Mo, Ni, Zn, Cu, Al, Ti, Fe) or alloys (NiCrAl, FeCrB, NiCr, NiAl, FeCrB, NiCrTi, NiCrMo) [55] onto large surfaces, in order to improve productivity, but in the same time the coatings quality is low. For oxides deposition (Cr_2O_2, Al_2O_3), also on large surfaces, are used high-power plasma spraying (HPPS) and water-stabilized plasma spraying (WSP) are used.

2.2.4.4 Nanostructured coatings

Nanostructured coatings enables small crystal grains (nanoscale) to be obtained inside the coatings. These methods use very fine powders, agglomerated or not, which transform during the spraying process into the desired coating material. Modifications to the existing techniques are related mainly to design of spray material feeders and of the spraying guns enabling the extra fine particles to be injected into a jet or flame [38].

The properties related to nano sized particles make nanopowders good candidates for wear resistance because of high hardness and fracture toughness in the same powder, as demonstrated for WC-Co, a staple in the coating industry for wear resistance [42]. In the last few years the nano invasion has penetrated into the spraying world in order to provide not only a good wear resistance of the sprayed coatings but also an optimal corrosion resistance aspect as well. Further work must be done to produce usable quantities of nanopowders at low cost if there is to be any impact in the thermal spray industry where cheap, good materials are a premium.

2.2.4.5 Spraying on inner surfaces

Inner surface spraying can be performed using specially developed spray torches. The construction form of these guns is smaller and has a special angle nozzle in comparison to those used only for external depositions. It has to be taken into account the peculiarities in controlling the temperature of the component to be coated, recirculating dusts, swirling, and the difficulties of frequently limited visual process monitoring. In order to avoid overheating the components, the performance level of the plasma or the HVOF flame has to be adapted to the component. A controlled dust and heat extraction by suction without causing unacceptable swirling in the spraying area is essential to ensure the quality of the finished coating. Plasma and high-velocity flame guns have enjoyed an innovation impulse due to the growing demands of and the developments in the aviations turbine market. Research in this area for compressor components and combustion chambers with complex geometries is conducted in the sectors of plasma as well as HVOF technology [56].

At the beginning of the last decade, high-velocity oxygen-fuel (HVOF) thermal spraying has become the method of choice, mostly to replace hard chrome plating on outside diameters (ODs) for commercial and military aircrafts. It was and is still used for landing gear pistons and axle journals, hydraulic rods, slat and flap tracks, engine shaft journals, and numerous other external surfaces, line-of-sight applications on wear, respectively corrosion components. However, HVOF was a line-of-sight spray technology that could not be used for many non-line-of-sight geometries such as internal diameters (IDs). It could only be applied for ID coatings if the ID can be reached from outside by angling the gun to a maximum of 60° off-normal (see figure 2.12 (a)), but the quality obtained was not as high as desired [2, 57].

a) with a standard external spraying device   b) internal spraying torch
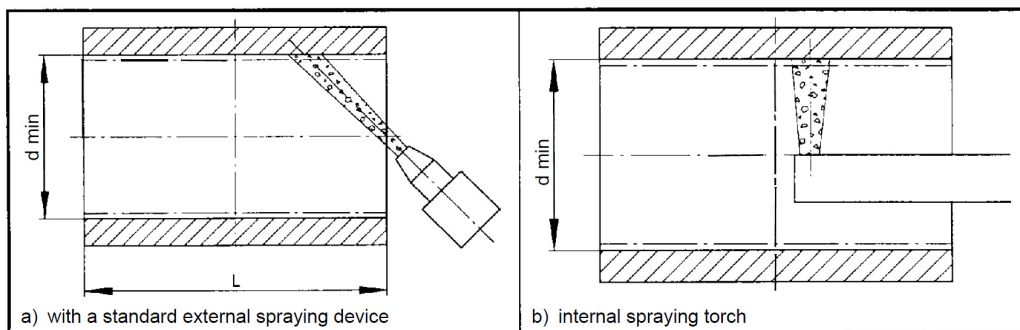
Figure 2.12 Coating of internal surfaces [35]

At that time the HVOF guns were quite large and required a standoff (distance from gun to surface), of about 300 mm, a lot more with regard to the plasma spraying (~ 40 mm). Additionally, due to the high thermal strain on the powders, the internal coating process based on HVOF guns was not extensively used [56].
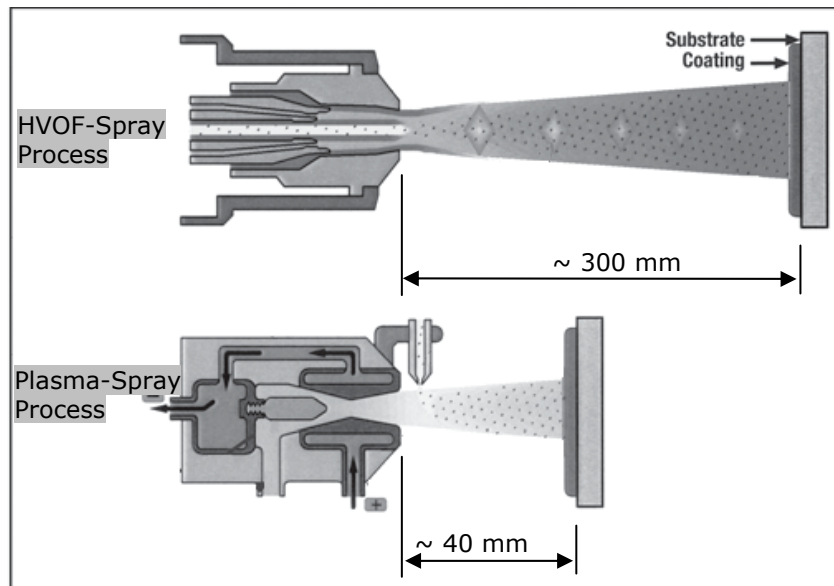
Figure 2.13 Flame standoff comparison between HVOF and Plasma spraying in the year 2000

The fact that standard HVOF guns can only be used for ID components above 350 mm restricts them to large internal diameters, or to shallow IDs whose depth is no greater than about one diameter, and which can be sprayed at a certain angle from outside.

For all these reasons another thermal spray technology, ID plasma spray, was developed for some limited internal diameters applications including also the ID chrome replacement on the cylinder of landing gears used in military aircraft [2].

Small plasma torches with angled plasma beams in the 5-30 kW performance range appeared to be a good way to coat inner surfaces with internal diameters (IDs) above 40 or 80 mm, in the early of last decade, this method was fast (can spray large area in short time) and can produce quite hard, low porosity material. Relatively low powder temperatures make it possible to use them for smaller component diameters. Applications based on CoMoWCrC alloys have established themselves for internal pipe coatings of heat exchanger or TBC combustion chamber coatings based on NiCrAl prepared surfaces and ZrO_2-Y_2O_3 top coats. Examples of such typical torches are: Thermico´s A60 and ID Axial III, Praxair SG 2700 miniature ID-gun, Sulzer Metco SM-F100 connex, SM-F300 and SM-F210 (see tabele 2.6). The latter gun uses several gas cooling jets that also serve to clear overspray from around the deposition region [56, 58].

The basic design of an ID plasma spray gun is shown in figure 2.14. Gas is fed into the gun while a potential between the cathode and anode creates plasma. Powder is injected either within the gun (as shown) or by a tube immediately outside the exit orifice. The powder is heated by the plasma and softens, while at the same time it is accelerated by the gas stream and lands on the substrate to form a coating. The spray direction is determined by the nozzle configuration and may be 0° (straightahead), 20°, 30°, 45°, 60°, 90° (normal to the wall of the ID), depending on the gun design. [2].
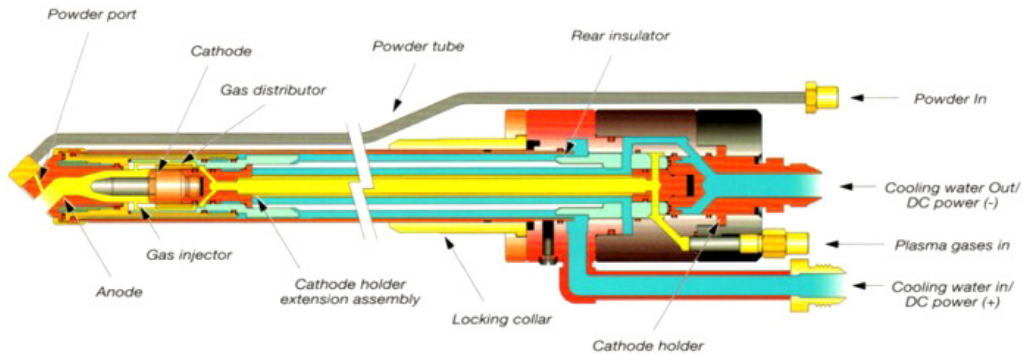
Figure 2.14 Constructive design of an ID plasma spray gun [2]

Moreover, the automated internal thermal arc spraying of aluminium for pipes with diameters of 180mm through 1000mm is another internal spraying technique for inner surfaces, designed, developed and implemented by Scott Ramey and Juan King, the principals of the Thermal Spray Specialists, company formed in October, 2005 [59].

Table 2.6 Summary of principal existing ID-Guns and their capabilities [2, 58, 55, 60-67].

ID-gun	Minimum ID [mm]	Spray rate [kg/h]	Operating power [kW] *	Spray angle [°]	Spray techniques	Standard lengths [mm] **
Praxair SG 2700	38	1.2	30	45; 90	APS	305; 610
SM-F100 connex	100	2.4	20	0;45; 90	ChamPro, APS	140; 280; 560
SM-F300	40	1.2	9	90	APS	250; 450
SM-F3	80		8	30	APS	
Plasma Gun F1-45; 90	70		25	45; 90	APS	500
SM-iPro 90	152		95	90	APS	1010
Plasma Gun F2-A	50		16	90	APS	640
SM-F210	60	1.2	12	0; 20; 30	APS	457; 660
Thermico ID A60	250		80	90	APS	
Thermico ID Axial III	320	3	135	90	APS	

Praxair SG 2086A	64	1.2	30	0; 45; 60	APS	305; 610
SM-6P-II guns[1]	168		35	0; 45; 80	FS	305; 610
SM-PPG SmartArc[2]	70	32[d]	≥24	0; 90	AS	330; 660
SM-DJ® guns[a]	180[b]/230[b] /280[c]/400[c]	9		45; 90	HVOF	690/700 /752/78 6
Termika-3	120	1.8		60	HVOF	1000
Thermico ID CoolFlow mono	80	2.4	50	70	HVOF	290
Thermico ID CoolFlow	150	3	50	70	HVOF	315
HVOF-P2000	250	6			HVOF	600

 * adjustable operating power
** all guns can typically be supplied with custom extensions to reach different depths
[a] HVOF-Diamond Jet® Guns with DJT series extension modules; [b] air-cooled gun configuration; [c] water-cooled gun configuration; [d] using zinc wires
[1] SM-6P-II Combustion Powder Flame Spray Guns with 6PT-II series extension modules
[2] PPG- Electric Wire Arc Spray Guns with PPGT series extension modules

Plasma spraying, flame spraying as well arc spraying could be used for almost all cylinder IDs, but the obtained coating is up to now too porous. Prior to this it was felt that this problem might be well solved by the use of ID-HVOF spray methods, which should also permit coatings to have better properties and to satisfy the required performance level.

After years of development new ID HVOF technologies are commercially available that overcomes the disadvantage of high thermal stress by overheating the components with internal diameters between 80 and 280 mm. HVOF technology usable for application of inner coatings required the reduction of the energy level of the flame stream from 100-200 kW down to 20 kW. In this, the required particle properties, such as high velocity and sufficient temperature, have to be realizable at short spraying distances [56].

In 2004 Thermico (www.thermico.de) announced the development of a new HVOF gun for spraying IDs using super-fine powders, unter the name of ID CoolFlow (see figure 2.16). This gun was described to be capable of spraying IDs down to 150mm diameter, to a depth limited essentially by the fixture on which the gun is placed, equipped with an 8 mm acceleration nozzle and dual radial power feed and with a deposition rate of 3kg/h. The spray rate should be equivalent to that of the plasma spray gun. However, because this is an HVOF gun, the coating quality and performance should be higher, providing a coating life longer than that in case of plasma coatings. The ID CoolFlow was inspired by a development project initiated by Cerma Shield in Boxburg / South Africa, who was also the first company to use the ID CoolFlow. This company had sprayed the cylinder liners of diesel railway engines with Cr_3C_2-NiCr and WC-CoCr layers in order to extend their repair cycle and to save fuel through reduced friction [68].
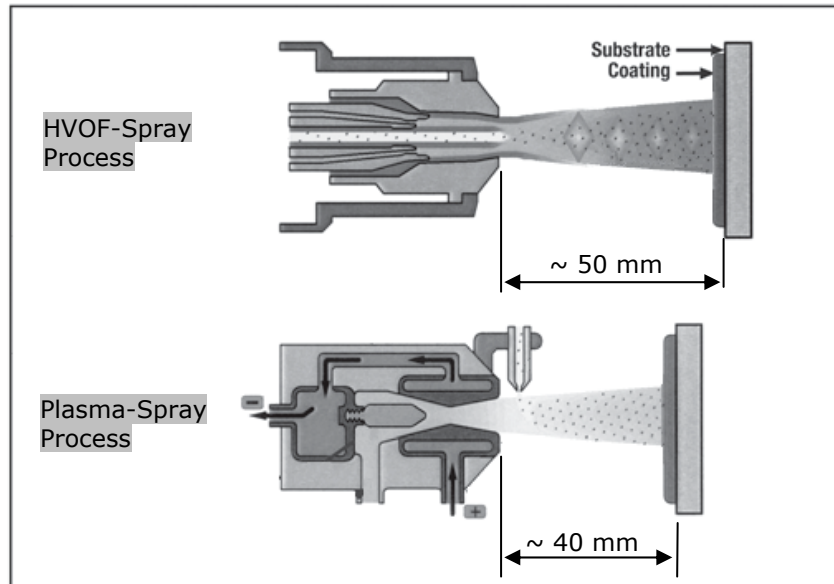
Figure 2.15 Flame standoff comparison between HVOF and Plasma spraying
in the year of 2010

Figure 2.16 HVOF-ID CoolFlow gun [www.thermico.de]

One year later a new HVOF gun was commercially available on the market, under
the name of ID CoolFlow Mono. This equipment is therefore mainly used for HVOF
IDs coatings down to approximately 80 mm, making HVOF internal coating
commercially viable for a variety of such applications. Thermico's ID CoolFlow M
HVOF spraying gun comes equipped with a 5mm acceleration nozzle and radial
powder feed, eliminates also the typical overheating problem [69]. The ID mono
gun was used during this work for the coatings deposition on the inner surfaces of
the cylindrical samples. More technical details about this type of gun will be
discussed in Chapter III.

Another important HVOF gun which has the possibility to spray inner surfaces is the
SM-Diamond Jet® family with the available DJT series extension modules, see figure
2.17, currently produced by Sulzer Metco Company. All DJT extension modules are
factory configured to spray at an angle of 90° and allow an easy access to very deep
inner surfaces. 45 and 60 degree heads are available as a purchasable option. They

are directly mounted onto the gun and use the same air caps, nozzles and siphon plugs used by DJ® guns.

The Diamond Jet® process uses oxygen, fuel gas and air to produce a high pressure annular flame, which provides uniform heating of the axially introduced powder spray material. The gas stream is accelerated through a converging/diverging nozzle to supersonic speeds. The axial powder injection focuses the coating material within the centre of the flame, eliminating coating material buildup on the walls of the extended air cap and minimizing wear.

Spray rates, depending on gun configuration and material applied, can be as high as 9 kg/h, thus reducing spraying time.

The Sulzer Metco Diamond Jet® family of spray guns for HVOF has been developed to produce high integrity coatings of metals, alloys, superalloys and carbides. Diamond Jet® guns can be supplied with a water-cooled front section, which allows the gun to produce higher particle velocities, maximizing coating substrate and interparticle bonding. In general, water-cooled SM-DJ guns also have higher coating densities, higher hardness and lower oxide content [62].
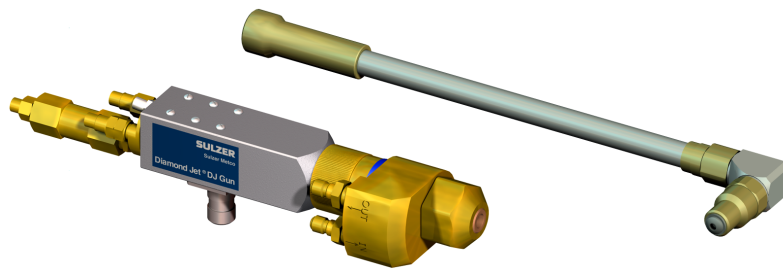
Figure 2.17 Diamond Jet® Gas-Fuel HVOF Spray Gun (left) and the extension modules (right) [www.sulzermetco.com] Reproduced by permission of Sulzer Metco AG, Switzerland

Further developments of HVOF torches are expected to bring spray guns, which would assure higher deposition efficiency, production rate and would allow smaller IDs to be coated. A wider optional window a temperature-velocity plane is also requirement emerging from the trend "higher quality at lower cost" [16].

2.3 High-velocity oxygen fuel spraying (HVOF)

The first industrial HVOF system was developed at the end of the 1970s and at the beginning of the 1980s. Many authors, Bick and Jürgens (1983) and Kreye et al. (1986), among others, agree that the initial work was carried out at the Thayer School of Engineering in Hanover, USA and by Browning Engineering in West Lebanon, also USA [38]. The system was commercialized by Deloro Stellite Corp, getting the name Jet Kote®. Since then a variety of different HVOF systems have been developed and commercialized for thermal spraying industry [16]. Therefore, the process has been used in numerous advanced applications and has become very popular within the thermal-spray industry over the last two decades. Presently, this method has become a standard one in the spraying of cermets for many applications in the aeronautical industry, such as Cr3C2-NiCr coatings sprayed on tip shroud of blades, as well as of MCrAlY coatings sprayed as an overlay or a bond layer for TBCs (more HVOF applications in section 2.3.2).
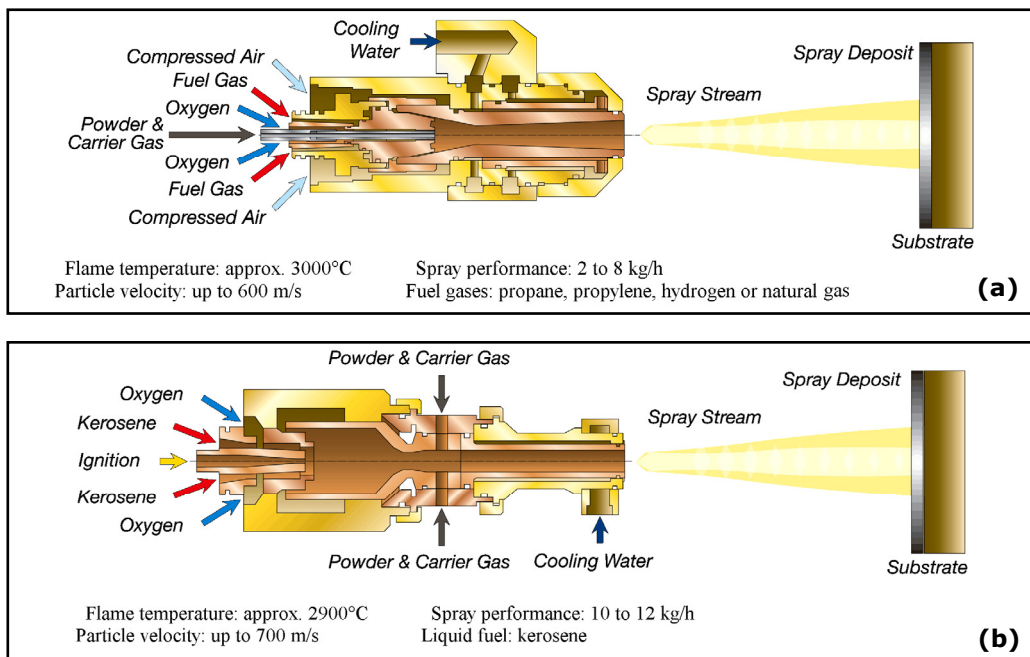
Figure 2.18 Principles of HVOF spraying using gas for fuel (a) or liquid fuel (b)
[http://www.sulzermetco.com] Reproduced by permission of Sulzer Metco AG, Switzerland

In the HVOF process, the fuel gas (Fig. 2.18 (a)) or fuel liquid (Fig. 2.18 (b)) is injected into the combustion chamber together with oxygen. An ignition initiates the combustion and the exhaust gas, formed by a nozzle, passes through a barrel and propels the powder feed stock at near supersonic speeds onto the substrate [59]. The powder can be introduced axially (Fig. 2.18 (a)) or radially (Fig. 2.18 (b)) into the high velocity gas stream. Depending on the flame temperature and also on the material's melting point, the particles can be completely or partially melted. Moreover, the degree of melting depends on the dwell time in which the particles ore in the flame. These are adjustable process parameters and they affect the properties of the coating [36]. The combustion chamber, nozzle and barrel are intensively cooled by water.

In high velocity flame spraying with liquid fuel like kerosene, N-paraffin a higher combustion pressure is applied compared to spraying with gaseous fuel. The combustion gases are expanded completely and already somewhat cooled down. This creates coatings of higher density and higher adhesive strength. Eventually, residual stresses on pressure may be generated in the coating [35]. The performance of HVOF processes generally depends on the type of fuel and the stoichiometry ratio, combustion pressure, as well as specific features of torches design, like powder injector position, nozzle and combustion efficiency [16].

The components of a typical HVOF setup are shown in figure 2.19. It includes the coating material to be applied, a powder feeder which deliver the feed stock material to the spray gun, an HVOF spray gun that will heat the powder material and propel it to the specimen, and a control unit which combines the ease of computer control with the precision of mass flow-controlled gas and kerosene lines in order to obtain the required flows for the HVOF combustion. In addition, as

peripheral equipment most HVOF spray installations require a cooling water system for the spray gun and also it is necessary to have cooling air to control the temperature of the specimen. Moreover, a noiseless cabin and an air filtration and exhaust system are necessary to protect the personnel and the environment.
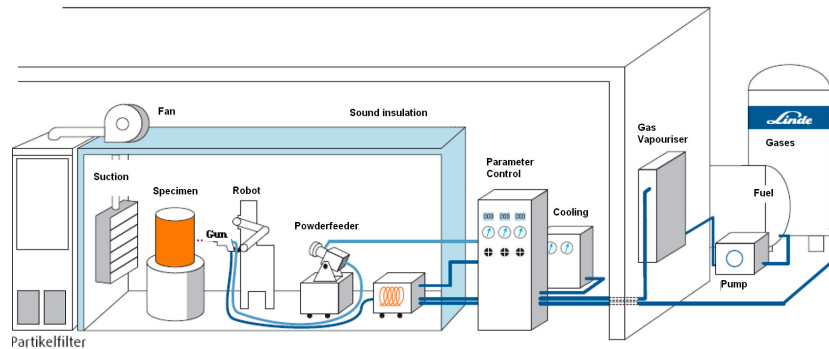
Figure 2.19 HVOF equipment and periphery [http://www.linde.com]

2.3.1 Characteristics of advanced HVOF technology

HVOF has proved to be one of the most suitable methods to deposit wear and corrosion resistant coatings. The high velocity and "low" temperature of the particles lead to a dense mixture of unmelted and semi-melted carbide particles in a fully melted metallic binder [70]. In case of hard metal spraying, HVOF shows less decarburization and building of sub- stoichiometric phases compared to the hotter APS or LPPS [16].

The advantage of HVOF is that it is a single technology, with a wide variety of materials that can be used to achieve just the right combination of properties for any purpose. The HVOF coatings, particularly the tungsten carbides, showed to be equal in performance to hard chrome in all of their measured properties, and significantly better than hard chrome in fatigue, wear and corrosion resistance [71].
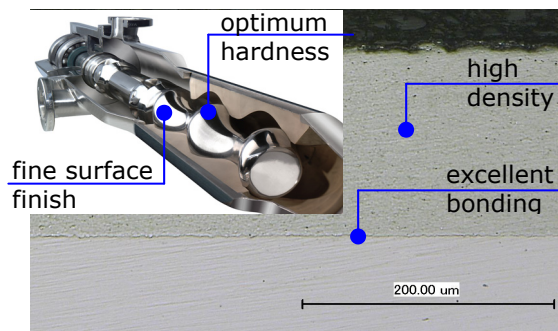
Figure 2.20 Main characteristics of HVOF spraying

Some of the advantages given by this method are listed below [62, 72, 73]:
- high density coatings;
- excellent bonding to the substrate;
- reduced oxidation risk, due to the very high velocities;

- minimal temperature effects;
- possibility to deposit different mixtures of materials;
- minimal metallurgical changes;
- optimum hardness;
- excellent wear and corrosion resistance;
- fine surface finishes.

2.3.2 HVOF cermet coatings applications

The HVOF coatings are often used for applications in which components operate under conditions that subject them to degradation mostly by various types of wear and corrosion processes. In such environments, the wear and corrosion resistant nature of certain ceramics and cermets enables improved performance, as compared to many metallic materials. Since it is often a combination of high hardness and toughness that provides good wear resistance, metal-ceramic systems such as cermets have been developed in order to benefit from both the hardness of the ceramic, providing a high wear resistance and also the toughness of the metal, responsible also for the corrosion resistance of those coatings [26, 74-75]. Therefore, the use of HVOF is broad among several industries, and is increasing in time. Examples of main application areas include aeronautical industry, where coatings are applied on different aero-engines components and also as a hard chromium replacement on landings gears, pumps, metalworking industry, such as cutting tool applications, oil and petrochemical industry, pulp and paper industry with coatings to rolls and blades, and automotive industry, which applications include piston rings and cylinder bores. In the following, some of these HVOF coating applications and materials are briefly presented accompanied by figures.

Aeronautical industry. HVOF thermally sprayed WC-Co coatings are currently being used for their impressive abrasive wear resistance and good behaviour at high temperatures in combustive environments on aero-engines components, like: bearing housings, compressor drive turbine shafts and compressor rear hubs [76].
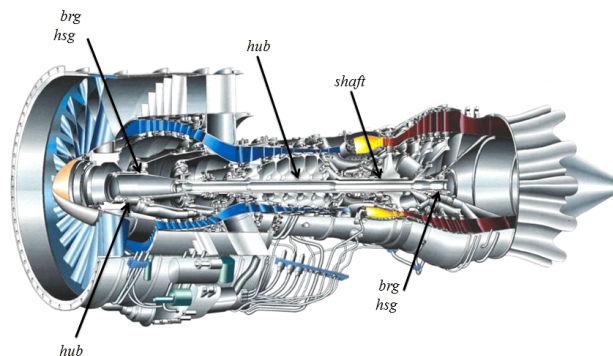
Figure 2.21 Schematic of a gas turbine engine using HVOF-sprayed components
[http://web.engr.oregonstate.edu/~sva/gt.html]

Hard chromium replacement. Hard chromium plating is used on aircraft and helicopters landing-gear components such as: inner cylinders, piston pivot bushings, pins, drag braces, struts and brake torque tubes is being replaced by HVOF spayed

WC-Co and WC-CoCr coatings for their superior performance and environmental friendliness.
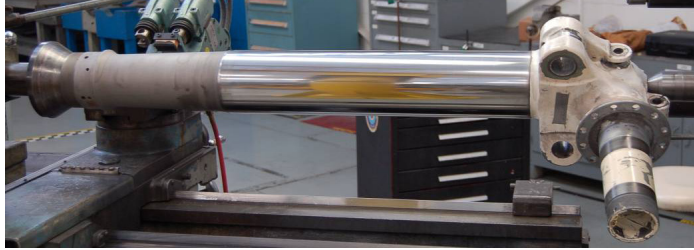
Figure 2.22 HVOF-sprayed landing gear component [http://www.asetsdefense.org]

Hydraulic pumps for seawater desalination (Fig. 2.23 (a)). Seawater desalination based on the reverse osmosis process requires a variety of hydraulic systems. The material concepts of these hydraulic systems are designed to reliably resist the corrosive properties of seawater and brine as well as the tribological loads. In pressure exchangers for energy recovery, high tribological loads occur on the rotors surfaces which usually operate with a clearance gap of 40-100 μm. Nowadays, thermally sprayed coatings are often used for the surface protection of these rotors. Coatings with high surface hardness have proven to be particularly successful. A coating system, based on WC, with a CoCr matrix, has been developed especially for these kind of applications [77]. Besides the above mentioned type of pump, more other housings and rotors geometries of pumps can be coated using HVOF technique, see figure 2.23, in order to improve the tribological and corrosion resistance of the exposed surface.

(a)

(b)

(c)

(d)
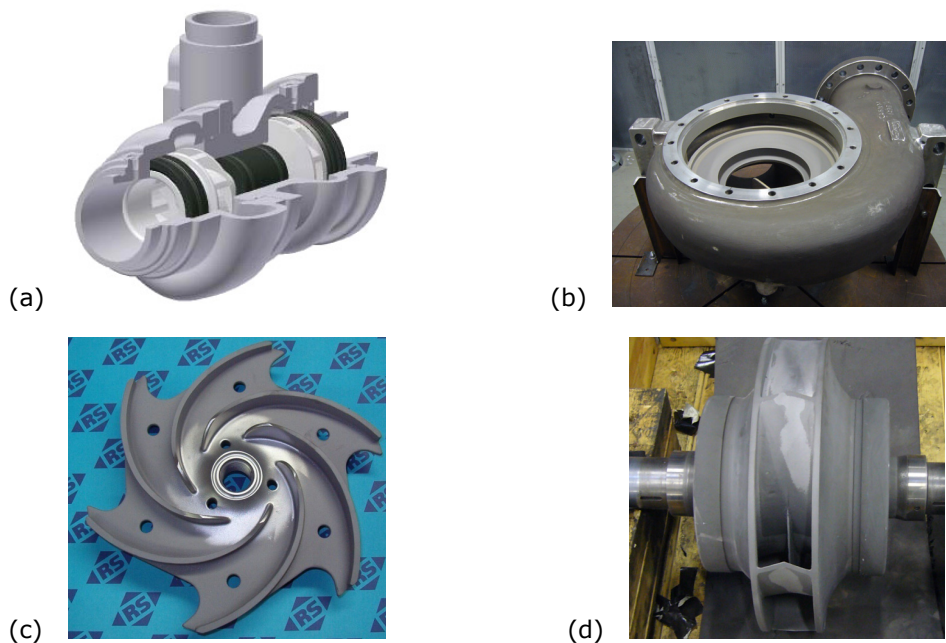
Figure 2.23 Different housings and rotors pumps for HVOF applications
(reverse osmosis pump (a); HVOF as-sprayed housing (b); HVOF as-sprayed rotors (c), (d))

Active surfaces for tools. HVOF thermally sprayed WC-CoCr coatings can be applied on the surface of active components that require high hardness, excellent wear and corrosion resistance. These types of coatings can be used for example in the metalworking industry with the purpose of improving the work capabilities and extend the lifetime of tools like: punches, dies, shear blades etc.
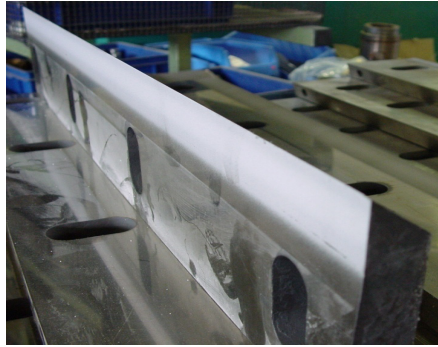
Figure 2.24 Guillotine shear blade

Oil and petrochemical industry. HVOF coatings are employed in the oil and petrochemical industry due to their ability to operate in the most extreme conditions of high pressure and temperature as well as in erosive, corrosive and abrasive environments. HVOF thermally sprayed WC-based coatings are usually applied on balls, seats and seals for sub-sea ball valves offering an excellent resistance to high pressure and abrasion and satisfactory gas seal. Similar, WC-based layers can be used in order to protect the outside surface of different rock bits legs against corrosion of aggressive fluids and also to extend the wear lifetime of the component during the drilling process.

(a)   (b)

Figure 2.25 Ball valve (a) [http://www.viarvalvole.com], rock bit (b)
[http://www.straightlinehdd.com]
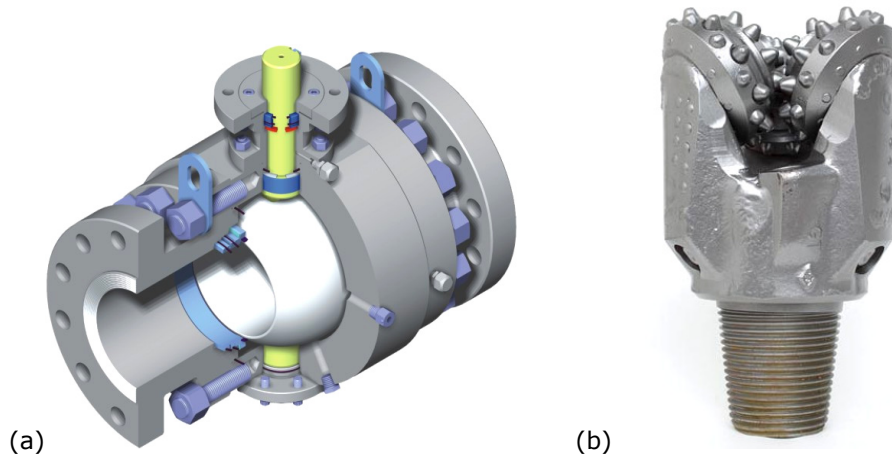
Interlayer to improve adhesion of CVD DLC (Diamond-like-carbon) coatings. HVOF sprayed WC-CoCr coatings are used as interlayer to increase adhesion of CVD DLC thin films to aluminum substrate. The WC-CoCr coatings also provide better mechanical support for the DLC-based film, better corrosion resistance (dictated by interlayer properties) and improve the sliding wear behaviour [78].
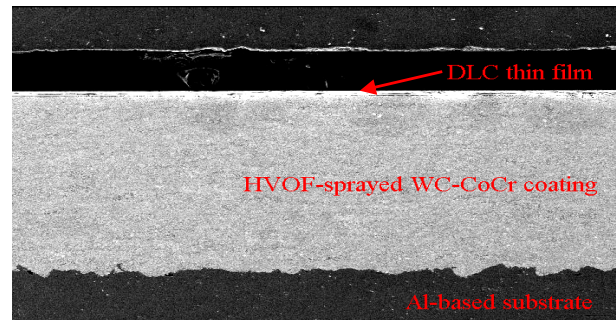
Figure 2.26 Micrograph of Al-based substrate with HVOF-sprayed WC-CoCr interlayer and DLC film [78]

Other versatile applications for HVOF coating include magnetic and biomedical use. HVOF sprayed ferromagnetic Fe-Si based deposits, which have been produced from nanostructured powder, can be used in several magnetic applications even at high temperatures. HVOF hydroxyapatite (HAp) coatings are applied in various biomedical applications due to excellent biocompatibility of HAp. The nanostructured HAp has been studied for biomedical use and the results are promising, as the coating exhibits high density and crystallinity, and good microstructural uniformity. In the biomedical field, HVOF-sprayed nanostructured titania coatings could be used for prosthetic devices and other applications, where superior mechanical behavior is required [79]. Besides of all these applications, the HVOF cermet coatings can be used for many other machinery components where corrosion and wear resistance are required.

2.4 Tribological behaviour of thermally sprayed coatings

2.4.1 Introduction

Tribology is defined as the science and technology of interacting surfaces in relative motion. It is a study of friction, lubrification and wear of engineering surfaces with a view to understanding surface interactions in detail and then prescribing improvements in given applications [80].
Today, mechanical components and tools are facing higher performance requirements [48]. Fortunately with the ability of thermal spray, to work with an almost limitless number of materials, well engineered wear resistant coatings can usually be produced to solve even some of the most complex wear issues [81]. The use of surface coatings opens up the possibility for a material design in which the specific properties are located where they are most needed. The substrate material can be produced for strenght and toughness while the coating is responsible for the wear resistance, thermal loads and/or corrosion attack. Coatings are now widely used to control friction and wear of different types of surfaces in contact. In the

most successful solutions the coefficient of friction has been reduced by two orders of magnitude and also the wear has been reduced by several orders of magnitude, depending on the material pair [48].

The diagnosis of friction and wear data of a tribosystem or corresponding laboratory test configurations and test specimens requires special attention because numerous characteristics, parameters, and factors must be taken into consideration. This is due to the fact that friction and wear are not intrinsic materials properties, but must be related to the entire system of interacting components, namely materials pairs and interfacial lubricants. This is obvious from a comparison between the test conditions to obtain friction and wear data.
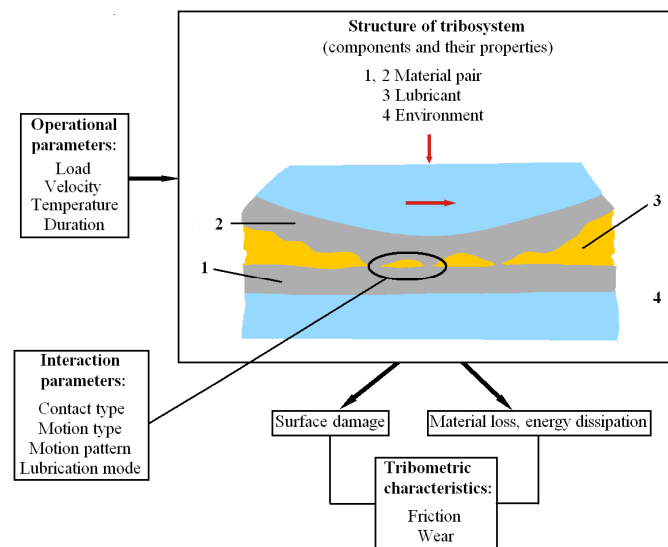
Figure 2.27 Characteristics and parameters of friction and wear

In a friction or wear test, the resistance against motion (friction) or the resistance against surface damage (wear) of a material/material pair (dry system) or a material/lubricant/material combination (lubricated system) in a given environment is determined under the action of a certain type of motion, such as sliding or rolling. The resulting tribometric characteristics, in particular the friction or wear data (Fig. 2.27), must understood as tribological systems characteristics associated with the following group of parameters:

- **Structural parameters**, which characterize the components: material pairing, hardness, roughness, lubricant, and environment
- **Operational parameters,** for example, load (F_N), velocity (v), temperature conditions (T) and test duration (t)
- **Interaction parameters**, which characterize, in particular, the action of the operating parameters on the structural components of the tribological system and define its motion type (sliding or rolling), motion pattern (continuous or oscillatory), contact type (point or line contact) and the lubrication mode [82, 83].

2.4.2 Friction

Leonardo da Vinci is generally credited with being the first to develop the basic concepts of friction, and his famous sketches inspired the French scientist Amontons to conduct experiments and later formulate his laws of friction. The classic laws of friction as they evolved from these early studies may be summarized as follows [80]:

- the friction force is proportional to load,
- the coefficient of friction is independent of apparent contact area,
- the static coefficient is greater than the kinetic coefficient and
- the coefficient of friction is independent of sliding speed.

It must be emphasized that these "laws" are very general in nature and that, while they are applicable in many instances, there are also numerous conditions under which they break down [84].

Friction is the tangential resistance to movement of one body over another found in relative motion. The bodies in question may be two solids (solid friction), a gas and a solid (aerodynamic friction) or a liquid and a solid (liquid friction). The experimental results of Amontons and Coulomb showed that the friction force F is proportional to the normal load F_N. The ratio of the friction force F to the normal load F_N has been termed the "coefficient of friction", generally noted with µ or f [82].

$$\mu = \frac{F}{F_N}$$

(Eq. 2.1)

In moving machinery, friction is responsible for dissipation and loss of energy. The energy lost to friction is an energy input that must continually be provided in order to maintain the sliding motion. This energy is dissipated in the system, primarily as heat which may have to be removed by cooling to avoid damage and may limit the conditions under which the machinery can be operated. Some of the energy is dissipated in various deformation processes, which result in wear of the sliding surfaces and their eventual degradation to the point where replacement of whole components becomes necessary [73].

2.4.2.1 Friction mechanisms of coated surface

In general, the mechanism of friction in sliding contacts has been explained by the adhesional effect between surface asperities, two main factors contribute to the friction generated between unlubricated surfaces in relative motion. The first, and usually the most important, factor is the adhesion which occurs at the regions of real contact, and the second may be described as a deformation term. This concept explains that when two metal surfaces are brought into contact under load, local welding occurs at the tips of the major asperities of the surfaces due to the materials adhesion (Fig. 2.28 (a)). When one of the bodies is moved in a tangential direction the micro welded joints will break but their shear strenght causes the resistance to motion [48, 80]. During sliding, new microweld joints are formed and broken continuously. In the case when a hard asperity or a hard particle penetrates into a softer material and ploughs a groove by plastic flow in the softer material this action creates a resistance to motion, known as ploughing effect as shown in figure 2.28 (b).
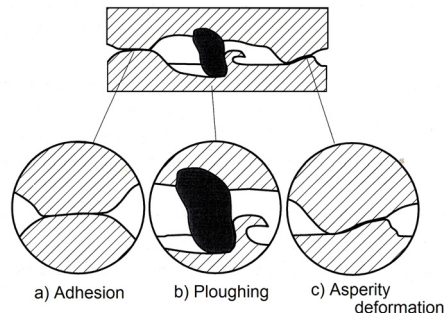
Figure 2.28 The three components of sliding friction [48]

Some authors have concentrated more on the effects of plastic deformation loses due to friction. They showed that resistance to motion arises from the work done when asperities are plastically deformed as they slide over each other [85], as is shown in figure 2.28 (c). In the normal case of dry sliding between rough surfaces, the coefficient of adhesional friction is generally at least twice as large as the deformation contribution. The friction mechanism responsible for the adhesion and deformation terms is widely different for metals; it depends on the materials type.

In case when one or two coated surfaces are in contact to each other, four main parameters which control the friction resistance can be defined such as: coating hardness, thickness of the coating, surface roughness and the size and hardness of wear debris in contact. The hardness of the coating is one of the most important parameters influencing a lot the tribological behaviour of a coated surface. A reduction in friction can be achieved by adding a thin soft coating on top of a hard surface, which can reduce the contact area and the interfacial shear strength.
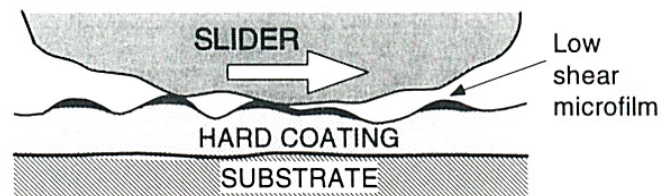
Figure 2.29 A low-shear microfilm on top of a hard coating [48]

Low friction can also be achieved with hard coatings if a low shear strength mircofilm is formed on top of the coating or on the asperity tips of the coating, see figure 2.29. Thus the shear will take place within the microfilm and the load is well supported by the hard coating, which in this case is playing the role of a hard substrate and the formed soft microfilm is playing the role of a coating. It is obviously advantageous for the substrate under the hard coating to have the ideal thickness and to be as hard as possible in order to avoid fracture of the brittle coating by deformation, to improve the load support and to reduce the real area of contact [40]. When the hard coating is thick enough (Fig. 2.30 (a)) it can carry part of the load, and the deformation of the substrate will be smaller. In the other case, if the coating is very thin it can not be able to sustain the load, see figure 2.30 (b). The function of the coating is to separate from the counterface and to prevent

ploughing by hardening the top layer of the surface [48, 86]. The prevention of shearing and ploughing reduces both the friction and the wear.
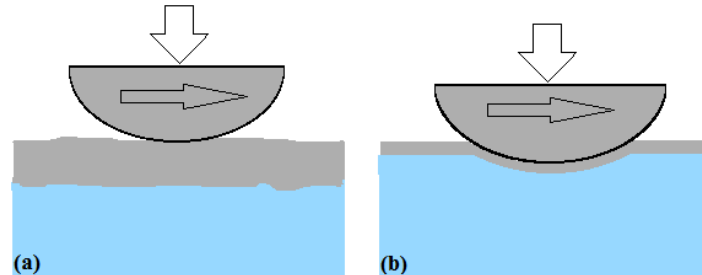
Figure 2.30 The thickness of the coating as load support: (a) thick coating, (b) substrate deformation in case of thin coatings

In sliding wear contacts, loose particles or debris are often present. They can either originate from the surrounding environment or be generated by different wear mechanisms in the sliding contact. Their influence on friction may be considerable in same contact conditions, depending on the particle size, coating thickness and surface roughness. For thin soft coatings, the influence of surface roughness is considerable. The penetration of the counterface asperities through the thin layer will cause increased shear resistance and ploughing of the substrate with an increase in friction as a result. Moreover, by reducing the roughness of the surfaces may increase both friction and wear if at the interface debris are present and they cannot hide in the valleys, so that the particles will interact with the sliding surfaces by scratching and interlocking. In case of rough surfaces the particles can be hidden in the valleys formed by the asperities while the sliding takes place at the asperitys tops, within the particles will have no great effect on either friction or wear.

2.4.2.2 Stages of friction coefficient

The typical friction-time curve during dry sliding consists of a simplified presentation of four stages of friction coefficient. A typical example for a metal/metal system is shown in in the following figure:
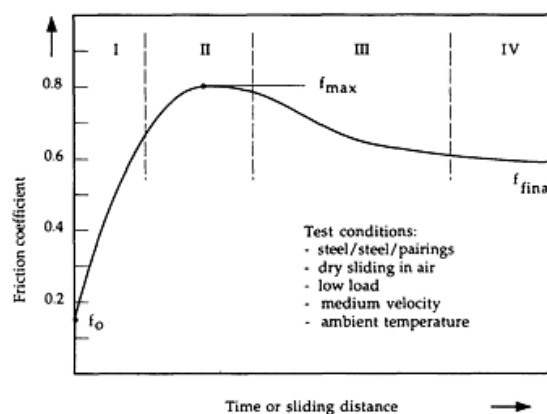
Figure 2.31 A friction-time master curve [82]

The initial value of the friction coefficient value of stage I, which is usually about f_0 = 0.1, is dependent on low loads, F_N, and on the shear resistance of surface contaminants, but is largely independent of material combinations, surface and environmental conditions. Surface layer removal and an increase in adhesion due to the increase in clean interfacial areas as well as increased asperity interactions and possible wear particle entrapment lead to a gradual increase in the friction coefficient.

Stage II, which produces the maximum value of the friction coefficient ($f$max 0.3 to 1.0 for most metal pairs), is reached when maximum interfacial adhesion and asperity deformation occur, and also when the wear particles are entrapped between the sliding surfaces as a consequence of higher wear rate.

In stage III, a decrease in the friction coefficient may occur due to the possible formation of protective tribochemical surface layers and a decrease in plowing and asperity deformation processes. In some cases, such as when a very hard stationary slider is slid against a soft specimen, the asperities of the hard surface are gradually removed, creating a mirror-like smooth surface. The frictional force decreases, due to the decrease of asperity deformation and ploughing.

Stage IV is characterized by steady-state interfacial tribological conditions leading eventually to almost constant friction coefficient values.

It should be noted that figure 2.31 shows a simplified smoothed friction graph, which in practice may be overlapped by shortterm fluctuations, friction peaks, or stick-slip effects. The above stages of initial friction can be different in other cases, for example in contacts where transfer layers are formed, and interfacial friction is then caused primarily by the combined effect of adhesion, ploughing and asperity deformation [48, 82, 84, 87].

2.4.3 Wear

Wear has been defined as the removal of material from solid surfaces as a result of one surface moving over another. Thus both friction and wear are simultaneously the results of the same tribological contact process that takes place between two moving surfaces [48, 73].

Depending on the amount of material which is lost from the element, the wear may be broadly classified as "mild wear" or "severe wear". Obviously this classification can be related to the composition of the surface or to the increasing or the decreasing of the normal load (F_N). In mild wear, the wear processes occur at the "outer" surface layers. The surfaces remain relatively smooth and are usually protected by surface oxide layers generated in rubbing. The worn debris consists of small particles down to some nanometers. In severe wear, the contact is metallic, the surfaces are deeply torn, and the worn debris consists of metallic particles up to some micrometers [82].

Figure 2.32 shows the abrupt transition from mild to severe wear for a brass pin rubbing on a hard steel disc. Below 1 kg load, the sliding surfaces become polished (with a micro finish of about 0.8 µ) and the wear debris appears as fine, dark powder. In the severe wear region, there is considerable subsurface damage; the wear debris consists of metallic flakes and the surface roughness is about 25 µ. Characteristics very similar to those observed in this figure are known to occur in the presence of lubricant films on the rubbing surfaces [80]. Clearly, the classification of wear into "mild" and "severe" is primarily a distinction in the scale of size [82].
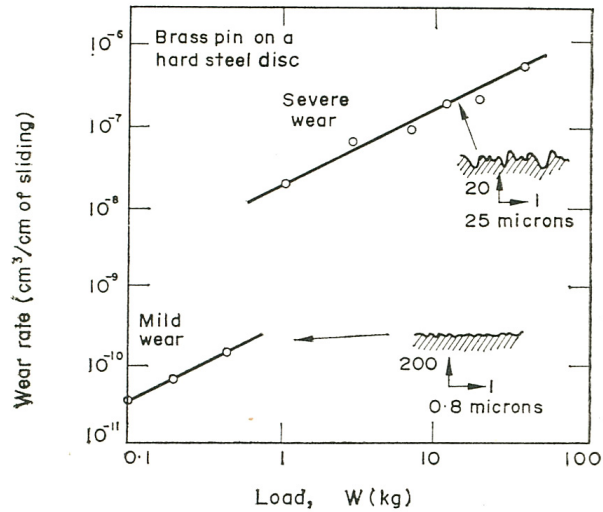
Figure 2.32 Transition from mild to severe wear by load increase [80]

2.4.3.1 Wear mechanisms of coated surfaces

In order to reduce wear, it is important to understand the mechanism by which it occurs in each case. There are a number of different wear mechanisms and each one requires a different practical approach to wear reduction [88]. Based on DIN 50320 the wear mechanisms are divided into four basic groups, see figure 2.33.
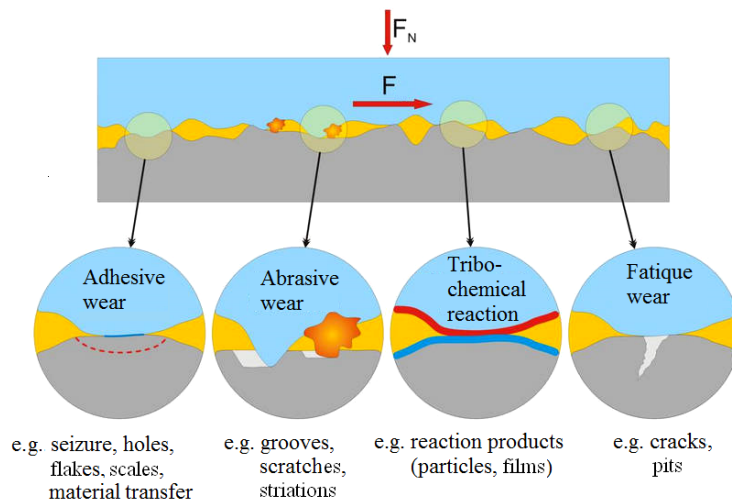
Figure 2.33 Wear mechanisms according to DIN 50320 and the wear appearance effects [89]

Metallic wear is a complex event that includes also complicating factors as work hardening, oxidation of exposed metal, material transfer, and phase changes in metallurgical composition.

Adhesive wear is the surface damage which can occur when two smooth surfaces rub against each other. Such surfaces are never perfectly smooth and have high spots where the rubbing occurs. These local areas experience concentrated contact loads and interactions tending to adhere strongly to each other and form asperity junctions or drag material away along the surface as shown in figure 2.34 [48, 88].

Most junctions shear at the interface (greatest weakness), but occasionally shearing will occur in one of the two materials. This will result in a wear material fragment being transferred from one surface to the other. Additionally, this type of wear mechanism can be considered as a cold welding of metal surfaces due to intimate metal to metal contact. A strong bond is formed but without much interdiffusion of atoms and recrystallization as would occur in a hot weld [90]. In adhesive wear the surface material properties, as well possible protecting surface films or contaminants, play important roles. For example a thin soft film applied in the sliding contact between two hard surfaces may remarkably improve the wear resistance of the interacting components [48].

This type of wear can occur in plain bearings, piston rings and cylinder, gears, cutting tools, chains, metals seals, valve trains and other interacting machine components, particularly if they are inadequately lubricated. The wear of brakes and clutches occurs by the same mechanism, and is kept under control by the use of dissimilar materials. Surfaces subject to adhesive wear can end up polished, with the generation of fine flakes of wear debris, or can show severe surface damage associated with surface dragging or even seizure [88].
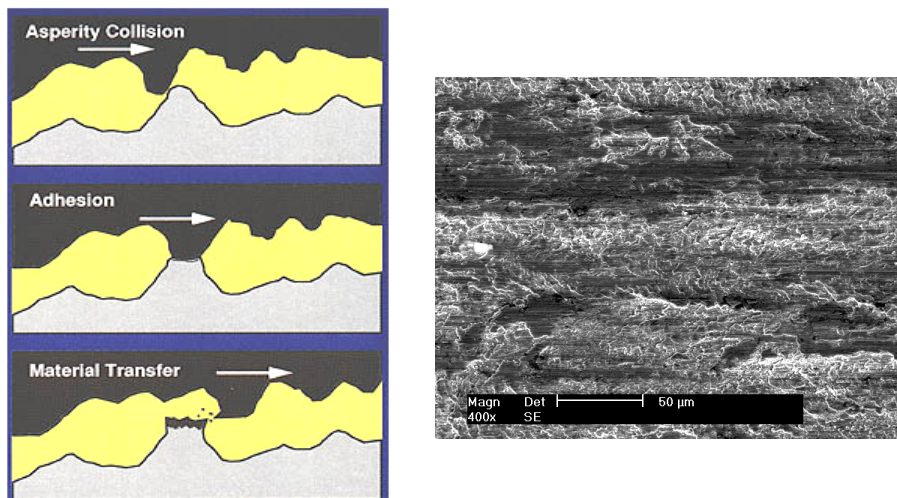
Figure 2.34 Adhesive wear mechanism [90] (theory-left, appearance of the worn surface-right)

Abrasive wear is typified by a hard rough slider sliding on a hard rough coating, with hard particles of sizes larger than the magnitude of the surface roughness present in the contact. The trapped particles have a scratching effect (Fig. 2.35-right) on both surfaces, and as they carry part of the load they will cause concentrated pressure peaks on both surfaces as they try to penetrate them. Abraded surfaces show damage which can range from fine scratching to deep gouges [88]. Two modes of abrasive wear are known as *two-body* and *three-body* abrasive wear, see figure 2.35-left. Two body wear occurs when the hard particles, are rigidly mounted or adhere to a surface and remove the material from surface.

Three-body wear occurs when the particles are not constrained, and are free to roll and slide down a surface [73, 91]. A rolling movement of the particles, which somteimes may even decrease the friction, is often present. Because of work hardening, phase transitions or third body formation, the microhardness of a steel wear surface can be about three times larger than the initial bulk hardness. Resistance to abrasion is defined as the ability to withstand non-elastic deformation as a result of groove formation [48, 80].

All the machine parts in relative motion are susceptible of abrasion damage. The most common industrial wear problem is the "wire wool" damage that appears on journal and thrust bearings. This occurs when a small particle of hard dirt or swarf gets embedded in the bearing material, but continues to rub against the steel counterface [92]. At high speed the temperature generated by the frictional rub carburises the chromium in the steel in the presence of hydrocarbon oil, producing hard chromium carbides that embed in the soft bearing material and act as cutting tools on the journal or thrust collar.
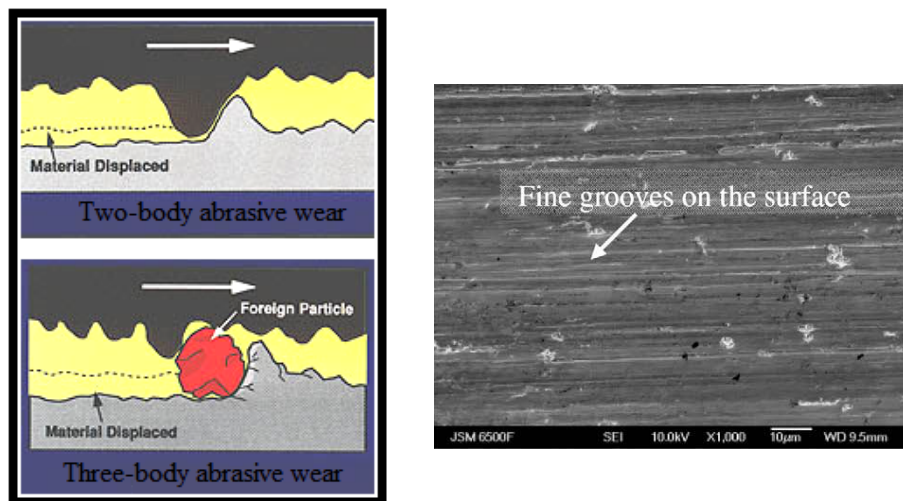
Figure 2.35 Abrasive wear mechanism (theory-left [90], appearance of the worn surface-right [1])

Fatigue wear. This type of wear is a phenomenon which results from loading and unloading of a surface, at a stress level that the material can not sustain if repeated many times. Moreover, another kind of fatigue wear is known under the name of delamination wear. This occurs on a more microscopic scale in sliding contacts when high spots of the surface repeatedly slide over each other and small cracks are propagated below the surface. There are two modes in which the cracks tend to propagate: parallel to the surface, when the load has a tangential cycling or perpendicular in case of normal cycling load, see figure 2.36.

Classic surface fatigue effects are observed to occur in journal bearings where the interacting surfaces are fully separated by a thick lubricant film [82]. It appears also in gears contacts, valve train parts etc. In rolling, where the stress field moves repeatedly over the surface, fatigue of the near surface material takes place. Material voids or dislocation pile-ups may form the nuclei for the first crack to occur [48].
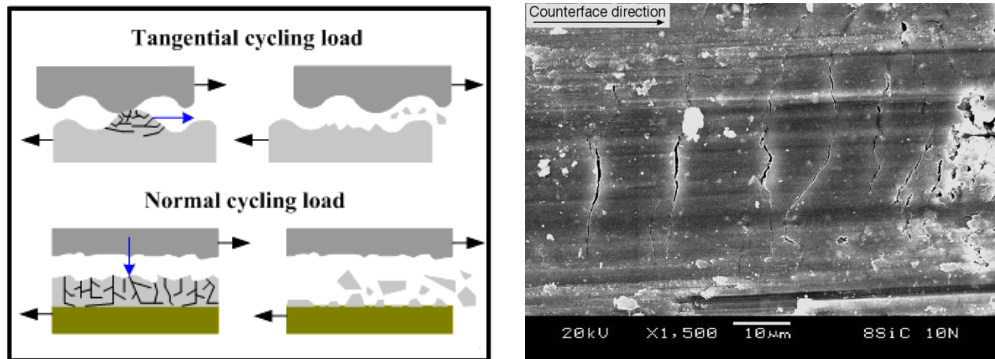
Figure 2.36 Fatigue wear mechanism (theory-left [93], appearance of the worn surface-right [94])

Chemical wear is defined as the degradation of materials in which both corrosion and wear are involved. The mechanism of surface fatigue wear, abrasive wear, and adhesive wear can be understood in terms of deformation and adhesion interactions between two contacting surfaces. In the case of tribo-chemical wear, the environment appears as a third component, see figure 2.37., in section 2.4. If the moving surfaces react with the environment, the rubbing of the surfaces together in such an environment results in the continuous formation and removal of reaction products [82]. This wear action most commonly takes place in two stages; first there is a chemical attack on the surface and then the sliding action wears off the corroded surface film (Fig. 2.37). Rubbing, in combination with the chemical reactions results in the removal of material and wear debris formation. The rubbing action results in increased temperatures at the surface and creates surface cracks which are favourable for more chemical reactions to take place [73, 95, 96]. The situation is further complicated for coatings, particularly porous coatings or those with substantial crack systems. Corrosion products can be transported from the surface contact through interconnecting porosity or crack networks to the substrate and in some cases can have a dramatically effect by chipping of the coating.
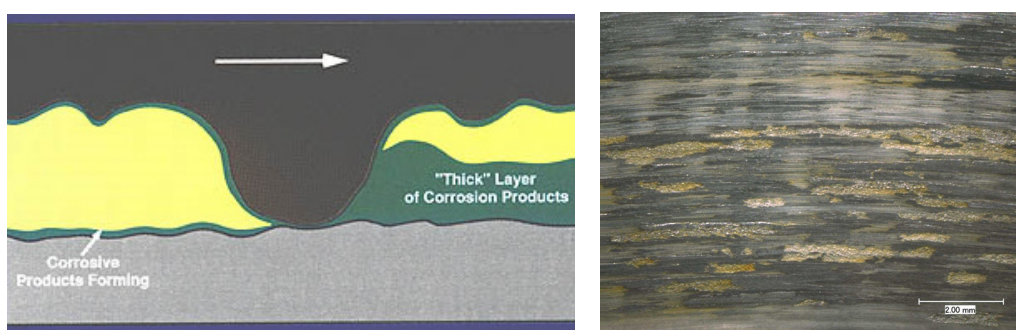
Figure 2.37 Tribochemical wear mechanism (theory-left [90], appearance of the worn surface-right)

A typical situation in which the chemical wear occurs are diesel engines from vessels that use inexpensive, high-sulfur fuel. Their combustion products contain sulphur

oxides and water vapour. These combine to form sulphuric acid, which is highly corrosive to the cast iron cylinders and piston rings. Other machine parts susceptible on chemical wear are: bearings, seals, chains, valve train, cylinder walls etc.

2.4.3.2 Wear measurement

Because of the diversity of the wear process, which depends on materials, contact conditions and environmental parameters, it has not been possible to formulate a universal equation of wear. A lot of authors have developed wear equations for different types of wear but all of them are quite limited in their range of validity. However, wear debris can be measured either as a weight loss or as a change in volume or dimension of one or both sliding components. The following five criteria have been proposed and used in order to calculate the wear resistance of the sliding members:

- Linear wear rate: $K_L = \dfrac{\text{thickness of layer removed}}{\text{sliding distance}} = \dfrac{h}{L}$ (Eq. 2.2)

- Volumetric wear rate: $K_V = \dfrac{\text{volume of layer removed}}{\text{sliding distance} \times \text{apparent area}} = \dfrac{\Delta v}{L A_a}$ (Eq. 2.3)

- Gravimetric wear rate: $K_W = \dfrac{\text{weight of layer removed}}{\text{sliding distance} \times \text{apparent area}} = \dfrac{\Delta W}{L A_a}$ (Eq. 2.4)

- Energetic wear rate: $K_E = \dfrac{\text{volume of layer removed}}{\text{work of friction}} = \dfrac{\Delta v}{F L}$ (Eq. 2.5)

- Coefficient of abrasion resistance: $\beta = \dfrac{\text{work of friction}}{\text{volume abraded}} = \dfrac{1}{K_E} = \dfrac{\mu}{A'}$ (Eq. 2.6)

where L is the sliding distance, F the friction force, μ the coefficient of friction and A' the abrasion factor. It can be observed that the energetic wear rate is equal to the reciprocal of the coefficient of abrasion resistance [80].

In a large proportion of reports that contain wear measurements, one finds the wear amount reported in volume units e.g. [mm^3] or in weight units [g], the latter is a straightforward method because most of laboratories have access to equipment that weighs objects. Depending on the amount of wear, this can influence the selection of measurement method. If large amounts of wear are experienced, then relatively simple, inexpensive measurement approaches, such as the all ready mentioned methods (volumetric and gravimetric) will be usually conducted successfully. Alternatively, if very small wear amounts are experienced, then more sensitive and costly techniques are necessary to detect minute changes of mass or volume.
Wear damage that leads to substantial loss of material is perhaps the most straightforward situation to describe quantitatively [97]. An important formal based on volume of material removed was developed by Holm and Archard in 1946 respectively 1953. The so called Holm wear relationship is often used for formulating the volumetric wear rate which is a practical and more general value for the amount of wear [48, 98]. This equation is illustrated as:

$$K = \frac{V}{w \cdot s}$$ [mm³/Nm]   (Eq. 2.7)

where: V - worn volume [mm³]
       w – normal load [N]
       s – sliding distance [m]

In order to determine the gravimetric wear rate of a tested specimen, it is necessary to weight the specimen before and after the wear test ($\Delta m = m_{before} - m_{after}$) using a precision balance. This value can be also negative in case of material transfer; the specimen weight is after the wear test higher than before. Thus, the wear rate will be "negative".

Knowing that the volume and mass are related to density, after the determination of the changes mass or weight and basing on the know density of the material, it is not more necessary to measure the width and depth, and the contact length of the worn track. In this case the wear rate will be calculated based on the following equation developed by "Lim and Ashby" in 1987 [99]:

$$W_V = k \cdot F_N \cdot s$$ (Eq. 2.8)

where: W_V – worn volume
       k – wear coefficient (wear rate)
       F_N – normal load
       s – sliding distance

It is known that: $W_V = \Delta V = \frac{\Delta m}{\rho}$, inserting $\frac{\Delta m}{\rho}$ in Equation 2.8 results:

$$\frac{\Delta m}{\rho} = k \cdot F_N \cdot s$$ (Eq. 2.9)

where Δm is the weight difference in [g] and ρ is the material density in [g/cm³].

From the above equations results the wear rate k, calculated on the basis of weight changes, Δm, as:

$$k = \frac{\Delta m}{F_N \cdot s \cdot \rho}$$ (Eq. 2.10)

having the following measurement unit: $\left[\dfrac{g}{N \cdot m \cdot \dfrac{g}{cm^3}} \right]$ or $\left[\dfrac{cm^3}{N \cdot m} \right]$

In this work the different tribological coatings are quantitatively compared to each other by determination of the friction coefficient and the wear rate. In the literature more often data for the coefficient of friction rather than for the wear rate is found. From a practical point of view it is much better to investigate both wear and friction properties of the coatings in order to correlate them.

2.4.4 Wear resistance of cermet coatings / Review

Wear resistance of thermally sprayed coatings is of high interest for many applications. In general, wear resistance of a coating in a particular environment is a system property influenced by the coating and substrate material and in particular the type of wear environment. Therefore, it is impossible to quantify the wear resistance of the coating accurately without knowing these factors [79]. Using cermet materials or hard oxide coatings to protect metallic components is an effective method to reduce wear. Understanding the factors that are causing wear to occur is very important to engineering the proper wear resistant coatings. Fortunately with the ability of thermal spray to work with an almost limitless number of materials, well engineered wear resistant coatings can usually be produced to solve even some of the most complex wear issues [81]. Some results of thermal spray coatings as a function of Vickers hardness are presented by the "Thermal Spray Technologies, Inc." in figure 2.38 (a), respectively as a function of wear resistance in figure 2.38 (b).
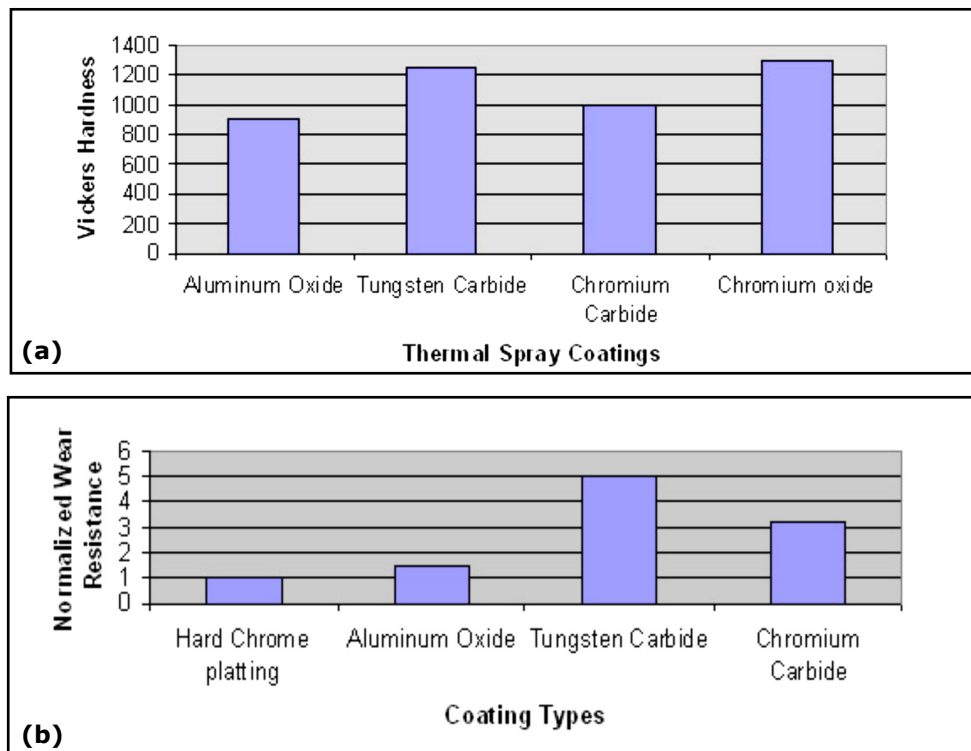
Figure 2.38 Hardness of typical wear resistance coatings (a) and thermal spray coating´s wear resistance vs. hard chrome plating, ASTM normalized G 65 wear test (b)[81]

This section contains a briefly presentation of some important researches regarding the wear resistance of different cermet coatings, conducted by some authors in the last few years. Tungsten carbide with cobalt seems to be the most frequently used and tested coating. A direct comparison of chromium carbide, Cr_3C_2 + 25 wt % NiCr, with tungsten carbide, WC + 12 wt % Co, shows a nearly two-orders-of-magnitude

better wear resistance for the latter one (Jin and Yang, 1996). The high wear resistance of tungsten carbide correlates strongly with (Qiao et al, 2001):

- high hardness of the deposits;
- high content of the WC phase and small content of the hard but brittle W_2C phase.

Qiao et al [100] study revealed that HVOF-sprayed WC+10Co (WC content, 90wt%) and WC+15Co (WC content, 85wt%) coatings tested by unlubricated pin-on-disc method against a Si_3N_4 monolithic sphere counter-body have a wear rate of 1.5 x 10^{-16} m^3/Nm and 6 x 10^{-16} m^3/Nm respectively, both under a load of 10 N. From these results, one can conclude that the higher WC content increases the wear performance.

L. Jacobs et al [101] tested HVOF and HVAF WC-Co-Cr coatings and a HVAF WC-Co coating by unlubricated sliding pin-on-disc (POD) method, with corundum counter-body, in ambient conditions. The HVAF sprayed WC-Co-Cr coatings showed a wear rate that was an order of magnitude lower than that of the HVOF WC-Co-Cr coatings. The HVAF sprayed WC-Co coating exhibited the best wear behaviour combined with a low wear of the counter-body. The authors concluded that the improved microstructure of the HVAF sprayed coatings reflects in an improved wear performance when compared to the HVOF coatings.
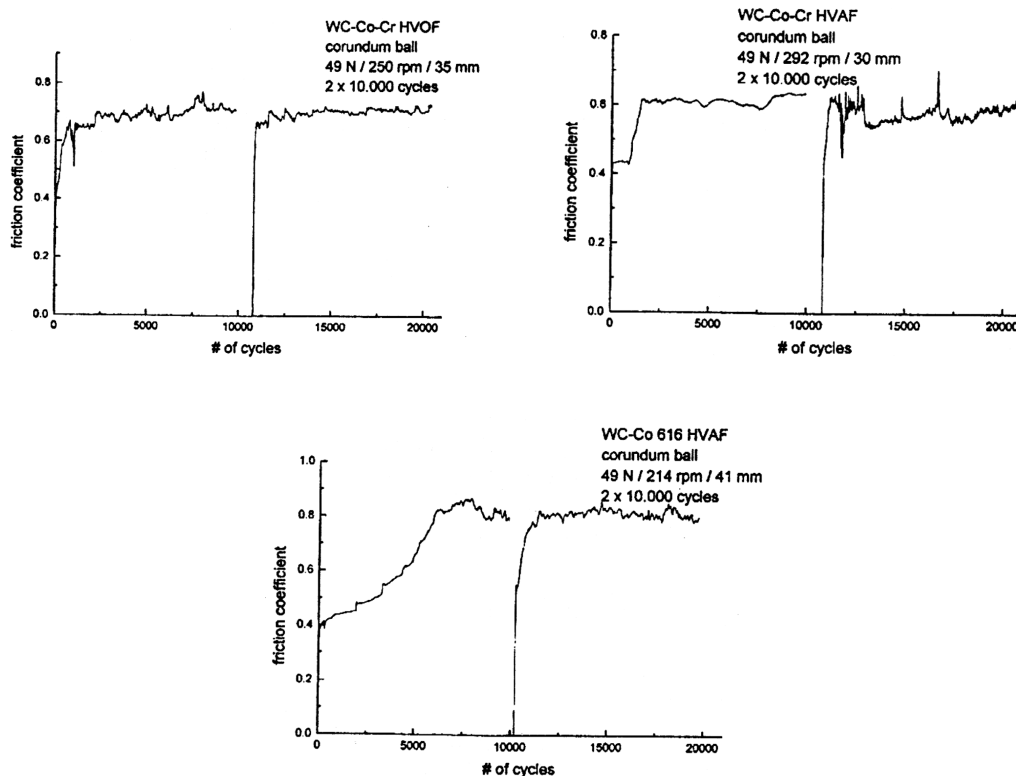
Figure 2.39 Evaluation of the coefficient of friction during POD wear tests [101]

T. Sahraoui et al [3] report that HVOF sprayed WC-Co coatings have a better wear resistance than that of Cr_3C_2- 25%NiCr HVOF sprayed coatings during Amsler wear tests carried out without lubrication and with extreme condition loadings. WC-Co coatings appear more adequate, with a good performance in case of lubrication and moderated loadings. Tests revealed that WC-Co exhibit lower weight loss.
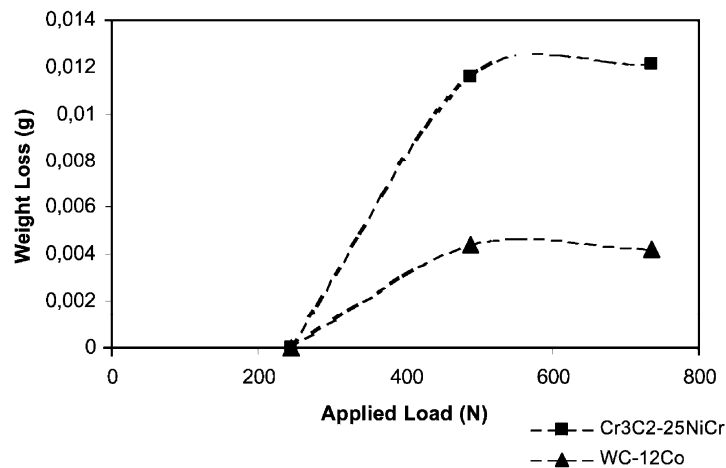
Figure 2.40 Evolution of the weight loss of HVOF coated samples during wear tests [3]

H. Chen et al [102] concluded from micro-scale abrasion tests that WC-Co coatings deposited by HVOF spraying with conventional WC grain size have a higher microabrasion wear resistance than the HVOF deposited WC-Co coatings with nanoscale WC grain size. This is due to the mechanism of material removal which consists of the preferential removal of the binder phase and subsequent undermining of the WC particle.

From their studies and tests, M. Barletta et al [103], (2009) conclude that HVOF sprayed WC-Co-Cr coatings on Al alloys are definitely preferable in applications where wear resistance is required, as the dry sliding wear rate of cermet coatings is lower than that of a hard anodized film by several orders of magnitude. Three torch scans seem to be enough to confer excellent wear resistance (close to 1×10^{-8} mm^3/Nm) to the WC-Co-Cr coating.

Table 2.7 Sliding wear rate of WC-Co-Cr coatings and anodized layers [103]

No. of scans	Sliding wear rate, 10^{-8} mm^3/Nm
2 scans	3,04 ± 0,49
3 scans	1,39 ± 0,16
4 scans	1,16 ± 0,42
5 scans	1,05 ± 0,18
Hard anodization	820 ± 647
Sealed anodization	Completely removed after 1000 m

C.W. Lee et al [104] studied the effects of mixing powders with various particle sizes on the fracture toughness and wear resistance of HVOF thermally sprayed WC-

10Co-4Cr coatings on S45C steel substrates. The wear properties of the coatings were assessed after 10,000 cycles on a pin-on-disk wear tester at ambient temperature without lubrication. The researchers observed that the wear loss of the coating layer sprayed with the mixed powder containing a high fraction (70%) of fine powder (10-38 µm) and a low fraction (30%) of coarse powder (20-73µm) was the lowest (see figure 2.41). Mixing of a small amount of coarse powders with fine powders resulted in the highest fracture toughness and wear resistance, due to the formation of coating layers having the lowest porosity.
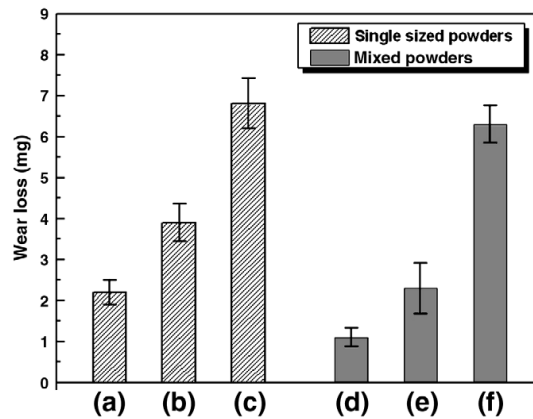
Figure 2.41 Wear loss of coatings sprayed with single sized powders and mixed powders: (a) fine, (b) medium, (c) coarse, (d) fine(70%) + coarse(30%), (e) fine(50%) + coarse(50%) and (f) fine(30%) + coarse(70%) [104]

J.A. Picas et al [105] examined the dry sliding tribological performance of three consolidation processing techniques to obtain coatings and bulk samples from WC-CoCr and WC-Co powders, namely, HVOF spray forming and laser engineered net shaping (LENS®) were used to deposit WC-Co coatings wile spark plasma sintering (SPS) was used to produce bulk WC-Co samples for comparison. The tribological behaviour under dry conditions was evaluated using POD tribometer (ball on disc configuration), according to ASTM wear testing standard G-99. The tests were carried out by sliding a 6mm WC-6wt.% Co pin against polished discs at a constant linear speed of 0,10 m/s with an applied force of 30N. All the tests were performed at 25°C with a relative humidity of approx. 50%. The wear of these WC-Co materials is generally considered to be a function of the WC particle size, the WC content, and bonding strength of the WC particle with the cobalt matrix. The results summarised in table 2.8, show that the disc wear rate was slightly lower in the case of the HVOF coating and SPS bulk sample compared to that of the LENS® coating. This was attributed to the high homogeneity of dispersed WC grains in these materials. The WC-matrix bonding in both the SPS bulk sample and the HVOF coating was better than for LENS® coatings, thus limiting the pull out of the carbide grains and exhibiting higher wear resistance.

Table 2.8 Tribological test results [105]

	HVOF coating	LENS®	SPS bulk sample
Friction coefficient	0,30	0,42	0,29
Specific wear rate (disc) (m^3/mN x 10^{-18})	3,6	8,9	3,5

2.5 Corrosion resistance of coatings

2.5.1 Introduction

The corrosion resistance of a given material depends on the environment and the conditions of exposure as well as on the condition of the test material. It is often the result of complicated interactions between the properties of a metallic surface and the adjacent environment to which it is exposed. Corrosion is defined as an electrochemical reaction between a material, usually a metal, and its environment that produces a deterioration of the material and its properties [106, 107].
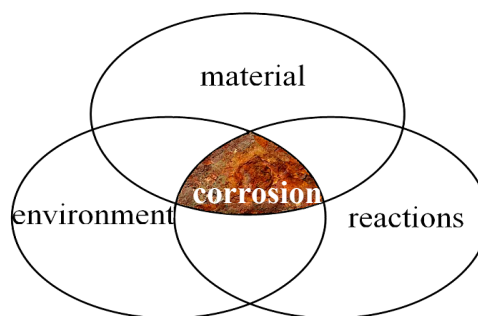
Figure 2.42 Corrosion process

Thermal spray coatings are frequently used to protect the surfaces of metals or alloys against aqueous corrosion. Such coatings mainly protect the substrate component in water, acids or bases [38]. The corrosion behaviour of a coating/substrate system is determined by the corrosion resistance of the coating material in the respective medium. However, this holds only for absolutely dense coatings that completely separate the aqueous corrosive medium from the underlying substrate material.

If the coating is a metal, the situation will vary according as the coating is cathodic or anodic to the basis metal. On steel, coatings of copper or nickel will be cathodic, whereas coatings of zinc and aluminium will usually be anodic.

Additonally, the aqueous corrosion resistant coatings on steel can be categorized as follows [38, 108]:

Anodic coatings or sacrificial coating, where the coating is less noble than the substrate, for example: Al, and Zn. In this case, if the electrolyte enters into contact with the coating and substrate, then the coating dissolves.

Cathodic coating or barrier coating, in which the coating is nobler than the substrate, e.g. Cu, Au, Ag, Pt. In order to obtain a maximal corrosion protection of the substrate, the quality of these coatings needs to be very high, in terms of low porosity or without pores, without cracks or any others defects. If the protective coating is porous or fine cracks are "visible", see figure 2.43, the corrosive environment will penetrate the coating along those defects up to the substrate. In most cases the coating will split off and the substrate will be severely corroded.

Inert coating, which protects the substrate in a physical way. The coating does not have any electrochemical activity with regard to the substrate.

Inhibitive coating, which is made of a material that slows down the corrosion rate. The corrosion rate can be measured by weighing a coated sample exposed to a corrosive environment as a function of exposure time. The rate is usually calculated as the loss of weight per unit area divided by the exposure time. [38, 109]. The most commonly methods used for testing the corrosion behaviour of the coatings are: electrochemical or polarization cell method (short-term test, see section methodology), artificial atmosphere-salt spray test based on DIN EN ISO 9227:2006 or water condensation with or without changing the climate based on DIN EN ISO 6270-2:2005 (long-term tests) [110, 111].

Generally, a laboratory accelerated test for determining the corrosion behaviour of different coatings uses severe conditions such as a higher applied stress (current), higher temperature and higher concentration of aggressive solutions than that of the actual service conditions, in order to minimize the testing time. Such severe conditions are useful for collecting valuable information in a short time, but cannot provide reliable data concerning the long-term performance, because the mechanism operating by short time test has not been proved to be identical to that governing long-time test performance in service.

2.5.2 Types of coating corrosion

Corrosion occurs in several widely differing forms. Classification is usually based on one of three factors [112]:

Nature of the corrodent: corrosion can be classified as "wet" or "dry". A liquid or moisture is necessary for the former, and dry corrosion usually involves reaction with high-temperature gases.

Mechanism of corrosion: this involves either electrochemical or direct chemical reactions.

Appearance of the corroded metal: corrosion is either uniform and the metal corrodes at the same rate over the entire surface, or it is localized, in which case only small areas are affected. The latter is the most common corrosion form that appears in domain of thermal spraying coatings.

2.5.2.1 Localized corrosion

Localized corrosion is described as corrosion that occurs at discrete locations on a material. The localization of corrosion reactions is essentially based on the fluctuation in electrochemical potentials among phases, discontinuities or porosity in structure, and areas of different density of either defects or segregation of chemical species. In addition, such environmental fluctuations as the concentration of reacting chemicals and the deposition of salts or corrosion products are to be considered. In understanding, simulating or accelerating localized corrosion, attention should be paid to formation and role of thin passive layer at interfaces between materials and their environments [113].

The following types of localized corrosion can appear with thermal sprayed coatings (see figure 2.43):

- Corrosion attack of the coating:

-*pitting corrosion*, which corresponds to the formation of corrosion points in the passivated film;

-*stress corrosion cracking*, which is a cracking process that requires the simultaneous action of tensile stress and a specific corrosive environment;

-*galvanic corrosion*, which occurs between the hard phase particles and the binder phase, in which only the metallic binder is affected;

-*crevice corrosion*, which occurs at coating/substrate interface because of an inadequate cleaning or pretreatment of the substrate.

• Substrate-corrosion attack:

-*due to coating porosity*, in which the corrosive environment penetrates the coating because of the interconnected porosity formed along the coating section;

-*due to coating micro-cracks*, in which the corrosive environment penetrates the coating up to the substrate along the interconnecting micro-cracks.
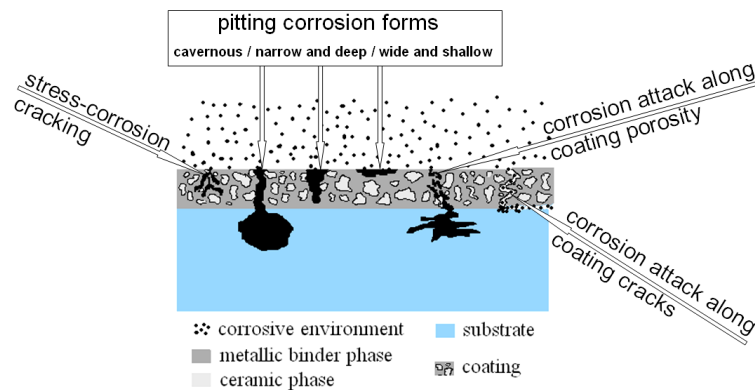
Figure 2.43 Schematics of the common forms of localized corrosion appeared by thermal spray coatings

2.5.2.1.1 Pitting corrosion

Pitting corrosion is characterized by local deep holes on an open surface, in that the holes can be small or large in diameter, but in most cases, they are relatively small. Pitting corrosion is influenced by many different parameters, including the environment, metal composition, potential, temperature, and surface condition. Important environmental parameters include aggressive ion concentration, pH, and inhibitor concentration [114]

Figure 2.43 shows some theoretical shape of pits and possible corrosive attack that can occur in thermal spray coatings. Furthermore some practical forms of pitting effect are illustrated in the figures 2.44, 2.45, respectively figure 2.46.
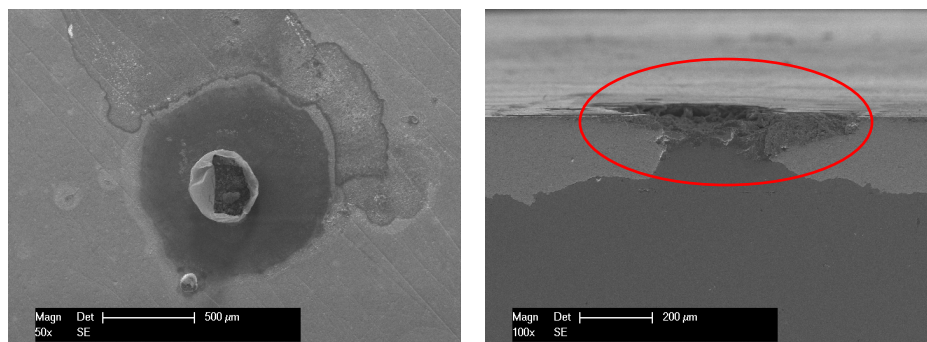
Figure 2.44 Corrosion pit with narrow and deep shape (top view-left, cross section-right)
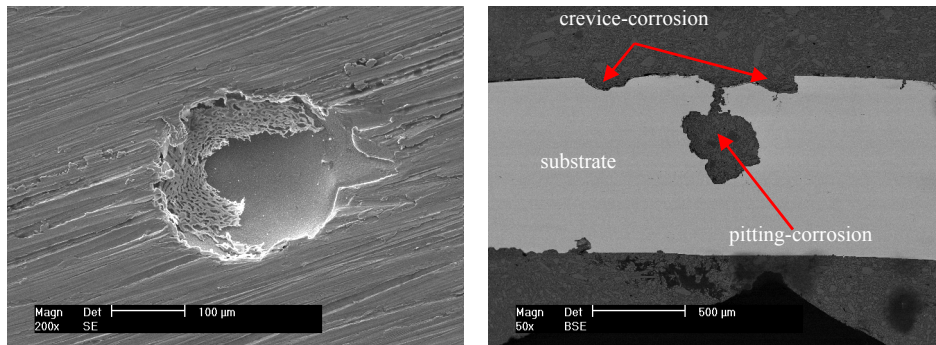
Figure 2.45 Corrosion pit with cavernous or subsurface shape (top view-left, cross section-right)

Deposition of a protective coating (noble coating), such as WC-CoCr, provides good corrosion resistance in the case of a pore-free and defect-free coating. Coatings defects, however, may allow severe local corrosion to occur, for example see figure 2.44 and 2.45. In case of figure 2.44, the substrate surface was inadequate finish-machined presenting a lot of material lifts. This fact leads, after the spraying process, to an irregular coating thickness that allows the corrosive environment, in some areas, to penetrate very easily the thin coating down to the substrate (see the marked zone). After a longer exposure to corrosion attack and also in case when crevice corrosion occurs at the coating/substrate interface, the coating will split off and the substrate will be severe corroded, see figure 2.45.

On the contrary, high quality coatings deposited on properly surface finished substrates (clean and without striations or lifts) will exhibit just a local corrosion attack that appears only superficial on the coating surface in form of wide pits as it can be seen in the figure below.
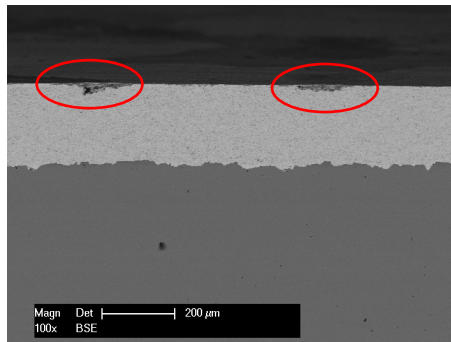
Figure 2.46 Corrosion pits with wide and shallow shape in cross section

2.5.2.1.2 Stress corrosion cracking

Stress corrosion cracking (SCC) is a complicated phenomenon that is affected by many factors, including metallurgical, environmental and structural or stress variables [113]. SCC is a localized form of corrosion characterized by the appearance of cracks (see figure 2.47) in materials subjected to both stress and a corrosive environment and leads to an early failure of the metallic coating. It usually

occurs in the presence of chlorides or other aggressive agents at moderate temperatures.
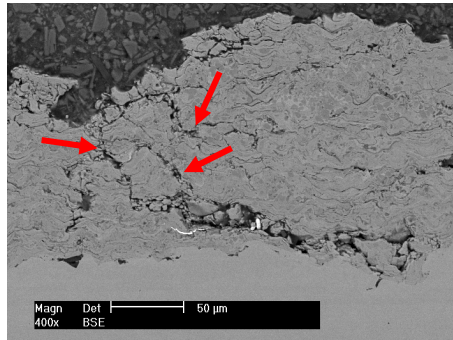
Figure 2.47 Stress corrosion cracking of HVOF Cr_3C_2-NiCr coating in cross section

A practical example of such a corrosion type (figure 2.47) was discovered in the case of a Cr_3C_2-NiCr coated piston, part of a food processing equipment. The SEM-micrograph shows the destruction of the entire coating down to the substrate. This damage occurred because of the local mechanical loadings and the environment in which the subjected piston had worked.

2.5.3 Corrosion behaviour of thermally sprayed coatings / Review

Besides the wear resistance review of thermally sprayed coatings presented in section 2.4.4, there is also necessary to know the corrosion behaviour of such coatings. Modern surface engineering research is looking into depositing a wide range of hard phases such as carbides along with corrosion resistant metal binder elements with the aim of achieving good adhesion between carbides and binders and therefore successfully combining corrosion and wear resistant elements together. Based on that, thermal spray techniques, especially HVOF, are increasingly being used for depositing wear-corrosion resistant coatings as a durable and protective barrier of the substrate [115, 116]. In general, the corrosion resistance of a coating/substrate system can be improved by producing dense coating structures through the optimization of deposition techniques and process parameters, by selecting noble coating materials, and by using dense and noble interlayers.

D. Toma et al [117] examined the erosion and corrosion resistance of HVOF cermet coatings at ambient temperature in 0.1 M NaOH and 0.1 M H_2SO_4 solutions containing sand. The combined erosion and corrosion tests have showed that a coating with a highly corroding matrix will suffer a much greater weight loss than a coating with less corroding matrix, see table 2.9. This work emphasises the importance of the corrosion resistance and passivity of the binder as coatings with less corrosion resistant matrix enhanced erosion. Among the tested materials the WC-Co coating was the least resistant. The addition of 4 wt% Cr or using other metallic binder, such as NiCr, seems to improve the corrosion resistance of the WC-based coating. D Toma showed also that the HVOF sprayed Cr_3C_2-NiCr coating is considered to be an excellent replacement for the thermal sprayed Cr_2O_3 coatings.

Table 2.9 Results from the electrochemical measurements and erosion-corrosion tests at 2.35 m s^{-1}, 100g l $^{-1}$ silica sand with a grain size between 100 and 500 µm, 20°C [117].

Coating	Electrochemical measurements Corrosion rate, mm a^{-1}			Erosion-corrosion test Erosion-corrosion rate, mm a^{-1}	
	NaOH	H$_2$SO$_4$	Sea water	NaOH	Sea water
WC-Cr$_3$C$_2$-Ni	0.38	0.15	–	0.4	–
Cr$_3$C$_2$-NiCr	0.17	0.077	–	0.17	–
WC-Co	–	–	0.76	–	1.6
WC-Co-Cr	–	–	0.32	–	0.55
Cr$_2$O$_3$-Al$_2$O$_3$-TiO$_2$	3.16×10^{-5}	3.64×10^{-5}	–	0.27	–
Cr$_2$O$_3$	7.6×10^{-4}	1.5×10^{-3}	–	0.35	–

Further observations about the corrosion resistance of HVOF WC-10Co4Cr and Cr$_3$C$_2$-25NiCr coatings were made by J. Laurila et al [4]. The corrosion results based on ASTM G48 test method showed that the Cr$_3$C$_2$-25NiCr coating was heavily corroded inside the coating material and also at the coating/surface interface after 24 hours and the WC-10Co4Cr exhibited the highest corrosion resistance even after seven days of exposure. Based on the results mentioned above by Toma et al, it is very hard to believe that Cr$_3$C$_2$-25NiCr posses such a poor corrosion resistance. Similar results can be obtained just in case of high porosity coatings in which the aggressive solution penetrates the coating in a very short time.

The role of binder corrosion in the corrosion degradation of HVOF thermally sprayed WC-Co-Cr coatings has been also studied by Souza and Neville [118] using electrochemical polarization tests in a 3.5% NaCl solution at varying temperatures. They report that the corrosion proceeds primarily by dissolution of the Co phase, depending on the integrity and thickness of the passive film on the binder phase. A series of electrochemical and long-term immersion tests were carried out by Cho et al [119], using a sulphuric acid (5 wt.% H$_2$SO$_4$) solution on HVOF sprayed WC cermet coatings with metallic binder of Co, Co-Cr, CrC-Ni and Ni. Considerable galvanic corrosion occurred between the WC particles and the metallic binder, and uniform corrosion occurred in the binder materials of the coatings without Cr. In spite of the presence of Cr, the overall corrosion resistance of the WC-Cr$_3$C$_2$-Ni coating was inferior to that of the WC-Co-Cr coating due to electrolyte penetration to the coating/substrate interface through interconnecting micro-cracks. Additionally, it was found that chemical composition of metallic binder materials and control of micro-cracks is the most important factors influencing the corrosion resistance of the HVOF sprayed WC cermet coatings.

M. Magnani et al [120] have studied the influence of HVOF parameters on corrosion resistance of WC-Co coatings sprayed on aluminium alloy using liquid nitrogen cooling prototype system. Electrochemical tests were conducted using open-circuit potential measurements and electrochemical impedance spectroscopy. The corrosion results reported show that a higher oxygen flux (higher flame temperature) produces the highest corrosion resistant coating in aerated and unstirred 3.5% NaCl solution. The influence of the spraying parameters (spraying distance, barrel length, fuel/oxygen rate and the powder feed rate) on the corrosion performance of cermet coatings has been studied also by Gil et al [121]. Their results indicated that all the spray parameters have a significant effect on the porosity and corrosion resistance of the HVOF coatings.
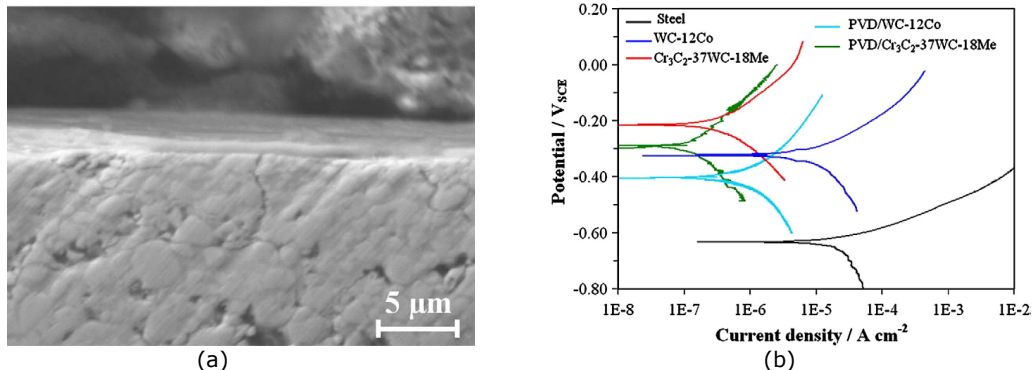
Figure 2.48: SEM micrograph of the PVD nanoscale multilayer NbN/CrN coating deposited on WC–12Co coating (a) and polarization curves recorded on bare steel or on coated steel specimens after 1 h immersion in 3.5% NaCl solution (b) [5].

Recently C. Monticelli et al [5] have investigated the corrosion performance in 3.5% Na Cl solutions of cermet and cermet/nanoscale multilayer CrN/NbN coatings deposited on steel specimens, respectively on WC-12Co coating, see figure 2.48 (a). Polarization curves recorded after 1 hour of immersion and polarization resistance values monitored during 3 days exposures showed that under free corrosion conditions the HVOF Cr_3C_2-37WC-18Me always exhibits low corrosion rates and efficiently protects the underlying substrate from corrosion. At short immersion times (1h), the HVOF WC-12Co coating presented a quite different corrosion behaviour, as the cobalt actively corrodes, while the NiCr matrix of Cr_3C_2-37WC-18Me is pasive in 3.5% Na Cl solution. However, after 3 days of exposure to this aggressive solution their corrosion behaviour becomes quite similar, due to the deposition of insoluble cobalt corrosion products on WC–12Co which slow down the cermet corrosion rate due to the slow penetration of the aggressive solution through the Cr3C2–37WC–18Me coating surface microcracks. Figure 2.48 (b) compares also the polarization curves recorded on steel specimens coated by thermally sprayed cermets or PVD/cermet coatings to those recorded on bare steel specimens and shows that the surface deposition of the nanoscale multilayer CrN–NbN film definitely improves the corrosion resistance of the WC–12Co coated specimens, while on PVD/Cr3C2–37WC–18Me coated specimens the corrosion behaviour is similar to that exhibited by the corresponding thermally coated specimens.

The effect (influence) of WC grain size on the corrosion behaviour of WC–Co based hardmetals is also important and can play a vital role in the coated system performance. Kellner et al [122] studied the corrosion characteristics of sintered hardmetals with different grain sizes in alkaline solutions using electrochemical methods. A clear tendency was observed: smaller the grain size, the higher the corrosion resistance. Laterally resolved Auger Electron Spectroscopy (AES) revealed that significant amounts of W and C diffuse into the Co binder matrix during the sintering process, and that the W and C concentration in the Co phase increases with decreasing grain size. They also affirmed that the dissolution of W and C in Co stabilize the fcc crystal structure of the Co binder which is otherwise not thermodynamically stable at room temperature. The small-grained hardmetals showed a higher amount of fcc Co in the structure, showing better corrosion behaviour than the hcp Co due to the higher thermodynamic stability.

Thermally sprayed coatings with compositions of WC-Co-Cr 86-10-4 or corrosion resistant alloys such as nickel aluminium bronze have been considered for wear and corrosion applications [118, 123, 124]. Beside of these, many other materials can be used to produce thermal spray coatings, thereby providing effective solutions for different corrosion problems [106].

2.6 Summary of literature-review

This summary synthesizes the current state of the art described in this chapter. Given the aim of this thesis, namely the wear and corrosion resistance of internal HVOF cermet coatings, this literature review was concentrated especially to find some scientific researches in the area of internal spraying. Unfortunately, there was no current research paper or book that explores this issue, just some final reports concerning the development of plasma spray method for ID chrome replacement in items such as hydraulic actuators and landing gears, described by the hard chrome alternatives team (HCAT) over the last decades. They report that HVOF is becoming accepted as the best alternative to replace the hard chrome plating on outside diameters (ODs), but cannot coat IDs less than 280 mm because of the flame standoff. At that time they used plasma spray in order to get into smaller diameters and tighter locations such as 76 mm ID tube used as sample holder for the spraying specimen under ID conditions. In that manner, no relevant results were found regarding the wear and corrosion resistance of internal HVOF coatings.

However, over the last few years new HVOF ID guns have been developed and are now commercially available. They can operate down to 80 mm ID. Also, the fine powder recommended for these types of guns, such as the nanopowder invasion has penetrated into the spraying world in order to provide good wear and corrosion resistance of the sprayed coatings. After all, in order to fully exploit the excellent properties of HVOF ID coatings, it is emphasized that optimization of the spraying process is mandatory. As compared to APS coatings, HVOF coatings offer a number of advantages in terms of coating microstructure and properties resulting in improved performance in many applications, especially in the case of cermet coatings. HVOF coatings are nowadays applied in a variety of industries. Major application areas are within industries where coatings are used to protect machinery components against wear, friction and corrosion. As it was mentioned before, no available researches were found about the wear and corrosion resistance of exactly internal HVOF coatings or their morphology. In analogy with that, a number of important researches with respect to wear and corrosion resistance of different cermet coatings were briefly presented. Commonly, the wear properties of the investigated materials were assessed using either the pin on disc test with or without lubrication according to ASTM wear test standard G-99 or according to ASTM G-65 abrasion test. Moreover, tungsten carbide with cobalt seems to be the most frequently used and tested carbide. On the other hand, the corrosion behaviour of the sprayed coatings was usually investigated using the electrochemical polarization tests. It was found that chemical composition of the metallic binder (e.g. NiCr, CoCr, Co) and the coatings porosity control are the most important factors influencing the corrosion behaviour of the HVOF cermet coatings. Many investigations show that the WC-Co-Cr coatings have a satisfactory corrosion resistance.

Both wear tester configurations mentioned before are designed only to test the outside surfaces of the as-sprayed specimens such as plate sample or external surface of a ring sample. Given the fact that the parameters of HVOF spraying process for outside diameters are totally different from those of the internal spraying diameters (different spray parameters, different spray guns and working in a "close" atmosphere) it is also necessary to investigate the main properties, for instance the wear or corrosion behaviour of such ID coatings. In order to overcome this problem a new wear tester was especially developed in the present work, in order to perform the wear tests for internal surfaces. More details about this wear tester are given in the following chapter.

Chapter III

EXPERIMENTAL PLAN AND METHODOLOGY

3.1 Investigation methods

The morphology and structure of the as-sprayed coatings as well as those of the feed stock powders were characterized by means of scanning electron microscopy (SEM) combined with energy dispersive spectrometry (EDS) and by X-ray diffraction (XRD) technique. The friction coefficient of the coatings was assessed using a pin-on-disc (POD) wear tester. The wear resistance of the coatings was investigated on a new sliding wear machine which was developed in the frame of this work, especially for testing inner surfaces. The corrosion behaviour of the coatings was investigated by potentiodynamic polarization method using 1 M NaCl testing solution and a three electrode open cell. Besides of these methods some investigations were also supported by precise stereo and light microscopes examinations.

3.1.1 Scanning electron microscopy (SEM)

The scanning electron microscope used for this work was a Philips XL 30 ESEM TMP. The XL 30 microscope is equipped with a field emission operating gun at an acceleration voltage up to 30kV and is able to achieve a very high resolution (2nm). The useful magnification range is about 1.000-250.000X. It is equipped with secondary electron and backscattered electron detector, as well as with energy dispersive X-Ray spectrometer.
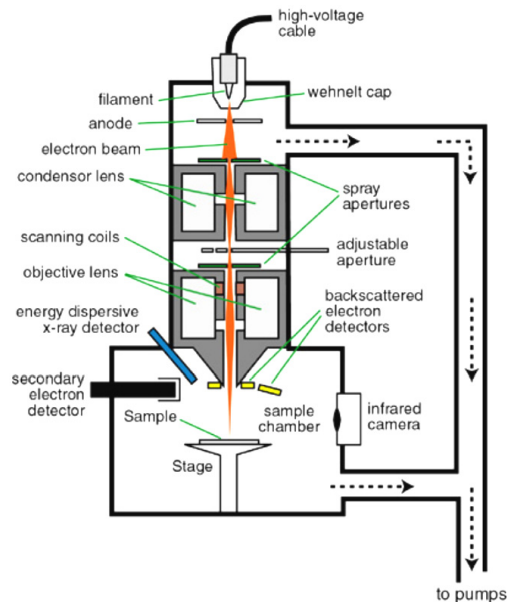

Figure 3.1 Principle of scanning electron microscopy
[http://www4.nau.edu/microanalysis/Microprobe-SEM/Instrumentation.html]

The principle of SEM (Fig. 3.1) is based on an electron column which consists of an electron gun and two electron lenses, which influence the paths of electrons travelling down an evacuated tube. The base of the column is usually taken up with vacuum pumps that produce a vacuum of about 10^{-4} Pa. The electron beam generates electrons and accelerates them to an energy in the range of 0.1-30 keV (100-30,000 electron volts). The spot size from a tungsten hairpin gun is too large to produce a sharp image unless electron lenses are used to reduce it and place a much smaller focused electron spot on the specimen. Two pairs of electromagnetic deflection coils (scan coils) are used to sweep the beam across the specimen. The first pair of coils deflects the beam off the optical axis of the microscope and the second pair bends the beam back onto the axis at the pivot point of the scan [126]. Detectors collect the secondary or back-scattered electrons, and convert them to a signal that is sent to a viewing screen, producing an image [127].

Secondary electrons (SE) are formed by interactions between the beam electrons and weakly bound conduction electrons of sample atoms [128]. The ratio of SE to incident electrons is called secondary electron yield (δ) and it is given by:

$$\delta = \frac{n_{SE}}{n_B} = \frac{i_{SE}}{i_B},$$

where n_{SE} is the number of secondary electrons emitted from a sample bombarded by n_B beam electrons, and i designates the corresponding currents [126]. Because SE yield is almost independent of the atomic number but strongly depends on the angle between the incident beam and the sample surface, secondary electrons are mostly used to image the surface morphology (topographic contrast). The energy spectrum of secondary electrons is independent of the energy of incident electrons and of the specimen material; it shows a pronounced maximum at approximately 3 eV. Seventy percent of the secondary electrons have energies below 15 eV, and at approximately 50 eV, the frequency of secondary electrons approaches zero. Conventionally, all electrons below 50 eV are considered to be secondary electrons and those having higher energy are considered to be backscattered electrons [129].

Backscattered Electrons (BSE) are beam electrons whose trajectories have intercepted a surface, usually, but not necessarily, the entrance surface, and which thus escape the specimen.
They are reflected or back-scattered out of the specimen interaction volume by elastic scattering interactions with specimen atoms. Since heavy elements (high atomic number) back-scatter electrons more strongly than light elements (low atomic number), and thus appear brighter in the image, BSE are used to detect contrast between areas with different chemical compositions.
Scanning electron microscopy offers possibilities for image formation that are usually easy to interpret and will reveal clear pictures of as-polished and etched cross sections as well as rough surfaces and particles. Beside of that, energy-dispersive x-ray microanalysis using equipment routinely attached to the scanning electron microscope features qualitative and quantitative analysis of the chemical composition with a typical lateral resolution of a micrometer and a typical depth resolution of a few tenths of a micrometer. Chemical analysis in the scanning electron microscope is performed by measuring the energy and intensity distribution of the x-ray signal generated by a focused electron beam. Due to the relatively easy handling, SEM has found a wide range of applications in materials research, materials development, failure analysis and quality control.

3.1.2 X-Ray diffraction

The X-ray diffraction examinations were performed using an X`Pert MPD apparatus from Phillips. This diffractometer is equipped with a high resolution vertical goniometer with long fine focus ceramic tube PW3373/00, Cu anode, wavelength 0.154 nm, max. 2.2 kW, 60 kV. Generally used on pure materials and simple mixtures, it can identify specific compounds on the basis of their crystal structure. In XRD, an aggregate of small crystal fragments, such as a powder, is irradiated with a monochromatic beam of X-rays. The beam is diffracted at angles determined by the planes of the atoms in the crystals. The intensity and spacing of these diffracted beams are unique to each type of crystalline material and can be identified by comparison to a published atlas.

Diffraction effects are observed when electromagnetic radiation impinges on periodic structures with geometrical variations on the length scale of the wavelength of the radiation. The interatomic distances in crystals and molecules amount to 0.15–0.4 nm which correspond in the electromagnetic spectrum with the wavelength of X-rays having photon energies between 3 and 8 keV. Accordingly, phenomena like constructive and destructive interference should become observable when crystalline and molecular structures are exposed to X-rays.

Generation of X-rays

X-rays are generated when electrons with kinetic energies in the keV range and above impinge on matter. The emission spectrum comprises a continuous part, called Bremsstrahlung, and some discrete lines indicative of the chemical elements of the target material. In laboratory x-ray tubes electrons are accelerated onto an anode plate made from a specific metal of high purity. The cross-section of such a tube is shown in figure 3.2.
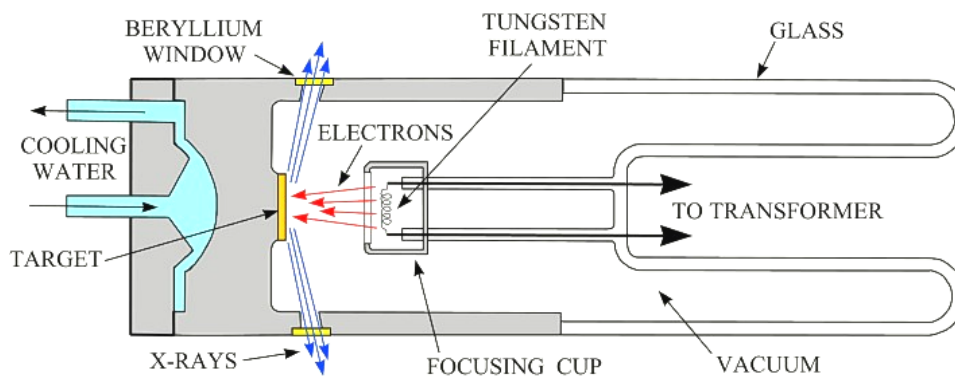
Figure 3.2 Schematic cross-section of an X-ray tube
[http://pubs.usgs.gov/of/2001/of01-041/htmldocs/images/xrdtube.jpg]

The electrons are emitted from the cathode filament and accelerated towards the anode plate. The anode is typically fabricated from copper, chromium, aluminium, molybdenum or another metal. The electron current between filament and anode may be adjusted by tuning the filament current in the range of some 10 mA. When impinging upon the anode the electrons are decelerated by their interaction with the target plate atoms leading to the emission of X-rays. The acceleration voltage (in

kV) must be greater than the energy of the characteristic radiation required by the experiment (in keV). Other x-ray tubes may be used if the diffraction pattern has to be contracted or expanded or if the excitation of x-ray fluorescence from the sample is to be avoided. A prominent example for the latter effect is given by Fe-containing samples that cause a strong background when Cu K α radiation is applied [130]. The crystal structure of an unknown material can be identified from the obtained diffraction patterns. In addition one can also determine factors such as the orientation of single crystals, or measure the size and shape of crystalline regions. There are several X-ray diffraction techniques. Two of the most common are:

Single crystal X-ray diffraction: used to solve structure of crystalline materials ranging from inorganic compounds to complex macromolecules such as proteins or polymers. One can learn everything about a crystal structure, but requires a single crystal. Although obtaining single crystals is difficult, single crystal X-ray crystallography is a primary method for determining the molecular conformations of biological interest such as DNA, RNA and proteins.

Powder X-ray diffraction: used to characterize crystallographic structure, grain size, and preferred orientation in polycrystalline or powder solid samples. This is a preferred method of analysis for characterization of unknown crystalline materials. Compounds are identified by comparing diffraction data against, a database of known materials. It can be used to follow phase changes as a function of variables such as temperature or pressure.

θ/2 θ Diffractometer. The basic measurement geometry of by far the most frequently used x-ray diffraction instrument is depicted in figure 3.3. The sample should preferably exhibit a plane or flattened surface. The angle of both the incoming and the exiting beam is θ with respect to the specimen surface. A vast number of organic and inorganic powder samples have been measured with these instruments from which the naming of powder diffractometer is understood. Its measurement geometry may also be applied to the investigation of thin films, especially if the layer is polycrystalline and has been deposited on a flat substrate, as is often the case.
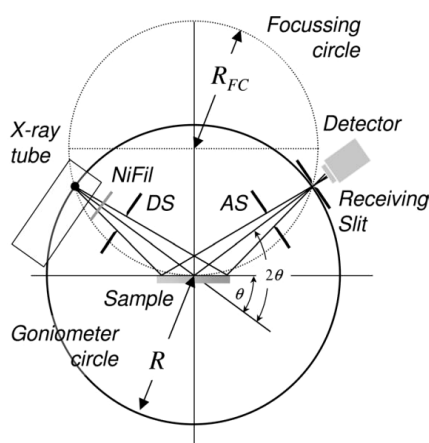

Figure 3.3 Schematic representation of θ/2 θ diffraction in Bragg–Brentano geometry [130]

The diffraction pattern is collected by varying the incidence angle of the incoming x-ray beam by θ and the scattering angle by 2θ while measuring the scattered intensity I (2 θ) as a function of the latter. Two angles have thus to be varied during a θ/2 θ scan and various types of powder diffractometers are in use [130].

3.1.3 Surface roughness tester

A quantitative complementary method to examine the surface morphology is obtained by analysing the surface roughness using surface profilometry. The surface roughness, *Ra* - value of the coated samples was measured using a Mitotoyo Surftest SJ-301 device. The SJ-301 is a stylus type surface roughness measuring instrument developed for shop floor use. It is capable to evaluate surface textures of various machine parts with a diversity of parameters according to different international standards. Additionally, the SJ-301 can be used also in order to measure the wear track profiles, knowing that the measuring range of the stylus stroke can rich 350µm on Z-axis and the detector traverse is about 12.5mm (X-axis). Besides of these specifications the display unit sustain a resolution between 0.01-0.4µm by 10µm respectively by 350µm measuring range.
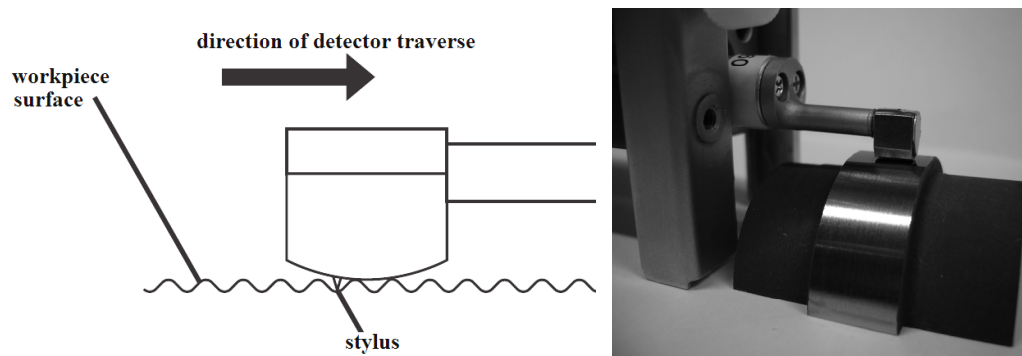
Figure 3.4 Surface roughness measurement

The surface roughness measurement principle (see figure 3.4) is based on vertical stylus displacement produced during the detector traversing over the work sample (specimen) surface irregularities, converting this displacement into electrical signals subjected also to various calculation processes. The measurement results (surface roughness) are digitally/graphically displayed on the touch panel, and output to the built-in printer (see the graphs in appendix).

3.1.4 Pin on disc

Friction tests were conducted on a pin on disc arrangement tribometer from CSM Instruments, test compliant to ASTM G99 & DIN 50324. The pin on disc method (Fig. 3.5 left) consists of a stationary sphere, pin or flat which is loaded onto the rotating test sample with a precisely known force. The pin is mounted on a stiff lever, designed as a frictionless force transducer. The friction coefficient is determined during the test by measuring the deflection of the elastic arm. Moreover, the wear degree of pin and disk materials can be calculated from the volume of material lost during the test.
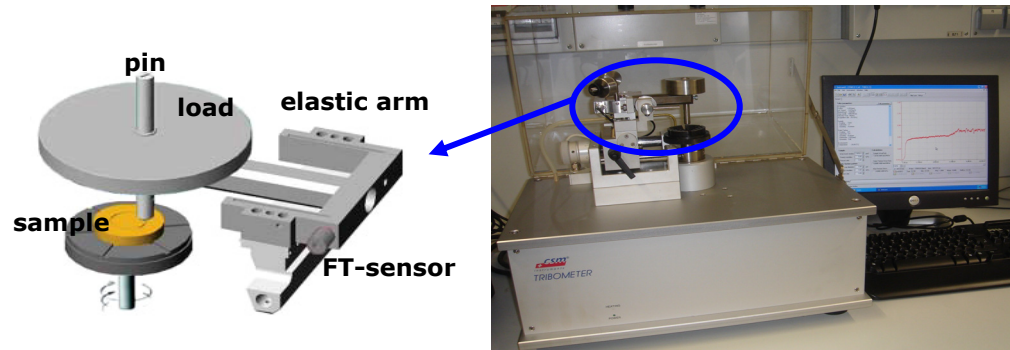
Figure 3.5 The principle of pin-on-disc (left); CSM Instruments-Tribometer (right)

This method facilitates the study of friction and wear behaviour of almost every external plane surface of solid state material combination with or without lubricant. Furthermore, the control of test parameters such as speed, frequency, contact pressure, time and environmental parameters (temperature, humidity and lubricant) allows simulation of the real life conditions of a practical wear situation. The specifications of this type of tribometer are presented below:

- load range: up to 10 N
- rotation speed: 0.3 – 500 rpm
- maximum test radius: 40 mm
- stationary partner: sphere Ø 6 mm; pin or flat
- air or gas input
- test conditions: with or without lubricant

The CSM Micro-Tribometer used in this work is presented in figure 3.5 right, assisted by computer software for displaying the test parameters and storing data for analysis. This method is very useful for determining the variation over time of the dynamic coefficient of friction by automatic calculation of mean coefficient of friction, standard deviation and maximum/minimum values from selected parts.

3.1.5 Cylinder on ring wear tester

Many different types of testing devices and other tribometers for measuring the friction and wear resistance of materials, under a wide variety of test conditions, are known in the art, but most of those devices are capable to test only the external surfaces of plane or cylindrical specimens. Cylinder on ring wear tester overcomes the above-discussed deficiency making the wear testing of coated or uncoated cylindrical inner surfaces possible. This wear tester was especially designed and developed during the PhD work in order to perform the wear resistance tests of the ring samples.
Cylinder on ring is a device for testing the wear resistance of lubricated and non-lubricated components especially developed for inner surfaces, which contains a stationary specimen in form of a cylinder or half cylinder pressed down to a rotating ring specimen generating thereby a line contact between the two components, see figure 3.6. The wear rate of the tested materials can be calculated based either on the mass loss of the specimen (gravimetric) or on the loss of material volume along

the cylindrical inner surface during the test. In this care, the volume of the rectangular wear track (volumetric) will be in this case calculated, see section 2.4.3.2.
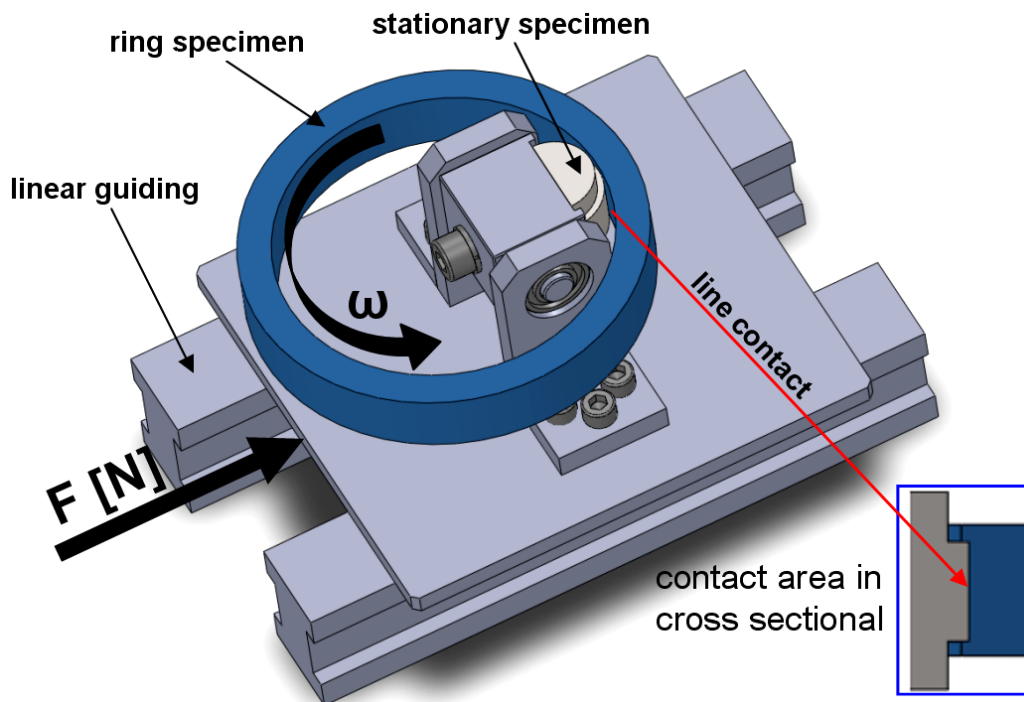
Figure 3.6 The principle of cylinder on ring wear tester

3.1.5.1 Technical and functional description

The cylinder on ring wear tester (Fig. 3.7) consists in a stationary round block (12) (as a counter part) which is loaded against a coated ring sample (13) fixed into a rotary chuck (11). The loading can be set by rotating the screw (6) mounted into a screw guiding support (17), which compresses the spring (7) with the help of a pipe nut (8) resulting in a wear track on the testing sample (5). The rotational speed of the sample is adjustable as well, depending on the engine frequency set from the control panel (3).
The upper part of the testing machine consists in a metallic frame (4) on which are mounted two sliding cylindrical columns (9) necessary for the vertical motion (Y-axis) of the electrical motor (2). This can be adjusted by a simple rotation (in one or the other direction) of the mounted crank (1). The connection between the motor shaft and the axis on which is fixed the chuck is made through the coupling connection (10).
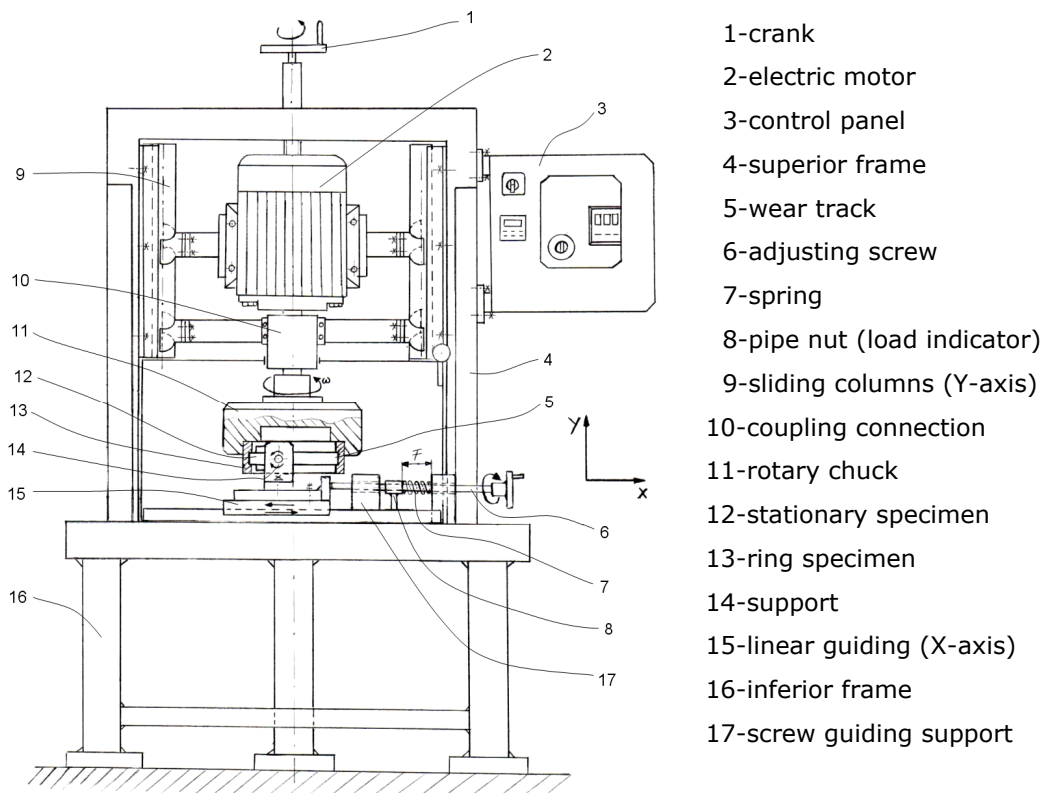
Figure 3.7 Cylinder on ring testing stand

1-crank
2-electric motor
3-control panel
4-superior frame
5-wear track
6-adjusting screw
7-spring
8-pipe nut (load indicator)
9-sliding columns (Y-axis)
10-coupling connection
11-rotary chuck
12-stationary specimen
13-ring specimen
14-support
15-linear guiding (X-axis)
16-inferior frame
17-screw guiding support

At the lower part of the wear testing stand exists another metallic frame (16) on which the linear guiding (15) is assembled enabling the linear motion (X-axis) of the stationary specimen-support (14). Given the fact that the stationary specimen has a round surface, forming a line contact between the tested specimens, it was absolutely necessary to mount two radial bearings (19) in the housing (20) in order to fulfill the optimal auto positioning of the stationary specimen (12) on the ring specimen (13) and also to ensure an uniform wear track during the test. The whole assembly is fixed onto the carrier plate (21), see figure below.
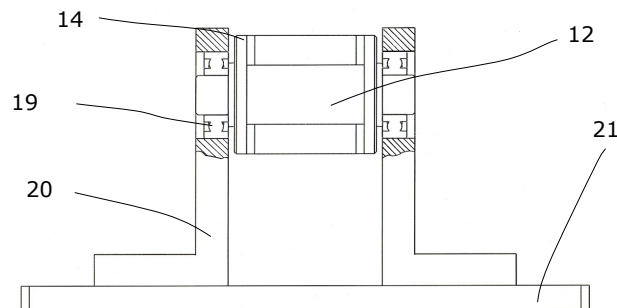
Figure 3.8 Assembly detail of the stationary specimen

3.1.5.2 Possible test configurations

The cylinder on ring wear tester is very flexible: it may run at various loads, velocities, and temperatures, different environments and also different contact types such as "ball on ring" (point contact, see figure 3.9) or standard as "cylinder on ring" (line contact, see figure 3.10). All these parameters are very important and necessary to be set in order to simulate the service conditions.
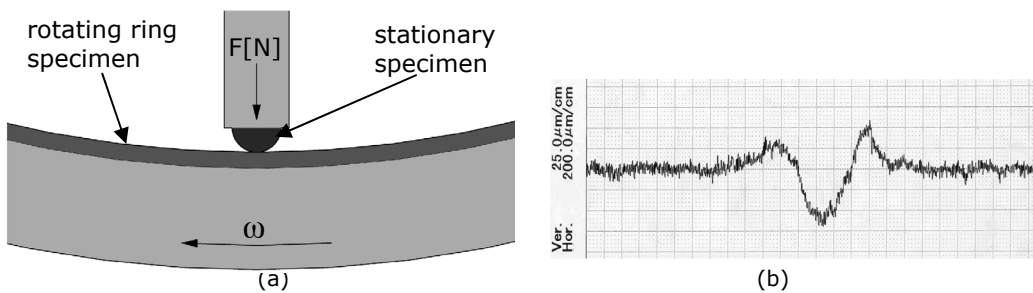
Figure 3.9 Point contact - Pin on ring test (a); The wear track profile (b)
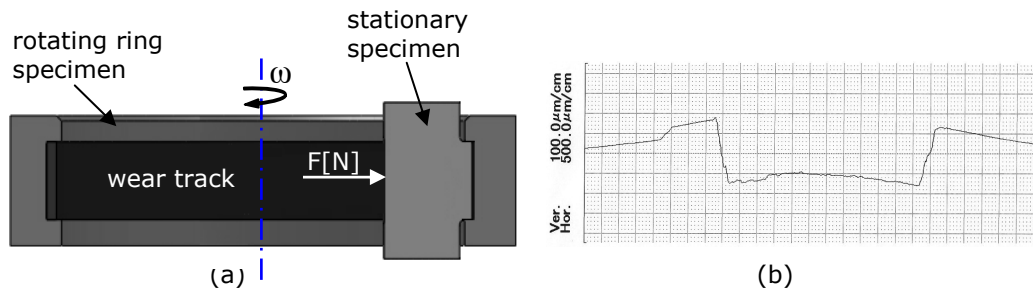
Figure 3.10 Line contact - Cylinder on ring test (a)*; The wear track profile (b)
*The test configuration is illustrated in transversal section for easier visualization of the contact type and the wear track

According to the test configuration, two different wear track profiles can be obtained, as shown in figure 3.9 (b) respectively in figure 3.10 (b). Based on these profiles, as already mentioned before, the volume generated by material loss during the wear test can be calculated. The resulting value will serve to the calculation of the volumetric wear rate.

Figure 3.11 and 3.12 illustrated the geometry of two stationary specimens designed for line contact wear tests. The one having a bushing geometry shape was developed, besides of the standard specimen (one test position), in order to improve the number of wear tests by using the same stationary specimen. This type allows up to 5 testing positions (Fig. 3.12) by rotating the specimen in the corresponded support after each test. From the economical point of view, it is an expensive component considering the machining process of such a complex geometry. On the other hand, this configuration is very useful when the stationary specimen needs to remain intact, without any kind of machining process after spraying or subsequent treatments.

These requirements are impossible to be fulfilled in the case of half cylinder specimen. As it can be seen in figure 3.11 this type of specimen requires post machining processes (cutting, drilling, threading) in order to mount it into the designated support. However, this specimen configuration is simple, with a cylindrical geometry, which can be very easily arranged for the spraying process.

Figure 3.11 The geometry of stationary specimen with a half cylindrical form (test positions: 1)

Figure 3.12 The geometry of stationary specimen having a bushing form (test positions: 5); solid shape of the stationary specimen support

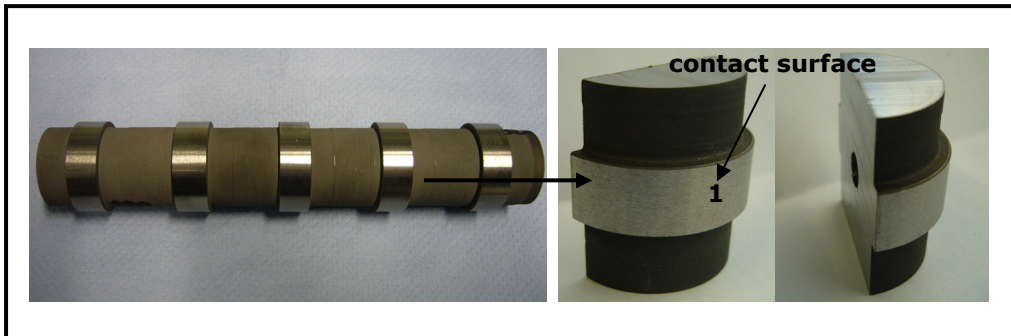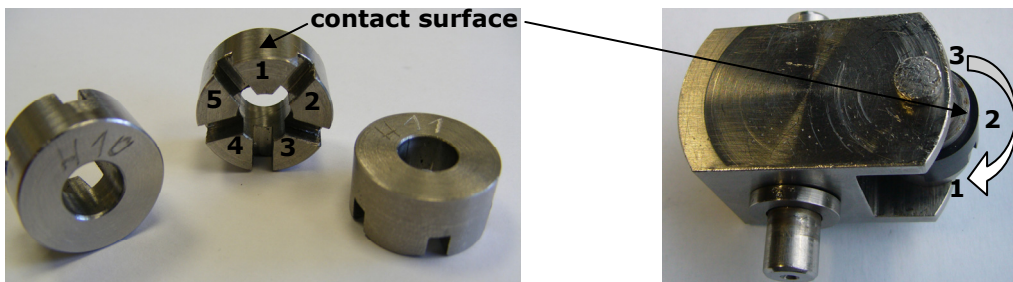The specifications* of cylinder on ring wear tester are briefly presented below:

Technical Data: Dimensions (H x W x D)……………………………1850 x 550 x 1100
                        DC motor power……………………………………………………..1100W
                        Max. number of revolutions……………......1420 min^{-1} (at 50 Hz)

Test Options: Cylinder on ring

Ring-clamping range:
    min. inner diameter………………………………….$\varnothing_{min.}$ 75 mm
    max. inner diameter………………………………….$\varnothing_{max.}$ 150 mm
    ring height……………………………………………10 to 45 mm

Stationary specimen-geometry:
    bushing with outer diameter………………………….$\varnothing$ 20 mm
       and contact length…………………………4 to 28 mm
        number of test positions…………………….max. 5
    half cylinder block with outer radius…………….10 to 15 mm
       and contact length………………………….2 to 28 mm
        number of test positions………………………….1

max. contact load………………………….110 N (at f_{spring}= 1,66N/mm)
contact type………………………………………………………………………line
load application type…………………………………………spring induced
testing environment…………………………………………user-defined
suitable for all material pairing

Pin on ring

Ring-clamping range:
    min. inner diameter……………………………………….$\varnothing_{min.}$ 75 mm
    max. inner diameter…………………………………….$\varnothing_{max.}$ 150 mm
    ring height……………………………………………….5 to 45 mm

Stationary specimen-geometry:
    ball diameter……………………………………………….$\varnothing$ 6 mm
max. contact load………………………………………………………….400 N
contact type…………………………………………………………………point
load application type…………………………………………by weight
testing environment…………………………………air or compressed air
material pairing depends on the ball

*specifications may be subject to change according to the applications which need to be simulated

3.1.5.3 The principal advantages of Cylinder on Ring wear tester

The introduction of a new manufacturing product or changing an older model involves important economical decisions as well as the selection of the optimal material. Thus, for a technical application that directly targets the wear resistance of inner cylindrical surfaces, materials to be used and placed in contact with each other should firstly be tested in order to provide the necessary knowledge about their

wear behaviour. This can be made possible by the present device, which facilitates the realization of such a wear test. This fact represents one of the biggest advantage of this testing device. Based on the results from these tests, one can select the optimal material for fabricating the new product, satisfying the structural and functional requirements. Some other important advantages of this wear tester are described below.

- Approach simulation of reality- possibility to test a wide variety of materials

The cylinder on ring tester is considered particularly advantageous thus to the stationary specimen geometry which surface can be easily coated with various materials (e.g. steels, cermets, titanium alloys etc) using different thermal spraying or other coating processes. A closer simulation of a given wear application can be realized by the means of the present wear device which allows to test different materials for the ring specimen and also for the stationary specimen rubbing against each other under a line contact type. Additionally, it facilitates also the possibility to optimize the spraying parameters used for deposition of cylindrical inner coatings in order to obtain a good wear resistance for the whole coating system.

- Force adjustment of the stationary specimen

A further advantage of this wear tester is the contact force adjustment mode of the stationary specimen realized by a spring loaded device. The spring assures a continuous contact between the ring inner surface and the counter-body (stationary specimen) during the whole wear test, even in case of possible oscillations and/or machining defects of the ring samples. These deviations can be successfully compensated with the aid of the existing spring damping.

- Possibility to vary the length of the contact line depending on the application that is intended to be simulated

Another advantage of this testing device is the possibility to vary the length of the contact line between the stationary specimen (counter-body) and the ring specimen. This can be achieved by simply machining the stationary block at desired dimensions and/or required by the engineering application that is attempted to be simulated.

- Line contact type - avoidance of premature wear of the counter-body

Due to the linear contact between the two bodies/surfaces, the forces involved during the test runs are evenly distributed on the surfaces, avoiding the premature wear of the stationary specimen (counter-body). At the same time this type of contact (surface vs surface) occurs more often in practice comparing with the pin on disc method where the contact type between the tested specimens is a point.

- Provides a wear track profile with a rectangular geometrical form

The wear tracks obtained at the end of the tests have an approximately rectangular geometry. This facilitates the subsequent calculation of the volume of material lost based on the section area of the obtained profile.

- Flexibility - possibility to perform tests in different environments

Considering all the above mentioned advantages, it can be concluded that this wear testing device, for inner cylindrical surfaces, is very flexible, easily adaptable to the requirements necessary to investigate the wear behaviour of a wide variety of materials usually employed in assemblies and/or subassemblies.

3.1.6 Electrochemical corrosion testing

During corrosion, at least two electrochemical reactions, an oxidation and a reduction reaction, occur at a metal-electrolyte interface. Because of the electrochemical mechanism of corrosion electrochemical techniques can be used to study corrosion reactions and their mechanism and kinetics.

A large number of electrochemical techniques are available for laboratory studies of various corrosion phenomena as well as for corrosion monitoring. The one selected for this work was the potentiodynamic measurement for large signal-polarization tests. In order to perform a polarisation scan on a particular metal/solution system, a certain experimental arrangement has to be prepared. The three-electrode electrochemical cell used to investigate the corrosion behaviour of the samples is illustrated in figure 3.13.

The working principle of the electrolytic cell used under potentiodynamic testing conditions is as follows: a potential is imposed between the sample and the reference electrode (SCE- saturated calomel electrode). As a consequence, the working electrode's (sample) potential is stepwise or at a constant rate, moved from the free corrosion potential (at which the recorded current I=0) in anodic or cathodic direction. The anodic or cathodic current thus imposed flows between the working and the auxiliary electrode and can be recorded, see the figure 3.14.
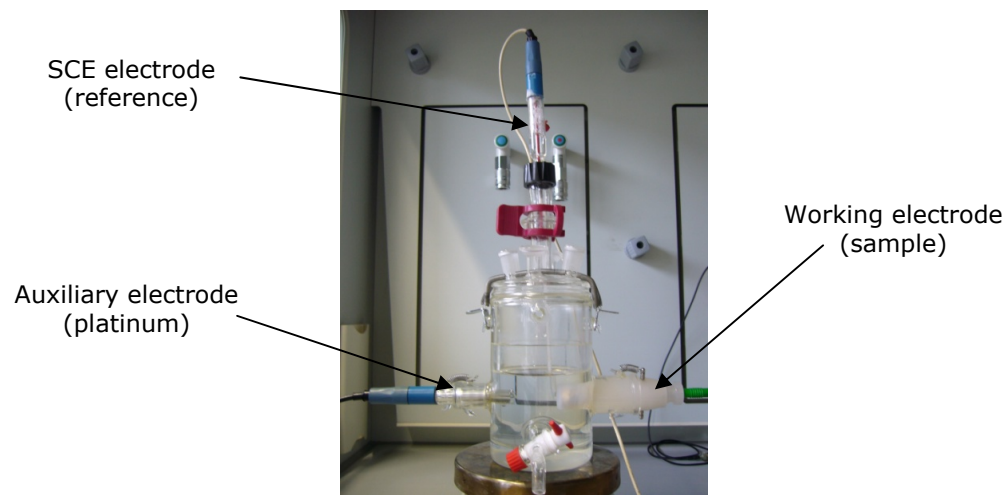

Figure 3.13 Three-electrode cell

A high-impedance voltmeter placed between the test and the reference electrodes prevents any significant current flow through the reference electrode, which then shows a negligible overpotential and remains very close to its equilibrium potential. As a result a polarization curve will be obtained.
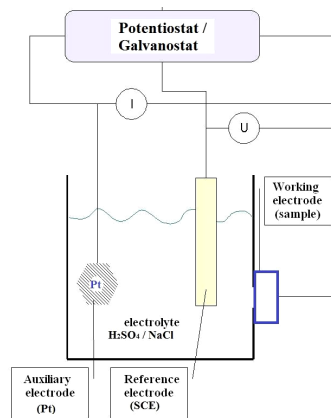
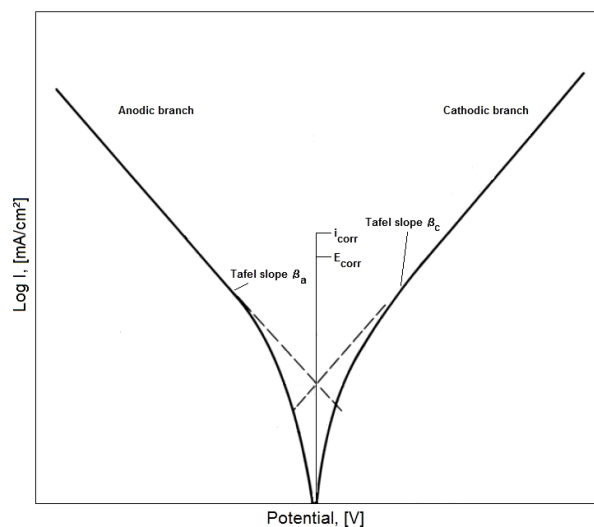Figure 3.14 Schematics of the electrochemical cell

Figure 3.15 Tafel extrapolation [131]

The polarization curve, is usually plotted as the applied potential E_{appl} versus the logarithm of the current density, i. A complete polarization curve consists of a cathodic branch and an anodic branch. The cathodic branch of the polarization curve contains information concerning the kinetics of the reduction reaction(s) occurring for a particular system. Depending on the solution composition, a mass- transport-controlled region can be reached at more negative potentials, at which the reaction rate (the measured current density) depends only on the solution composition and the hydrodynamic conditions. The particular features of the anodic branch of the polarization curve depend strongly on the metal-electrolyte system. Usually, a charge-transfer-controlled region occurs at potentials close to E_{corr}. So-called passive metals show an active-passive transition followed by a passive region and the region of oxygen evolution at higher potentials. For those metals, which are susceptible to localized corrosion, a large increase of the current occurs in the passive region when the pitting potential, E_{pit}, has been exceeded. In general, only

qualitative information, such as changes in the polarization characteristics in the passive region or changes of E_{pit} due to the presence of inhibitors or alloying, is extracted from a full polarization curve. However, it is possible to determine from such curves quantitative information that is related to the kinetics of the corrosion reactions and the corrosion rate.

The relationship between the applied potential, E_{appl}, and the current density, i, in the Tafel region is given by:

$E_{appl} = E_{corr} + \beta a \log (i/i\text{corr})$, for the anodic polarization curve;   (Eq. 3.1)
$E_{appl} = E_{corr} - \beta c \log (i/i\text{corr})$, for the cathodic polarization curve.   (Eq. 3.2)

Plots of E_{appl} versus $\log i$ are called Tafel plots. The corrosion current density, i_{corr}, can be determined according to Eq 3.1 and 3.2 by extrapolation of the Tafel lines to $E_{appl} = E_{corr}$, where $i = i_{corr}$ (Fig. 3.15.).

This method of obtaining corrosion current density is called the Tafel extrapolation method. Extrapolation of the Tafel region in either cathodic or anodic polarisation curve to the corrosion potential will give corrosion current density i_{corr}, and it can be used to calculate corrosion rate. It is advantageous to use computer software to record polarization curves and analyze the experimental data in terms of parameters such as βa, βc, and i_{corr}. From the numerical values of βa and βc, conclusions concerning the rate- determining step in the reaction mechanism can be made. From i_{corr}, the corrosion rate can be calculated using Faraday's law. The results of electrochemical measurements can be converted to rates of uniform corrosion [106].

3.2 Substrate materials and specimen geometries

According to the test condition requirements different types of specimen geometries have been chosen for the coatings deposition. Furthermore, in the case of friction investigations (pin on disc test) standard Almen strips were used and for the sliding wear resistance test of inner surfaces (cylinder on ring tests) there were employed ring specimens (d_{min}=130) and cylinder bars (as the stationary specimen). Additionally, disc-like specimens (Ø 14mm) were necessary in order to perform the corrosion tests, see the figure below.
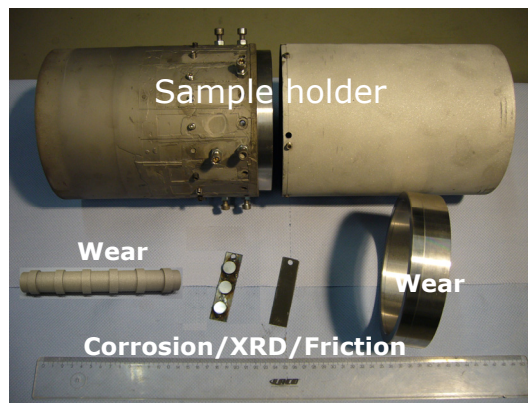

Figure 3.16 ID sample holder and the specimens geometry

The ring material is a quality steel, unalloyed, with a hardness of 47 HRC based on 1.0580 (S52) material. This is a hot rolled product of structural steel in accordance with DIN EN 10297 (2003) for steel construction, having a tensile strength between 500-680 N/mm^2. Based on the UV spectral analyses the chemical composition of this steel is presented in table 3.1.

Table 3.1 Chemical composition of the ring specimen

Element	C	Si	Mn	S	Cr	Fe
*Weight %	0.16	0.19	1.31	0.004	0.05	98.0

* average values based on five measurements

Table 3.2 Chemical composition of the stationary specimen (counterbody)

Element	C	Si	Mn	S	Cr	Fe
*Weight %	0.42	0.27	0.65	0.022	0.25	97.9

* average values based on five measurements

The substrate material of the stationary specimen was a carbon tool steel 1.1730 (C45W) with a tensile strength of 1200 N/mm^2 in compliance with DIN EN ISO 4957 (02/2001) and a hardness of about 42 HRC. Its chemical composition is presented in table 3.2.

3.2.1 Preparation of test specimens (Substrate pre-treatment)

To obtain optimum adhesion between the sprayed layer and substrate, an appropriate pretreatment of the substrate surface is mandatory. First, gross impurities, such as grease and rust must be removed. The subsequent blasting process increases the surface roughness of the base material and guarantees the mechanical interlocking of the sprayed particles as well as the interdiffusion and microwelding phenomena between the base material and the sprayed coating. Not to reduce the tensile adhesive strength due to oxidation or other environmental influences, the recently blasted component must be directly coated.
For the blasting process one should apply only sharpfaced particles of high purity. Rounded edges of the beam particles have a negative impact and harden the surface by a forging effect.
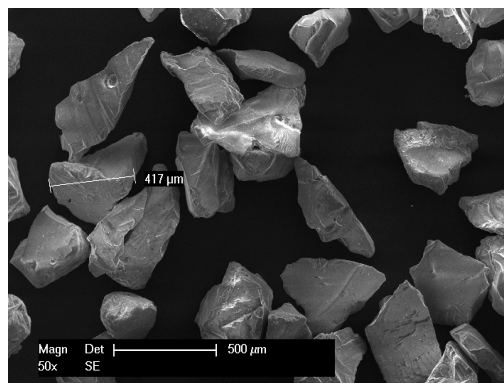

Figure 3.17 Al_2O_3 grit blasting powder

In this work the substrate was degreased, roughened and cleaned prior to the coating process.

For this procedure, the substrate was placed in a gritblasting cabin and treated with 500µm grain size alumina particles (see figure 3.17) achieving round about 3µm as a roughness size on the substrate surface. To ensure a maximum blasting effect, after each set of test specimens, the grit was renewed. It is known that the adhesion of the coating to the substrate can be largely influenced by the grit blasting process. Moreover, this fact could have a negative effect on the tribological performance of the coatings because of the mechanical interlocking splats degree [1]. Thus care in the substrate preparation is paramount to good coating performance.

3.2.2 Preparation steps of the substrate specimen (Example)

One of the objectives of this work was to simulate as near as possible the real work conditions of the moving wear parts coated with different cermet materials. Therefore, the substrate preparation of the specimens used for the wear tests (e.g. ring and stationary specimen) was performed in the same required way as under industrial conditions. The main steps of the surface preparation process are schematically presented in the figure 3.18.
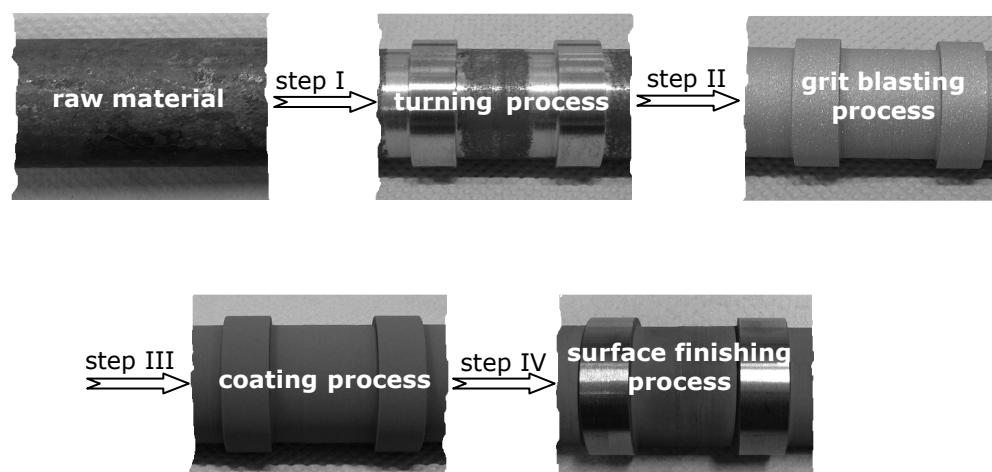
Figure 3.18 The prearrangement steps of the stationary specimen (counterbody)

The ring specimens were prepared similar with the stationary specimen. They were cut at the desired dimensions (d_{max}=150mm; d_{min}=130mm; w=35mm) from a tubular raw material. After the surface finishing process of the coatings, the range of surface roughness (ring, counterbody) was between 0.4µm and 0.9µm according to the powder material used during the spraying process. All the final roughness values will be spreadsheet presented in section 4.4 (Sliding wear resistance of HVOF coatings sprayed on inner surfaces).

3.3 Powder feed-stock materials

Two different commercially available agglomerated/sintered and crushed cermet powders from Thermico GmbH&Co Company were used for the experimental program. Feedstock powders from type WC-Co-Cr 86 10 4 and WC-Cr_3C_2-Ni 70 23 7, with different particles grain seizes were investigated. As already mentioned, each powder type, three fractions of particles were used having the size as follows: -10+2μm, -25+5μm, -45+20μm for the first powder and -10+2μm, -22+5μm, -30+5μm for the latter one. These powders are known to exhibit good wear resistance, due to the ceramic phase and high resistance against corrosion, due to the metallic phase.

3.3.1 WC-Co-Cr powder

Figure 3.19 left shows the SEM micrographs demonstrating the shape and size of the three fractions of WC-Co-Cr powders. On the right side, the X-ray diffraction analysis confirmed the predominance of a large percentage of ceramic phase, WC, between 62 wt.% and 73 wt.%, but not as large as expected considering that the theoretical amount of these powders has to be about 86%. Additionally, a substantial amount of cobalt and tungsten containing subcarbides as Co_2W_4C, was also recorded by all the investigated powders. Moreover, it can be observed that the quantity of Co phase is very low ~ 5 wt.% instead of 10 wt.% (theoretical wt.%). This fact indicates that during the powder processing (sintering) a metallurgical reaction between Co and WC occurred, diminishing thereby the Co content and that of the WC phase as well. In terms of Cr content, this corresponds with the theoretical one in the case of all powders.

3.3.2 WC-Cr_3C_2-Ni powder

In contrast to the previous powder type, the recorded XRD patterns (Fig. 3.20 right) of both ceramic phases WC and Cr_3C_2 indicate approximately the similar phase composition given by the powder producer, namely for WC=70 wt.% and for Cr_3C_2=23 wt.%. Consequently, it should be noticed that the identified metallic binder (Ni) content of the fine and medium sized powders (Fig. 3.20 d and e) shows a lower value (3 wt.% in both cases) in comparison with the coarse powder (Fig. 3.20 f) which has a Ni amount near to the theoretical one, namely 6 wt.% instead 7 wt.%. The amount of Ni may be influenced by the particle size of the WC or Cr_3C_2-powder. A finer powder fraction means a larger specific surface area and implies the probability to "hide" better the Ni-particles whereas these are better detected during X-ray measurements of the coarse powder.
The XRD spectrum of the coarse powder (Fig. 3.20 f) shows also an unusual ceramic phase which is the Cr_7C_3. Generally, these kinds of powder should contain the ceramic phase in form of Cr_3C_2.
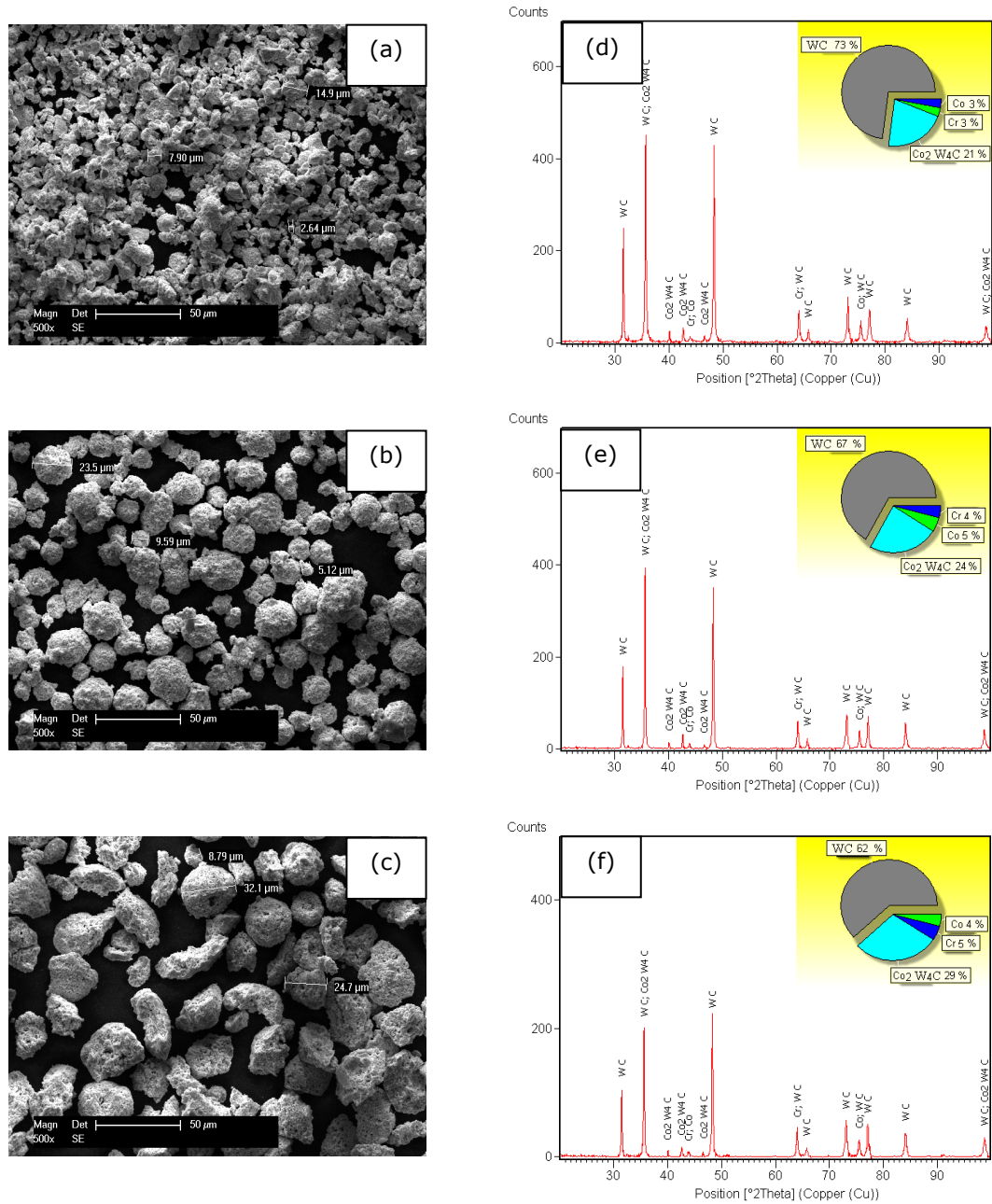
Figure 3.19 SEM morphology of the WC-Co-Cr 86-10-4 powders (left side): (a)-fine, (b)-medium and (c)-coarse powder; the corresponding X-ray diffraction patterns (right side)
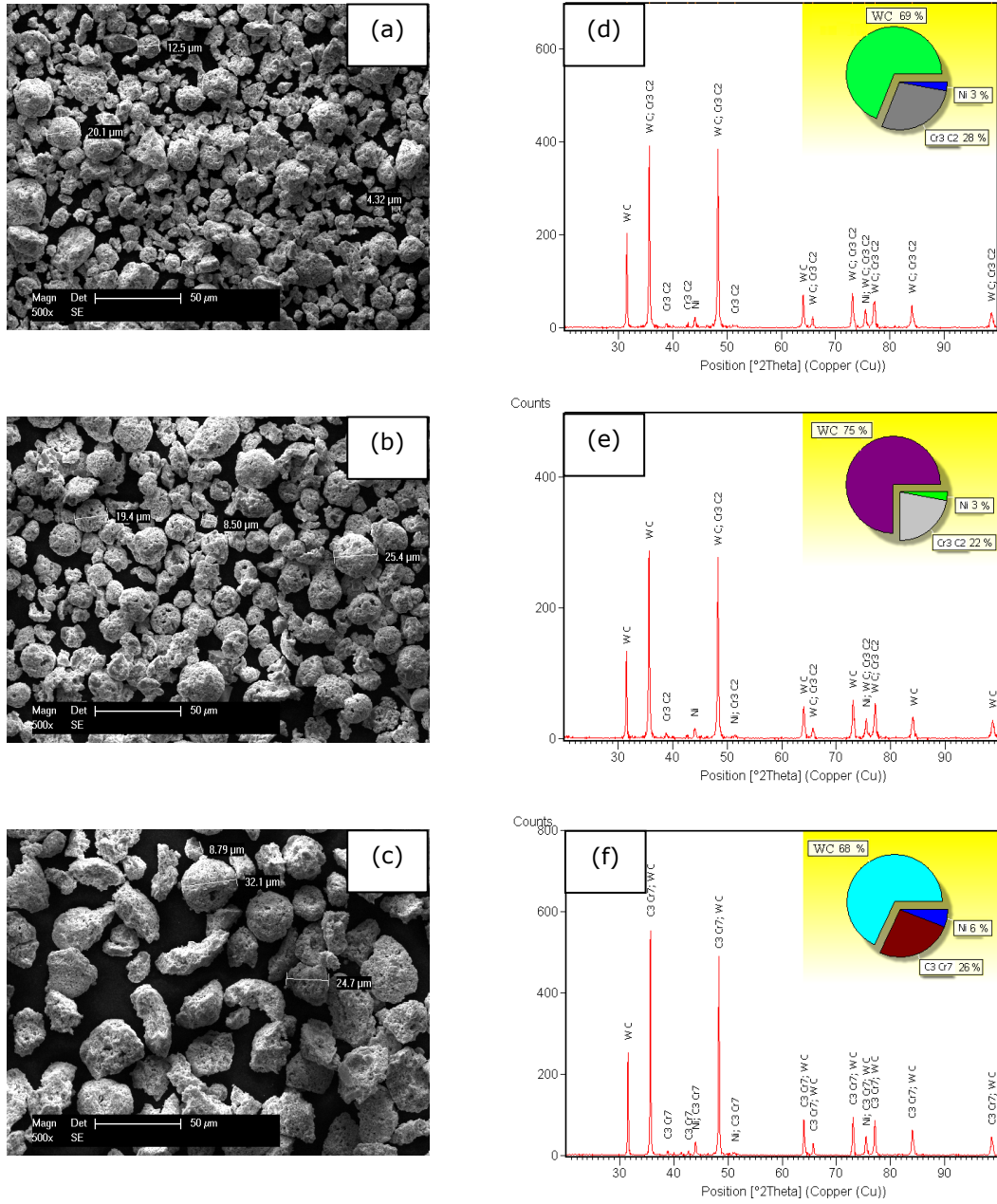
Figure 3.20 SEM morphology of the WC-Cr$_3$C$_2$-Ni 70-23-7 powders (left side): (a)-fine, (b)-medium and (c)-coarse powder; the corresponding X-ray diffraction patterns (right side)

3.4 HVOF spraying process on inner surfaces

The HVOF coating process for all the specimens used in this work was carried out at the company Thermico GmbH. The carbide containing coatings were produced by HVOF using two different systems: the fine and medium powders were sprayed using an ID CoolFlow Mono gun developed especially for inner surfaces (Fig. 3.23) and the coarse powders (-30+5µm, respectively -45+20µm) were sprayed with a CJS gun by angling it to maximum of 60° off-normal (Fig. 3.22 (a)). The usage of the latter one was necessary, because of the inability to spray coarse powder with the ID gun. Moreover, for a practical simulation of typical wear resistance parts, the stationary specimen (cylindrical axle) was coated also by CJS gun (Fig. 3.22 (a)) and the ring specimen, as already mentioned, with the ID gun. This is another important aspect which has to be considered during sliding wear of two components with complementary geometries (an OD coating will slide against an ID coating).

A special sample holder was designed for the ID CoolFlow spraying process in order to realize the coating deposition under the same conditions on all the specimen geometries which are required for different investigation tests. Thus the same coating properties are guaranteed.
The holder consists of two 152mm ID steel tubes with threaded holes (see figure 3.16) through which the corresponding set screws are fixing the rings and also the others specimens, as it can be seen in figure 3.21, left side. All the specimens were coated from inside the tubes using the ID gun, see figure 3.21, unless otherwise noted above or in figures.

This alignment (sample holder) was fastened on a turntable which rotates at a constant revolution speed of 181 rpm. To ensure evacuation of the backscattered particles and the hot flue gases, the turntable is equipped with an internal exhaustion system. During and after the HVOF process, the substrate was cooled by an air nozzle and the temperature monitored by an infrared temperature sensor, see figure A.1 in appendix.

Figure 3.21 Special test set-up for internal coatings using ID CoolFlow Mono Gun; sample holder
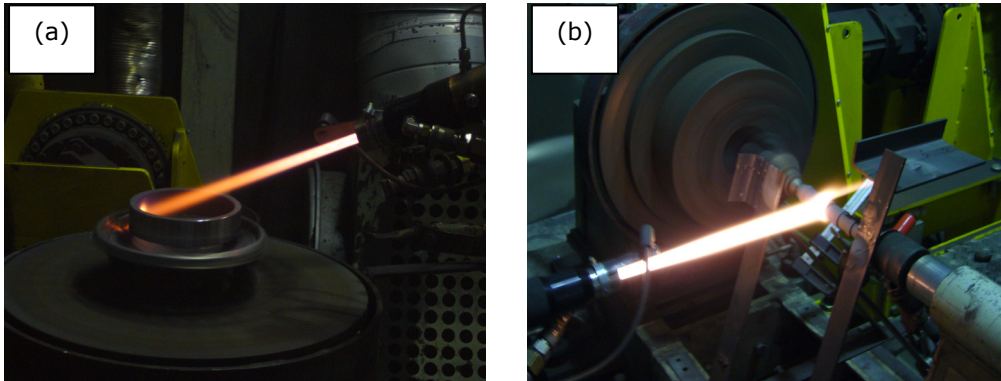
Figure 3.22 OD-HVOF spraying process: ID coating of the ring specimen (a) and OD of the stationary specimen using a CJS-gun* (b)
*only in case of coarse powders and also for the coating deposition of the stationary specimen

Smallest Internal Diameter:
80mm
Power:
5–50kW
Oxygen:
200 – 500 l /min
Kerosene:
1,0– 5 l/h
Hydrogen:
50 –120 l /min
Combustion chamber pressure:
7–18 bar
Powder carrier gas:
Nitrogen 7– 23 l /min
Powder Feedrate:
Max. 40 g/min
Coolant:
Water
Coolant pressure:
Min. 8 bar
Cooling power:
17–40kW
Weight of gun:
2.0 kg

Figure 3.23 ID-CoolFlow Mono HVOF torch [www.thermico.de]

As it was already mentioned above, the inner coatings (excepting the coarse powder) were sprayed using an ID CoolFlow mono gun developed by Thermico Company, see figure 3.23. This gun is a HP HVOF system for high pressure, but cold internal HVOF spraying, designed especially for nano-HVOF applications. Operating at reduced power levels, the ID Cool-Flow mono applies coatings at reduced substrate temperatures. This gun is equipped with a single radial powder injector and designed to spray internal diameters of at least 80 mm. It has a full metal housing equipped with standard extensions for a maximum spray depth up to 1.5meters. The combination of the ID CoolFlow mono with the CPF powder feeder for ultra fine powders of <10 μm is ideal for the spraying of thermo-sensitive components. Powder is applied at up to 40 g/min with a DE of up to 50 %. This high performance is the result of the unique combustion chamber design. The ID CoolFlow mono achieves a combustion chamber pressure of 7 to 18 bars. The use of fine powders allows a power level affecting the substrate of less than 20kW [66]. WC-Co-Cr with powder size fractions between -25+5μm and -10+5μm can be sprayed at reduced power levels. The latter one is much more recommended for usage on ID HVOF applications. These low power levels, combined with an additional air cooling, allow a very short spray standoff (distance from gun to surface) while maintaining a substrate temperature below 200° C, see graph 1 attached in appendix.

Thermico's other gun, namely the Carbide Jet System (CJS) is a highly flexible HVOF gun based on a sophisticated radial powder injection system and adaptable nozzle configurations to guarantee optimum spraying conditions for all powder types and sizes [66]. This gun was developed for OD coatings but it can also be employed for ID coatings, as already was done in this work (Fig. 3.22 (a)). However, it can be only used for IDs if the ID can be reached from outside by angling the gun to a maximum of 60° off-normal. This method has the disadvantage that a good deposition rate and/or high quality coatings may not be achieved. The CJS gun has a high combustion operations pressure of up to 25 bars. The jet temperature is controlled by a kerosene-oxygen system, while the jet speed is controlled by a hydrogen-oxygen system.

3.4.1 Process parameters

Due to the spraying conditions namely, different powders, specimen geometries and also different HVOF guns, it was necessary to change the process parameters corresponding to each situation. These are presented in the following two tables. The first one shows the spraying parameters by using the ID CoolFlow mono gun, respectively the second one by using the CJS gun.

Table 3.3 HVOF spraying conditions in the case of ID mono gun

Specimen geometry	ring/almen strip/disc			
Powder type [µm]	-10+2	-25+5	-10+2	-22+5
	WC-Co-Cr 86 10 4	WC-Co-Cr 86 10 4	WC-Cr$_3$C$_2$-Ni 70 23 7	WC-Cr$_3$C$_2$-Ni 70 23 7
Oxygen [l/min]	160	210	170	210
Nitrogen [l/min]	100	40	100	30
Hydrogen [l/min]	140	140	140	140
Kerosene [l/h]	3.0	4.3	3.5	4.7
Carrier gas [l/min]	11	9	10	10
Spraying distance [mm]	60	60	60	60
Spraying angle [°]	70	70	70	70
table speed [min^{-1}]	181	181	181	181
Robot speed [mm/sec]	6.03	6.03	6.03	6.03
Coating thickness [µm]*	204/320	207/320	182/280	139/280

* the first value is the real coating thickness of the almen strips and discs specimens, see the SEM micrographs, and the second one is the theoretical thickness of the coating rings measured by a thickness gauge after the spraying process

As it can be observed in both tables, the obtained coating thickness was different: the rings and also the stationary specimens have a coating thickness of about 300µm and in case of the other specimens it is up to 200µm. The thickness size for the first two specimens was necessary for obtaining of thicker coatings in order to have sufficient rest coating even after the surface finishing process. Consequently, this process was mandatory for the wear resistance tests, see section 4.4.

It should be also mentioned that, spraying from outside under a 60° angle leads to a very low deposition rate and inevitably the overlaps number is increasing. Additionally, the WC-Co-Cr powder presents a high coating efficiency in contrast with the WC-Cr$_3$C$_2$-Ni powder, especially the medium and the coarse one, exhibiting also (e.g. 60° spraying angle) a low deposition rate, see table 3.3 and 3.4.

Another important issue observed during the spraying process is that according to the powder used (fine, medium or coarse) the spraying distance needs to be changed. For example, the coarser the powder is the bigger the spraying distance must be. Hence, the fine powders are more required to be used for ID HVOF coatings (small spraying distance) and the other one are recommended for OD coatings because no constrained environment occurred (higher spraying distance).

Concerning the spraying process, it can be concluded that for each powder type and/or specimen geometry different process parameters must be used. In the next section there is a short description of the influence of spraying process parameters on the coating properties.

Table 3.4 HVOF spraying conditions in the case of CJS gun

Specimen geometry	ring/almen strip/disc		stationary specimen	
Powder type [μm]	-45+20	-30+5	-45+20	-10+2
	WC-Co-Cr 86 10 4	WC-Cr$_3$C$_2$-Ni 70 23 7	WC-Co-Cr 86 10 4	WC-Co-Cr 86 10 4
Oxygen [l/min]	850	850	850	560
Nitrogen [l/min]	-	-	-	450
Hydrogen [l/min]	110	110	110	140
Kerosene [l/h]	17	16	17	15
Carrier gas [l/min]	16	16	16	16
Spraying distance [mm]	320	320	320	280
Spraying angle [°]	60	60	90	90
table speed [min^{-1}]	180	180	540	540
Robot speed [mm/sec]	12	12	36	36
Coating thickness [μm]	184/320[*]	152/324[*]	300[**]	300[**]

[*] the first value is the real coating thickness of the almen strips and discs specimens, see the SEM micrographs, and the second one is the theoretical thickness of the coating rings measured by a thickness gauge after the spraying process; [**] the theoretical coating thickness measured by a thickness gauge after the spraying process

The above mentioned spraying parameters were established after a long experimental period of time in which a lot of deposition conditions were set for the production of coatings with good morphological and structural properties. One example of the procedure used in order to find out some optimal deposition conditions is given in the follow section.

3.4.2 Procedure to establish optimal spraying conditions

This section describes an ID HVOF process optimization that includes interaction studies between spraying parameters, such as liquid fuel /oxygen ratio, total gas flow, carrier gas and also the standoff distance. Therefore, five samples at different spraying parameters were produced, see table 3.5.
The quality of the obtained WC-Co-Cr coatings was investigated mainly in cross-section micrographs using the optical and scanning electron microscopy. X-ray diffraction was also used for the crystal structures characterization of the as-sprayed coatings. The magnitude of the displayed micrographs is different from coating to coating, depending on its representative microstructure skills.

Table 3.5 HVOF thermal spraying process parameters:

Sample Nr.	1	2a	2b	3a	3b	4a	4b	5
Gun type	ID COOL FLOW M							
Powder type [μm]	-25+5	-25+5		-25+5		-25+5		-25+5
Oxygen [l/min]	210	210		140	300	210		210
Hydrogen [l/min]	140	140		140		140		140
Kerosene [l/h]	3.6	3.6		2	5	3.6		3.6
Carrier gas [l/min]	10,8	10,8		10,8		7	14,8	10,8
Spraying distance [mm]	58	20	70	58		58		58
Spraying angle [°]	70	70		70		70		70
Speed table [min⁻¹]	181	181		181		181		181
Robot speed [mm/sec]	5.8	5.8		5.8		5.8		5.8
Sample temperature [°C]	120	225	105	105	145	120		>400*

* without cooling the substrate using compressed air and without exhaustion system

- Sample 1 (Default parameters)

Sample 1 is called also the master-sample due to its good properties (low porosity, good adhesion and no cracks – see figure 3.24). The spraying parameters of this sample are considered as optimized after a meticulous comparison with the other five which are displayed in table 3.5.
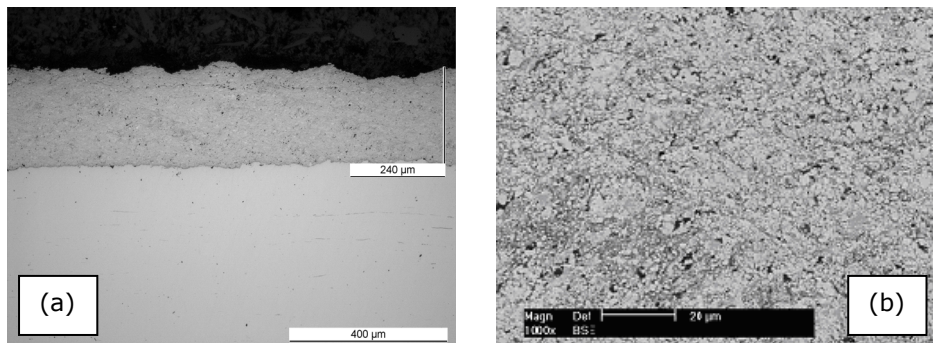
Figure 3.24 Optical microscope images 100x (a); SEM micrograph of the WC-Co-Cr coating (b)

The XRD-spectrum, figure 3.25, displays the phase analysis of the sample 1. One can observe that the W_2C signal is lower than that corresponding to the WC phase. This remark is very important from theoretical point of view; one should avoid the phase transformation WC into W_2C during spraying, due to the fact that the main property, namely the hardness, will be reduced by a high quantity of W_2C phase.
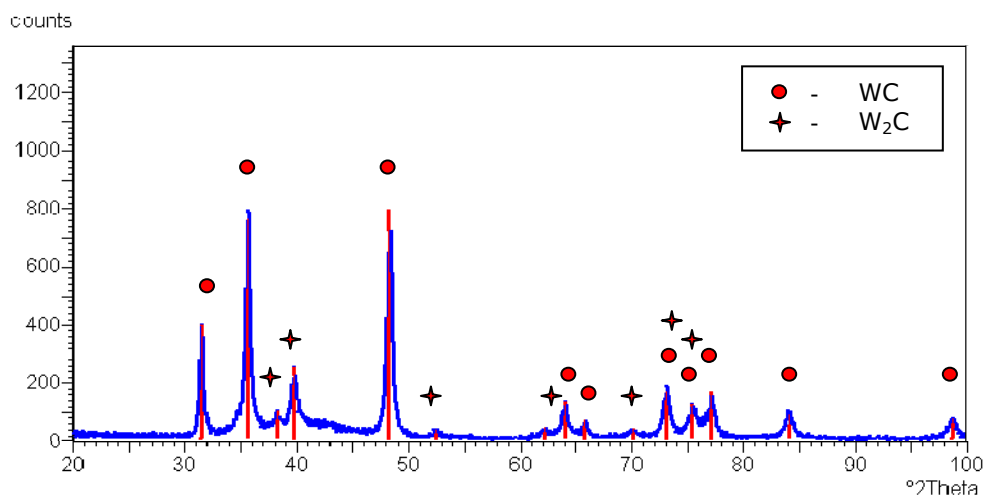
Figure 3.25 X-ray diffraction spectrum-sample 1

- Sample 2 (Spraying distance)

Sample 2 was obtained by modifying the spraying distance in comparison with that used for the coating of sample 1. Therefore, two samples were obtained: sample 2a by reducing the distance down to 20 mm and sample 2b by increasing it to 70 mm.
The microstructure of sample 2a is shown in the cross-section micrograph, figure 3.26. The coating has a reduced thickness due to the high impact of the sprayed particles onto the substrate. The spraying conditions induced a lot of internal stress into the coating leading to the appearance of some cracks and consequently a

partial spallation. This observation explains the irregular coating thickness of this sample.

Moreover, the reduced spraying distance leads to an increase of the sample temperature during spraying, as it can be seen in table above.
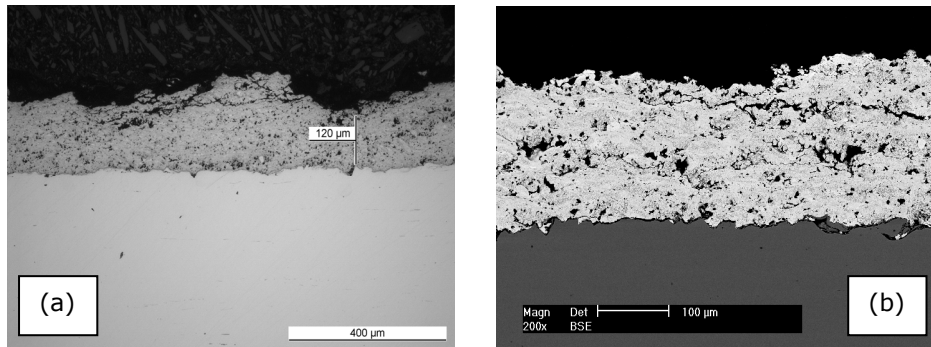

Figure 3.26 Optical microscope images 100x (a); SEM micrograph of WC-Co-Cr coating (b)

The ratio between the WC respectively the W_2C signal is quite reduced in this case, that means that the introduced thermal energy during the coating deposition was higher than that of the sample 1 (compare figure 12 with figure 14). Microhardness measurements should confirm the phase transformation.
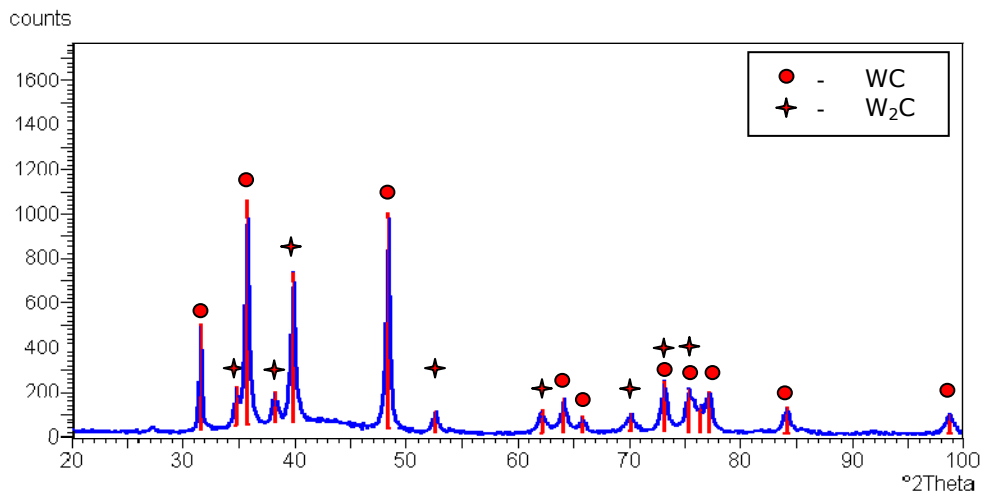

Figure 3.27 X-ray diffraction spectrum-sample 2a

In comparison with sample 2a, the microstructure of the sample 2b in cross-section (Fig. 3.28) shows a better quality (uniform thickness distribution and no cracks). A negative aspect of the properties of this coating is the high degree of internal oxidation (see oxide strings in figure 3.28 b) due to the high spraying distance which means a longer exposure of the particles to the oxidizing atmosphere. On the other hand, a positive aspect is that the sample temperature is lower compared to

sample 2b (see table 3.5) assuring a good adhesion of the coating to the substrate, see figure 28 (a).
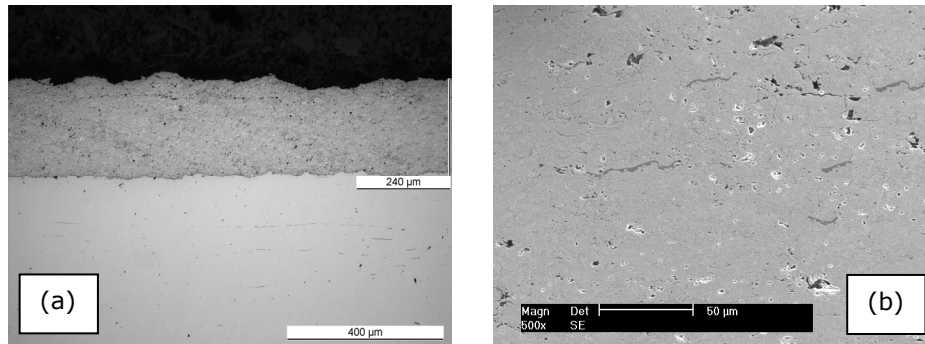

Figure 3.28 Optical microscope images 100x (a); SEM micrograph of WC-Co-Cr coating (b)

The XRD-spectrum (Fig. 3.29) of the sample 2b is similar with that of the sample 2a. This observation confirms that the spraying distance has no great influence on the phase transformation.
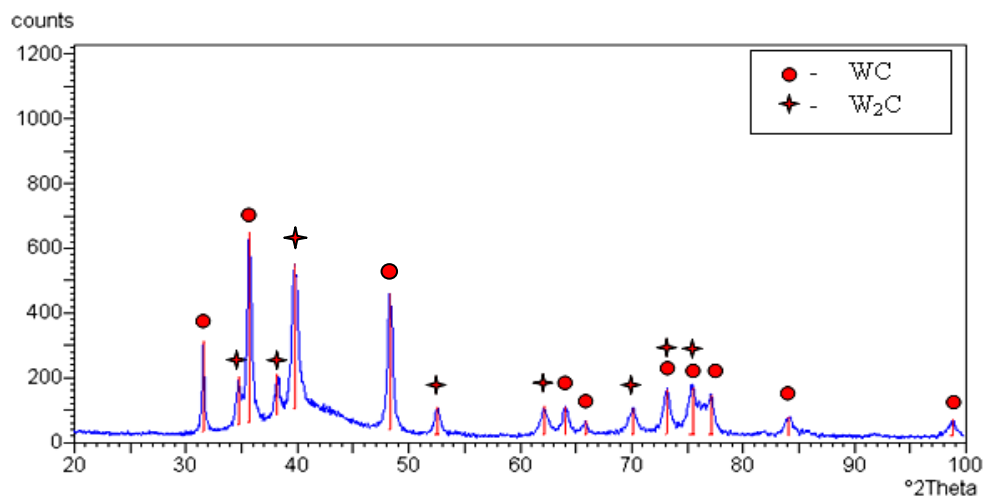

Figure 3.29 X-ray diffraction spectrum-sample 2b

- Sample 3 (Gas feed)

In the case of this sample, the variable parameter is the gas flow: the sample 3a was coated using a lower kerosene flow (2 l/h) respectively oxygen flow (140 l/min) and the sample 3b was obtained by applying higher kerosene and oxygen flow rate (5 l/h respectively 300 l/min).
The degree of flattening stage decreases at diminished gas flows, fact that explains a high coating thickness as it can be observed in figure 3.30 (a). Due to the

presence of unmelted or partially melted particles, the coating has a high degree of porosity, see figure 3.30 (b).
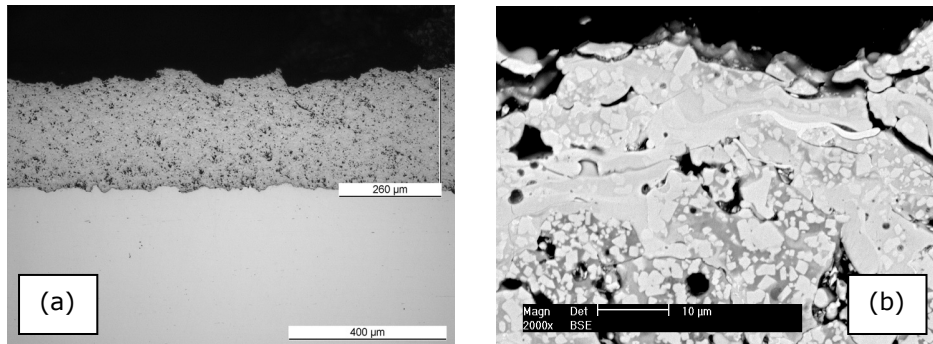

Figure 3.30 Optical microscope images 100x (a); SEM micrograph of WC-Co-Cr coating (b)

Moreover, the peak corresponding to the W_2C phase is very small, see figure 3.31. This phenomenon may be explained by the reduced kerosene flow rate which cannot guarantee an efficient melting of the sprayed particles.
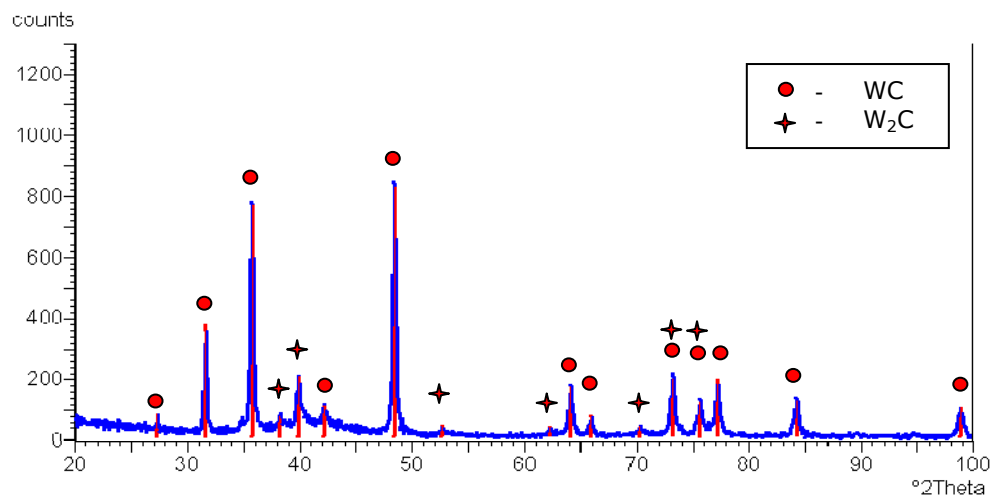

Figure 3.31 X-ray diffraction spectrum-sample 3a

Comparing sample 3a, figure 3.30, with sample 3b, figure 3.32, an improved quality of the coating is observed. This was achieved by enhancing the kerosene and oxygen flow rate, at a constant hydrogen flow.
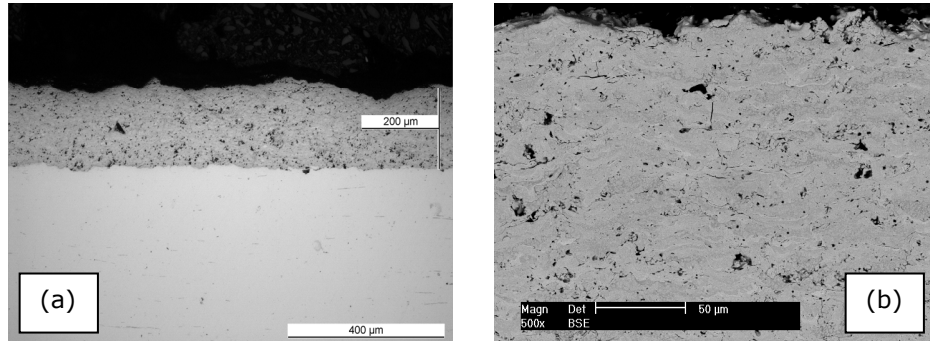
Figure 3.32 Optical microscope images 100x (a); SEM micrograph of WC-Co-Cr coating (b)

Increasing the gas flow rates will inevitably lead to a high thermal energy of the system which will favourize the formation of the W_2C phase, see the XRD-diffraction pattern in figure 3.33, the intensity of the W_2C peak is clearly higher in comparison with the WC signal.
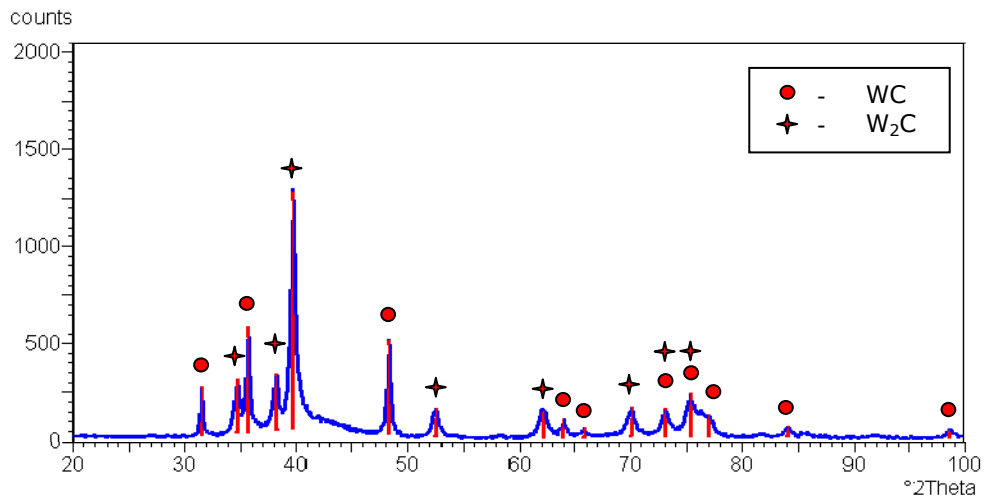

Figure 3.33 X-ray diffraction spectrum-sample 3b

- Sample 4 (Carrier gas-nitrogen)

As a sequentially step in the samples production, the flow rate of the carrier gas was also modified. By reducing the gas flow rate from 10.8 down to 7 l/min the sample 4a was obtained and similarly, the sample 4b was produced by increasing the flow rate up to 14.8 l/min. In figure 3.34 one can observe that by reducing the nitrogen flow rate (carrier gas) the porosity degree of the coating is very high due to the insufficient powder feeding rate. This factor leads to a reduced coating thickness as well.
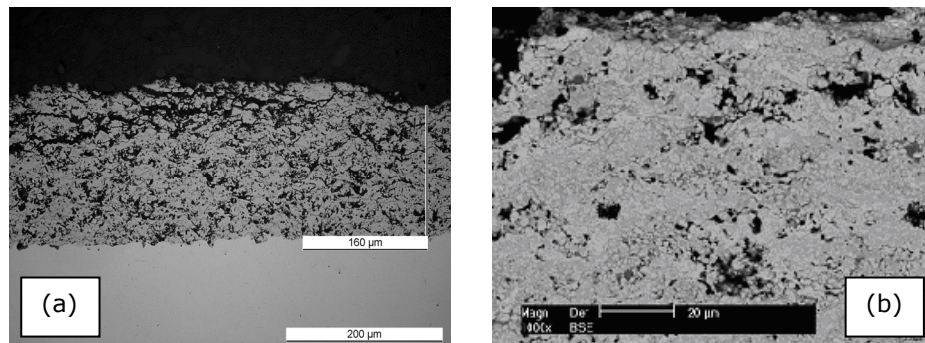
Figure 3.34 Optical microscope images 200x (a); SEM micrograph of WC-Co-Cr coating (b)

A second aspect concerning this sample, having as a principal characteristic the constant thermal energy, similar like in the case of the other samples, but with a much lower powder feeding velocity. The XRD spectrum (Fig.3.35) has identified as a predominant signal the peak of the W_2C phase as a consequence of the unusual ratio between the energy input and the quantity of powder.
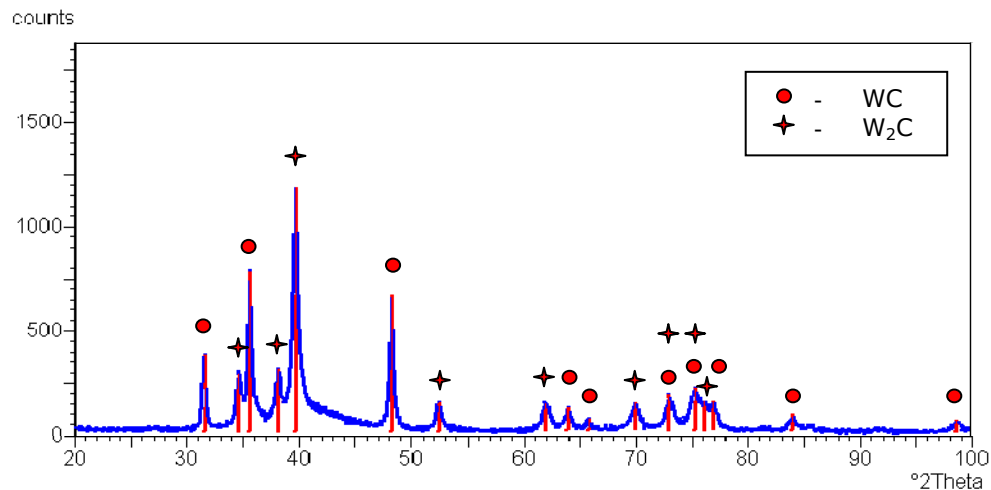

Figure 3.35 X-ray diffraction spectrum-sample 4a

The optical micrograph of the sample 4b in cross section presented in figure 3.36a shows the quality of the coating obtained at high nitrogen flow rate during spraying. The thermal energy seems to be quite low for such conditions especially regarding the powder feeding rate. As a consequence some unmelted or partially melted particles in the coating may be clearly observed in the micrographs (Fig. 3.36b).
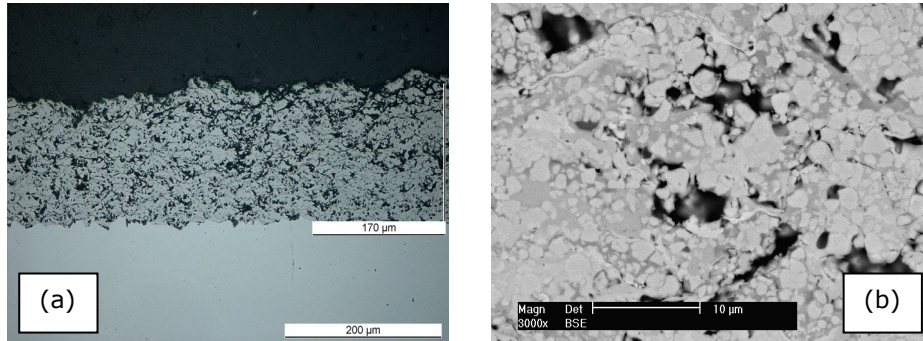
Figure 3.36 Optical microscope images 200x (a); SEM micrograph of WC-Co-Cr coating (b)

The XRD-pattern (Fig. 3.37) recorded a minimal phase transformation, an expected phenomenon for such spraying conditions (constant thermal energy and high nitrogen flow rate, introduced in the system).
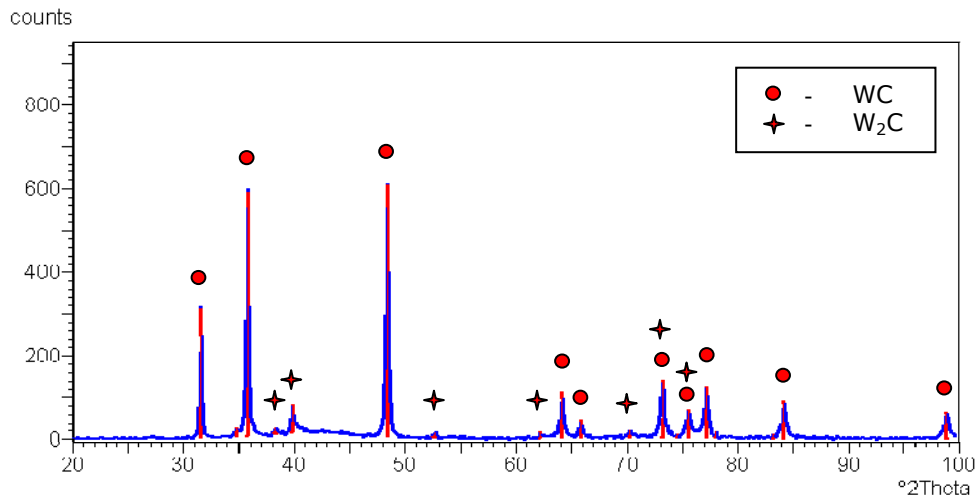

Figure 3.37 X-ray diffraction spectrum-sample 4b

- Sample 5 (Without exhaustion)

For further investigation regarding the influence of some spraying parameters on the coatings properties, the exhausting and the substrate cooling systems were switched off. There is expected a substantial increase of the sample temperature which should have a great impact on the adhesion of the coating to the substrate.
During the deposition process, the sample temperature was higher than 400°C and therefore the depletion of the applied coating occurred immediately after finishing the process, see figure 3.38. Due to the improper spraying conditions, an increase in the W_2C phase is also observed (see diffraction pattern figure 3.39).
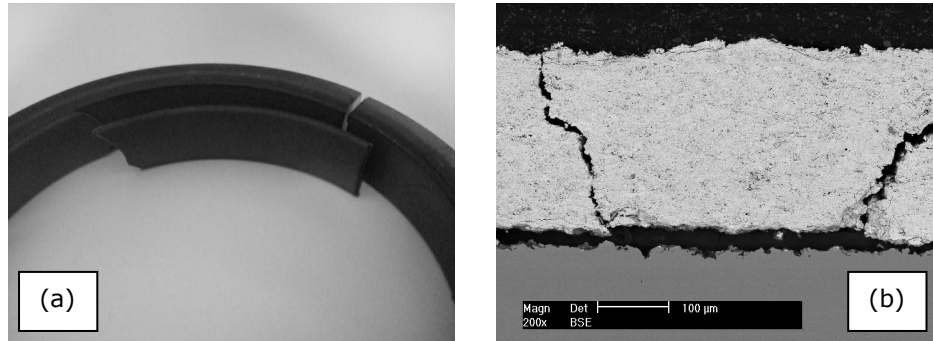
Figure 3.38 Photograph of the coated ring (a); SEM micrograph of WC-Co-Cr coating (b)
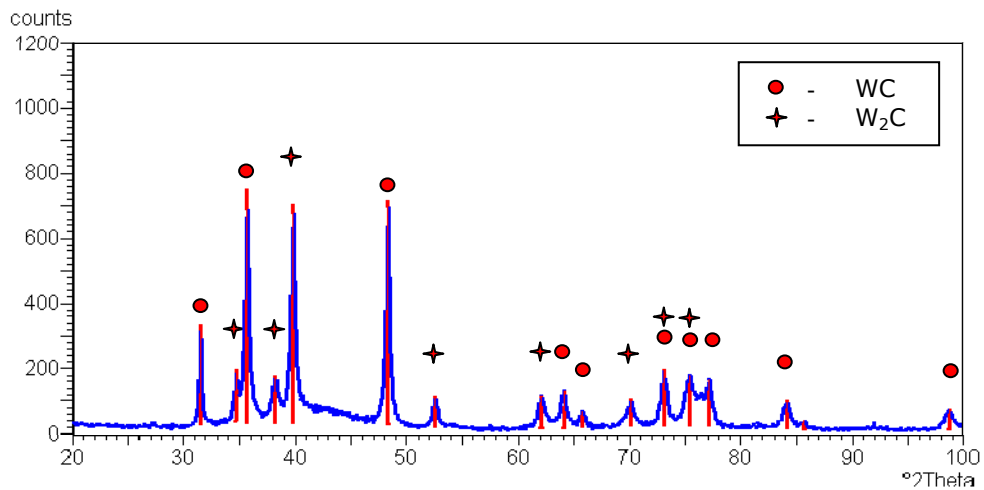

Figure 3.39 X-ray diffraction spectrum-sample 5

Spraying the fine grained powder under the same operating conditions like the coarse one, the generated thermal energy is distributed to a relatively higher total surface of the deposited material. Reported to a single particle, there is a rescue to volatilize certain powder particles due to the overheating phenomenon, fact which will increase the coating porosity. Beside the already mentioned tasks, there is expected to identify a high quantity of W_2C phase.

Chapter IV

RESULTS AND DISCUSSION

4.1. Microstructure of thermally sprayed coatings

All the sprayed coatings were cross-sectioned, polished and examined by the means of scanning electron microscopy (SEM), equipped with energy dispersive spectrometry (EDS), see section 3.1.1. The magnification used when examining the cross-sections varied from 250x to 5000x, in order to assess the coating/substrate interface, coating thickness as well as morphology and microstructure. Moreover, the phase composition was determined by means of X-Ray diffraction measurements.

As it is already known, the microstructure of an HVOF sprayed coating is a complex mixture of lamellas formed from melted or semi-melted particles as well as from some irregularities. These types of coatings may typically contain oxide strings due to the oxidation of the particles in the hot flame and also some cracks due to the relaxation of residual stresses.
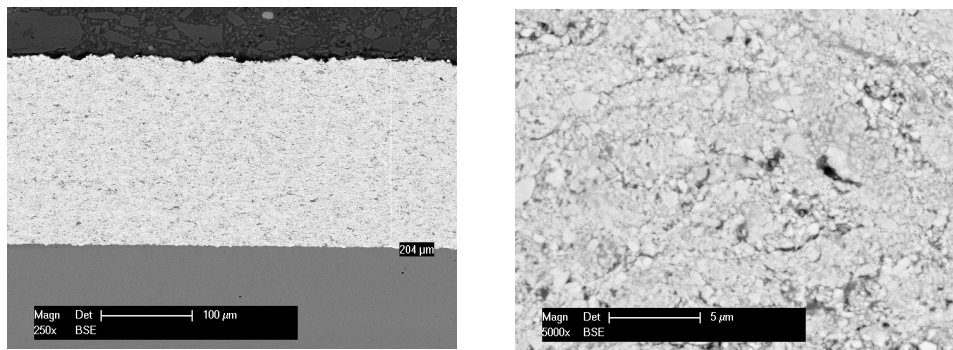

Figure 4.1 SEM micrographs of the WC-Co-Cr (-10+2µm) coating
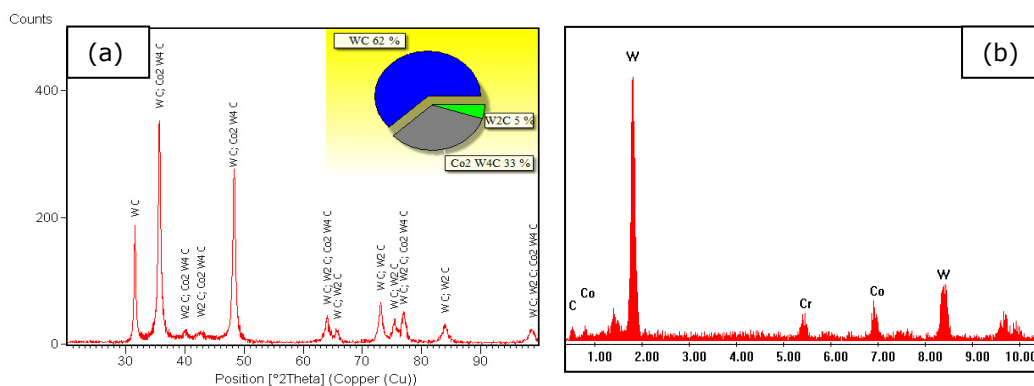

Figure 4.2 X-Ray diffraction pattern (a) and EDS analysis (b) of the WC-Co-Cr (-10+2µm) coating

Besides of the previous defects stated above three typical groups of porosity can be identified: interlamellar pores, interconnected pores and/or globular pores. Generally, all the investigated coatings showed a good adhesion to the substrate, but various microstructures and amounts of porosity. Figure 4.3 shows a high degree of interconnected pores. These pores are formed mainly due to the melting stage and the impact velocity of the particles which are influenced by the spraying process parameters. Another cause of such a porous coating is the WC grain size, measured in figure 4.3-right, different from grain to grain which means also different melting stages that conducted to a reduced cohesion between the splats.

However, the XRD patterns show a light transformation (between 2%-5%) of the WC-phase into the W_2C-phase, which normally by such coatings may occur more pronounced during the deposition process. A positive aspect, knowing that a high decomposition of WC leads to a fragile mixture of W_2C, WC and free carbon (graphite) in the coating composition.
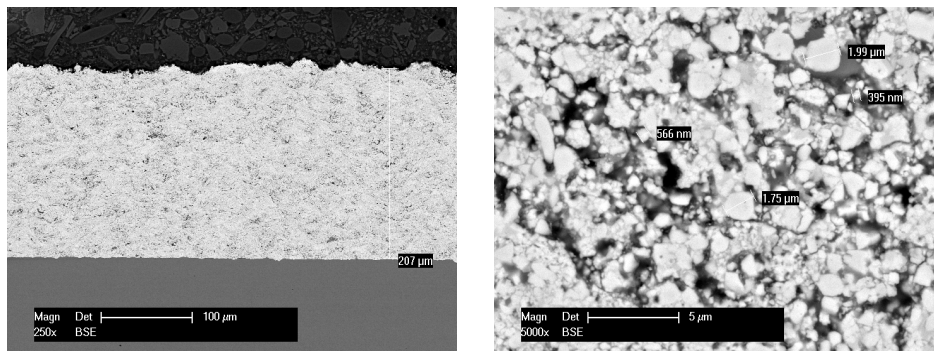

Figure 4.3 SEM micrographs of the WC-Co-Cr (-25+5µm) coating

Figure 4.4 X-Ray diffraction pattern of the WC-Co-Cr (-25+5µm) coating
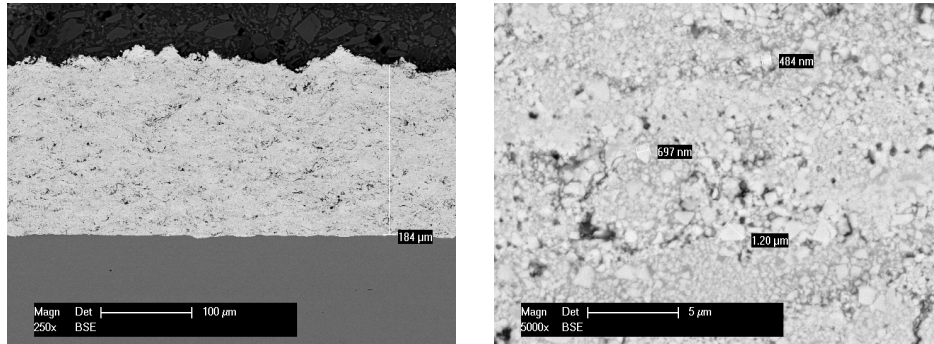
Figure 4.5 SEM micrographs of the WC-Co-Cr (-45+20µm) coating
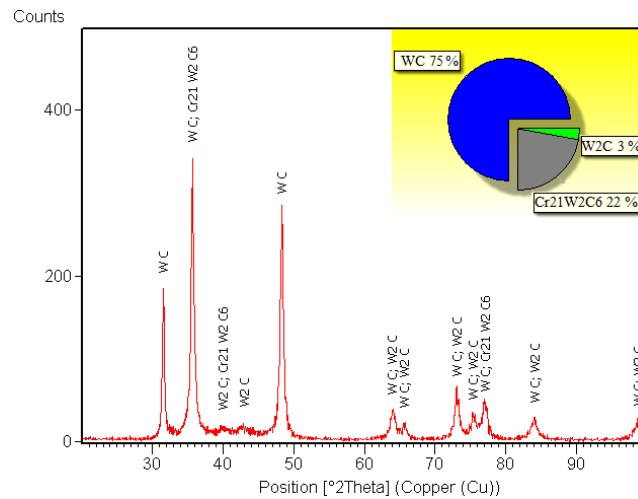

Figure 4.6 X-Ray diffraction pattern of the WC-Co-Cr (-45+20µm) coating

Figure 4.7 SEM micrographs of the WC-Cr$_3$C$_2$-Ni (-10+2µm) coating
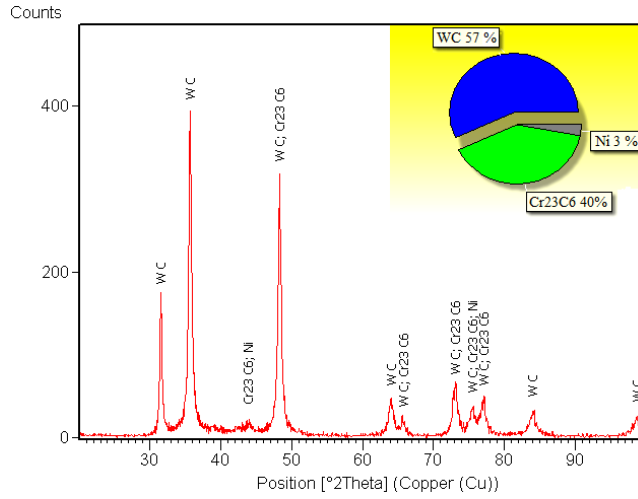
Figure 4.8 X-Ray diffraction pattern of the WC-Cr$_3$C$_2$-Ni (-10+2μm) coating
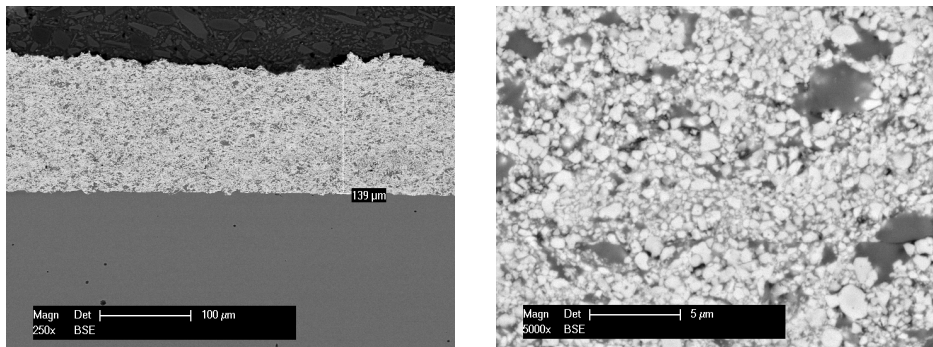
Figure 4.9 SEM micrographs of the WC-Cr$_3$C$_2$-Ni (-22+5μm) coating
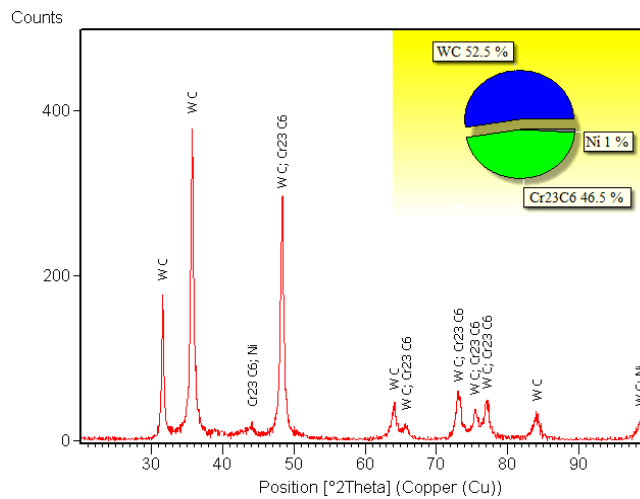
Figure 4.10 X-Ray diffraction pattern of the WC-Cr$_3$C$_2$-Ni (-22+5μm) coating
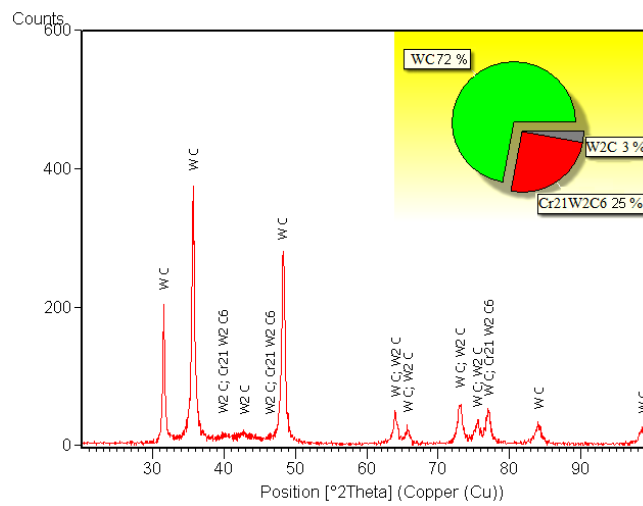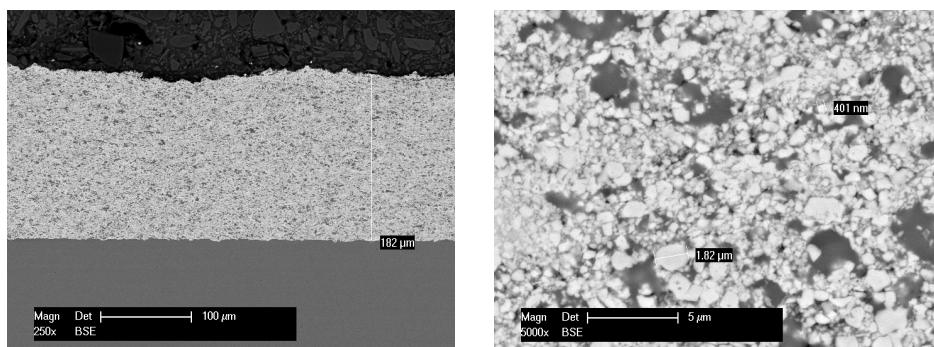
As expected the EDS point analysis (Fig. 4.11 b) illustrates, the predominance of the ceramic phases WC (see 1) and Cr_3C_2 (see 2) dispersed in a metallic Ni binder (see the arrows 3).

By comparing the thickness of all the investigated coatings it can be concluded that the WC-Co-Cr coatings are generally thicker than the WC-Cr_3C_2-Ni layers. This statement is based on better deposition rate for the CoCr based cermet powder during the spraying process. Furthermore, it was demonstrated that using fine powders, the structure of the obtained coatings (under ID conditions) is denser and finer. However, the most important factors which influence the coating microstructure are the spraying parameters.
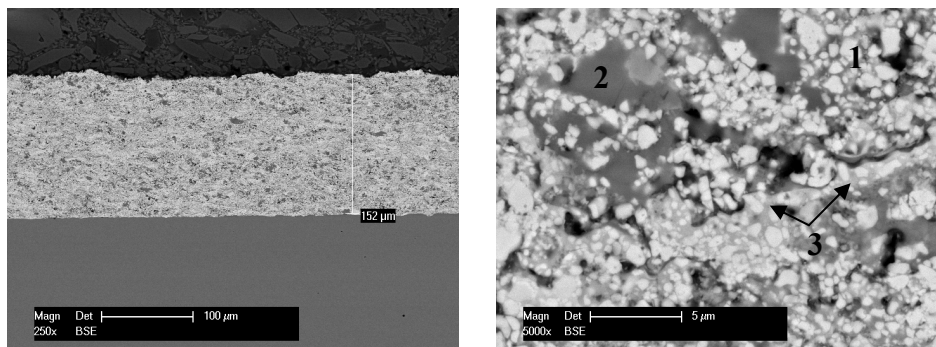
Figure 4.11 SEM micrographs of the WC-Cr_3C_2-Ni (-30+5µm) coating
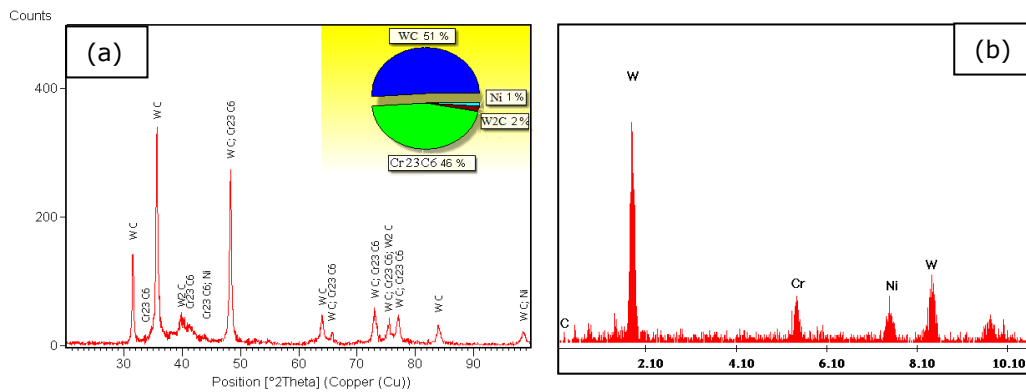
Figure 4.12 X-Ray diffraction pattern (a) and EDS analysis (b) of the WC-Cr_3C_2-Ni (-30+5µm) coating

4.2 Microhardness measurements

It is generally known that hardness is an important factor which significantly affects the sliding and abrasive wear resistance of materials. Therefore, the microhardness measurements were performed along the polished cross-section of the coatings in eight random locations using a microhardness tester. Figure 4.13 shows the modality of Vickers indentation measurements (rhombus diagonals) using a digital microscope. The load used for determining the Vickers microhardness was 300 pounds/15 seconds by each measurement (HV 0,3\15s).
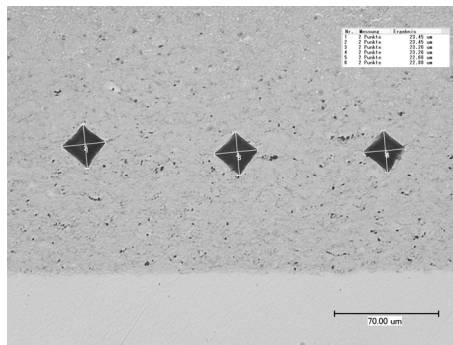
Figure 4.13 Vickers indentation measurements

The microhardness results of the investigated coatings are presented in figure 4.14. There are no significant differences between the tested specimens, even in the case of different phase composition. The lowest value was measured for the coating obtained from the coarse WC-Cr_3C_2-Ni powder (983 HV 0.3) and the highest value corresponds to the coating sprayed with -22+5µm WC-Cr_3C_2-Ni powder. Correlating the coating microhardness with the obtained microstructures (see figures 4.3 and 4.11) one may observe that the porosity degree has the highest influence on the microhardness.
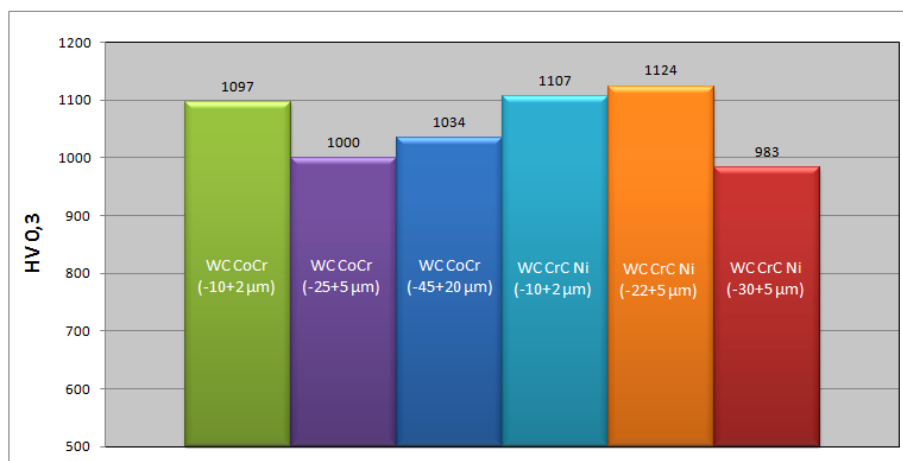
Figure 4.14 Vickers microhardness HV 0.3 of the HVOF coatings

The XRD-patterns of all tested specimens show a certain amount of η-phase ($Cr_{21}W_2C_6$, and/or Co_2W_4C) which is known as hard and brittle. The results of the microhardness measurements for WC-Co-Cr coatings correlate in a good manner with the quantified amount of the η-phase. The higher the ratio of the brittle phases, the higher is the coating hardness.

The presence of such phases has been not confirmed by the measured XRD-spectra of the WC-Cr_3C_2-Ni coating. Therefore, the $Cr_{23}C_6$ phase was identified in the as-sprayed coatings, instead of Cr_3C_2 or Cr_7C_3 observed by the X-ray diffraction patterns of the powders (section 3.3.2). Only the WC from the chemical composition of the coarse powder suffered during thermal spraying a light decarburization to W_2C, phenomenon which slightly influence the coating microhardness.

4.3 Friction behaviour of HVOF coatings sprayed on inner surfaces

The friction tests were performed using a pin on disc arrangement (POD), see section 3.1.4. This test design was chosen because the cylinder on ring wear tester is not equipped with a friction coefficient transducer providing on-line measurement of the friction force. Consequentially, the coated almen strips were used as test specimens rotating against a static WC-Co ball of 6 mm diameter as counterbody under ambient conditions. WC-Co ball was selected in order to assure similar testing conditions like those of the cylinder on ring sliding wear tests, where the counterbody was coated with fractions of WC-Co-Cr powders (see the next section).

However, the pin on disc testing parameters were required to be first optimised in order to be able to deliver consistent and accurate results and to achieve a stability level of the friction coefficient, as well. Therefore, a number of tests were performed. Three of the most important tests, where the linear speed and the number of laps (cycles) were varied are attached in appendix.

After the process optimisation it was concluded that these coatings (WC-based) required besides a longer test duration (100 000 laps) also a high intensity test (40cm/s), in order to achieve the value of a stabilized level for the friction coefficient (μ_{max}, see appendix). The optimised testing parameters (work parameters) were kept constant for all the tested specimens and are presented in the table below:

Table 4.1 Pin on disc test parameters

counter-body	normal load [N]	linear speed [cm/s]	rotational speed [min^{-1}]	radius [mm]	stop condition [lap]	sliding distance [m]	test duration [s]
WC-Co ball	10	40	475	8	100 000	5150	12900

Due to the fact that the maximum load which can be applied on the tested specimens with this wear tester is about 10N, there was necessary to optimise the testing conditions, especially the testing time until coefficient of friction fixes on a steady level.

Prior to the tests, all the specimens surfaces were polished to an average roughness (Ra) of 0.13µm, cleaned with acetone and dried in hot air. The temperature and the relative humidity varied between 20 and 25 °C and between 45 and 55%,

respectively. Additionally, it has to be mentioned that each test was minimum three times repeated in order to achieve reproducible results.

4.3.1 Friction behaviour of WC-Co-Cr and WC-Cr$_3$C$_2$-Ni coatings

The coefficient of friction was continuously monitored during the POD tests. All the WC-Co-Cr coatings exhibited a stable frictional behaviour with no evidence of a significant increase of friction coefficient after 100 000 laps, see figure 4.15. An exception makes curve 1: throughout the first 2500 laps the friction coefficient raises to approximately 0.48μ_{max} and afterwards it decreases and remains stable. The coating obtained from coarse powder (curve 3) exhibits the lowest coefficient of friction and also the lowest standard deviation value, see table 4.2. From the test results it appears that there is no significant difference between friction behaviour of the WC-Co-Cr coatings sprayed with fine, medium and coarse powder. Based on the maximum values of the friction coefficient, these are ranged between 0.3μ_{max} and 0.5μ_{max}. However, the average coefficient of friction of the WC-Co-Cr coating can be approximated with 0.4μ.
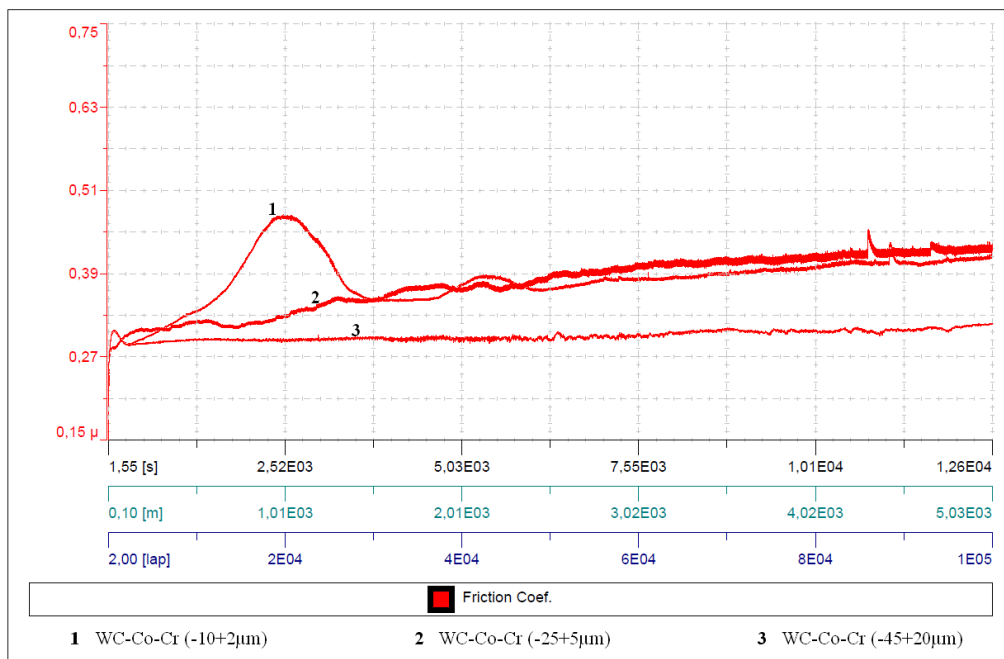

Figure 4.15 Friction coefficient of the WC-Co-Cr coatings

Table 4.2 Friction coefficient (μ) values of the WC-Co-Cr coatings

Sample name	μ_{min}	μ_{max}	μ_{mean}	Standard deviation
WC-Co-Cr (-10+2µm)	0.16	0.48	0.38	0.037
WC-Co-Cr (-25+5µm)	0.10	0.50	0.37	0.028
WC-Co-Cr (-45+20µm)	0.20	0.32	0.30	0.007

In contrast to the above described results, the values for the friction coefficient of the HVOF sprayed WC-Cr$_3$C$_2$-Ni rised up to μ_{max} 0.7. Additionally, the curves display an unstable frictional behaviour with lot of fluctuations, see figure 4.16. Comparing curve 6 with curve 3 from figure 4.15 it seams that in both cases the coatings obtained from coarse powder exhibits an superior friction stability, fact confirmed also by the standard deviations values (the lower ones), see table 4.2 and 4.3. This observation can be explained by correlating the hardness values (see figure 4.14) of these coatings with the corresponding friction curve. Consequently, both coatings have a hardness of around 1000 HV 0.3 which involves also smoother surfaces in comparison with the other one (~1100 HV 0.3). Based on that, this friction stability (see curve 3 and 6) can be attributed to a rapid polishing process during the sliding test, establishing a smooth wear track surface, by ploughing away the smooth surface asperities or roughness peaks. As the test proceeds further, the wear track becomes smoother and the coefficient of friction fixes on a steady level. On the other hand, the instabilities of the others friction curves should be due to a continuous breaking and regeneration of micro-junctions and indicate a continuously changing interaction (interlocking) at the ball on specimen contact surface.
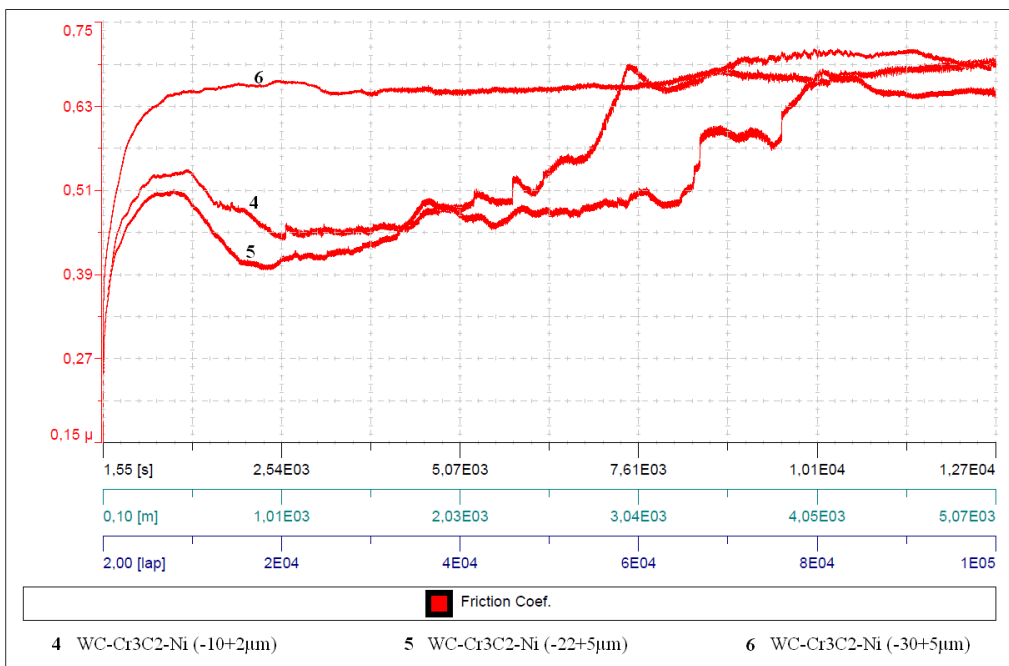
Figure 4.16 Friction coefficient of the WC-Cr$_3$C$_2$-Ni coatings

Table 4.3 Friction coefficient (μ) values of the WC-Cr$_3$C$_2$-Ni coatings

Sample name	μ_{min}	μ_{max}	μ_{mean}	Standard deviation
WC-Cr$_3$C$_2$-Ni (-10+2µm)	0.15	0.71	0.57	0.098
WC-Cr$_3$C$_2$-Ni (-22+5µm)	0.21	0.68	0.52	0.089
WC-Cr$_3$C$_2$-Ni (-30+5µm)	0.25	0.70	0.66	0.039

Based on a general comparison of all obtained values for friction coefficient, one can conclude that the WC-Co-Cr coatings revealed a superior friction performance (lower values of friction coefficient) than the WC-Cr_3C_2-Ni coatings.

In addition, some other investigation were carried out in order to elucidate (quantified by means of XRD-measurements) the above mentioned results. Therefore, the content of hexagonal WC of each sprayed coating was compared with the coresponding μ_{mean} values, see figure 4.17. It was demonstrated that the higher the WC content the lower is the friction coefficient. This observation correlates very well with theoretical refrences which mention that materials containing a high amount of hexagonal phases exhibit a good sliding wear behaviour.
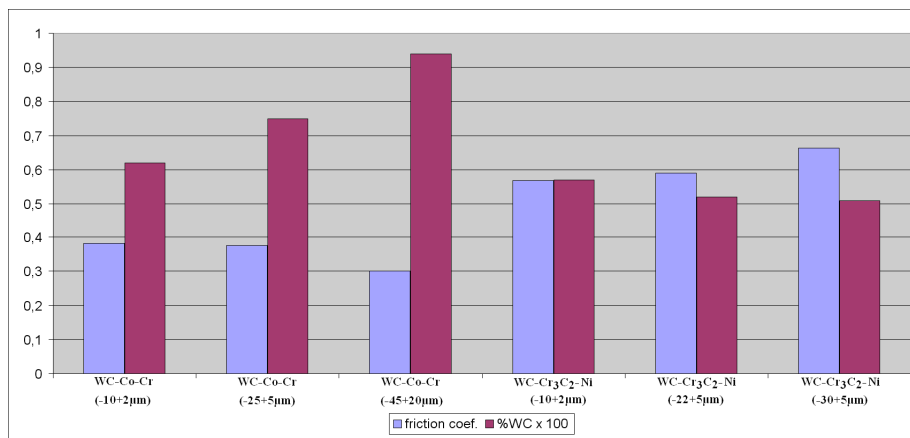
Figure 4.17 Friction coefficient as a function of WC content

As it can be observed in figure 4.18, examination of the coating surfaces with the resulted wear track, white powder in form of wear debris was formed during the friction tests. This phenomenon was observed for all the investigated specimens. The appearance of this powder on the surface specimens was quite different, depending on the phase composition. For the WC-Co-Cr coatings the formed powder was displayed as a continuous layer along the worn track edges (Fig. 4.18 a). In the case of WC-Cr_3C_2-Ni coatings it exhibited a fractured appearance (Fig. 4.18 b). This observation demonstrates once again that the sliding wear behaviour of hcp structures has a better tribological response than fcc structure.
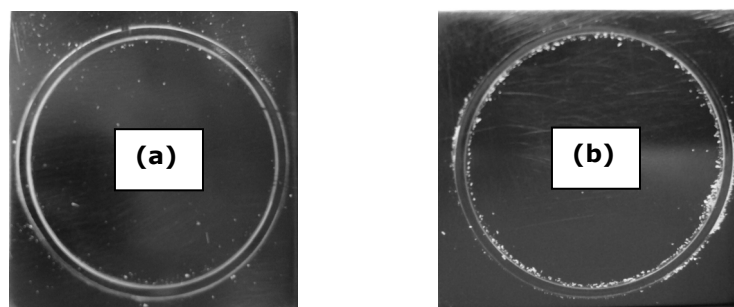
Figure 4.18 The appearance of the worn track: WC-Co-Cr coatings (a); WC-Cr_3C_2-Ni coatings (b)

A closer examination of the resulted wear debris by means of EDS analysis (Fig. 4.19) identified a high amount of tungsten and chromium oxides (oxidation products). Unfortunately there was not sufficient powder for an XRD analysis in order to attest the affirmations done by EDS.

Figure 4.19 The EDS analysis of the collected wear debris

According to the obtained wear tracks it appears that the 10N normal load is not optimal (not high enough) for testing such hard coatings. Unfortunately, this equipment was the only available one and therefore, the testing conditions needed to be adapted in concordance with the tester's capabilities. However, conclusions can be drawn from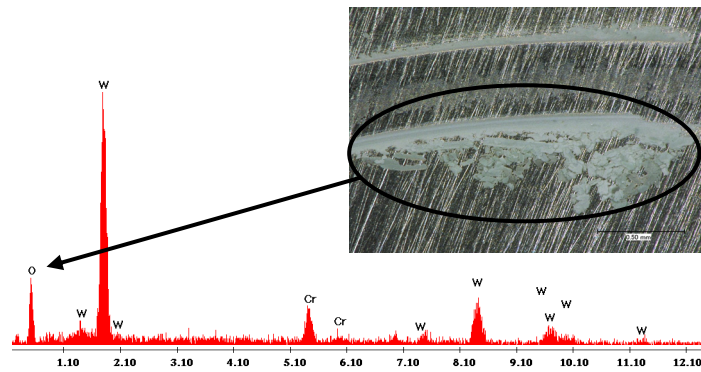 these tests and the results should be taken into consideration, for the specified parameters, although they probably can not offer information about the friction behaviour of such coatings under higher normal loads.

4.4 Sliding wear resistance of HVOF coatings sprayed on inner surfaces

For a complete tribological investigation of the inner HVOF sprayed coatings, besides of the friction investigations, a new wear tester was developed in order to test the sliding wear resistance. The principle of this method is presented in chapter 3. The cylinder on ring method was chosen for two main reasons: practical approach simulation by testing the surfaces under a line contact condition (surface on surface) and the facility with which counterbodies (stationary specimen) from a wide variety of materials can be supplied. Therefore, the counterbody used to examine the wear behaviour of the ring specimens inner surface could be coated with different fractions of WC-Co-Cr powder (-10+2µm and -45+20µm), using thermal spraying processes (e.g. HVOF), see previous chapter. In contrast to this, the pin on ring method which involves specific counterbodies produced through different fabrication methods than HVOF (e.g. sintered ball), implies a difficult purchasing of the desired counterbody.

The stationary specimens (conuterbodies) were loaded against rotating ring type specimens which prior to the tests both required surface finishing with a diamond grinding wheel, see figure A.2 in appendix. Surface roughness measurements of the finished specimens were performed in the perpendicular direction to the grinding direction. The results of these measurements are displayed in concordance with the powder fraction in the following tables.

Table 4.4 Roughness of ring type specimens

Ring nr.*	Roughness Ra/Rz [µm]**	
	as-sprayed	surface-finish
M 1.1	2.20/14.84	0.55/4.08
M 1.2	2.50/17.29	0.56/4.27
M 2.1	4.42/29.09	0.49/3.62
M 2.2	4.42/29.03	0.52/3.82
M 3.1	6.47/39.62	0.58/4.26
M 3.2	6.56/39.23	0.53/4.07
M 4.1	9.03/68.99	0.96/6.38
M 4.2	8.89/67.58	0.90/6.16
R 1.1	5.45/36.09	0.56/4.28
R 1.2	5.40/34.26	0.53/3.97
R 2.1[a]	3.18/22.52	0.51/3.82
R 2.2[a]	6.89/44.21	0.74/5.06
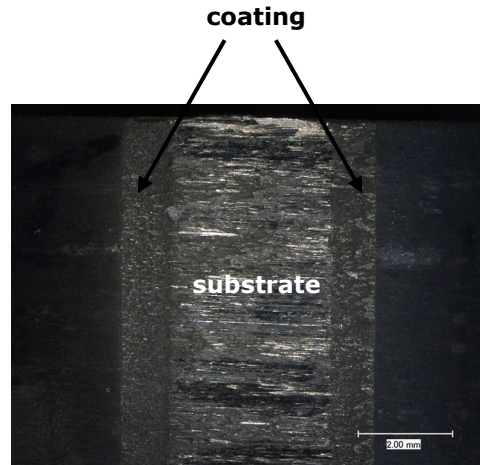
Figure 4.20 Premature wear of the stationary specimen

*see table A.1 in appendix
**average values based on 5 measurements for each specimen
[a] sprayed with the same parameters and powder, but not at the same time

Table 4.5 Surface roughness of the stationary specimens

Stationary specimen WC-Co-Cr powder (**-10+2**µm)	Surface-finish	Stationary specimen WC Co-Cr powder (**-45+20µm**)	Surface-finish
	Ra/Rz [µm]**		Ra/Rz [µm] **
2.1	0.64/4.25	1.1	0.42/3.04
2.2	0.50/3.68	1.2	0.39/2.80
2.3	0.50/3.65	1.3	0.43/3.29
2.4	0.60/4.03	1.4	0.42/3.03
2.5	0.62/4.20	1.5	0.53/3.38
2.6	0.67/4.70	1.6	0.41/3.38
2.7	0.48/3.43	1.7	0.39/2.90
2.8	0.63/4.30	1.8	0.42/3.18
2.9	0.60/4.18	1.9	0.46/3.34
2.10	0.64/4.52	1.10	0.39/2.96
2.11	0.55/4.02	1.11	0.45/3.25
2.12	0.61/4.04	1.12	0.47/3.27
Average value Ra/Rz	0.58/4.08	Average value Ra/Rz	0.43/3.15

**average values based on 5 measurements for each specimen

Additionally, after the wear test, the surface roughness of the wear track on both tribopairs was also measured perpendicular to the sliding direction. Based on that, the Ra difference (Δ Ra) could be calculated, see table A1 in appendix.

From the above roughness measurements one can observe that the stationary specimens sprayed with WC-Co-Cr coarse powder have a lower average roughness that those sprayed with finer powder. This result can be attributed to the CJS gun designed for OD coatings which generally is employed to spray coarse powder and one may assume that the spraying parameters were not sufficiently optimized. Therefore, the WC-Co-Cr coating obtained from fine powder probably exhibits a higher degree of porosity which conducts to an inferior surface quality after the surface finishing process (higher roughness). Such surface roughness differences may occur also when two specimens are not sprayed at the same time, see table 4.4, specimen R 2.1 and R 2.2.

Cylinder on ring wear behaviour test was conducted by applying optimised parameters in order to avoid a premature wear of one or both tribopairs before test ends. In other words a premature wear which implies inadequate test parameters (high loads, distance) can lead to the rapid removal of such thin coatings (~250μm), thereby reaching the substrate material (Fig. 4.20) during testing, significantly influencing the wear test results. Consequentially, the wear experiments were carried out using the following test parameters presented in table 4.6, under dry (ambient atmosphere) and wet (water) conditions. Two ring specimens coated with the same material were necessary to accomplish a complete wear test (4 test combinations). On each ring, two wear tracks were obtained under both testing conditions (Fig. 4.21-left) by using the same stationary element (e.g. WC-Co-Cr sprayed with fine or coarse powder).

Table 4.6 Cylinder on ring test parameters

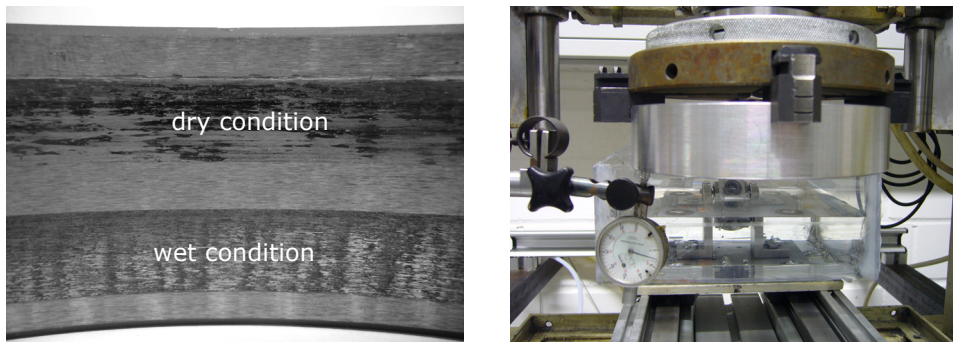| counterbody	normal load [N]	linear speed [cm/s]	rotational speed [min⁻¹]	motor frequency [Hz]	stop condition [lap]	sliding distance [m]	test duration [s]
WC-Co-Cr coatings (10+2μm) (-45+20μm)	80	300	475	15.9	25000	10000	3330

Figure 4.21 Cylinder on ring wear tracks (left); The ring centering process into the clamping chuck (right)

It should be also noted that, all the ring specimens required a mandatory balancing before starting the wear test. This was necessary in order to achieve an uniform wear track and for a roundly test course as well. Therefore, the wear tests were performed to a maximum deviation of 0.03mm measured with a comparator gauge, see figure 21-right.

The generated wear was quantified gravimetrically from the mass loss of the specimen. This method was chosen instead of the volumetric one, because the obtained worn tracks of all the investigated specimens were not deep enough in order to perform an optimal surface scanning topography.

For the gravimetric wear rate determination of the tested specimens, it is necessary to weigh the specimen before and after the wear test ($\Delta m = m_{before} - m_{after}$) using a digital balance which offers a capacity of 2100g and an accuracy of 0.01g. This value can be also negative in case of material transfer; the specimen weight is higher than before. Thus, the wear rate will be "negative", see table A.1 in appendix.

In this case, the wear rate (k) of both sliding pairs was calculated based on the following equation:

$$k = \frac{\Delta m}{F_N \cdot s \cdot \rho} \qquad \left[\frac{cm^3}{N \cdot m} \right] \qquad \text{(Eq. 2.10)}$$

where:

Δm – weight loss   [g]
F_N – normal load   [N]
s – sliding distance   [m]
ρ - coating density   [g/cm^3]

As one can see in the previous equation, the coating density was the only unknown value and needed to be determined. In order to overcome this problem, the density of all the investigated coatings was measured by using a pycnometer. The obtained densities of the coatings are presented in the table below:

Table 4.7 Coatings density

Coating type	WC-CoCr (-10+2 μm)	WC-CoCr (-25+5 μm)	WC-CoCr (-45+20 μm)	WC-Cr$_3$C$_2$-Ni (-10+2 μm)	WC-Cr$_3$C$_2$-Ni (-22+5 μm)	WC-Cr$_3$C$_2$-Ni (-30+5μm)
Coating density [g/cm^3]	9.49	9.36	9.88	9.15	8.44	6.28

Besides of the wear rate calculation, the resulted wear debris were analysed by XRD examination. After the sliding wear test, the collected wear debris was separated from water by filtering, using a small vacuum pump, see figure 4.22.

As it was already mentioned, the wear tests were performed in air and also under wet condition. Therefore, in the first case the temperature evolution of both tribopairs was measured using an infrared thermometer gun and in the other case, the water temperature was also measured before and during the entire wear test, see the corresponding graphics in the next two sections.
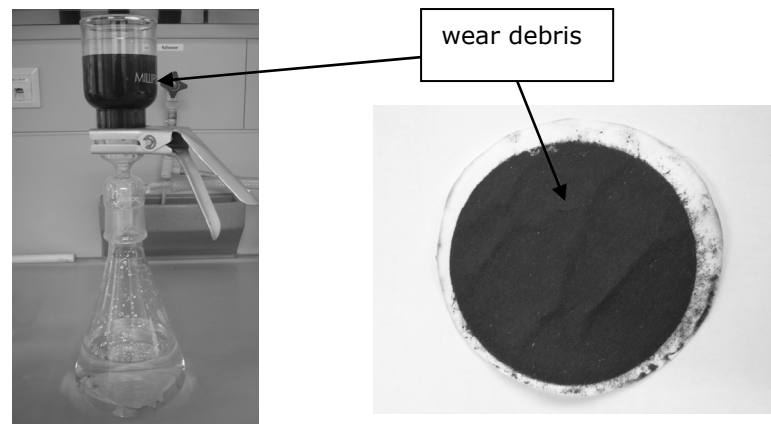
Figure 4.22 Filtering process of the wear debris

4.4.1 Sliding wear resistance under dry condition (ambient atmosphere)

The results of the investigated coatings under dry sliding wear conditions visualise some differences between the wear track surfaces. The WC-Co-Cr coatings exhibit darker traces on the worn scars, whereas in case of WC-Cr$_3$C$_2$-Ni coatings, the traces are only slightly visible, see table A2-A4 attached in appendix. Generally, the WC-Co-Cr surface of the ring specimens shows negative wear rates (see the black marked histograms presented in figures 4.23 and 4.24) while wear occurred mainly on the counterface (stationary specimen). For an easier overview of the wear rate results for both tribopairs, two types of wear rate order were used ([10^{-8} cm^3/Nm] for tables and [10^{-10}cm^3/Nm] for the histograms).

However, comparing table 4.8 with 4.9, the WC-Co-Cr coatings exhibit a better wear resistance (negative wear rates) under the same testing conditions due to a high process of material transfer from the stationary specimen. This fact was also confirmed by the higher wear rates of the counterbodies. In contrary, the specific wear rates of all the stationary specimens sliding against the WC-Cr$_3$C$_2$-Ni coatings exhibit lower values, which demonstrate according to the solicited surface area, that the WC-Co-Cr coatings have a significantly better sliding wear resistance than the latter one.

Visual observation of the wear track surface from both sliding components indicate that lower wear damage occurs when dissimilar coating materials are used (different chemical composition and different powder grain sizes). For example for a dry sliding wear contact, one may use coarse powder for the stationary specimen and fine or medium powder for the ring specimen. In this case the stationary specimen will be the sacrificial component with the most wear degree. Additionally, this type of stationary specimen has in general a positive effect on the performed sliding wear tests in respect of smoothly run, without vibrations, increased or excessive noise or any other disturbing elements. However, note that in most actual components it is the wear of the total system that is most important. Sometimes one component is designed to be sacrificial, but in general the aim is to ensure good wear life for both components. Thus a component that does not itself wear but that causes excessive wear in the counterface is usually unacceptable.

Table 4.8 The wear rates of the tribopairs (WC-Co-Cr vs WC-Co-Cr) under dry conditions

Wear rate [10^{-8} cm^3/Nm]	WC-Co-Cr coatings					
	fine powder		medium powder		coarse powder	
Ring	0.39	-0.26	-0.14	-0.72	-0.12	-0.25
Counterbody	0.47*	0.67**	1.42*	1.05**	0.32*	1.34**

Table 4.9 The wear rates of the tribopairs (WC-Cr$_3$C$_2$Ni vs WC-Co-Cr) under dry conditions

Wear rate [10^{-8} cm^3/Nm]	WC-Cr$_3$C$_2$-Ni coatings					
	fine powder		medium powder		coarse powder	
Ring	8.74	8.74	4.59	7.10	6.17	6.36
Counterbody	0.19*	0.25**	0.35*	0.29**	0.09*	0.16**

* counterbody coated with fine powder; ** counterbody coated with coarse powder; the wear degrees of both types of tribopairs are presented spreadsheet in appendix.
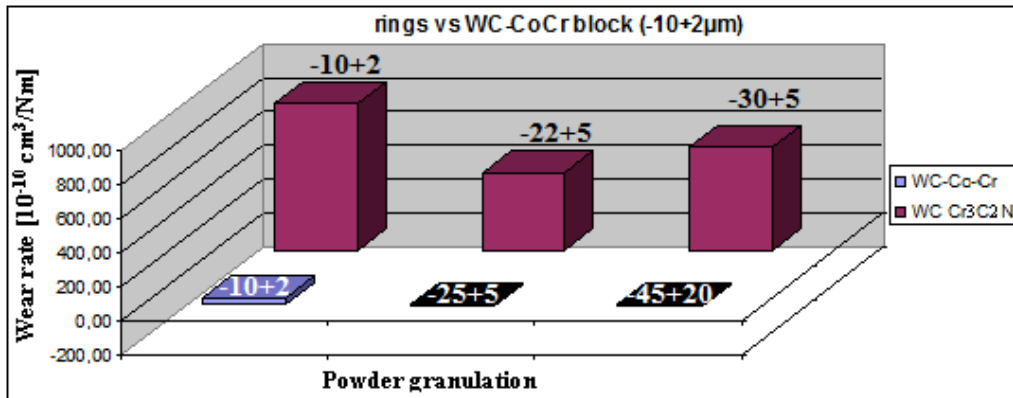

Figure 4.23 Sliding wear resistance of the ring specimens vs WC-Co-Cr (-10+2μm) stationary specimen under dry conditions
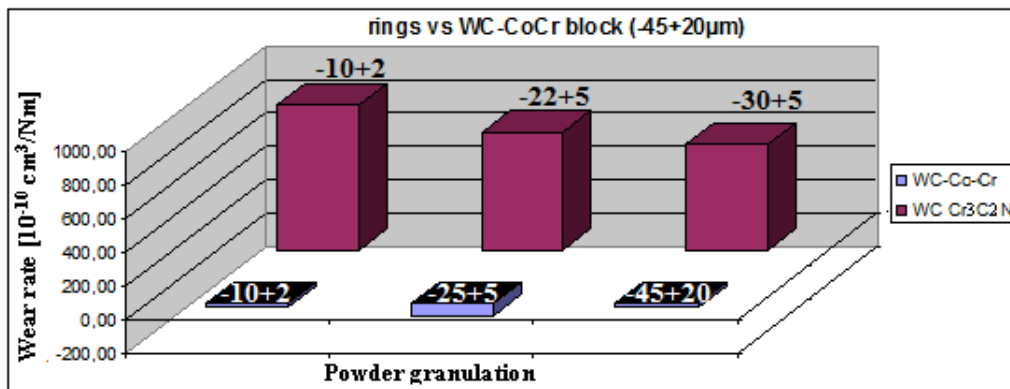

Figure 4.24 Sliding wear resistance of the ring specimens vs WC-Co-Cr (-45+20μm) stationary specimen under dry conditions

Figure 4.25 shows the temperature evolution of the tribopairs in case of WC-Co-Cr coatings recorded during the wear test. In the early stage, the temperature increases up to the maximum level, remains constant for approximately 3000 laps and than decreases slowly down to a stable value. It is very important to be pointed out, that the maximum of temperature corresponds to the formation of the thin lubrication film which has a significant influence on the evolution of the specimens temperature during the remaining test period. This phenomenon is associated also with the transition from the severe wear intensity to a mild one, reaching finally a light wear regime. The stationary specimen follows the same pattern of temperature evolution during the sliding wear test. All the investigated WC-Co-Cr coated specimens (rings and counterbodies) exhibit this temperature phenomenon only with some variations in temperature (±15°C). It should be mentioned that the wear rate of these coatings depends on the period of time, respectively the number of laps in which the specimens will reach the maximal temperature (the sooner the better) which corresponds to the tribofilm formation and of course the transition between the two types of wear regimes.
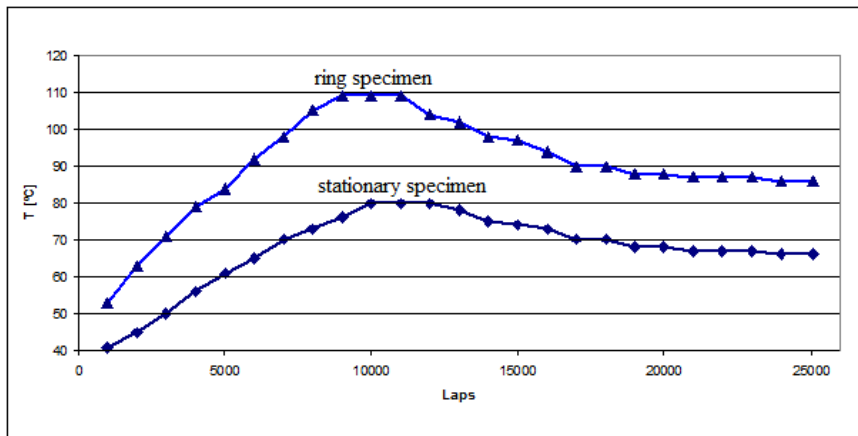

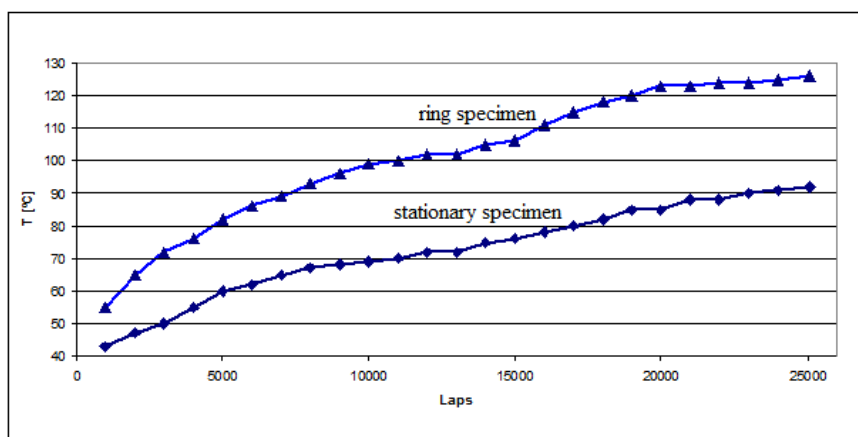Figure 4.25 The evolution of ring and stationary specimen temperature of WC-Co-Cr coatings

Figure 4.26 The evolution of ring and stationary specimen temperature of WC-Cr$_3$C$_2$Ni coatings

In contrast to the temperature evolution of the WC-Co-Cr coatings, figure 4.26 shows the temperature of the ring and stationary specimens sprayed with WC-Cr_3C_2Ni powder. The temperature increases continuously without any stability domain which can be correlated with the absence of the tribofilm on the wear track surface (see tables A2-A4 in appendix), maintaining a severe wear process for the duration of the entire test. This explains also the higher wear rates in comparison with of WC-Co-Cr coatings.

During the previous dry sliding tests, a significant difference between the wear behaviour of WC-Co-Cr and that of WC-Cr_3C_2-Ni coatings has been ascertained. Based on the wear theory, which affirms that the wear may be broadly classified as "mild wear" or "severe wear, this can be associated in the same order with the present wear behaviour of WC-Co-Cr and WC-Cr_3C_2-Ni coatings. Figure 4.27 illustrates a general wear course as a function of the laps number. For all tribopairs, the wear degree increases abruptly during the first sliding laps, corresponding to a severe wear. After a "running-in" stage, this decreases to mild wear and than reaches an equilibrium state in which the wear degree remains approximately constant (light wear domain) as a function of sliding distance, see the WC-Co-Cr graph. In contrast, the wear degree of WC-Cr_3C_2-Ni coatings remains at the severe wear level until the end of the sliding test (25000 laps), which confirms the above mentioned continuous increasing of the tribopairs temperature.
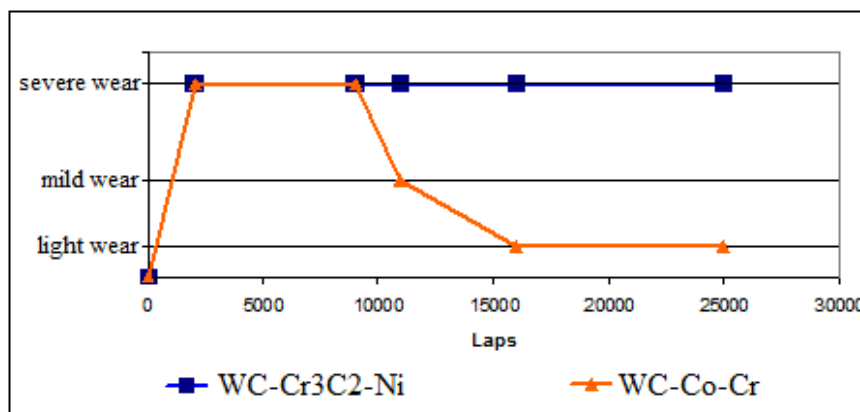
Figure 4.27 Example of the ring specimens wear behaviour as a function of sliding distance

This behaviour is not due to an increase or decrease in the normal load or due to the wear debris particles size (nano or micro-scale), it depends only on the phase composition of the contact surface between the tribopairs.

4.4.2 Sliding wear resistance under wet conditions (in water)

The sliding wear rate results for both WC-Co-Cr and WC-Cr_3C_2-Ni coated ring specimens tested under wet condition are shown in figure 4.28 and figure 4.29 respectively. As in the previous section, the wear rate results of both tribopairs are summarized in the following two tables for a better comparison between the results.

Table 4.10 The wear rates of the tribopairs (WC-Co-Cr vs WC-Co-Cr) under wet conditions

| Wear rate [10^{-8} cm^3/Nm]	WC-Co-Cr coatings					
	fine powder		medium powder		coarse powder	
Ring	-0.26	-0.13	0.57	0.28	19.3	2.65
Counterbody	0.13*	0.42**	0.52*	0.46**	1.48*	1.35**

Table 4.11 The wear rates of the tribopairs (WC-Cr$_3$C$_2$Ni vs WC-Co-Cr) under wet conditions

Wear rate [10^{-8} cm^3/Nm]	WC-Cr$_3$C$_2$-Ni coatings					
	fine powder		medium powder		coarse powder	
Ring	21.8	19.9	21.4	19.5	45.3	38.2
Counterbody	0.05*	0.07**	0.06*	0.35**	0.43*	1.61**

* counterbody coated with fine powder; ** counterbody coated with coarse powder; the wear degrees of both types of tribopair are presented spreadsheet in appendix.

All the ring specimens coated with WC-Co-Cr powder show higher wear resistance (lower wear rate) under the same testing conditions than those coated with WC-Cr$_3$C$_2$-Ni powder. For both it can be observed that the specific wear rate drops with the decrease in the powder grain sizes. A different wear behaviour comparing the WC-Cr$_3$C$_2$-Ni coatings tested under dry condition, in which the resulted wear rates decrease with the increasing of the powder grain sizes. The WC-Co-Cr coatings obtained from fine powder exhibit a negative wear rate during sliding against both types of stationary specimens (-10+2µm and -45+20µm), which means that during the wear test, the process of material transfer from the counterbody onto the ring specimens surface has occurred, see the black marked histograms.
Besides of the ring specimens wear rate results, one may observe from table 4.10 and 4.11 that the wear rate of the stationary specimen increases with the increase of the powder grain size (fine, medium, coarse powder) used for the coating deposition on the ring specimens.
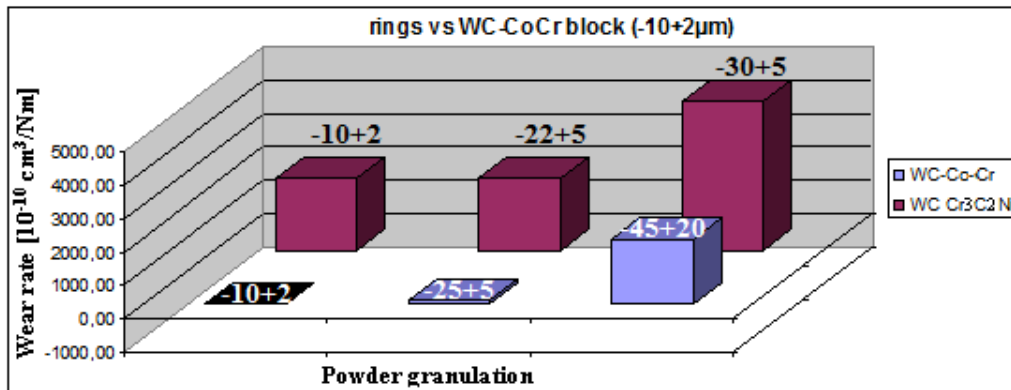
Figure 4.28 Sliding wear resistance of the ring specimens vs WC-Co-Cr (-10+2µm) stationary specimen under wet conditions
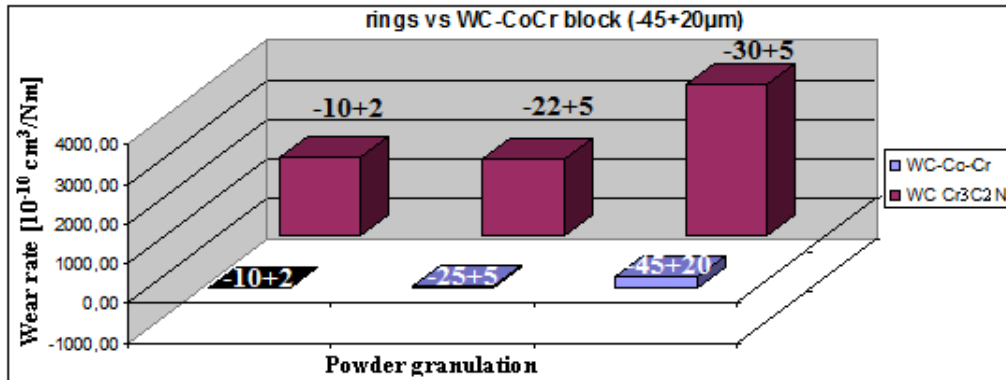
Figure 4.29 Sliding wear resistance of the ring specimens vs WC-Co-Cr (-45+20μm) stationary specimen under wet conditions

Based on these results, the conclusion is that the largest wear damage occurs in the case of WC-Cr$_3$C$_2$-Ni coatings (coarse powder) sliding against WC-Co-Cr counterbody coated with coarse powder, which also suffered the highest wear degradation reaching even the specimen substrate, as it can be seen in figure 4.30.
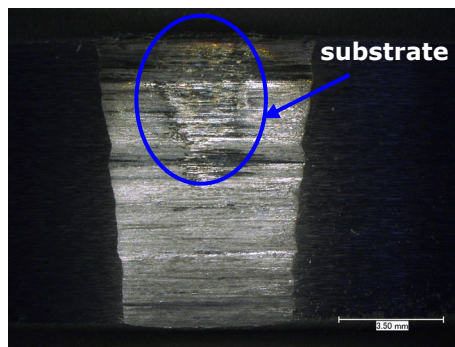

Figure 4.30 Stationary specimen with the highest degree of deterioration

The above presented case demonstrates that coarse powders sliding against each other are unrecommended as material paring for wear subjected components.

Under these test conditions, the water temperature was measured before and during the test in order to observe if the temperature evolution presents similar trendlines as those recorded in the case of dry sliding wear tests. From figure 4.31 and 4.32 it can be clearly seen that the water temperature follows closely the temperature of the corresponding tribopairs. All the WC-Co-Cr coatings exhibit a maximal water temperature around 25°C (±0.5°C) with an exception attributed to the WC-Co-Cr tribopairs (ring specimen coated with coarse powder sliding against a counterbody coated with fine powder) which had registered 29°C, a normal value considering that this tribopairs showed the higher wear rate, see table 4.10. The maximal water temperature in case of WC-Cr$_3$C$_2$Ni coatings was approximately 29°C (±0.5°C).
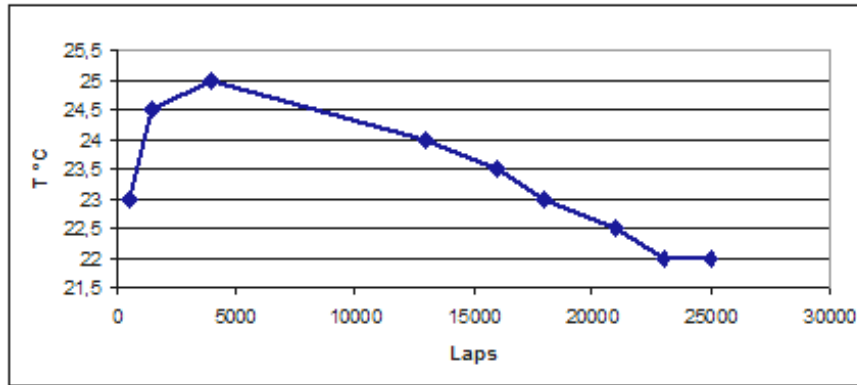
Figure 4.31 The evolution of water temperature during testing of WC-Co-Cr coatings
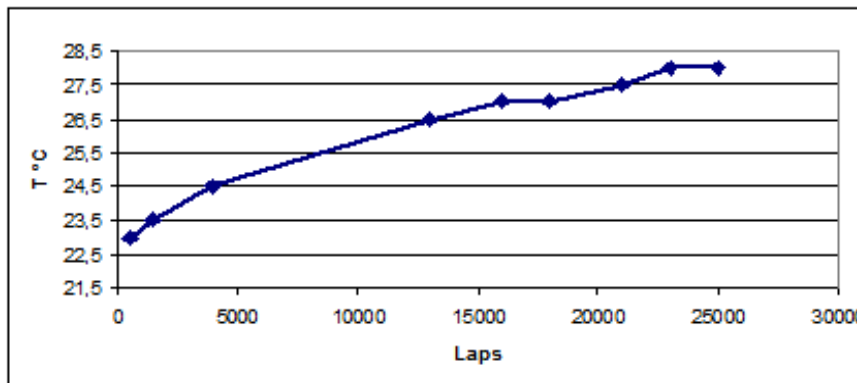

Figure 4.32 The evolution of water temperature during testing of WC-Cr$_3$C$_2$Ni coatings

From all the above temperature graphs obtained under dry and wet testing conditions, one can conclude that the WC-Cr$_3$C$_2$Ni coatings are disadvantageous in some applications due to the persistence of the severe wear behaviour. Furthermore, under both testing conditions the temperature of water and specimens had followed similar evolution corresponding to the coating types.

As mentioned before, it seams that the sliding wear behaviour of these types of coatings depends mostly on the composition of the contact surface between the tribopairs. After the wet sliding wear tests, similar types of worn track surfaces (dry conditions) were observed. The WC-Co-Cr coatings present darker traces that repeatedly did not appear in case of WC-Cr$_3$C$_2$-Ni coatings. This phenomenon can be explained by the change in appearance of the water involved in the test, which for the latter coating is much darker in comparison with the one resulted after the wear test of the WC-Co-Cr coatings, see figure A.3, respectively A.4 attached in appendix. Therefore, the water was filtered (see figure 4.22) in order to collect the wear debris generated during the test. The X-ray diffraction analyses of these debris, presented in figure 4.33, show a very high amount (81%) of carbon in form of graphite with a rhombhoedral crystal structure, nickel and wolfram oxide and a small amount of tungsten carbide (4%).

Correlating the water appearance with the resulted wear track surfaces, it was clear that in case of WC-Co-Cr coating the adhesion of the thin graphite film on surface is pronounced (clear water after the test), in contrast to the WC-Cr$_3$C$_2$Ni coatings where the graphite did not adhere to the underlying material surface, falling into the water.
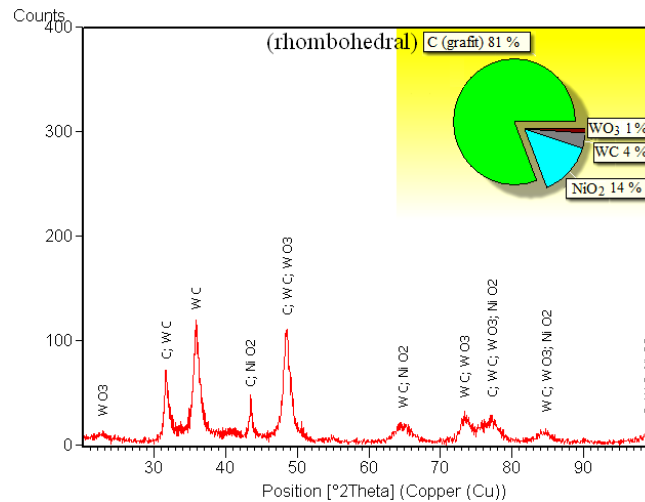

Figure 4.33 X-Ray diffraction pattern of the collected wear debris (WC-Cr$_3$C$_2$-Ni coatings)

The dependency of wear resistance on the formed graphite tribofilm which adhers or not on the coating surface can be clearly observed by correlating the tables A2, A3 and A4 attached in appendix, with the corresponding wear rate results.

The formed graphite on the worn track acts as a lubricating, ductile, dense and cohered tribofilm protecting the coating surface from further wear, decreasing in case of the WC-Co-Cr coatings, the wear rates during the sliding tests. This fact is commensurate with the theory of a thin soft film applied in the sliding contact between two hard surfaces which may remarkably improve the wear resistance of the interacting components. These kinds of surfaces are subjected to adhesive wear and can end up polished (e.g. case of the investigated coatings) or can suffer severe surface damage associated with surface dragging or even seizure.

Moreover, the WC-Co-Cr ring specimen coated with coarse powder (-45+20μm) exhibits a lower wear resistance when loaded against a counterbody coated with fine powder (-10+2μm). During the sliding test a high amount of vibrations and rubbing was encountered, leading to the most significant deterioration of both components, in comparison with the other WC-Co-Cr tested tribopairs. Additionally, for this tribopairs the adhesion degree of the thin lubricating film was not as good as expected when two WC-Co-Cr coatings are sliding against each other. This fact was confirmed also by the water appearance (more cloudy) resulted after the wear test. It seams that in case of high vibrations leading to supplementary forces during the sliding test, the porous tribofilm adhere poorly on the contact surface. Consequently, the wear debris from water were filtered and also investigated by means of XRD. In this case (Fig. 4.34), the identified carbon based structure has a hexagonal lattice (d$_{002}$=2.1112), different from the one detected for WC-Cr$_3$C$_2$-Ni

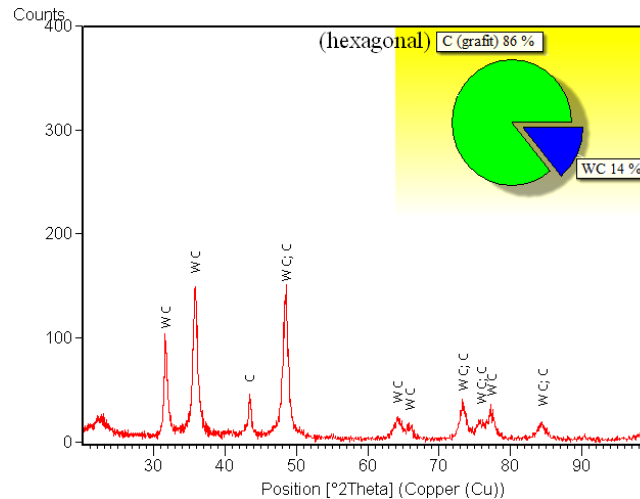coatings d_{002}=11.1500 (rhombohedral), but corresponding to the same graphite phase, see table 4.12.

Figure 4.34 X-Ray diffraction pattern of the collected wear debris (WC-Co-Cr coatings)

Comparing the testing conditions (dry and wet) one may conclude that in the case of dry conditions the resulted wear rates for both investigated coatings are significantly lower than in the case of wet conditions. This is mostly attributed to the graphite thin soft film formed on the sliding contact, which adheres (dry conditions) or has a poor adhesion (wet conditions) leading to a lower or higher friction level between the two tribopairs.

Based on the fact that a decarburization process occurs at high temperatures, no concluding reasons could clarify how during a sliding wear test, graphite is formed on the wear track, knowing that the maximum measured temperature at the rings OD was about 130°C. The only one possible supposition is that the carbon generated through a certain decarburisation degree during spraying was not entirely oxidized to CO_2 due to the high velocity of the deposition process which influence the kinetics of the chemical reaction. Even in this case, is very hard to understand the existence of such a high amount of free carbon (practically impossible) which could rapidly diffuse to reach the coating surface and thus, to form the graphite tribofilm during the sliding tests. Concerning this situation SEM investigations were performed in order to find a credible explanation regarding the appearance of this kind of tribofilm. Cross sections of both tested coatings (Fig. 4.37, 4.39) show significant structural changes in the nearby surface area consisting of a thin layer (~3.5µm) with a fine grain structure composed from extra fine WC particles bounded into a metallic matrix containing W, Co and Cr. This implies the presence of high temperature as well as of high cohesions forces at the tribopair contact surface (microscale) which may lead to the formation of the graphite tribofilm detected in the X-ray diffraction patterns, see figure 4.33, 4.34.
The formation of the graphite microfilm can be associated with Holmbergs and Matthews theory [48] regarding the tribochemical mechanisms which may occur in sliding contacts between hard coatings (see figure 2.29 in chapter 2, section

2.4.2.1). They write that in case of ceramic sliders sliding on diamond or diamond-like coatings the formation of a graphite microfilm can take place. Moreover, they affirmed that the transformation temperature for diamond to graphite is near 900K in the presence of oxygen and above 1800K in the absence of oxygen and that the temperature at microcontacts in the sliding of hard materials may often be sufficient for the transformation to occur (between 1000°C and 2000°C).

According to the above hypothesis and based on the SEM micrographs, one may assume that at the microcontact region such temperature were achieved and a certain decarburization degree of WC-phase occurred during the sliding process.

Besides the decomposition reaction of WC ($2WC \rightarrow W_2C+C$) as well as that of the W_2C ($W_2C \rightarrow WC+W$), normally occurred at approx. 1250°C, one should consider the possibility of certain oxidation reactions of WC (>300-500°C) as follows: $2WC+O_2 \rightarrow W_2C+CO_2$. As a consequence of these degradation reactions, some C is dissolved in the matrix. A part from this carbon will react with oxygen forming CO/CO_2 thus losing part of the C from the original powder. Depending on the degree of decarburization, metallic W can precipitate along boundaries where a C depletion occurred, when oxygen reacts with the carbon from WC and forms volatile CO_2.

All the above discussions are only suppositions regarding the formation of graphite tribofilm during the sliding wear test. Unfortunately, the contact temperature between the tribopairs could not be measured and thus, to clearly affirm that the decomposition temperature of WC was achieved.

Additionally, the surface of the worn tracks was investigated by means of X-ray diffraction to provide information about their crystalline lattice. The specimens coated with WC-Co-Cr (Fig. 4.41) exhibit a predominant hexagonal crystalline structure in contrast to that on the WC-Cr_3C_2-Ni (Fig. 4.42) which presents a rhombohedral/cubic packing arrangement. Based on theoretical statements that the hcp structure exhibits a good sliding wear behaviour (see solid lubricants based on graphite or MoS_2), the experimental results attest also good sliding wear (especially low friction coefficient) for the coatings with hexagonal carbon structure on the top. The adherence of the formed tribofilm is strongly influenced by the content in other hexagonal phases included in the coating composition (especially WC-hexagonal). If during sliding, the formed tribofilm is distributed on a coating surface which contains a high amount of hexagonal WC (e.g. WC-Co-Cr coatings ≥ 60 %), the forces generated beside the applied normal load are appreciably lower than that produced in situations when the amount of hexagonal phases is lower. This affirmation is confirmed by the identified rhombohedral carbon present in the tribofilm on the top of the WC-Cr_3C_2-Ni coatings (1%) and also in the collected wear debris (81%). This film contains definitively in the incipient testing period predominantly hexagonal carbon. The fact that in the phase composition of the WC-Cr_3C_2-Ni coatings, besides the hex WC phases there is a considerable amount of cubic Cr_3C_2, leads to the appearance of strong acting forces (hertzian-, shear-, radial-forces) as confirmed by the values of friction coefficient. These forces, especially the shear one are able to transform the …ABAB…graphite layer stacking into the …ABCABC…stacking which corresponds to the rhombohedral graphite, see figure 4.35. H.P. Boehm et al [132] affirmed that the hexagonal graphite phase is thermodynamically stable but in particular thanks to grinding processes a large percentage of rhombohedral form can be obtained.

Considering the results from the pin on disc tests, especially the appearance of the wear debris (the gray powder), which in case of WC-Co-Cr coatings (predominance of hcp structure) presents a continuous layer and on the WC-Cr_3C_2-Ni coatings

(predominance of fcc structure) a fractured one, it is obvious that there are two different wear debris structures that are formed after the sliding tests.

Correlating the SEM-micrographs from figures 4.37-4.40 especially that from figure 4.43 with the phase composition of the worn surface, one may conclude that the WC ceramic particles are fine distributed into a Cr-W-Co metallic matrix. On top of this region a very thin film of WO_3 was observed. This oxide layer is highly porous and cracked due to the generation of CO and CO_2 during oxidation (T° > 600°C): $WC+2O_2 \rightarrow WO_3+CO$ and $CO+1/2O_2 \rightarrow CO_2$.
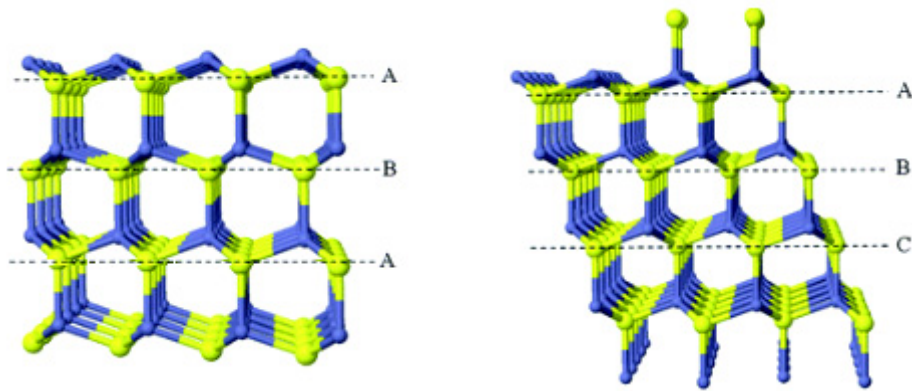

Figure 4.35 Stacking arrangement of the investigated graphite: hexagonal structure detected on the WC-Co-Cr coatings (left); rhombohedral structure detected on the WC-Cr_3C_2-Ni coatings (right)
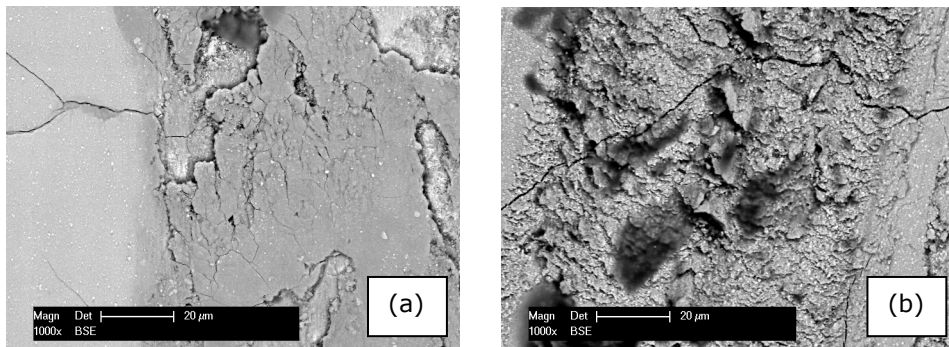

Figure 4.36 SEM micrographs of the wear track surface: WC-Co-Cr coatings (a); WC-Cr_3C_2-Ni coatings (b)
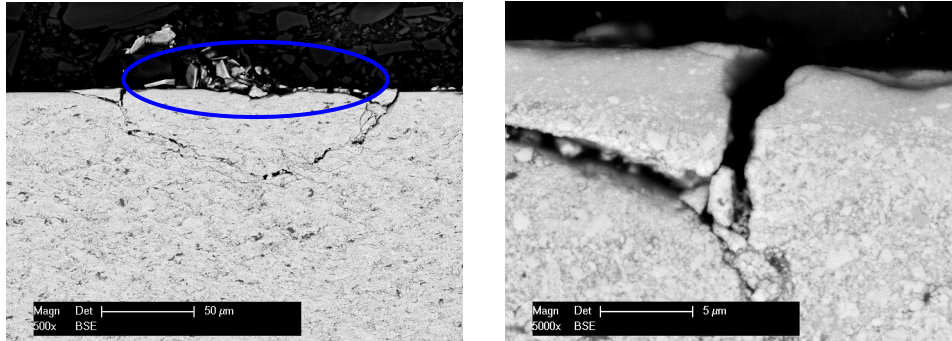
Figure 4.37 Cross sections of WC-Co-Cr coatings after dry sliding wear test
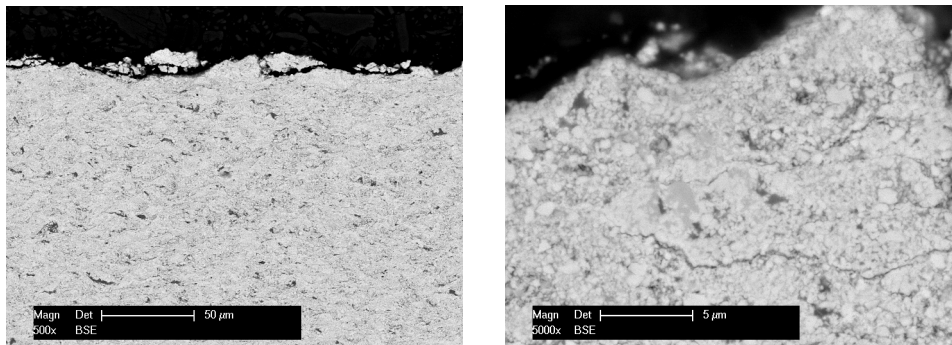

Figure 4.38 Cross sections of WC-Co-Cr coatings after wet sliding wear test

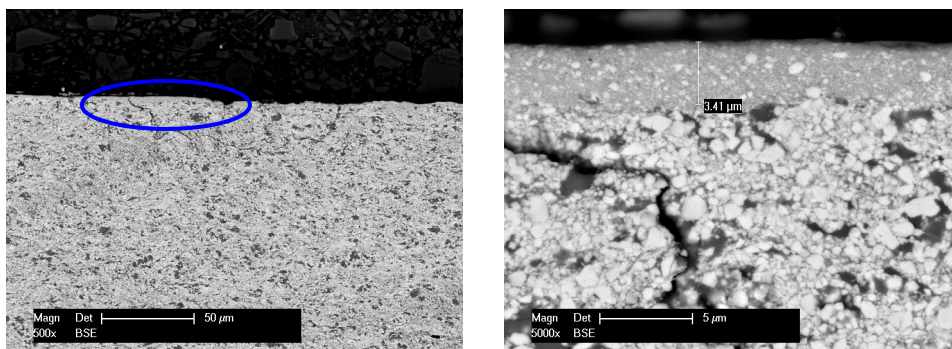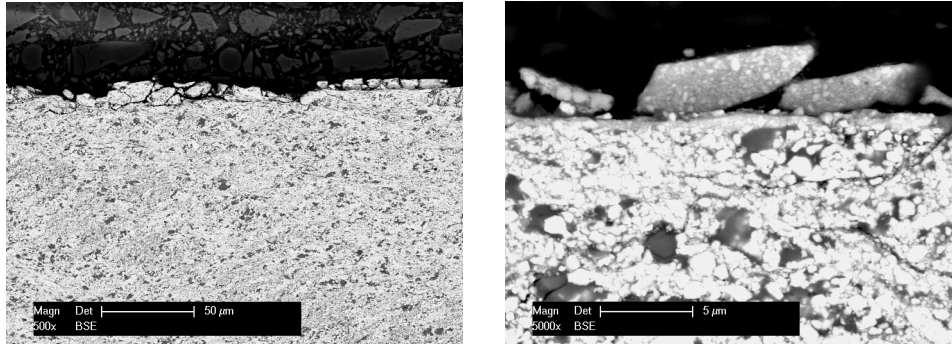Figure 4.39 Cross sections of WC-Cr$_3$C$_2$-Ni coatings after dry sliding wear test

Figure 4.40 Cross sections of WC-Cr$_3$C$_2$-Ni coatings after wet sliding wear test
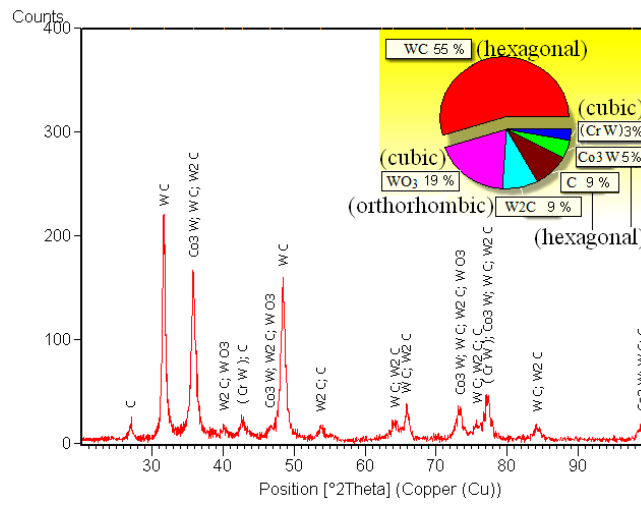

Figure 4.41 X-Ray diffraction pattern on the wear track surface of WC-Co-Cr coatings
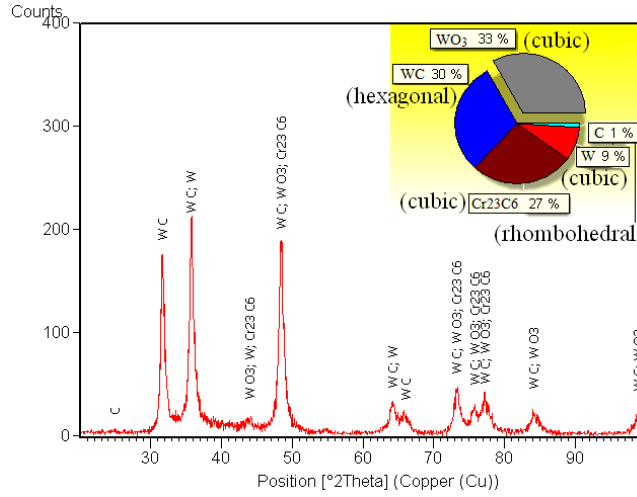
Figure 4.42 X-Ray diffraction pattern on the wear track surface of WC-Cr$_3$C$_2$-Ni coatings

Table 4.12 Crystal structure analyses

coating	filtered carbon			carbon on surface		
	crystal structure					
	a	b	c	a	b	c
WC-Co-Cr	2.5221	2.5221	8.2371	2.4560	2.4560	6.6960
lattice constant [Å] (100%)	d$_{002}$=2.1112 (hexagonal)			d$_{002}$=3.3480 (hexagonal)		
WC-Cr$_3$-C$_2$-Ni	2.4600	2.4600	33.4500	2.5221	2.5221	43.2450
lattice constant[Å] (100%)	d$_{002}$=11.1500 (rhombohedral)			d$_{002}$=2.0593 (rhombohedral)		

Examinations of the wear track surfaces (Fig. 4.36) indicate same microcracks propagation and also the formation of the graphite thin tribofilm due to the adhesive wear. The WC-Co-Cr coatings present a delimitation phenomenon, fact which in the case of WC-Cr$_3$C$_2$-Ni leads to an abrasive wear mechanism. The latter one presents a rougher surface after the wear test which has been confirmed by the roughness measurements illustrated in table A1 from appendix (e.g. specimen M3.1: Ra$_{before}$= 0.58μm and Ra$_{after}$=1.08μm). Based on the cross sections micrographs illustrated above one can observe that the microcracks are propagated first perpendicular (normal cycling load) and than parallel (tangential cycling load) to the surface. However, both kind of coated specimens show a predisposition to fatigue wear.

A higher material loss under wet sliding conditions can be clearly observed from the SEM micrographs (Fig. 4.38. 4.40 respectively), where the exposed coating surface presents a high amount of fractured particles. In contrast, the dry conditions produced an almost continuous (unfractured) layer, without significant material loss. These observations are also supported by the corresponding wear rate results.

Even in case of WC-Co-Cr coatings which have demonstrated very low wear rates under dry sliding conditions; these can be dramatically modified due to the presence of the fatigue phenomena. As it can be observed in figure 4.37 a large amount of coating could be removed after a longer testing time because of the interconnected

cracks which are propagated in the subsurface region. This effect can be accentuated when the surface tribofilm can not support the inducing forces and will split-off from the contact surface, see the marked area in the same figure. Therefore, on this area lifts are formed which conducted to an excessive normal load and of course the appearance of high vibrations, an optimum situation for cracking propagation. This phenomenon is available also in case of WC-Cr_3C_2-Ni coatings.

Based on all the discussed wear results it can be concluded that the wear rates and also the water and the specimens temperature can be very well correlated with the obtained coefficient of friction investigated in the previous section. For example the WC-Co-Cr coatings exhibit a lower friction coefficient which was confirmed by the lower wear rates and also by the graphics temperature (first the temperature increase and than decreases). In contrast, the WC-Cr_3C_2-Ni coatings exhibit a higher friction coefficient that leads to a higher wear rate and also to higher temperatures of the specimen as well as from the water which increases during the entire sliding wear tests (see the corresponding graphics).

All the above wear results can be attributed to the size and type of the surface contact which was made possible with the aid of the cylinder on ring wear tester. Therefore, the test specimens are subjected to high loads and at the same time to a large contact area between the tribopairs. These facts lead to high test temperatures that affect even the structure of the testing specimen. The line contact type (width 10mm wear track) permits a severe wear testing method that leads to a better simulation of real conditions.
Comparing the surface contact of this method with the one obtained by the pin on ring test, the latter offers a point contact which regarded to the ring specimen size can not exhibit such high wear test intensity due to the premature wear. Moreover, it was demonstrated that the sliding tests performed under dry conditions improve the wear resistance of both types of tested coatings due to the self-lubricated properties.

For a better understanding of the wear mechanism which occurred under these testing conditions, a schematical overview regarding the wear behaviour of the WC-Co-Cr coating directly influenced by the formation and stability of the tribofilm, is presented in the figure below.
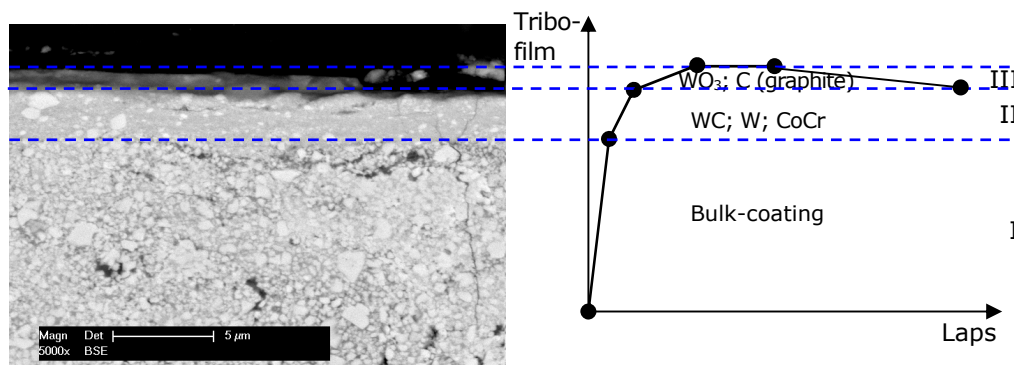

Figure 4.43 Formation and stability of the tribofilm during the sliding wear test

In case of WC-Cr$_3$C$_2$-Ni coatings the third domain does not exist due to the poor adhesion of the graphitic tribofilm to the coating surface leading to a lower wear resistance of this type of coatings. The tribochemical mechanisms that have been observed by these tribological contacts can be divided into two main surface phenomena for which the chemical effects are essential, such as: the formation of thin tribofilm and the oxidation process.

4.5 The influence of compressed air onto the wear resistance of WC-Co-Cr coatings

Additionally, to the already performed wear investigations the influence of compressed air onto the wear behaviour of WC-Co-Cr coating was also assessed. In this case the pin on ring testing method was chosen, instead of the cylinder on ring, because some of these types of wear tests were already performed and therefore, it was better to use the same testing method. At that time, the cylinder on ring tester was in the conception phase.

The principle of the pin on ring test is shown in chapter 3 and consists of a stationary WC-Co ball, as counterpart, loaded against the surface of an ID coated ring specimen in relative motion with or without using the compressed air under different test parameters. It needs to be mentioned that the air was blowing with a pressure of 2 bar toward the tribopairs contact zone. The first pin on ring test was performed at the beginning of this PhD thesis by using the following parameters: linear speed of 200 min^{-1} and 40 N as normal load for a testing distance of 5000 m. Under these parameters, figure 4.44 shows two significant differences between the wear tracks. Comparing their widths, it can be observed that by the usage of compressed air the wear degree changes dramatically. The correspondent wear degree of this counterbody and of all the other counterbodies used for this research are illustrated in table A.8 attached in appendix.

A closer SEM examination of the wear track surfaces illustrates two different wear mechanisms. The wear track resulted without the influence of compressed air presents a smooth surface (Fig. 4.45-left) which relates to a low wear degree due to the emergence of the thin tribofilm.

The most likely source of the transition to reduced wear rate regime is the formation of the tribofilm by reattaching the wear debris. In contrast, with the use of the compressed air during the sliding test, leads to a total removal of the tribofilm from the coating surface and due to that, to a very rough surface (Fig. 4.45-right) with a scratching effect. Therefore, under these testing conditions two types of wear mechanisms occurred namely, the abrasive wear (compressed air usage) and the adhesive one for the other case.

Cross sections of the wear track, shown in figure 4.46, prove the influence of the compressed air, which prevents the formation of the thin layer with fine structure, responsible for a smooth sliding between the tribopairs.
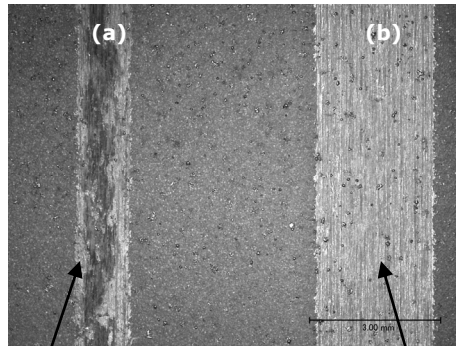
Figure 4.44 SM-micrograph, 30x of the wear tracks: without (a) and with compressed air (b)
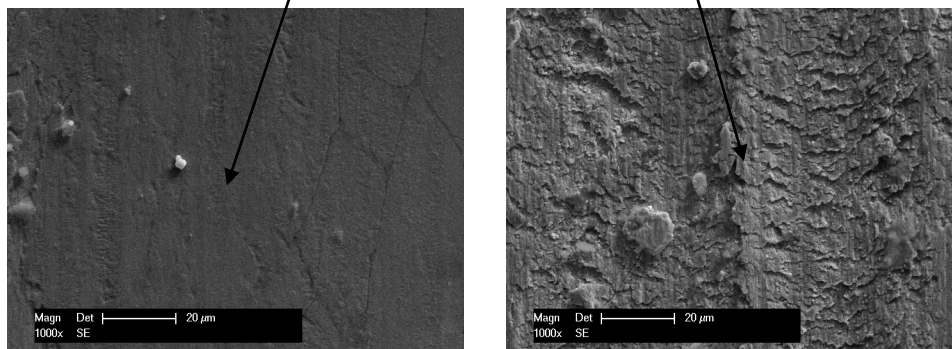

Figure 4.45 SEM micrographs of the wear track surface: without (left); with compressed air (right)
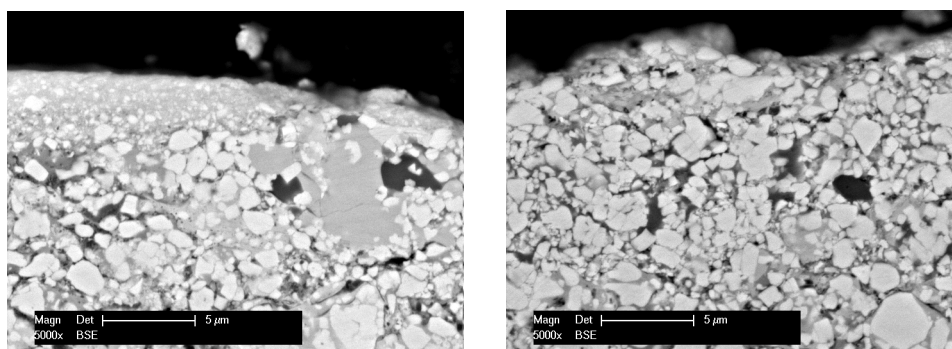
Figure 4.46 Cross section through the wear tracks illustrated in figure 4.45: without (left) and with compressed air (right)

Besides of the above mentioned parameters further sliding wear tests were performed by using eight further testing conditions by modifying the normal load and the rotational speed respectively (with and without compressed air), see table 4.13. After using the first parameters set (1.1 and 1.2), an unexpected result

namely, two similar wear tracks as well as identical wear degree on the counterbodies were obtained. Comparing with the first pin on ring test (40N and 200rpm) it was demonstrated that under these testing conditions (80N and 475rpm) the addition of compressed air has no effect onto the wear behaviour of the investigated coating.

Table 4.13 Pin on ring test parameters

Parametres	normal load [N]	rotational speed [min⁻¹]	motor frequency [Hz]	stop condition [lap]	sliding distance [m]	compressed air [bar]
Set 1.1	80	475	15.9	25000	10000	-
Set 1.2	80	475	15.9	25000	10000	2
Set 2.1	40	475	15.9	25000	10000	-
Set 2.2	40	475	15.9	25000	10000	2
Set 3.1	40*	200*	7*	25000	10000	-
Set 3.2	40*	200*	7*	8000	~3000**	2*
Set 4.1	80	200	7	25000	10000	-
Set 4.2	80	200	7	3000	~1200**	2

*identical test parameters as by the first pin on ring test
** stop condition because of the very high wear degree of both tribopairs

Figure 4.47 illustrates that both wear tracks present the same surface structure with the thin tribofilm traces, which based on the wear results from the previous section can be associate with the formation of the graphitic film that lubricates the tribopairs surface. Therefore, some additional cross section examinations of the wear track were carried out.

Similar, but not as pronounced as in the case of the cylinder on ring tests, at the nearby surface one can observe significant structural changes of the coating which consist of a very thin gray layer (see the arrow in figure 4.48). According to the EDS analysis of this layer, a high amount of WO_3 and C was found, demonstrating once again that a certain degree of decomposition of the WC phase into metallic W and free carbon occurred. During the sliding wear test, it can be assumed that a part from the metallic W was oxidized to WO_3 and some carbon was similarly oxidized to CO_2, but there was still enough graphitic carbon left in order to contribute to the tribofilm formation. The increased intensity of the oxygen peak leads clearly to a high content of metallic oxides, especially W, on the surface of the wear track.
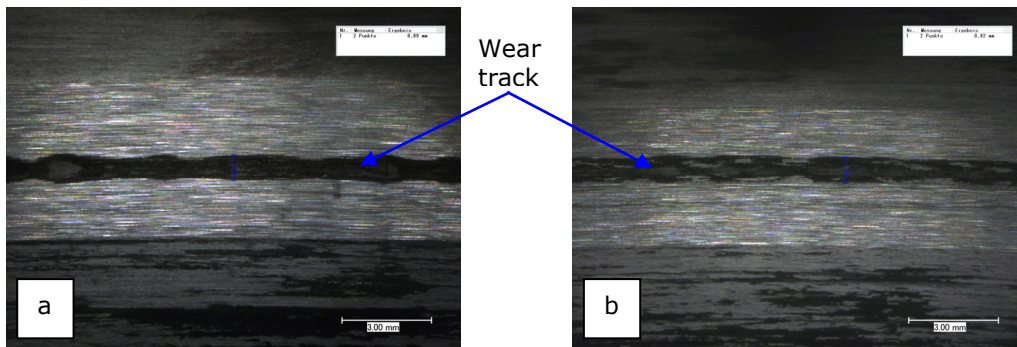
Figure 4.47 SM-micrograph of the wear tracks obtained with set 1.1 (a) and 1.2 (b) parameters
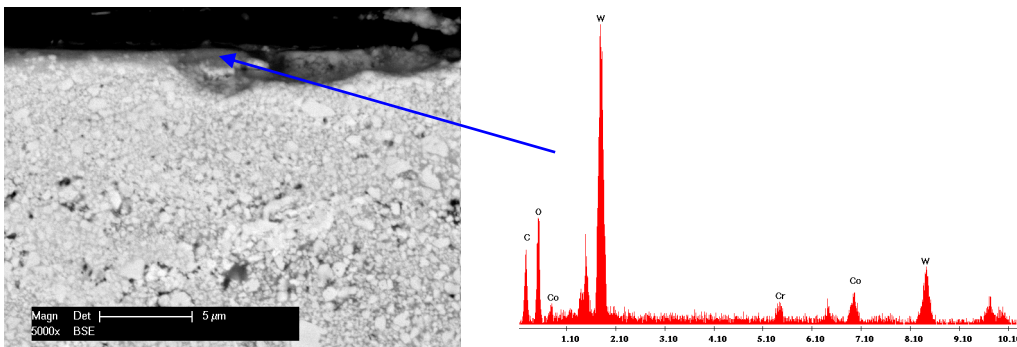

Figure 4.48 Cross section through the wear tracks illustrated in figure 4.47 (80N; 475rpm, without compressed air) and EDS point analyze (see the arrow)

Considering the additional use of the compressed air during the sliding wear test, which maintains a constant temperature of the specimen (~35°C), it is interesting to note that the structural changes of the coating (tribofilm formation) are mostly influenced by the strong acting forces (shear forces) which are generated during the test. This statement was also confirmed in the previous section.

Based on the first pin on ring test, for the second set of parameters (2.1 and 2.2) a lowering of the normal load down to 40 N was assigned. Figure 4.49 indicate the resulted wear tracks, presenting the same surface structures as the previous tests, only that the worn widths and the counterbodies wear degrees are smaller, as expected, because of the lower pressure. It seems that the formation and adhesion of the tribofilm are not affected by the load size.

Figure 4.49 SM-micrograph of the wear tracks obtained with set 2.1 (a) and 2.2 (b) parameters

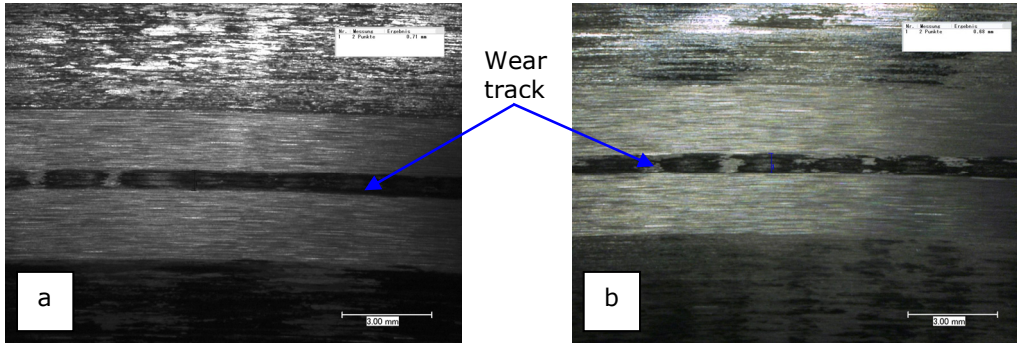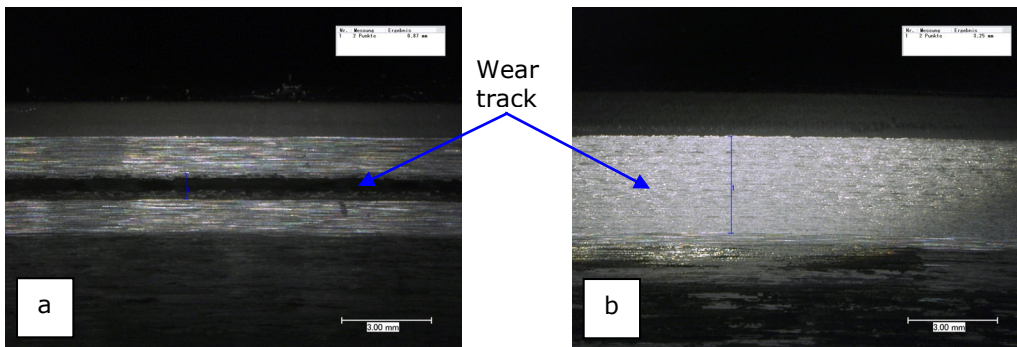Figure 4.50 SM-micrograph of the wear tracks obtained with set 3.1 (a) and 3.2 (b) parameters
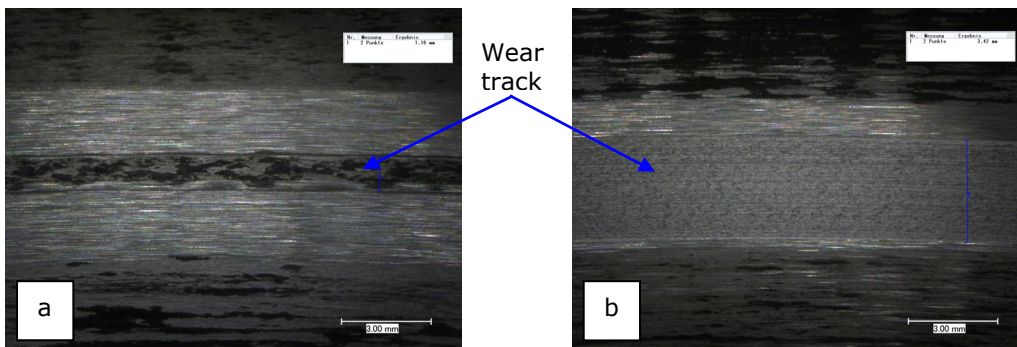

Figure 4.51 SM-micrograph of the wear tracks obtained with set 4.1 (a) and 4.2 (b) parameters

Consequently, the third set of parameters (3.1 and 3.2) was used, by keeping constant the (40N), whereas the rotational speed was decreased from 475rpm to 200rpm. These testing conditions are identical with the first pin on ring test, only

that the WC-Co-Cr coating morphology (Fig. 4.48) is different (see the WC grain size) compared to the first coating illustrated in figure 4.46. However, the obtained wear tracks present the same characteristics as the ones mentioned before (Fig. 4.50). Namely, a narrower track for the test that did not implied compressed air (Fig. 4.50 a) and a wider track for the other one (Fig. 4.50 b). In the case of the latter one it was necessary to stop the test after 8000laps due to the extremely high wear degree of the counterbody, see table A.8 from appendix.

In order to assess if a high contact pressure leads to a better wear behaviour without being influenced by the addition of compressed air, the last set of parameters (4.1 and 4.2) were used. Consequently, the results of this last test (Fig. 4.51) are similar to the previous with the exception that the experiment had to be stopped even earlier, at 3000 laps due to the combination of compressed air and high load. This test demonstrates that a higher contact pressure (80N), when using compressed air has no influence on the tribofilm adhesion, contrary to the case when high rotational speed is applied. The wear debris generated during the sliding test, which form the thin lubricating film could not adhere onto the coating surface and due to that a premature damage of the conterbody was obtained, see figure A.8 in appendix.

All the above highlighted results lead to the statement that the wear behaviour of such coatings has a close connection to the testing conditions. It was found that the addition of compressed air during the wear experiments has a negative influence on the sliding wear resistance, when testing under lower intensities (e.g. 200 rpm). Contrary, at high testing speed the compressed air has "no time" to remove the formed tribofilm and due to that, the tested coatings exhibit a high wear resistance. Based on this, one can conclude that these types of coatings require high intensity working conditions in order to "defend" themselves against wear. Therefore, under the first and the second set of parameters, the graphite tribofilm adhesion had proved to be very strong, due to the high sliding speed (475 rpm). Even in the case of lower normal loads (40N instead 80N) the compressed air has no effect on the wear behaviour of the tested specimens.

Moreover, it was also proved that the WC grain sizes used for the WC-Co-Cr coatings depositions have less influence onto the wear behaviour under these testing conditions. The fine and the coarse powder showed similar performance during the sliding wear tests.

These investigations results may be correlated with the friction coefficient behaviour of the WC-Co-Cr coatings presented in section 4.3, where after the pin on disc process optimization it was concluded that such kind of coatings required especially high rotational speed of the tested specimen and longer sliding distance to reach the steady state.

With regards to the above mentioned discussions one can conclude that the appearance of the graphite tribofilm on the coating surface assures a good sliding wear resistance, lubricating the exposed surface and decreasing also the friction coefficient. This fact is valid only in the case when no compressed air is used or in case of high intensity tests.

4.6 Corrosion resistance of HVOF coatings sprayed of inner surfaces

This part of the work describes the corrosion behaviour of both investigated coatings. Disc-like coated specimens, in the form of round test pieces (disc-like, see figure 3.16) with a substrate of heat-treated steel, were electrochemical investigated by using the potentiodynamic polarization testing method and the three electrode open cell. The working principle of this type of cell was described in the previous chapter.

Before the corrosion tests, the coated surfaces were grinded and polished to roughness values (Ra measurements-perpendicular to the grinded direction) as illustrated in table 4.14. The specimens were sealed (teflon band was applied around the specimen boundary) and than mounted into a special sample holder (working electrode) in order to expose the surface of the coating to the testing solution, without any influence from the specimen substrate. Hence only the exposed coating surface (approx. Ø 12mm) was electrochemically active. Similar to the other investigations, these tests were also repeated at least three times for each type of coating under identical testing conditions. Moreover, the surface roughness was measured after the corrosion test in order to calculate the roughness difference ΔRa, see table 4.14. Besides of that, the solid, powder-like residues in the aqueous solution were filtered in order to examine their composition, using the vacuum pump illustrated in the previous section.

Table 4.14 Specimens roughness before and after the corrosion test

Coating type	WC-Co-Cr (-10+2μm)	WC-Co-Cr (-25+5 μm)	WC-Co-Cr (-45+20 μm)	WC-Cr_3C_2-Ni (-10+2 μm)	WC-Cr_3C_2-Ni (-22+5 μm)	WC-Cr_3C_2-Ni (-30+5 μm)
Roughness before [μm]	0.10	0.13	0.11	0.10	0.11	0.10
Roughness after [μm]	1.74	1.36	1.58	1.87	1.82	2.65
Roughness difference ΔRa [μm]	1.64	1.23	1.47	1.77	1.71	2.55

The corrosion tests were carried out in 1 molar NaCl solution at room temperature. The applied potential was varied between -1500 and 1500 mV versus SCE electrode (saturated calomel electrode) at a scan rate of 10 mV/s.

It is known that, the chemical compositions of the metallic binder, the amount and the size of the carbide particles, the phase transformations during the deposition process, as well as the coating porosity are some of the additional factors, which should be taken into account at the examination of the corrosion behaviour of such cermet sprayed coatings [117, 133].
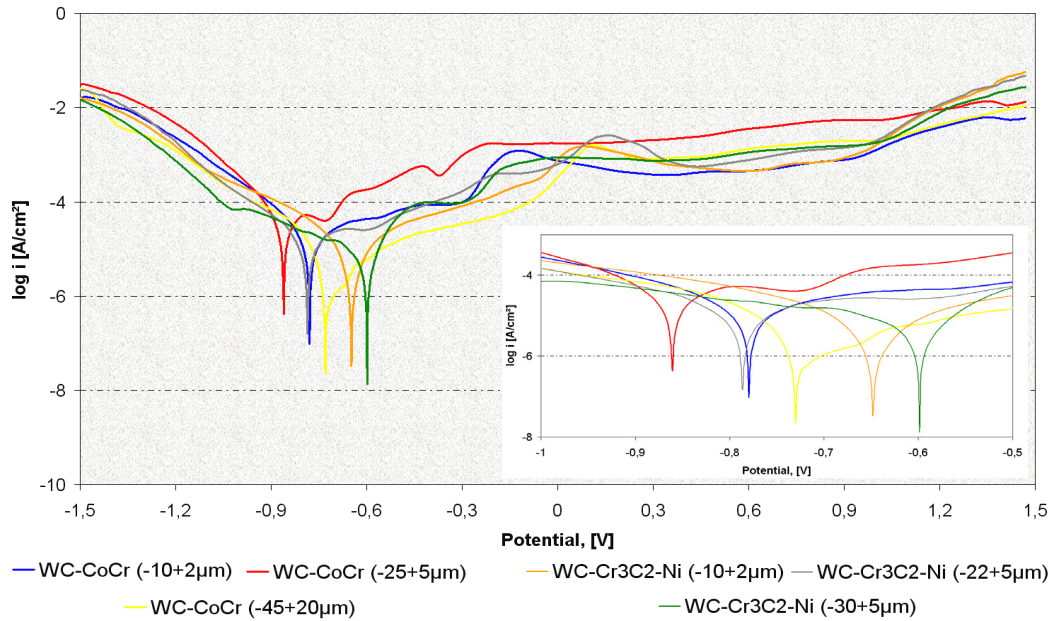
Figure 4.52 Anodic potentiodynamic polarization curves recorded during the corrosion tests

Figure 4.52 shows the polarization curves measured at free corrosion potential of all the investigated coatings. The rates of corrosion, expressed in current density i_{corr} at the corrosion potential E_{corr} of those coatings are presented in table 4.15. The results reveal a shift of the corrosion potential from -593 mV to about -855 mV and an decrease of the corrosion rate (based mainly on the low value of 1.30 $\mu A/cm^2$) corresponding to the WC-Co-Cr coating obtained from coarse powder. The WC-Cr_3C_2-Ni coating (-30+5μm powder) exhibited a similar current density value, but the corrosion potential was different.

Table 4.15 Electrochemical data for the WC-based coatings in 1 M NaCl

Coating type	WC-CoCr (-10+2 μm)	WC-CoCr (-25+5 μm)	WC-CoCr (-45+20 μm)	WC-Cr_3C_2-Ni (-10+2 μm)	WC-Cr_3C_2-Ni (-22+5 μm)	WC-Cr_3C_2-Ni (-30+5 μm)
E_{corr} [mV]	-772.9	-855.5	-755.7	-639.3	-780.6	-593.1
i_{corr} [μA/cm²]	6.22	17.7	1.30	2.78	4.83	2.12
v_{corr} [mm/y]	0.28	0.8	0.059	0.18	0.34	0.16

Correlating the obtained roughness changes of the tested surfaces with the corrosion results, no conclusive explanation can be given. It can only be assumed, that in case of low corrosion resistance due to the coating microcracks and/or porosity, the corrosion attack is propagated mostly along these, affecting just superficially the exposed surface during the entire test, see coating WC-Co-Cr (-25+5μm) in table 4.14 (the most corroded specimen showed the lowest ΔRa). This coating has recorded the highest current density leading to the lowest corrosion resistance of all the tested specimens. Figure 4.53 illustrates the surface of this

specimen after the electrochemical corrosion test. It can be observed that the exposed surface reveals localized corrosion appeared in form of pittings concluding in cracks propagations. Consequently, there are some definite locations in the coating where the electrolyte can reach the steel substrate very easily. In those locations, the anodic dissolution of the substrate is partially fast, so that a very large amount of corrosion products accumulates along the coating/substrate interface and detaches the coating, lifting it off the substrate surface. The corrosion products can therefore emerge to the specimen surface, giving rise to the iron oxide spots visually noticeable in the same figure. When the coating spalls off, it cannot exert any protective action toward the substrate, which can be directly accessed by the electrolyte leading to an increase in the corrosion rate up to 17.7 µA/cm2, see table 4.15. This is explained by the severe galvanic corrosion occurring on the exposed substrate while the surrounding coating acts as a cathode. Simultaneously, during the test many more gas bubbles appear: this indicates a definite acceleration in the chatodic reaction, witnessing an increase in the overall rate of the electrochemical corrosion reaction.
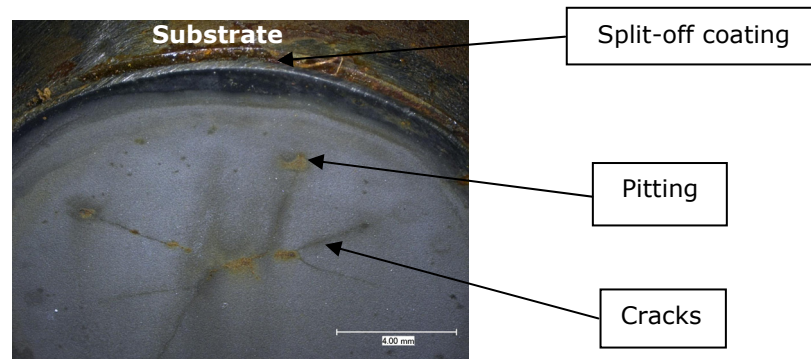

Figure 4.53 SM-micrograph of the highest corroded specimen (WC-Co-Cr (-25+5µm) powder)

A similar corrosion behaviour was observed in the case of the specimen coated with WC-Cr$_3$C$_2$-Ni medium sized powder, see table A.9 attached in the appendix (for the corroded surface appearance of all the specimens consult the same table). All the other specimens excepting the already mentioned one, present corrosion attack all over the exposed surface, which is known as the mechanism of uniform corrosion. In this case, no effect of accelerated local corrosion of the substrate occurred. Minor amounts of corrosion products precipitating inside the coating defects are present, which allow just a slowly penetration of the electrolyte throughout the dense coating.

After polarization experiments up to +1500mV, the coatings were investigated by means of scanning electron microscopy supported be EDS analysis in order to investigate the morphology of the corroded zones. The SEM examination (Fig. 4.54) of the specimen surface illustrated above, provides a closer image of the formed pitting and also the cracks propagations. The cross section of this corroded area shows the presence of many cracks mostly oriented toward the depth of the coating that will clearly reach the substrate concluding in high material damage. It was difficult to find exactly the pitting propagation area in which the cracks are reaching the substrate because of the coating brittle structure.
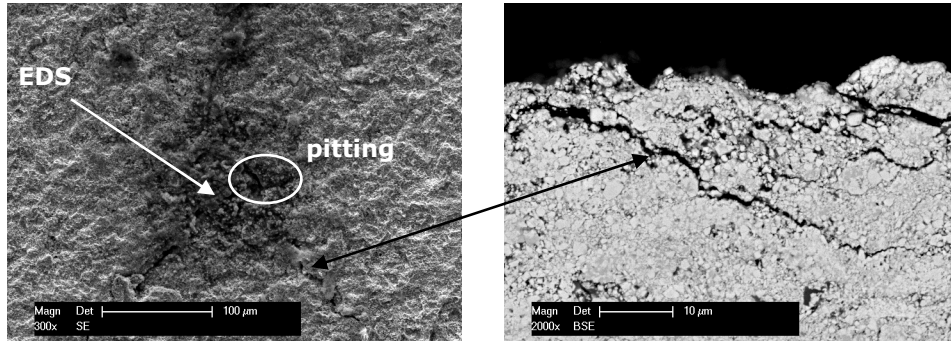
Figure 4.54 SEM micrograph of the corroded surface (after polarization up to +1500mV) illustrated in figure 4.53 and the corresponding cross section

The following EDS spectrum (measured in the area marked by the arrow in figure 4.54) identifies an increased signal for both iron and oxygen which confirms the existence of iron oxide leaching out from the substrate on the coating surface due to the electrochemical reactions. Besides these two main signals, as expected the C, W, Cr belonging to the coating chemical composition and the Cl peak signal corresponding to the electrolyte solution are also present in the related spectrum.
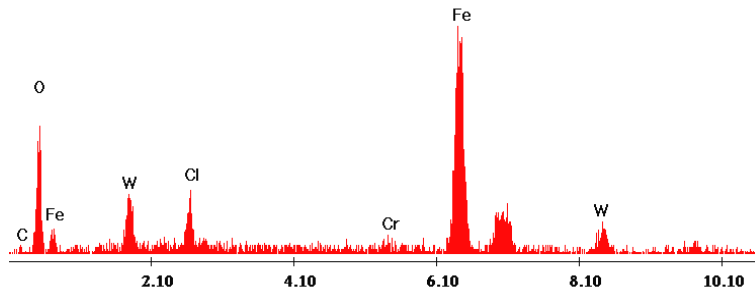

Figure 4.55 EDS spectrum of the corroded surface presented in figure 4.54

Correlating the E_{corr} (nobler potential) recorded of the WC-Co-Cr (-25+5µm) coating with the figure 4.3 from section 4.1, many interconnected pores between the top surface and the substrate interface therefore can be observed, making the resistance against electrolyte penetration in the coating low and the anodic dissolution of the substrate easy. In such cases the increase in thickness and the remarkable decrease in coating porosity will improve the substrate protectiveness. On the other hand, it is known that the grater the coating thickness is the higher the deposition costs are. Therefore, a thin coating with a high density structure is desired, representing the optimal solution under such corrosion conditions.

Further SEM micrographs of specimens cross sections (Fig. 4.56 a; b) show that both metallic binder seams to corrode very fast under the testing conditions and undermines the carbide particles. In the case of WC-Co-Cr coatings, cobalt seems to corrode actively, while chromium steel forms a passive oxide layer, which offers corrosion protection for a defined time. This fact was also confirmed by the EDS spectrum of the very fine corrosion residues presented in figure 4.57. Moreover, the

XRD investigations (Fig. 4.58) confirms the EDS results, recording high amounts of Co_3O_4 (~56%), Fe_3O_4 (4%) and WO_3 oxide.

The corrosion products formed during the potentiodynamic measurements of the WC-Cr_3C_2-Ni coatings were filtered from the electrolyte and investigated by means of X-ray diffraction. The phase composition identified besides NaCl, a high amunt of NiO_2 (37%) and WO_3 (19%) as well. The negligible amount of CrO_2 is explained by the chemical phase of chromiumcarbide present in the coating composition. In such situations, there is evidently that during the exposure into the electrolyte, the metallic binder will be first of all susceptible to oxidation.

As these investigated coatings have a complex compositions, it could be mentioned that the possibility of micro-galvanic corrosion activity between the different microstrucuture and the composition is likely to undermine surface integrity. Considerable micro-galvanic corrosion occurred between the hard WC particles and the metallic binder, and uniform corrosion occurred in the binder materials.
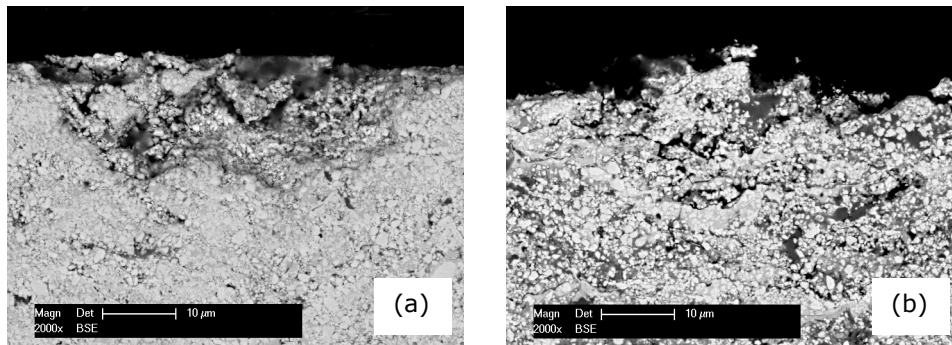

Figure 4.56 Cross sections of the corroded WC-Co-Cr (a) and WC-Cr_3C_2-Ni (b) coatings
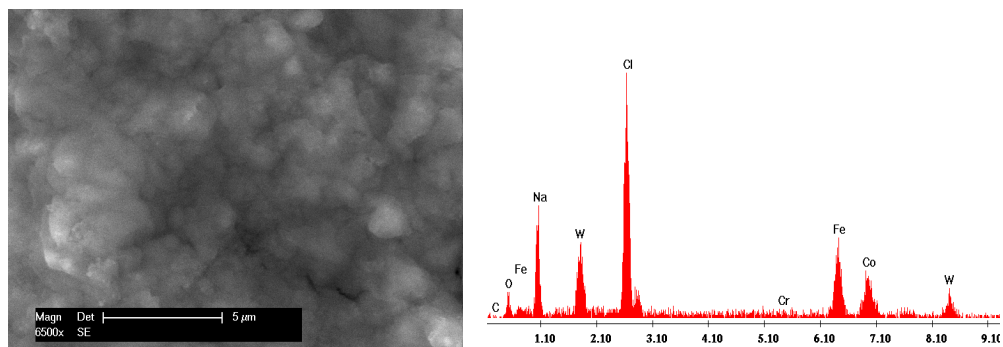

Figure 4.57 The resulted corrosion residues in case of WC-Co-Cr coating and the corresponding EDS
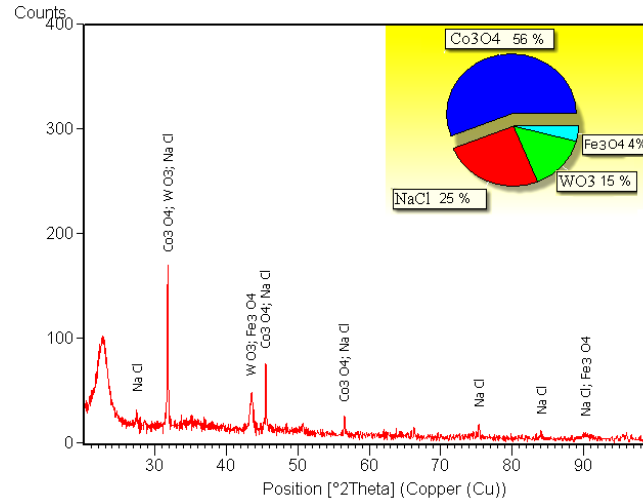
Figure 4.58 The XRD diffraction patterns of the corrosion residues collected after the electrochemical test (WC-Co-Cr coatings)
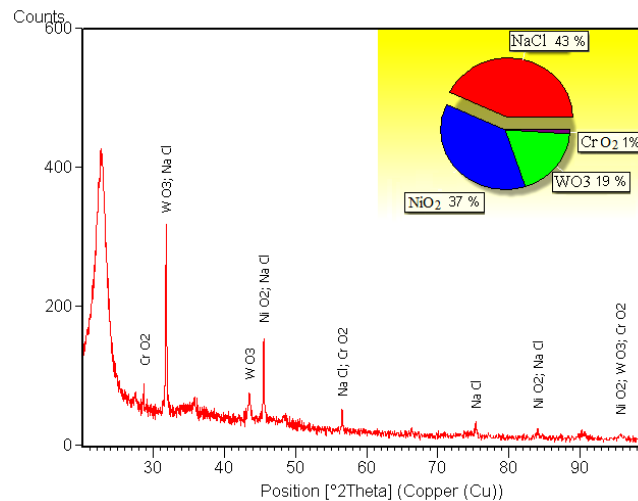

Figure 4.59 The XRD diffraction patterns of the corrosion residues collected after the electrochemical test (WC-Cr$_3$C$_2$-Ni coatings)

Besides of the above investigations, it is important to be noted that after the electrochemical tests, the electrolyte has shown different shades depending on the chemical composition and the amount of corrosion residues. According to this, in case of all the investigated coatings obtained from WC-Cr$_3$C$_2$-Ni powders, the electrolyte exhibits a yellow appearance, different than that of WC-Co-Cr coatings, see figure A.5 attached in appendix. The analysing of this electrolyte remains as outlook for further work in order to see which kind of dissolution takes place.

For a better overview of the corrosion results, figure 4.60 summarized the spread of the corrosion resistance of both investigated coatings as a function of corrosion rate mm per year. Based on the overall corrosion rates, the WC-Cr$_3$C$_2$-Ni coatings seem

to offer a slightly better (stable) corrosion protection that the WC-Co-Cr coatings. An exception to this is the WC-Co-Cr coating obtained from coarse powder, which shows also the best corrosion resistance. However, both types of coatings exhibit an optimal corrosion resistance excluding the ones with high porosity degree, considering that the best recorded corrosion rate was approximately 60µm/year under these severe testing conditions.
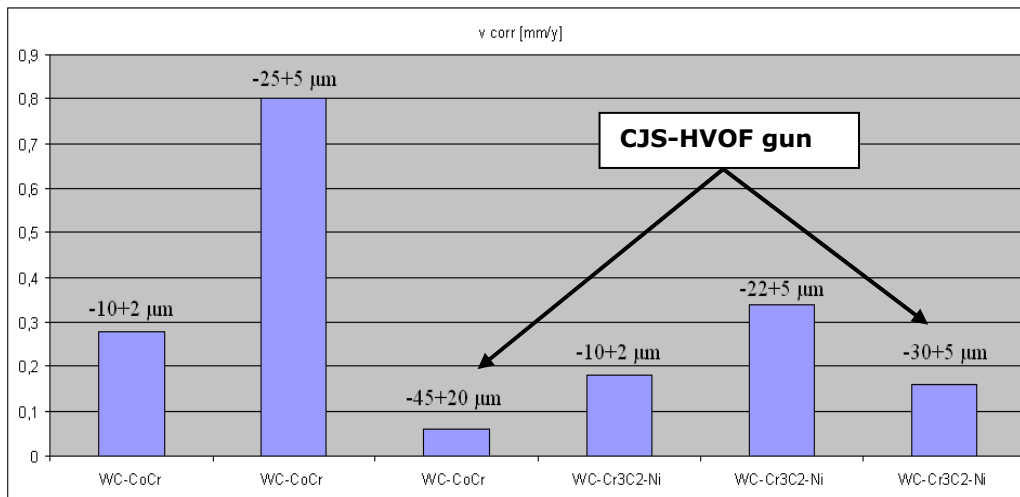

Figure 4.60 The corrosion rate of the investigated coatings

As in the figure above may be observed, the corrosion rates show a dependence on the type of HVOF spraying process. Therefore, the specimens coated with the CJS-HVOF gun from outside (coarse powders), reveal the best corrosion behaviour followed closer by the other two coatings obtained from fine powders by using the ID CoolFlow mono gun.

The higher corrosion resistance of both WC-based coatings sprayed by CJS technique may therefore be ascribed to the process parameters, which are well known and have been applied in practice for a long time for the depositions of such coarse powders. Contrary to medium powders, which from empirical results appear to create problems in finding the appropriate parameters for spraying on inner diameters (constrained environment) because they tend to form coatings with high porosity. This phenomenon induces automatically a lower corrosion resistance. Due to that, during the corrosion test the corrosive electrolyte penetrates along the formed cracks or interconnected pores and reaches the substrate causing the detachment of the coating.

Some authors, affirmed that the corrosion behaviour of hardmetals obtained from different grain sizes and tested in various solutions shown a clear tendency that the smaller the grain size, the higher the corrosion resistance. Whereas, the results of this research stipulate that the highest influence over the corrosion resistance of such coatings belongs to the spraying parameters instead of the powder granulometric fraction and/or the chemical composition. On the other hand, the powder characteristics (mentioned above) could exhibit an important roll for the corrosion resistance in case of a very stable spraying process (control of the porosity degree of the coatings). Even in this case, when low porosity coatings are

obtained, but the existing pores are somehow interconnected, the corrosive electrolyte will penetrate up to the coating/substrate interface leading to large corrosion damage. Contrary, porous coatings could exhibit better corrosion resistance, when random pores are not interconnected in comparison with the latter case. Under these circumstances it may be conclude that the corrosion investigations of such coatings are very difficult to perform in order to achieve reproducible results and thus, clear corrosion performance to predict.

Chapter V

CONCLUSIONS, ORIGINAL CONTRIBUTIONS AND OUTLOOK

5.1 Conclusions

The purpose of this work was to investigate the tribological and corrosion behaviour as well as the morphology of WC-based cermet coatings sprayed under ID conditions. For that, two different cermet powders (WC-Co-Cr 86-10-4 and WC-Cr_3C_2-Ni 70-23-7), each having three granulometric fractions were deposited. The spraying process was performed using a special ID sample holder and two different spraying systems according to the powder grain size, a new developed ID CoolFlow mono gun for the fine and medium sized powders and a classic CJS gun for the coarse ones. The use of the latter gun was a compromise because the coarse powder is not recommended for ID gun, so that the coatings were deposited from outside by angling the CJS gun into the cylinder.

It was clearly pointed out that the coating density, including splat flattening and interlamellar adhesion, are important in order to produce high quality coatings and that they must be prioritized in the coating parameter optimization. Moreover, it was demonstrated that for each powder type, different process parameters must be used due to the different melting degrees.

The coatings microstructures were characterised and correlated with the spray system, powder grain size and spray parameters. The WC-Co-Cr coating obtained from fine powder (-10+2µm) provides the densest and most uniform coating and can be further recommended due to its high deposition efficiency under ID conditions. In contrast, the WC-Co-Cr (-25+5µm) powder showed the highest porosity degree after the spraying process, which indicates that this granulometric fraction can not be recommended to be sprayed with ID HVOF guns. The WC-Cr_3C_2-Ni coatings showed similar microstructures only that the deposition efficiency of this powder is lower in comparison with the WC-Co-Cr one. This lower deposition efficiency was also observed when spraying the ring specimens from outside by angling the CJS gun to 60° off-normal.

Based on the results of this work, some limitations of ID HVOF spraying process can be stated: for coating inner surfaces with diameters of 130mm it is highly recommended to use fine powders; in general this method is not suitable for coating IDs below 100mm due to the short standoff distance (distance from gun to surface ~ 30mm); the spraying depth as well as the extraction of the overspray are problematic. Depth is limited firstly, by the length of the custom extension that carries the gun and secondly by the overspray extraction. The standard lengths are generally 20-150mm; longer custom extensions can usually be supplied by the manufacturer in order to reach different spraying depths. If the extension is too long the gun will pose problems due to lack of rigidity. The minimum coatable diameter is

defined by the size of the HVOF gun and also by the powder grain size, which have a direct influence onto the required standoff.

Due to the use of fine powders granulations (smaller standoff) and also to Thermico's new ID CoolFlow Mono gun which subjects the components to only moderate thermal strain, avoiding overheating, the HVOF for ID coatings has become a realistic technology. Moreover, this type of gun allows spraying of high-hardness and low-porosity ID coatings with a low degree of WC-phase decomposition. Regarding the coatings microhardness, no significant differences were recorded between the as-sprayed coatings (from 980 to 1124 HV0.3).

The most important challenge of this PhD thesis was the conception and construction of a special wear tester (cylinder on ring) which made possible the sliding wear testing of inner cylindrical surfaces. Moreover, due to its design, the counterbody can be coated with any kind of coating required for a specific sliding wear test. This opportunity allows the optimal tribopairs selection when different types of coatings are rubbing against each other. The contact type between the tribopairs is in form of a "line-surface", which overcomes the well known premature wear of the counterbody (see the pin on disc arrangement) as well as allows a closer simulation of the working conditions. Until today such types of wear testers were not practicable, while all the other available were suitable only for outer surfaces.
The cylinder on ring wear tester has demonstrated to be a very useful and flexible tribometer in the area of tribological testing of inner thermally sprayed surfaces. Such wear tests are useful in order to develop an efficiency increase in wear resistance of these kind of coatings.

The tribological examinations were performed by analyzing first, the friction coefficient and then the wear resistance under dry (ambient atmosphere) and wet (in water) conditions. Because of the inability of the cylinder on ring to measure the friction coefficient, this was determined by using the pin on disc test method based on the ASTM G99 & DIN 50324. It was demonstrated that the friction coefficient of WC-Co-Cr exhibit lower values than that of WC-Cr$_3$C$_2$-Ni coatings regardless of the granulometric fraction used. This result was associated with the higher amount of hexagonal phases recorded in the first coating which conform to others researches, allows a better sliding behaviour. Moreover, it was showed that, the test parameters need to be chosen very carefully in order to obtain representative results.

The cylinder on ring sliding wear tests have revealed similar results as the pin on disc tests namely that the WC-Co-Cr coatings exhibit a significantly better sliding wear resistance in comparison with the WC-Cr$_3$C$_2$-Ni one under both testing conditions.
Under dry condition, the specific wear rates of the WC-Co-Cr coatings were mostly negative, due to the material transfer from the counterbody to the inner surface of the ring specimens.
In contrast, the WC-Cr$_3$C$_2$-Ni coatings have exhibit higher wear rates without the existence of material transfer phenomena. Similar results were observed also under wet testing conditions.

The wear results were attributed to the formation and most important to the adhesion or not of the graphite tribofilm onto the specimen surfaces. The tribofilm

adhesion was demonstrated to be strongly influenced by the crystalline structure of the coatings (the higher the hcp structure, the better the adhesion). In contrary, the high amount of fcc structure ($\sim$ 70%) identified on the worn track surface in case of WC-Cr$_3$C$_2$-Ni, leads to the appearance of strong acting forces (especially the shear one) which are able to transform the hexagonal graphite packing arrangement into a rhombohedral one. As a consequence of this, the tribofilm adheres poorly to the coating surface during the entire sliding wear test, conducting to high wear rates.

The mechanism for the formation of the thin graphite film could be mainly based on the following two reasons: due to the existence of free carbon (decomposition of WC into W$_2$C and not entirely oxidized to CO_2) separated from the tungsten carbide particles during the spraying process and which could rapidly diffuse to reach the coating surface during testing or according to Holmbergs and Matthews theory [48], one should consider that some tribochemical reactions which can take place on the surfaces, during the sliding contact and can be strongly influenced by the high local pressures and the flash temperature, often between 1000°C and 2000°C, occurring especially at spots of asperity collisions of hard coatings. Therefore, a possible decarburisation degree of the WC-phase during the sliding wear tests has to be taken into consideration. Only this additional phenomenon may explain the high amount of graphite detected by the XRD-measurments. Unfortunately, there was no accessible instrument or method in order to measure the contact temperature between the two tribopairs and thus, to confirm clearly that a decomposition of WC into W$_2$C took place during the sliding tests. These challenge remains as outlook for further research works.

Correlating the pin on disc results with the cylinder on ring one, the formation and adhesion of the graphite tribofilm onto the WC-Co-Cr coatings, explains the lower coefficient of friction recorded by this type of coating, besides of the hypothesis regarding the hcp structures discussed above.
It can be said that the WC-Co-Cr coatings are intrinsically able to give both low friction and wear, conferring them a very important characteristic, knowing that only a very limited number of materials (outstanding examples: carbons, graphite, and some polymers) has such capability. The tribological properties of these coatings are markedly improved by the adhesion of the thin graphite tribofilm onto the coating surface. The dense soft film protects the surface from further damage, thereby reducing the initial higher wear rate to a relatively lower steady wear state. In other words the formation of this film corresponds with the transition from the severe wear regime to a very mild one that occurs between the tribopiars. This affirmation was supported also by the temperature of the tested specimens (water as well) measured during the sliding wear tests.

Accordingly to the results of preliminary wear tests, one can select which of the moving elements is desired to be the interchangeable part into a working assembly. For example, when the ring (housing) is coated with fine powder and the cylinder (axle journals or pistons) with coarse powder, the latter one is designed to be the sacrificial part and needs to be periodically chanced. Moreover, specimens coated with powder from the same chemical composition and fraction (especially fine grain size) sliding against each other, usually lead to high wear rates of both tribopairs.

Additionally to the wear test investigations, the influence of the compressed air onto the wear behaviour of WC-Co-Cr coatings was studied. It was showed that, depending on the working conditions, one may produce self lubricating surfaces.

The one common issue regarding the corrosion resistance, seen across all the coating composition types and powder fractions investigated, is the need for high quality and fully dense coatings to remove substrate corrosion influences, to improve coatings life and to stop spallation. It was demonstrated that the corrosion behavior of the investigated coatings depends mostly on the spraying parameters which have direct influence onto the coating porosity. According to the best recorded corrosion rate, namely 60µm/year, it can be concluded that the investigated coatings exhibit lower corrosion resistance after exposure to severe testing conditions (1M NaCl). The field of protecting components against corrosion remains a challenge for the HVOF process due to the risk of interconnected pores, which lead to a very difficult corrosion rate estimation. Therefore, the corrosion effect on coated components working in aggressive environments will be hard to anticipate. These coatings can be recommended to be used against corrosion only for components that do not affect other parts in case of coating spallation (no risk) and can be easily overhauled by respraying.

Based on all the investigations proceeded in this work, it can be concluded that the WC-Co-Cr coatings obtained from fine powder (-10+2µm) presents the best compromise between the wear and corrosion behaviour, when exposed to severe conditions. Moreover, this type of coating exhibits also optimal deposition efficiency during the HVOF process, thus minimizing the spraying costs. It can be said that this work was dealing with questions that are essential for a good performance of HVOF thermal spraying coatings for inner surface components. All these pieces of information and results have to be documented in such a way that they can be used as a knowledge base for the future.

5.2 Original contributions

Theoretical and experimental researches conducted during this PhD work have lead to the accomplishment of HVOF cermet coatings sprayed on inner cylindrical surfaces with enhanced wear and corrosion resistance. In respect to these, the main purpose, namely the production and testing of ID HVOF coatings, had to be established for the achievement of a better applicability in practice. Therefore, a new design of sample support was constructed in order to provide spraying conditions as close as possible to those encountered during the coating of inner cylindrical surfaces. On the other hand, the wear resistance of the investigated ID coatings was possible to be performed due to the construction and development of the cylinder on ring wear tester that allows the opportunity to coat both tribopairs with the desired type of material.

According to the sliding wear tests, optimal test parameters were obtained: reaching the stability level of the friction coefficient, as well as the possibility to observe which kind of wear mechanisms occur under severe test conditions using the same or different types of coatings for the tribopairs. Based on that, changes in coatings structure and also the formation of a graphite tribofilm were detected after the sliding wear tests. The structure and properties of the resulted wear debris were established. It was determined under which conditions, the formed graphite

tribofilm may adhere or not onto the coating surface. An overview regarding the influence of the testing atmosphere and/or environment on the wear behaviour of this type of coatings was also contoured. For example, it was demonstrated under which circumstances, the compressed air has or has not an influence onto the wear behaviour, when two cermet coatings are sliding against each other. Moreover, due to the prescription of the optimal spraying parameters high quality coatings were obtained, that are able to assure the best compromise between the wear and corrosion resistance under severe operating conditions.

5.3 Outlook

The theoretical and experimental studies conducted in the present thesis emphasises the current trends of the HVOF cermet coatings properties, deposited under ID conditions, as well as the vastness of this domain.
In this regard, some further research directions can be outlined as:
- experimental coatings using new powder types – e.g. plasma treated;
- attempts to spray inner cylindrical surfaces with very small diameters (e.g. Ø 80mm), employing fine (nanotype) plasma treated powders;
- attempts to spray inner diameters with depths higher than 500 mm;
- assessment of the deposition efficiency of various types of powders during spraying under ID conditions in order to evaluate the deposition costs;
- investigations of the "white powder" resulted in the POD test;
- investigations regarding the friction coefficient of the same type of coatings as the ones presented in the thesis, applying different loads;
- fitting the testing device (cylinder-on-ring) with a friction coefficient sensor, temperature measurement sensor, and a data recording and analysing computer system;
- development of an advanced modelling software for the cylinder on ring sliding wear simulation;
- tests regarding the mechanical properties (e.g. adhesion, flexural strength, tensile strength etc) of the as-sprayed specimens;
- cylinder on ring wear testing of tribopairs materials (same chemical composition) using different environments as well as other material combinations, especially to follow if the graphite tribofilm appears or not;
- further research regarding the unstable structure of graphite during the sliding wear tests;
- further potentiostatic analysis to determine the coatings corrosion resistance;
- analysis of the water resulted after the corrosion tests.

References

[1] Robert J.K. Wood "Tribology of thermal sprayed WC–Co coatings", Int. Journal of Refractory Metals & Hard Materials, vol. 28, p 82–94, Elsevier 2010

[2] K. O. Legg, B. D. Sartwell, et al, "Investigation of Plasma Spray Coatings as an Alternative to Hard Chrome Plating on Internal Surfaces", SERDP Project WP-1151 Final Report, 2006

[3] T. Sahraoui et al, "Structure and wear behaviour of HVOF sprayed Cr_3C_2-NiCr and WC-Co coatings", Materials and Design 24, p 309-313, 2003

[4] J. Laurila, K. Niemi et al, "Degradation mechanisms of thermally sprayed coatings in chloride containing electrolytes", International Thermal Spray Conference & Exposition, Thermal Spray: Global Solutions for Future Application (DVS-ASM), p 762-767, 2010

[5] C. Monticelli, A. Balbo, F. Zucchi, "Corrosion and tribocorrosion behaviour of cermet and cermet/nanoscale multilayer CrN/NbN coatings", Surf. Coat. Technol., vol. 204, p 1452-1460, 2010

[6] A. Souza and A. Neville, "Linkining electrochemical composition behaviour and corrosion mechanisms of thermal spray cermet coatings (WC-CrNi and WC/CrC/CoCr)", Materials Science and Engineering A352, p 202-211, 2003

[7] M. Perry, A. Neville, and T. Hodgkiess, "A Comparison of the Corrosion Behavior of WC-Co-Cr and WC-Co HVOF Thermally Sprayed Coatings by In Situ Atomic Force Microscopy (AFM)", Journal of thermal spray technology, vol. 11, p 536-541, 2001

[8] L. Fedrizzi, L. Valentinelli, S. Rossi, and S. Segna, "Tribocorrosion Behaviour of HVOF Cermet Coatings", Corros. Sci. 49, p 2781-2799, 2007

[9] R. Tinklepaugh, W.B. Crandall, "Cermets", Chapter 1, Reinhold, 1960

[10] N-R.V. Bangaru, C. Chun et al, "Advanced erosion-corrosion resistant boride cermets", US Patent 7,157,687 B2, 2007, url: http://www.freepatentsonline.com/7175687.html

[11] E.C. Van Schoick, Ed., "Ceramic Glossary", The Ceramic Society, 1963

[12] R. Nunes, J.H. Adams et al, "Properties and Selection: Nonferrous Alloys and Special-Purpose Materials", ASM Handbook, ISBN 0-87170-378-5, vol. 2, 1990

[13] P. Ettmayer and W. Lengauer, "The Story of Cermets", Powder Metal, vol. 21, p 37-38, 1989

[14] E. Rudy, "Boundary Phase Stability and Critical Phenomena in Higher Order Solid Solution Systems", J. Less-Common Met., vol. 33, p 43-70, 1973

[15] A.J. Sturgeon, et al, "British Ceramic Proceedings", vol. 54, p. 57, 1997

[16] K.E. Schneider, V. Belashchenko, M. Dratwinski, S. Siegmann, A. Zargorski, "Thermal spraying for power generation components", Weinheim, ISBN: 3-527-31337-0, p. 25;26, 2006

[17] K. Schroeter, U.S. Patent 1,549,615, 1925

[18] H. Moissan, "The Electrical Furnace", V. Lenher, Trans., Chemical Publishing Company, 1904

[19] E.K. Storms, "The Refractory Carbides", Academic Press, 1978

[20] M. Hansen and K. Anderko, "Constitution of Binary Alloys", McGraw-Hill, 1958

[21] S. V. Nagender Noldu and P. Rama Rao, "Phase diagram of binary tungsten alloys", The Indian Institute of Metals, Electronic Publishing Center, new Delhi, India, p 37, 1991

[22] Zhengui Yao, Jacob J. Stiglich and T. S. Sudarshan, "Nano-grained Tungsten Carbide-Cobalt (WC/Co)", Materials Modification, Inc. 2929, 2002

[23] J He, Y. Liu et al, "Metallurgical and Materials Transactions", A 32, p 145-147, 2002

[24] D.A. Stewart, P.H. Shipway, D.G. McCartney, "Abrasive wear behaviour of HVOF sprayed WC-Co coatings", Surf. Coat. Technol., vol. 105, p 13-24, 1998

[25] Y. Qiao, T.E. Fischer, A. Dent, "The Effects of Fuel Chemistry and Feedstock Powder Structure on the Mechanical and Tribological Prop-erties of HVOF Thermal-Sprayed WC-Co Coatings with Very Fine Structures", Surf. Coat. Technol., vol. 172, p 24-41, 2003

[26] K.H. Baik, J.H. Jang, S.Y. Hwang, "Nanostructured WC-Co Coatings from Different Feedstock Powders" Mater. Sci. Forum, vols. 449-452, p 1293-1296, 2004

[27] J. Li, Y. Zhang, J. Huang, C. Ding, "Mechanical and tribological properties of plasma-sprayed Cr_3C_2-NiCr, WC-Co and Cr_2O_3 coatings", Journal of Thermal Spray Technology, vol. 7(2), p 246, 1998

[28] C. Richard, J.Lu, J.F Flavenot, F.Decops, "Study of Cr_3O_2 coating materials and characterization by an interfacial test of coating/substrate adherence", Thermal spray, ASM international, p 11-16, 1992

[29] E.F. Rybicki and E.D. Case, "Elastic modulus determination of coatings layers as applied to layered ceramic composites", Mater. Sci. Eng., vol. A 132, p 39-47, 1991

[30] B. Winkler, E. A. Juarez-Arellano et al "Reaction of titanium with carbon in a laser heated diamond anvil cell and reevaluation of a proposed pressure-induced structural phase transition of TiC", Journal of Alloys and Compounds, vol. 478, p 392–397, 2009

[31] R. Nunes, J.H. Adams et al, "Surface Engineering", ASM Handbook, ISBN 0-87170-377-7, vol. 5, 1994

[32] http://www.sandvik.com

[33] K. Simunovic, "Thermal spraying", Welding engineering and technology, Encyclopaedia of Life Support Systems (EOLSS), 2004

[34] Prof. Knight, "Thermal Spray: Past, Present and Future, A Look at Canons and Nanosplats", Thermal Spray Term Paper – MATE-580, Philadelphia PA 19104, 2008

[35] DIN EN 657, "Thermal spraying; Terminology, classification ", 2005

[36] E. Turunen, "Diagnostic tools for HVOF process optimization", VTT Technical Research Centre of Finland, VTT Publications 583, p 66 p + app. 92, Espoo 2005

[37] E. Turunen, A. Hirvonen et al, "Application of HVOF Techniques for Spraying of Ceramic Coatings", Advances in Technology of Materials and Materials Processing Journal, vol. 9, p 63-68, 2007

[38] L. Pawlowski, "The Science and Engineering of Thermal Spray Coatings", Second Edition, ISBN 978-0471-49049-4, 2008

[39] J.R. Davis, "Handbook of Thermal Spray Technology", Thermal Spray Society, ASM International, Materials Park, OH, USA, p 338, 2004

[40] P. Heinrich, "Thermal spraying - Facts and state of the art", Sonderdruck, E10/92, p 28, 1992

[41] L. Pawlowski, "The science and engineering of thermal spray coatings", John Wiley & Sons, New York, NY, USA, p 432, 1995

[42] A. Kulkarni, J. Gutleber, S. Sampath, A. Goland, W.B. Lindquist, H. Herman, A.J. Allen & B. Dowd, "Studies of the microstructure and properties of dense ceramic coatings produced by high-velocity oxygen-fuel combustion spraying" Materials Science and Engineering A369(2004), p 124-137

[43] D.A. Ramm, T.W. Clyne, A.J. Sturgeon & S. Dunkerton, "Correlations between spraying conditions and microstructure for alumina coatings produced by HVOF and

VPS" Proceedings of the 7th National Thermal Spray Conference, 20.24 June, 1994, Boston, Massachusetts, USA, p 239-244, 1994

[44] A.J. Sturgeon, M.F. Harvey & F.J. Blunt,"The influence of fuel gas on the microstructure and wear performance of alumina coatings produced by the High Velocity Oxyfuel (HVOF) thermal spray process", British Ceramic Proceedings, Vol. 54, p 57-64, 1997

[45] A. J. Sturgeon, "Recent advantages and applications of thermal sprayed ceramic coatings", British Ceramic proceedings, vol. 55, p 3-12, 1996

[46] S. Sampath, X. Jiang et al, "Development of process maps for plasma spray: case study for molybdenum" Materials Science and Engineering, vol. A348, p 54-66, 2003

[47] E. Turunen, T. Varis et al, "Parameter optimization of HVOF sprayed nanostructured alumina and alumina–nickel composite coatings", Surface & Coatings Technology, vol. 200, p 4987-4994, 2005

[48] K. Holmberg, A. Matthews, "Coatings Tribology-Properties, Techniques and Applications in Surface Engineering", tribology series, 28, Elsevier, 1994

[49] Bhatia, „Thermal Spraying Technology and Applications", Continuing Education and Development, Inc. 9 Greyridge Farm Court Stony Point, NY 10980, EM 1110-2-3401, 1999

[50] http://www.gordonengland.co.uk/tsc.htm

[51] D.S Rikerby and A. Matthews, "Ceramic coating by physical vapour deposition", Reviews an powder metallurgy and physical ceramics, vol. 3-4, p 155-295, 1991

[52] D. E. Crawmer, "Coating Structures, Properties, and Materials", Thermal Spray Technologies Inc., as published in Handbook of Thermal Spray Technology, J.R. Davis (Ed.), ASM International, p 49, 2005

[53] http://stellite.com/ProductsServices/CoatingServices/ThermalSpraying/tabid/316/Default.aspx

[54] Y. Ishikawa, J. Kawakita and S. Kuroda, "Effect of Spray Condition and Heat Treatment on the Structure and Adhesive Wear Properties of WC Cermet Coatings", Vol. 46 No.07, p 1671-1676, 2005

[55] R. Polak; F. Kremser, "Thermal Spraying between erosion and corrosion challenges", TSL surface engineering, 2008

[56] G. Matthäus Thermico GmbH & Co.KG, A. Sturgeon TWI Ltd, "Application of the HVOF process to internal coatings of cylinders, and hard-and software for internal coating technology of complex components", Advanced coating solutions, Thermico, 2006

[57] P. Ruggiero, M. Froning, "The Effect of Off-angle Spraying on the Structure and Properties of HVOF WC-Co-Cr", Air Force Plating Working Group, 2003

[58] K. Legg, B. Sartwell et al, "Thermal Spray Coatings for Internal Diameters", AeroMat,   2002
http://www.rowantechnology.com/Documents/Chrome%20Replacement/Aeromat%20ID%20Cr.pdf

[59] http://www.thermalsprayspecialists.com

[60] http://www.praxair.com/na/us/pst/pst.nsf/0/EF992BC8C1F6CFA8852576A500590967?OpenDocument

[61] http://www.asianaerospace.com/   novadocuments/247

[62] http://www.sulzermetco.com

[63] http://www.plasma-hvof.com/index.php/plasma-gun-f1.html

[64] http://www.sulzermetco.com/en/portaldata/13/Resources//documents2/flyer/Flyer_HVOF-Plasma_Gun_Portfolio_EN4.pdf

[65] http://www.wix.com/atermika/atermika-hvof#!i.d.gun

[66] http://www.thermico.de

[67]http://www.metatherm.de/index.php?option=com_content&view=article&id=59&Itemid=70&lang=de

[68] G. Matthäus Thermico GmbH & Co.KG, A. Sturgeon TWI Ltd, "Application of the HVOF process to internal coatings of cylinders, and hard-and software for internal coating technology of complex components", Advanced coating solutions, Thermico, 2006

[69] G. Matthaeus, W. Brandl, I.-F. Secosan, G. Marginean, V. Chirila, D. Ackermann, "Standard HVOF process compared to the HVOF process for internal coating with fine powders", Thermal Spray Crossing Borders (DVS-ASM international), p 473-476, 2008.

[70] V. Stoica, R. Ahmed, S. Tobe, "Wear of hot isostatically pressured (HIPed) thermal spray cermet coatings", Wear, vol. 257, p 1103-1124, Elsevier, 2004

[71] K. Legg, B. Sartwell, "Hard Chromium Alternatives Team Update – Improving Performance While Reducing Cost", AESF-EPA Paper, 2000

[72]http://www.stellite.de/ProcessesOutline/CoatingServices/ThermalSpraying/tabid/118/language/en-US/Default.aspx

[73] C. M. Pogan, "Wear Resistance Improvement of Titanium by Surface Alloying using Electron Beam Irradiation", PhD Thesis, ISBN 978-606-554-251-8, 2011

[74] J. Nerz, B Kushner, A Rotolico, " Microstructural evaluation of tungsten carbide-cobalt coatings", Thermal Spray Thechnology, 1996

[75] B. Marple, B. Arsenault, J. Voyer, "Performance of WC-Based, Hvof-Processed Coatings in Sliding Wear", ASM International, USA, 1997

[76] Bruce D. Sartwell, Keith O. Legg et al, "Replacement of chromium electroplating on gas turbine engine components using thermal spray coatings", Environmental Security Technology Certification Program, 2005

[77] A. Dwars, W. Kochanowski et al, "Application of thermally sprayed coatings of the type WC/CoCr in reverse osmosis processes for seawater desalination", Materials and Corrosion, , ISSN 0947-5117, vol. 59(11), p 870-877, 2008

[78] G. Bolelli et al, "HVOF- sprayed WC-CoCr interlayer to improve adhesion of CVD DLC coatings to aluminium substrate", Department of Materials and Environmental Engineering Modena, Italy, 2011

[79] M. Oksa, E. Turunen et al, „Optimization and Characterization of High Velocity Oxy-fuelSprayed Coatings: Techniques, Materials, and Applications" Coatings, ISSN 2979-6412, p 17-52, 2011

[80] Desmond F. Moore, "Principles and Applications of Tribologiy", International series in materials science and technology, vol. 14, ISBN 0-08-017902-9, 1975

[81] http://www.tstcoatings.com/wear_resistant_coatings.html

[82] H. Czichos, "Tribology-a systems approach to the science and technology of friction, lubrication and wear", vol. 1, Elsevier, ISBN 0-444-41676, 1978

[83] L. Deters, A. Fischer, E. Santner, "Tribologie: Definition, Begriffe, Prüfung", GfT, Arbeitsblatt 7, 2006 (http://www.gft-ev.de/pdf/2002_AB_7.pdf)

[84] Jorn Larsen-Basse, "Introduction to Friction", National Science Foundation, ASM Handbook, vol. 18, ISBN 0-87170-380-7, 1992

[85]. D.A. Rigney, J.P. Hirth, "Plastic deformation and sliding friction of metals", Wear, p 345-370, 1979

[86] S.J. Bull, D.S. Rickerby, "Compositional, microstructural and morphological effects on the mechanical and tribological properties of chromium nitrogen films", Surface and Coating Technology, p 732-744, 1990

[87] P.J. Blau, "Friction and wear transitions of materials: Break-in, Run-in, Wear-in", Noyes Publications, New Jersey, USA, 1989

[88] M. J. Neale and M. Gee, "Wear Problems and Testing for Industry", William Andrew Publishing, LLC, ISBN 0-8155-1471-9, USA, 2001

[89] www.lubcon.com/typo3temp/pics/dd543524ac.jpg

[90] http://www.stle.org/resources/lubelearn/wear/default.aspx

[91] M.H Jones, D. Scott, "Industrial Tribology: the practical aspects of friction, lubrication, and wear", Elsevier Scientific Publishing Company, 1983

[92] http://www.tribology.co.uk/services/investigate/pb09-2.htm

[93] http://www.substech.com

[94] http://www.eng.nus.edu.sg/EResnews/0310/rd/rd_5.html

[95] D.H. Buckley, "Surface Effects in Adhesion, Friction, Wear and Lubrication", Elsevier, 1981

[96] H Czichos, K. Habig, "Tribology Handbook – Friction and Wear", Vieweg, 1992

[97] A.W. Ruff, "Wear Measurement" Friction, Lubrication and Wear Technology, ASM Handbook, vol. 18, p 687-715, 1992

[98] J.F. Archard, "Contact and rubbing of flat surfaces", J. Appl. Phys. 24, p 981-988, 1953

[99] H. Czichos, K.-H. Habig, "Tribologie-Handbuch", Auflage 3, ISBN 978-3-8348-0017-6, 2010

[100] Y. Qiao et al, "Sliding and abrasive wear resistance of thermal-sprayed WC-Co coatings", J. Therm. Spray Technol., vol. 10, p 118-125, 2001

[101] L. Jacobs et al, "Wear behaviour of HVOF and HVAF sprayed WC-cermet coatings", Proceedings of 15th ITSC'98, Nice, France, p 169-174, 1998

[102] H. Chen et al, "Micro-scale abrasive wear behaviour of HVOF sprayed and laser-remelted conventional and nanostructured WC-Co coatings", Wear, vol. 258, p 333-338, 2005

[103] M. Barletta et al, "Wear and corrosion behaviour of HVOF-sprayed WC-CoCr coatings on Al alloys", ASM International, Journal of Thermal Spray Technology, vol. 19(1-2), p 358-366, 2010

[104] C.W. Lee et al, "A study on powder mixing for high fracture toughness and wear resistance of WC-Co-Cr coatings sprayed by HVOF", Surface & Coatings Technology, vol. 204, p 2223-2229, 2010

[105] J. A. Picas et al, "Microstructure and wear resistance of WC-Co by three consolidation processing techniques", Int. Journal of Refractory Metals & Hard Materials, vol. 27, p 344-349, 2010

[106] T. A. Adler, M.K. Adler Flitton et al, "Corrosion: fundamentals, testing and protection" ASM Handbook, vol. 13A, ISBN 0-87170-705-5, 2003

[107] B.S. Covino, Jr. and S.D. Cramer, "Introduction to forms of corrosion", Corrosion: fundamentals, testing, and protection, vol. 13A, ASM Handbook, ASM International, p 189, 2003

[108] R. F. Bunshah, "Metallurgical application", in Handbook of Deposition Technologies for Films and Coatings, 2nd Edition, R.F. Bunshah (Ed.), Noyes, P. Ridge, NJ, USA, p 740-762, 1994

[109] W. H. Ailor, "Handbook of Corrosion data and evaluation", John Wiley & Sons, Inc., New York, USA, 1971

[110] DIN EN ISO 6270-2:2005, Beschichtungsstoffe-Bestimmung der Beständigkeit gegen Feuchtigkeit-Teil 2: Verfahren zur Beanspruchung von Proben in Kondenswasserklimaten

[111] DIN EN ISO 9227:2006 Korrosionsprüfungen in künstlichen Atmosphären-Salzsprüh- nebelprüfungen

[112] http://www.asminternational.org/content/ASM/StoreFiles/06691G_Chapter_1.pdf, "The Effects and Economic Impact of Corrosion", ASM International, 2000

[113] F. Hine, K. Komai, K. Yamakawa, „Localized corrosion", Current Japanese Materials Research, vol. 4, Elsevier Applied Science, ISBN 1-85166-213-8, 1988

[114] G.S. Frankel, "Pitting Corrosion", Corrosion: Fundamentals, Testing, and Protection, vol. 13A, ASM Handbook, ASM International, p 236–241, 2003

[115] R. J. K. Wood, "Tribo-corrosion of coatings: a review", Surface Engineering and Tribology Group, School of Engineering Sciences, Highfield, University of Southampton, p 5502-5521, 2007

[116] A. Scrivani, S. Ianelli et al, "A contribution to the surface analysis and characterisation of HVOF coatings for petrochemical application", Wear, vol. 250, p 107–13, 2001

[117] D. Toma, W. Brandl, G. Marginean, "Wear and corrosion behaviour of thermally sprayed cermet coatings", Surface and Coatings Technology, vol. 138, p 149-158, 2001

[118] V. A. Souza and A. Neville, "Corrosion and synergy in a WC–Co–Cr HVOF thermal spray coating-understanding their role in erosion–corrosion degradation", Wear, vol. 259, p 171-180, 2005

[119] J. E. Cho, S. Y. Hwang and K. Y. Kim "Corrosion behaviour of thermal sprayed WC cermet coatings having various metallic binders in strong acidic environment", Surf. Coat. Technol., vol. 200, p 2653–2662, 2006

[120] M. Magnani, P.H. Suegama et al, "Influence of HVOF parameters on the corrosion and wear resistance of WC-Co coatings sprayed on AA7050 T7", Surf. Coat. Technol., vol. 202, p 4746-4757, 2008

[121] L. Gil, M.H. Staia, "Influence of HVOF parameters on the corrosion resistance of NiWCrBSi coatings", Thin Solid Films, vol. 420-421, p 446-454, 2002

[122] F.J.J. Kellner, H. Hildebrand, S. Virtanen, "Effect of WC grain size on the corrosion behavior of WC–Co based hardmetals in alkaline solutions", Int. Journal of Refractory Metals & Hard Materials 27, p 806 812, 2009

[123] R. C. Barik, J. A. Wharton, R. J. K. Wood, K. S. Tan and K. R. Stokes, "Erosion and erosion–corrosion performance of cast and thermally sprayed nickel–aluminium bronze", Wear, vol. 259, p 230–420, 2005

[124] R. J. K. Wood, A.J. Speyer, "Erosion-corrosion of candidate HVOF aluminium-based marine coatings", Wear, vol. 256, p 545–556, 2004

[125] http://www.sciencedirect.com

[126] J. Goldstein, D. Newbury, D. Joy, C. Lyman, P. Echlim, E. Lifshin, L. Sawyer, J. Michael, "Scanning Electron Microscopy and X-Rays Microanalysis", 3rd edition, Kulwer Academic / Plenum Publishers, New York, 2003

[127] S.L. Flegler, J.W. Heckman, K.L. Klomparens, "Elektronenmikroskopie: Grundlagen, Methoden, Anwendungen", Spektrum/ Akademische Verlag, 1995

[128] H.E. Exner and S. Weinbruch, "Scanning Electron Microscopy, Metallography and Microstructures", Vol 9, ASM Handbook, ASM International, 2004

[129] H.E. Exner, R.W. Cahn, P. Haasen "Qualitative and Quantitative Surface Microscopy, in Physical Metallurgy", R.W. Cahn, 3rd ed., North-Holland, 1983

[130] M. Birkholz, "Thin Film Analysis by X-Ray Scattering" WILEY-VCH Verlag GmbH & Co. KGaA, ISBN: 3-527-31052-5, Weinheim, 2006

[131] F. Mansfeld, "The Polarization Resistance Technique for Measuring Corrosion Currents", ASM Handbook vol.13, 2003

[132] H.P. Boehm, V. Hofmann, "Anorganische und allgemeine Chemie", Vol. 58, p 278-299, 1995

[133] C. Verdon, A. Karimi et al, „A study of High Velocity Qxy-Fuel Thermally Sprayed Tungsten carbide Based Coatings. Part I: Microstructures", Mat. Sci. & Eng. A, 246: 11-24, 1998

List of Publications

[1] G. Matthaeus, W. Brandl, **I. F. Secosan**, G.Marginean, V. Chirila, D. Ackermann, "Standard HVOF process compared to the HVOF process for internal coating with fine powders", International Thermal Spray Conference & Exposition, USA, Thermal Spray Crossing Borders (DVS-ASM international), p 473-476, 2008

[2] A. Asavei, **I. F. Secosan**, D. Frunzaverde, G. Marginean, W. Brandl, E.-Rainer Sievers "Testing of the wettability during brazing", University Annals "Eftimie Murgu" Resita, Manual of Engineering, year XV, nr.1, 1453-7394 B+, 2008

[3] D. Utu, G. Marginean, D. Buzdugan, **I. F. Secosan**, V.A. Serban „The influence of deposition process on corrosion and sliding wear behavior of WC-Co coatings", Scientific Bulletin of the „Politehnica" University of Timişoara, Romania, Transactions on Mechanics, Tom 54 (68), Fasc. 2, p 11-16, ISSN 1224 – 6077, 2009

[4] **I. F. Secosan**, G. Marginean, V.A. Serban ,W. Brandl "Influence of phase composition of HVOF-sprayed WC-CoCr coatings on the sliding wear and corrosion behaviour", Junior Euromat Conference, University of Lausanne, Switzerland 2010

[5] C. Pogan, **I. F. Secosan**, I. Mitelea, W. Brandl, "The influence of electron beam scanning modus on the properties of titanium surfaces alloyed with tungsten carbide powder", International Conference ModTech, Republic of Moldova, 2011

[6] **I. F. Secosan**, D. Utu, V.A. Serban "The influence of process parameters on the characteristics of internal HVOF sprayed WC-CoCr cermet coatings", Scientific Bulletin of the „Politehnica" University of Timişoara, Romania, Transactions of Mechanics, vol. 56 (70), Iss. 1, p 37-42, ISSN 1224 – 6077, 2011

[7] **I. F. Secosan**, W.Brandl, "Prüfstand für die Untersuchung des Verschleißverhaltens an Zylinder-Innenflächen", DE Utility Model with file number 20 2011 105 181.5, Patent application with the number 10 2011 117 558.3 submitted to the German Institute for Patent and Trademark, 2011

[8] **I. F. Secosan**, D. Utu, V.A Serban, W. Brandl "Wear Resistance of Internal WC-CoCr Coatings Produced by High Velocity Oxy-Fuel Spraying", Solid State Phenomena vol. 188, p 416-421, Trans Tech Publication, Switzerland, 2012
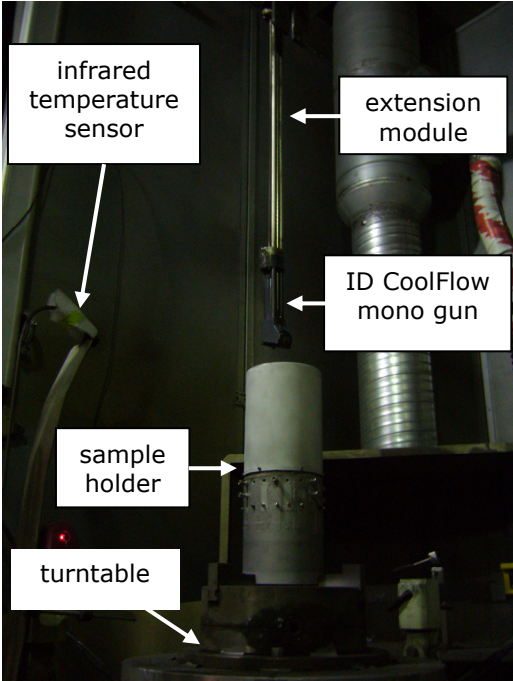
Figure A.1 The arrangement of the ID HVOF spraying process
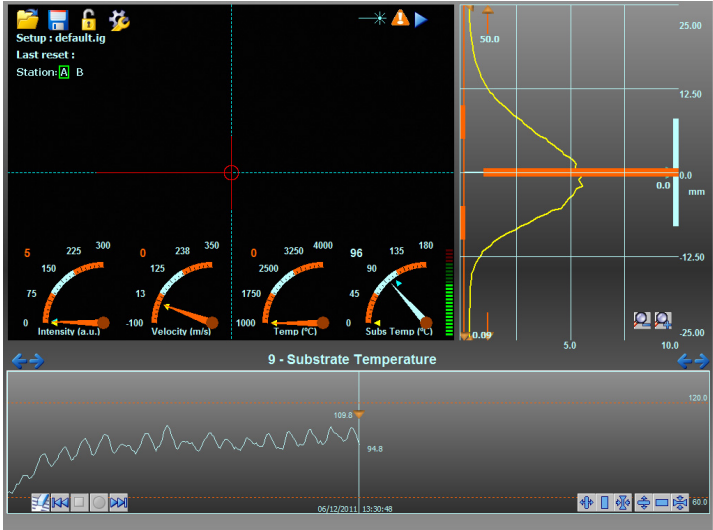
Graph 1 Measurement of the substrate temperature from outside during the spraying process

Pin on disc - parameters optimisation (test 1)

Test 1

Reference :   Almenstreifen
Substrate :   Steel
Layer n° 1 :   WC-CoCr [150,00 µm]

Tribo measure

Tribo parameters

Acquisition
Radius   : 8,30 [mm]
Lin. Speed   : 40,00 [cm/s]
Normal load   : 10,00 [N]
Stop condit.   : 50000 [lap]
Effective Stop : Laps
Acquisition rate : 10,0 [Hz]

Sample
-Coating   : WC-CoCr
-Substrate : Steel
-Cleaning   : Acetone

Static Partner
-Coating   : WC-Co
-Substrate : WC-Co
-Cleaning   : Acetone
-Dimension : 6,00 [mm]
-Geometry : Ball

Environment
Temperature   : 20,00 [°C]
Atmosphere   : air
Humidity   : 50,00 [%]

Sample
Worn Track Section : 0,0 µm2
Young's Modulus : 0,0 GPa
Poisson Ratio : 0,000

Static Partner
Worn Cap Diameter : 290,0 µm
Young's Modulus : 690,0 GPa
Poisson Ratio : 0,240

Calculations
Sample Wear Rate : 0 mm3/N/m
Partner Wear Rate : 4,444E-009 mm3/N/m
Max Herzian Stress : 0 GPa

Curve

Start : 0,163	Min : 0,163	Max : 0,351	Mean : 0,311	Std. Dev. : 0,031

Friction Coef.
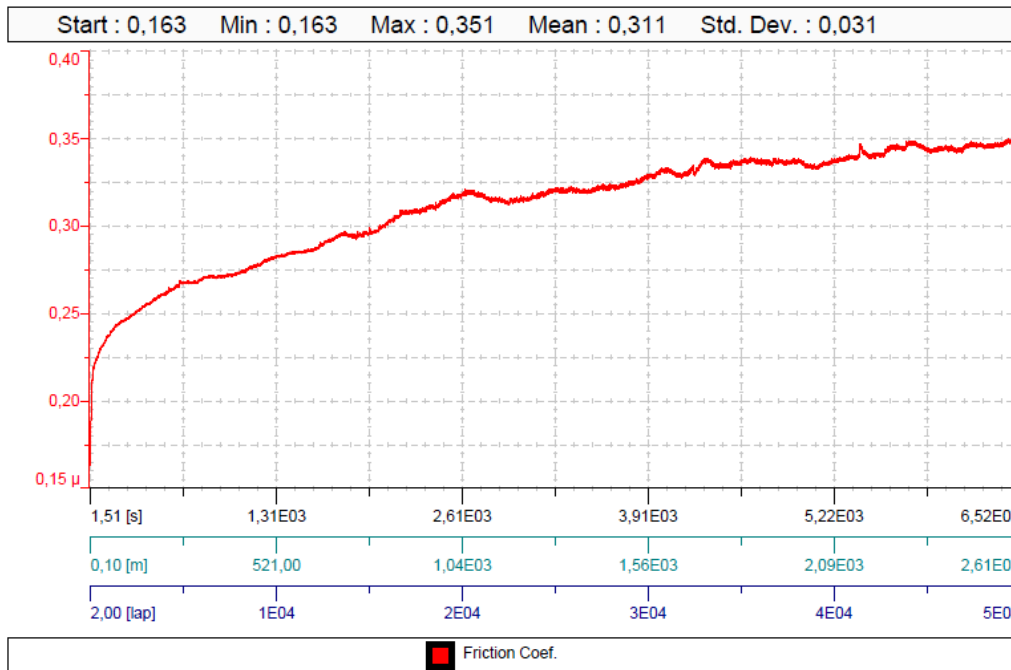
Pin on disc - parameters optimisation (test 2)

Test 2

Reference :   Almenstreifen
Substrate :   Steel
Layer n° 1 :   WC-CoCr [150,00 μm]

Tribo measure

Tribo parameters

Acquisition
Radius   : 7,23 [mm]
Lin. Speed   : 20,00 [cm/s]
Normal load   : 10,00 [N]
Stop condit. : 100000 [lap]
Effective Stop : Laps
Acquisition rate : 10,0 [Hz]

Sample
-Coating   : WC-CoCr
-Substrate : Steel
-Cleaning   : Acetone

Static Partner
-Coating   : WC-Co
-Substrate : WC-Co
-Cleaning : Acetone
-Dimension : 6,00 [mm]
-Geometry : Ball

Environment
Temperature   : 20,00 [°C]
Atmosphere   : air
Humidity   : 50,00 [%]

Sample
Worn Track Section : 0,0 μm2
Young's Modulus : 0,0 GPa
Poisson Ratio : 0,000

Static Partner
Worn Cap Diameter : 370,0 μm
Young's Modulus : 690,0 GPa
Poisson Ratio : 0,240

Calculations
Sample Wear Rate : 0 mm3/N/m
Partner Wear Rate : 6,76E-009 mm3/N/m
Max Herzian Stress : 0 GPa

Curve

Start : 0,174	Min : 0,174	Max : 0,365	Mean : 0,309	Std. Dev. : 0,039

Friction Coef.
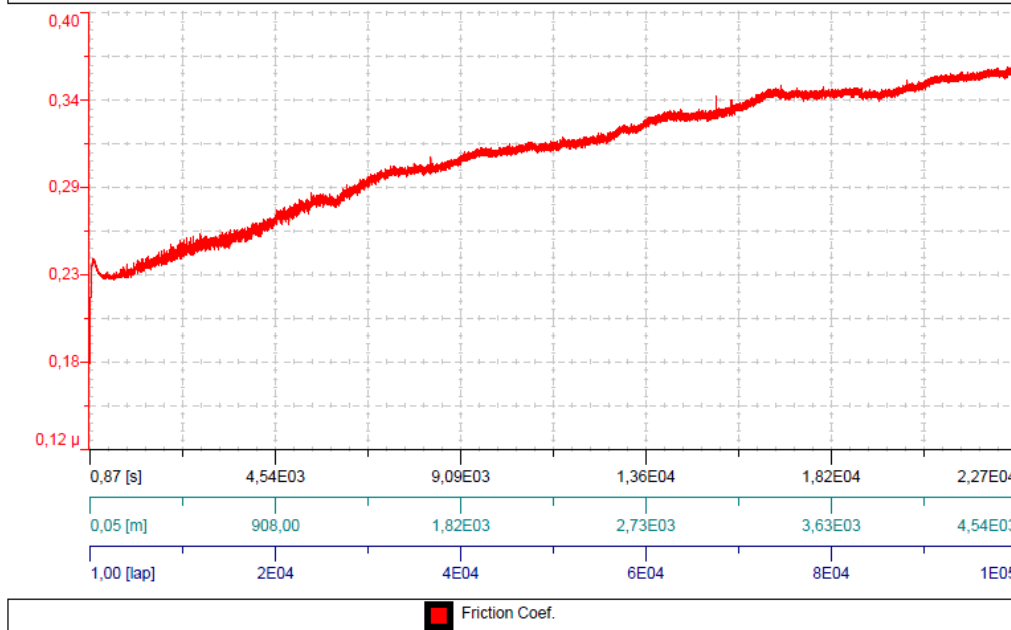
Pin on disc – optimised parameters (were set for the experimental work)

Test 3

Reference :   Almenstreifen
Substrate :   Steel
Layer n° 1 :   WC-CoCr [150,00 µm]

Tribo measure

Tribo parameters

Acquisition
Radius   : 8,19 [mm]
Lin. Speed   : 40,00 [cm/s]
Normal load   : 10,00 [N]
Stop condit. : 100000 [lap]
Effective Stop : Laps
Acquisition rate : 10,0 [Hz]

Sample
-Coating   : WC-CoCr
-Substrate : Steel
-Cleaning   : Acetone

Static Partner
-Coating   : WC-Co
-Substrate : WC-Co
-Cleaning   : Acetone
-Dimension : 6,00 [mm]
-Geometry   : Ball

Environment
Temperature : 20,00 [°C]
Atmosphere   : air
Humidity   : 50,00 [%]

Sample
Worn Track Section : 0,0 µm2
Young's Modulus : 0,0 GPa
Poisson Ratio : 0,000

Static Partner
Worn Cap Diameter : 365,0 µm
Young's Modulus : 690,0 GPa
Poisson Ratio : 0,240

Calculations
Sample Wear Rate : 0 mm3/N/m
Partner Wear Rate : 5,649E-009 mm3/N/m
Max Herzian Stress : 0 GPa

Curve

Start : 0,177   Min : 0,177   Max : 0,395   Mean : 0,348   Std. Dev. : 0,042

Friction Coef.
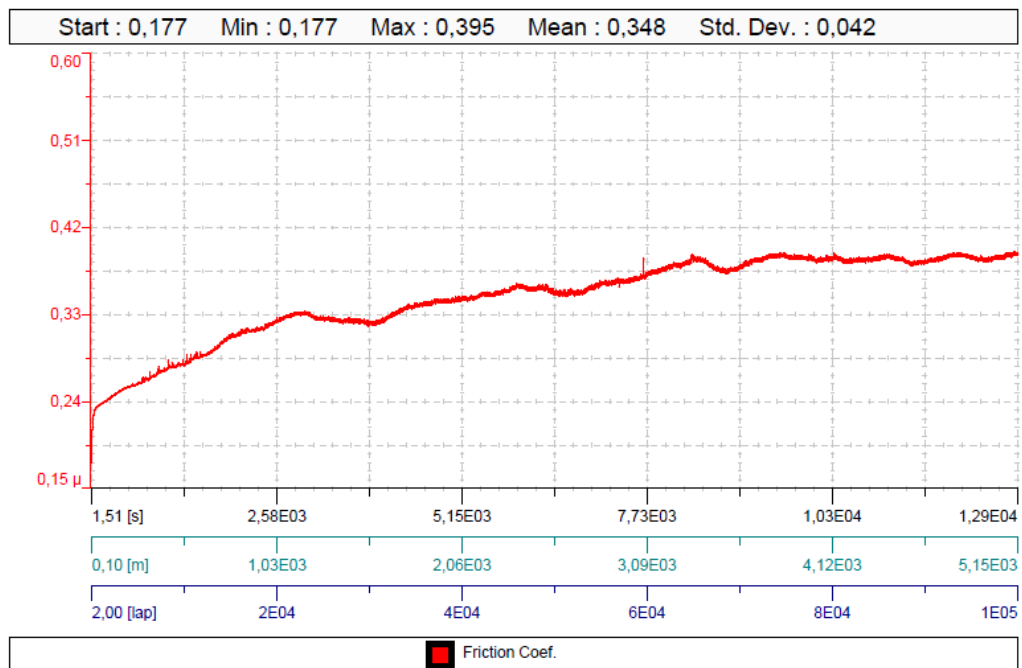
Table A.1 The main table including all the information used for the cylinder on ring wear test investigations

sample nr.	Worn number	Ring Material	Ra-Ring [µm] before	after	ΔRa-R	Block Material / nr.	Ra-Block [µm] before	after	ΔRa-B	R-Weight [g] before	after	Δw-R [g]	B-Weight [g] before	after	Δw-B [g]	Water-Tmax [°C] before	after
M1.1	worn 1	WC-CoCr (-10+2)	0.55	0,47	-0,08	WC-CoCr (-10+2) 2.1	0.64	0.12	-0,52	1138.59	1138.61	+0.02	68.694	68.684	- 0.01	23	25
M1.2	worn 1	WC-CoCr (-10+2)	0.56	0,55	-0,01	WC-CoCr (-45+20) 1.7	0,39	0.27	-0.12	1133.89	1133.90	+0.01	62.629	62.594	-0.035	23	25
M2.1	worn 1	WC-CoCr (-25+5)	0.49	0,62	+0.13	WC-CoCr (-10+2) 2.7	0.48	0.21	-0.27	1135.33	1135.29	-0.04	64.062	64.022	-0.04	23	25
M2.2	worn 1	WC-CoCr (-25+5)	0.52	0,54	+0.02	WC-CoCr (-45+20) 1.2	0.39	0.35	-0.04	1133.04	1133.02	-0.02	57.104	57.067	-0.037	23	25
M3.1	worn 1	WC-CrC-Ni(-10+2)	0.58	1,08	+0.50	WC-CoCr (-10+2) 2.3	0.50	097	+0.47	1080.42	1078.82	-1.60	67.087	67.083	-0.004	23	28
M3.2	worn 1	WC-CrC-Ni(-10+2)	0.53	1,29	+0.76	WC-CoCr (-45+20) 1.3	0.43	1.39	+0.96	1113.84	1112.38	-1.46	66.538	66.532	-0.006	23	28
M4.1	worn 1	WC-CrC-Ni(-22+5)	0.96	1,17	+0.21	WC-CoCr (-10+2) 2.4	0.60	1.14	+0.54	1127.48	1126.03	-1.45	64.596	64.591	-0.005	23.5	28
M4.2	worn 1	WC-CrC-Ni(-22+5)	0.90	2,10	+1.20	WC-CoCr (-45+20) 1.4	0.42	1.72	+1.30	1124.46	1123.14	-1.32	62.001	61.973	-0.028	22.5	28.5
R1.1*	worn 1	WC-CoCr (-45+20)	0.56	0,90	+0.34	WC-CoCr (10+2) 2.5	0.62	1.65	+1.03	1131.90	1130.37	-1.53	55.662	55.554	-0.108	23.25	29.5
R1.2*	worn 1	WC-CoCr (-45+20)	0.53	0,79	+0.26	WC-CoCr (-45+20) 1.5	0.53	0.23	-0.30	1109.91	1109.70	-0.21	64.257	64.150	-0.107	22.75	27.5
R2.1*	worn 1	WC-CrC-Ni(-30+5)	0.51	0,99	+0.48	WC-CoCr (-10+2) 2.6	0.67	0.97	+0.30	1117.79	1115.51	-2.28	60.448	60.415	-0.033	23	29
R2.2*	worn 1	WC-CrC-Ni(-30+5)	0.74	2,05	+1.31	WC-CoCr (-45+20) 1.6	0.41	1,47	+1.06	1129.91	1127,99	-1,92	67,846	67.718	-0,128	23,5	29

Test condition-water; *rings coted with CJS-external gun by angling the gun to a maximum of 60° off-normal
R-ring specimen
B-stationary specimen

sample nr.	Worn number	Ring Material	Ra-Ring [µm] before	after	ΔRa-R	Block Material	Ra-Block [µm] before	after	ΔRa-B	R-Weight [g] before	after	Δw-R	B-Weight [g] before	after	Δw-B	Tmax [°C]** Ring	Block
M1.1	worn 2	WC-CoCr (-10+2)	0.55	0,83	+0.28	WC-CoCr (-10+2) 2.2	0.50	0.25	-0.25	1138.61	1138.57	- 0.03	62.656	62.622	-0.034	100	75
M1.2	worn 2	WC-CoCr (-10+2)	0.56	0,69	+0.13	WC-CoCr (-45+20) 1.1	0.42	0.30	-0.12	1133.89	1133,89	+0.01	64.897	64.844	-0.053	103	73
M2.1	worn 2	WC-CoCr (-25+5)	0.49	1,17	+0.68	WC-CoCr (-10+2) 2.8	0.63	0.54	-0.09	1135.29	1135.30	+0.01	61.871	61.763	-0.108	114	91
M2.2	worn 2	WC CoCr (-25+5)	0.52	0,68	+0.16	WC-CoCr (-45+20) 1.8	0.42	0.28	-0.14	1133.02	1133.07	+0.05	64.504	64.421	-0.083	109	80
M3.1	worn 2	WC-CrC-Ni(-10+2)	0.58	0,59	+0.01	WC-CoCr (-10+2) 2.9	0.60	1.56	+0.96	1078.82	1078.18	-0.64	66.881	66.866	-0.015	108	77
M3.2	worn 2	WC-CrC-Ni(-10+2)	0.53	0,73	+0.20	WC-CoCr (-45+20) 1.9	0.46	1.81	+1.35	1112.38	1111.74	-0.64	68.305	68.285	-0.020	109	77
M4.1	worn 2	WC-CrC-Ni(-22+5)	0.96	1,15	+0.19	WC-CoCr (-10+2) 2.10	0.64	0.52	-0.12	1126.03	1125.72	-0.31	66.977	66.950	-0.027	126	92
M4.2	worn 2	WC-CrC-Ni(-22+5)	0.90	1,20	+0.30	WC-CoCr (-45+20) 1.10	0.39	1.49	+1.10	1123.14	1122.66	-0.48	72.962	72.939	-0.023	104	75
R1.1*	worn 2	WC-CoCr (-45+20)	0.56	0,74	+0.18	WC-CoCr (-10+2) 2.11	0.55	0.25	-0.25	1130.37	1130.36	+0.01	62.073	62.048	-0.025	111	88
R1.2*	worn 2	WC-CoCr (-45+20)	0.53	1,13	+0.60	WC-CoCr (-45+20) 1.11	0.45	0.35	-0.10	1109.70	1109.72	+0.02	68.100	67.994	-0.106	120	90
R2.1*	worn 2	WC-CrC-Ni(-30+5)	0.51	0,76	+0.25	WC-CoCr (-10+2) 2.12	0.61	0.68	+0.07	1115.20	1115.20	-0.31	65.340	65.333	-0.007	97	76
R2.2*	worn 2	WC-CrC-Ni(-30+5)	0.74	0,80	+0.06	WC-CoCr (-45+20) 1.12	0.47	1.45	+0.98	1127.67	1127.67	-0.32	62.776	62.763	-0.013	102	75

Test condition-atmosphere; *rings coted with CJS-external gun by angling the gun to a maximum of 60° off-normal; ** block and ring temperature before the wear tests ~26.5 °C
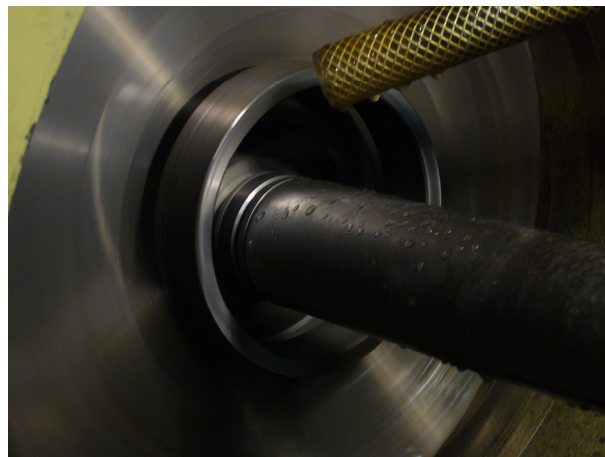
Figure A.2 Surface finishing process of the ring specimens

Graph 2 Roughness measurements of the finished surface of the ring specimens

WC-Co-Cr (-10+2µm)	WC-Co-Cr (-25+5µm)	WC-Cr$_3$C$_2$-Ni (-22+5µm)	WC-Cr$_3$C$_2$-Ni (-30+5µm)
Notiz: M1.1	Notiz: M2.1	Notiz: M3.1	Notiz: M4.1

	M1.1		M2.1		M3.1		M4.1
Norm	JIS2001	Norm	JIS2001	Norm	JIS2001	Norm	JIS2001
Profil	R	Profil	R	Profil	R	Profil	R
Filter	GAUSS	Filter	GAUSS	Filter	GAUSS	Filter	GAUSS
Ausw.-L	4.0mm	Ausw.-L	4.0mm	Ausw.-L	4.0mm	Ausw.-L	4.0mm
N	5	N	5	N	5	N	5
λc	0.8mm	λc	0.8mm	λc	0.8mm	λc	0.8mm
λs	2.5µm	λs	2.5µm	λs	2.5µm	λs	2.5µm
Neigungscom	Pen. alle	Neigungscom	Pen. alle	Neigungscom	Pen. alle	Neigungscom	Pen. alle
M-Gesch.	0.5mm/s	M-Gesch.	0.5mm/s	M-Gesch.	0.5mm/s	M-Gesch.	0.5mm/s
Bereich	AUTO	Bereich	AUTO	Bereich	AUTO	Bereich	AUTO
	ESC		ESC		ESC		ESC
Vor/Nach	ON	Vor/Nach	ON	Vor/Nach	ON	Vor/Nach	ON
Vorschub	STAND	Vorschub	STAND	Vorschub	STAND	Vorschub	STAND
R-PROFIL		**R-PROFIL**		**R-PROFIL**		**R-PROFIL**	
Ausw.-L	4.0mm	Ausw.-L	4.0mm	Ausw.-L	4.0mm	Ausw.-L	4.0mm
λc	0.8mmX5	λc	0.8mmX5	λc	0.8mmX5	λc	0.8mmX5
Ra	0.56µm	Ra	0.50µm	Ra	0.56µm	Ra	0.92µm
Rz	4.11µm	Rz	3.55µm	Rz	4.21µm	Rz	6.40µm
Rq	0.70µm	Rq	0.63µm	Rq	0.72µm	Rq	1.17µm
R-PROFIL		**R-PROFIL**		**R-PROFIL**		**R-PROFIL**	
Ausw.-L	4.0mm	Ausw.-L	4.0mm	Ausw.-L	4.0mm	Ausw.-L	4.0mm
λc=0.8mmX5		λc=0.8mmX5		λc=0.8mmX5		λc=0.8mmX5	

→×5K   →×5K   →×5K   →×2K

×50   ×50   ×50   ×50

Ver.	2.0µm/cm	Ver.	2.0µm/cm	Ver.	2.0µm/cm	Ver.	5.0µm/cm
Hor.	200.0µm/cm	Hor.	200.0µm/cm	Hor.	200.0µm/cm	Hor.	200.0µm/cm

Graph 3 Roughness measurements of the finished surface of the ring specimens

WC-Co-Cr (-45+20µm)

Notiz:	R1.1
Norm	JIS2001
Profil	R
Filter	GAUSS
Ausw.-L	4.0mm
N	5
λc	0.8mm
λs	2.5µm
NeigungscomPen.	alle
M-Gesch.	0.5mm/s
Bereich	AUTO
	ESC
Vor/Nach	ON
Vorschub	STAND

R-PROFIL

Ausw.-L	4.0mm
λc	0.8mmX5
Ra	0.54µm
Rz	3.64µm
Rq	0.68µm

R-PROFIL

| Ausw.-L | 4.0mm |
| λc=0.8mmX5 | |

→×5K
×50

| Ver. | 2.0µm/cm |
| Hor. | 200.0µm/cm |
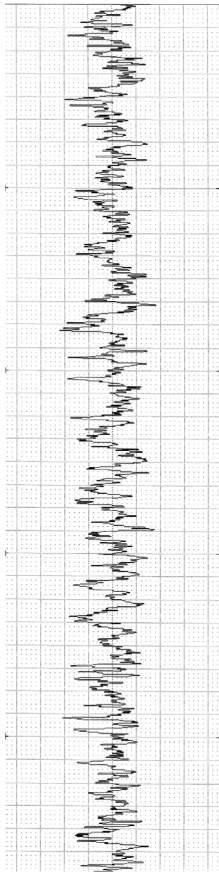
WC-Cr$_3$C$_2$-Ni (-30+5µm)*

Notiz:	R2.1*
Norm	JIS2001
Profil	R
Filter	GAUSS
Ausw.-L	4.0mm
N	5
λc	0.8mm
λs	2.5µm
NeigungscomPen.	alle
M-Gesch.	0.5mm/s
Bereich	AUTO
	ESC
Vor/Nach	ON
Vorschub	STAND

R-PROFIL

Ausw.-L	4.0mm
λc	0.8mmX5
Ra	0.51µm
Rz	3.92µm
Rq	0.66µm

R-PROFIL

| Ausw.-L | 4.0mm |
| λc=0.8mmX5 | |

→×5K
×50

| Ver. | 2.0µm/cm |
| Hor. | 200.0µm/cm |
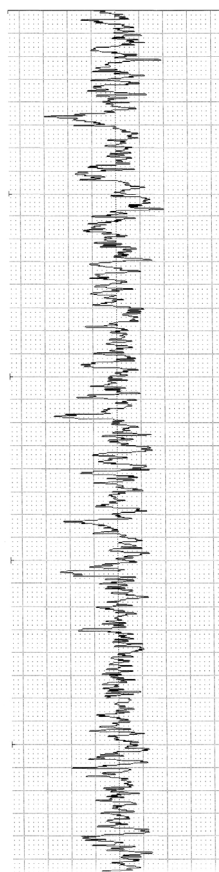
WC-Cr$_3$C$_2$-Ni (-30+5µm)*

Notiz:	R2.2*
Norm	JIS2001
Profil	R
Filter	GAUSS
Ausw.-L	4.0mm
N	5
λc	0.8mm
λs	2.5µm
NeigungscomPen.	alle
M-Gesch.	0.5mm/s
Bereich	AUTO
	ESC
Vor/Nach	ON
Vorschub	STAND

R-PROFIL

Ausw.-L	4.0mm
λc	0.8mmX5
Ra	0.74µm
Rz	5.15µm
Rq	0.94µm

R-PROFIL

| Ausw.-L | 4.0mm |
| λc=0.8mmX5 | |

→×5K
×50

| Ver. | 2.0µm/cm |
| Hor. | 200.0µm/cm |
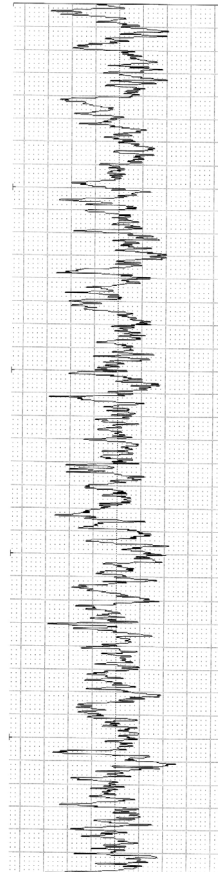
*same coating and spray parameters, but not deposited at the same time under a 60° angle
(first ring, Ra= 0.51µm and the second one, Ra=0.74µm => no reproducibility)

Graph 4 Roughness measurements of the finished surface of the cylinder bars

WC-Co-Cr (-10+2μm)
Notiz: CYLIND.B-1

Norm	JIS2001
Profil	R
Filter	GAUSS
Ausw.-L	4.0mm
N	5
λc	0.8mm
λs	2.5μm
Neigungscompen. alle	
M-Gesch.	0.5mm/s
Bereich	AUTO
	ESC
Vor/Nach	ON
Vorschub	STAND
Ra	0.43μm
Rz	2.97μm
Rq	0.54μm
Ver.	1.0μm/cm
Hor.	200.0μm/cm
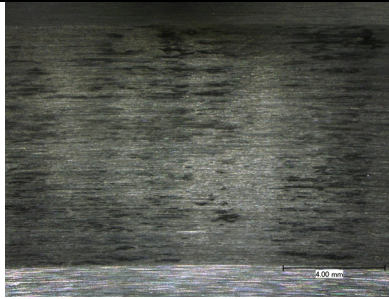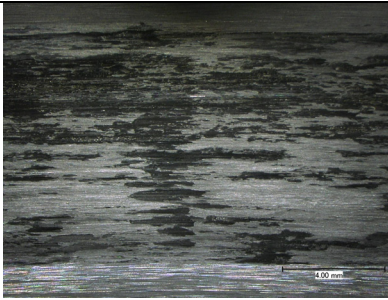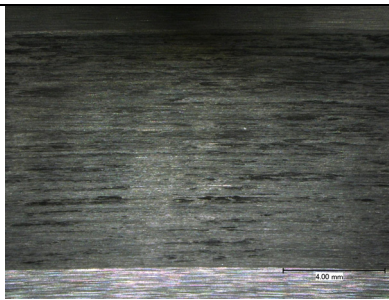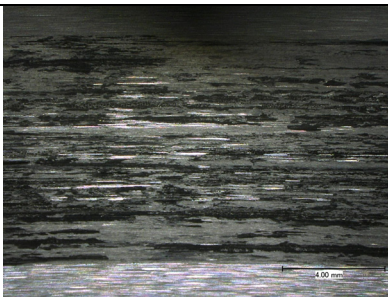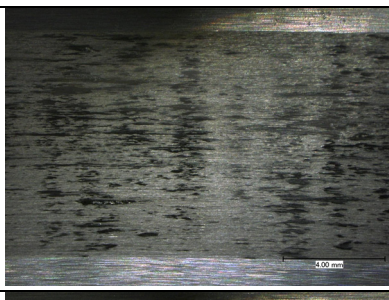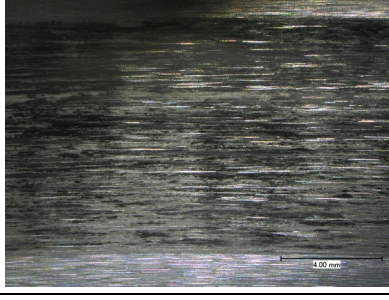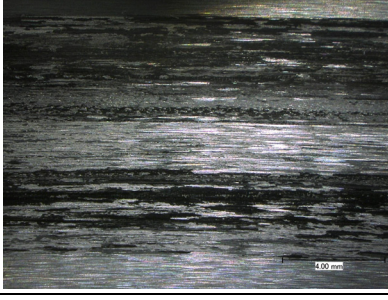
WC-Co-Cr (-45+20μm)
Notiz: CYLIND.B-2

Norm	JIS2001
Profil	R
Filter	GAUSS
Ausw.-L	4.0mm
N	5
λc	0.8mm
λs	2.5μm
Neigungscompen. alle	
M-Gesch.	0.5mm/s
Bereich	AUTO
	ESC
Vor/Nach	ON
Vorschub	STAND
Ra	0.58μm
Rz	4.12μm
Rq	0.73μm
Ver.	2.0μm/cm
Hor.	200.0μm/cm
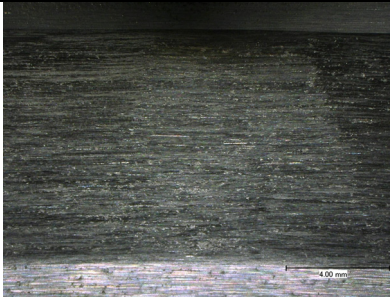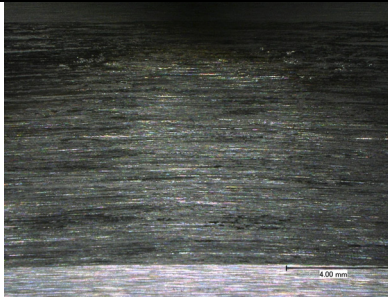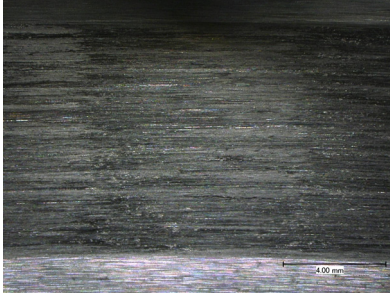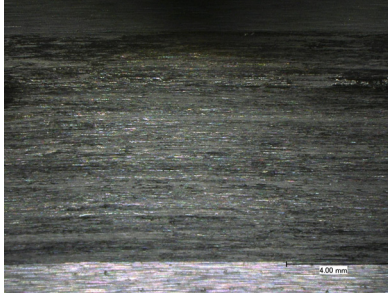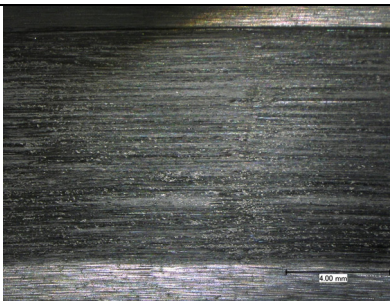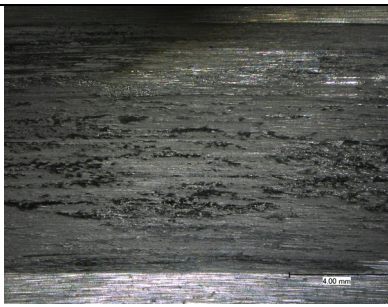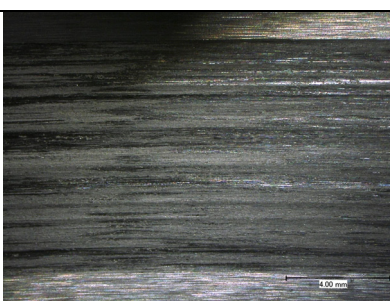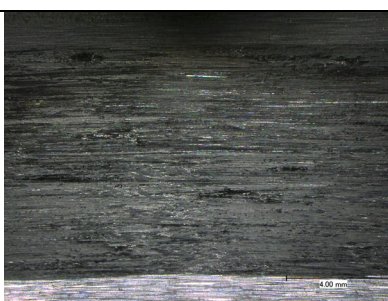
Table A.2 The wear tracks surface of the ring specimen after the cylinder on ring test

WC-Co-Cr Ring-specimens (ID coolFlow mono gun)			
Sample nr. *	Test condition		
	Water	Sample nr. *	Atmosphere
M1.1 worn 1		M1.1 worn 2	
M1.2 worn 1		M1.2 worn 2	
M2.1 worn 1		M2.1 worn 2	
M2.2 worn 1		M2.2 worn 2	
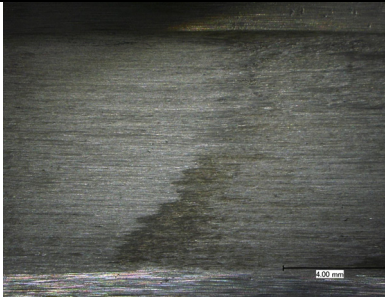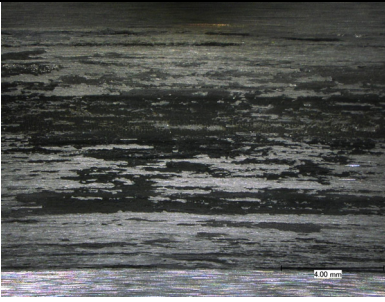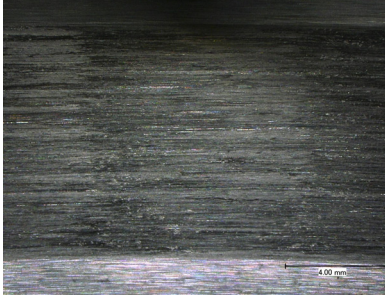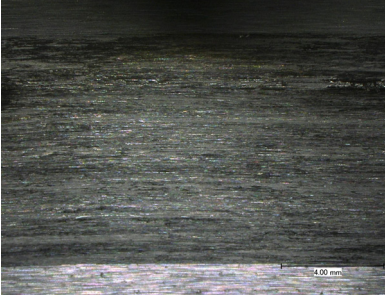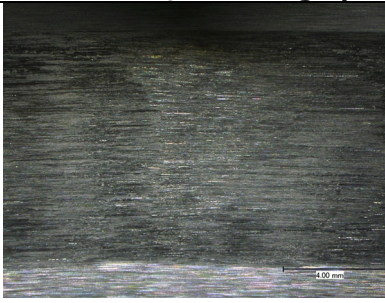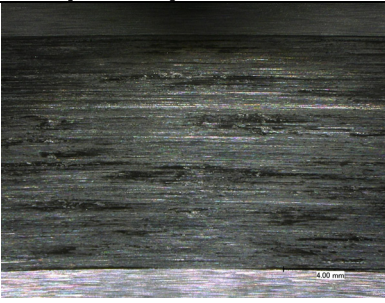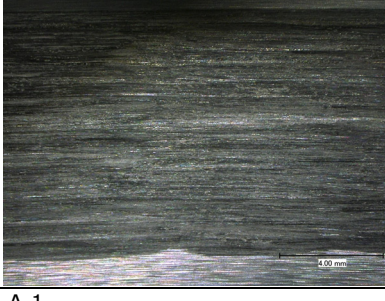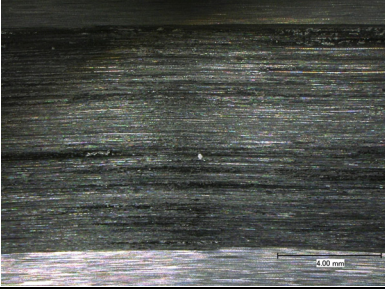
* see table A.1

Table A.3 The wear tracks surface of the ring specimen after the cylinder on ring test

WC-Cr$_3$C$_2$-Ni Ring-specimens (ID coolFlow mono gun)				
Sample nr. *	Test condition			
	Water	Sample nr. *	Atmosphere	
M3.1 worn 1		M3.1 worn 2		
M3.2 worn 1		M3.2 worn 2		
M4.1 worn 1		M4.1 worn 2		
M4.2 worn 1		M4.2 worn 2		
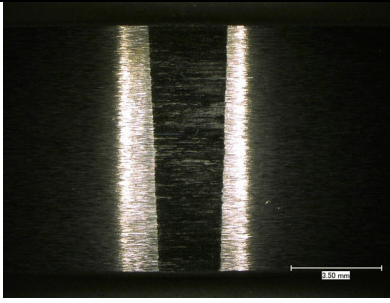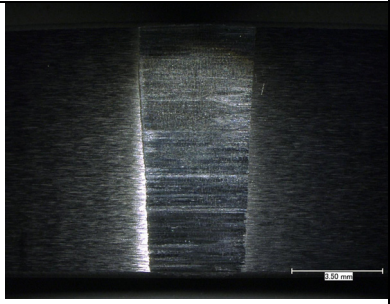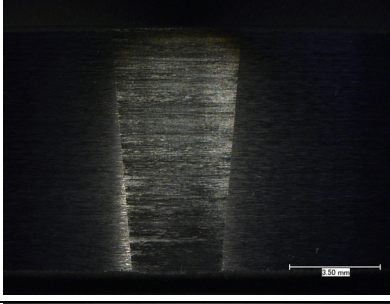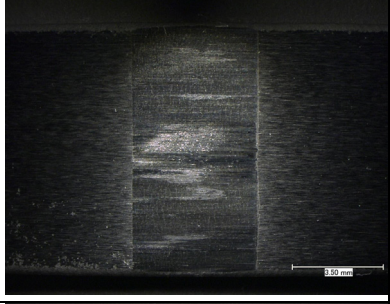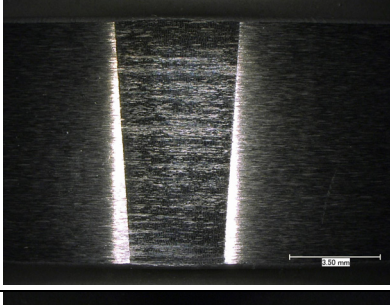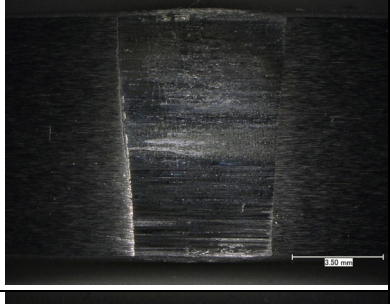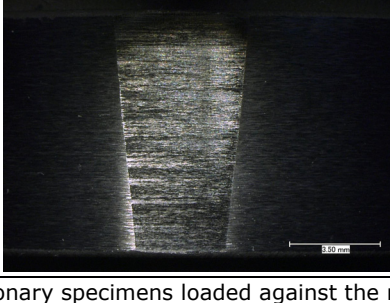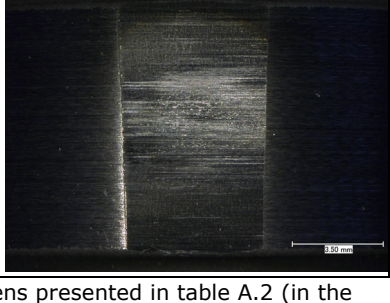
* see table A.1

Table A.4 The wear tracks surface of the ring specimen after the cylinder on ring test

WC-Co-Cr Ring-specimens (CJS gun-coarse powder)			
Sample nr.*	Test condition		
	Water	Sample nr. *	Atmosphere
1.1 worn 1		1.1 worn 2	
1.2 worn 1		1.2 worn 2	
WC-Cr$_3$C$_2$-Ni Ring-specimens (coarse powder)			
2.1 worn 1		2.1 worn 2	
2.2 worn 1		2.2 worn 2	
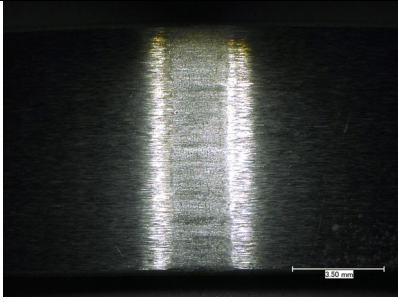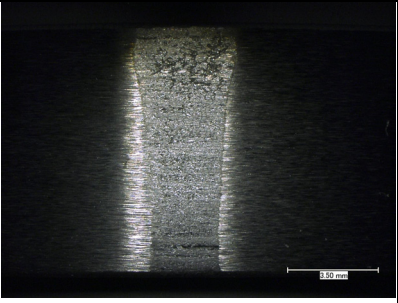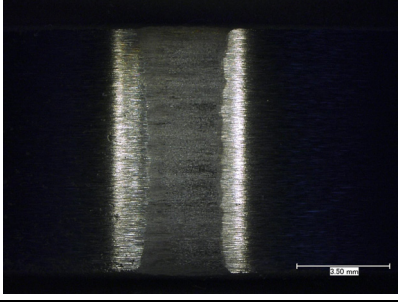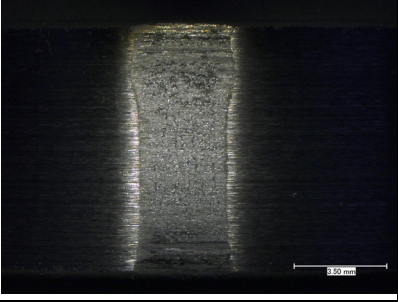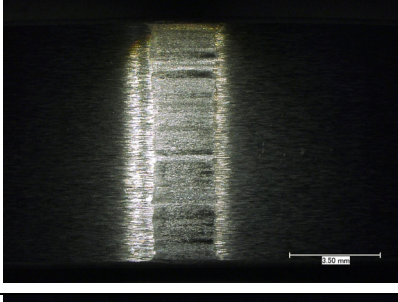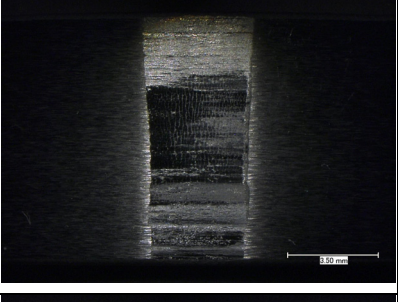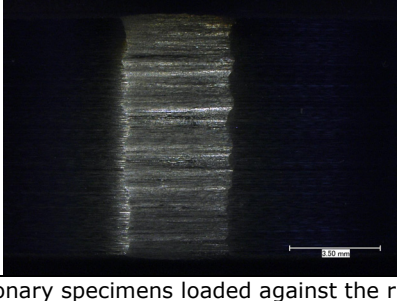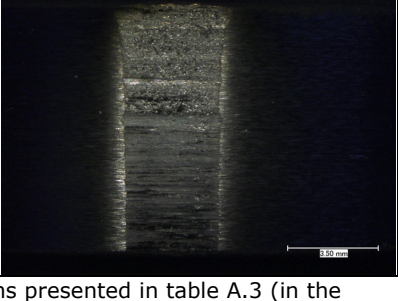
* see table A.1

Table A.5 The wear degree of the stationary specimen after the cylinder on ring test

WC-Co-Cr Ring-specimens (ID coolFlow mono gun)			
Sample nr. *	Test condition		
	Water	Sample nr. *	Atmosphere
2.1		**2.2**	
1.7		**1.1**	
2.7		**2.8**	
1.2		**1.8**	
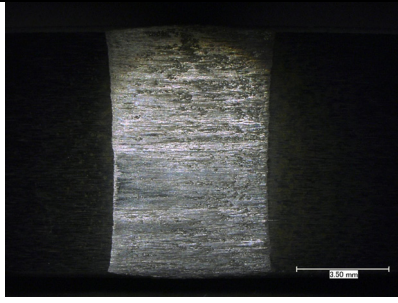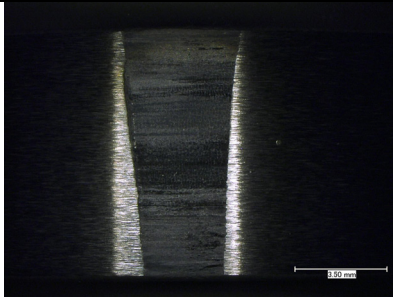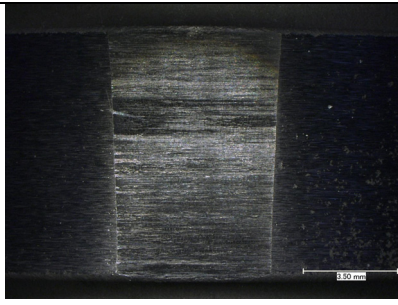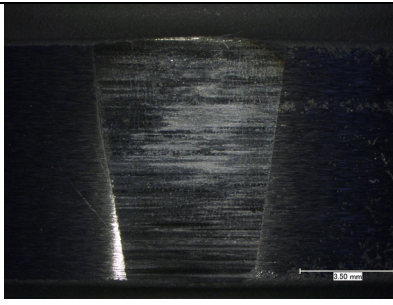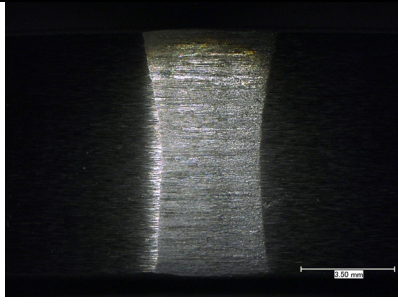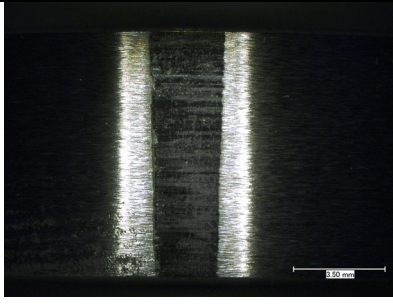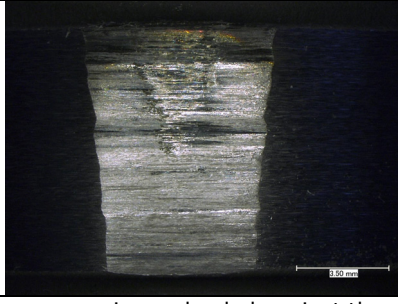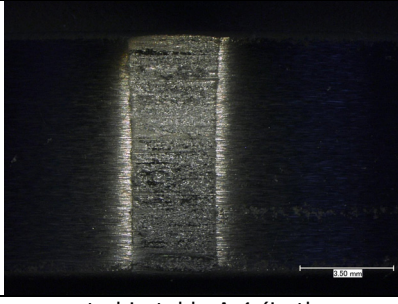
* the stationary specimens loaded against the ring specimens presented in table A.2 (in the same order: 2.x – WC-Co-Cr fine powder; 1.x – WC-Co-Cr coarse powder)

Table A.6 The wear degree of the stationary specimen after the cylinder on ring test

WC-Cr$_3$C$_2$-Ni Ring-specimens (ID coolFlow mono gun)				
Sample nr. *	Test condition		Sample nr. *	
	Water			Atmosphere
2.3			**2.9**	
1.3			**1.9**	
2.4			**2.10**	
1.4			**1.10**	

* the stationary specimens loaded against the ring specimens presented in table A.3 (in the same order: 2.x – WC-Co-Cr fine powder; 1.x – WC-Co-Cr coarse powder)

Table A.7 The wear degree of the stationary specimen after the cylinder on ring test

WC-Co-Cr Ring-specimens (CJS gun-coarse powder)			
Sample nr.*	Test condition		
	Water	Sample nr. *	Atmosphere
2.5		2.11	
1.5		1.11	
WC-Cr₃C₂-Ni Ring-specimens (coarse powder)			
2.6		2.12	
1.6		1.12	

* the stationary specimens loaded against the ring specimens presented in table A.4 (in the same order: 2.x – WC-Co-Cr fine powder; 1.x – WC-Co-Cr coarse powder)
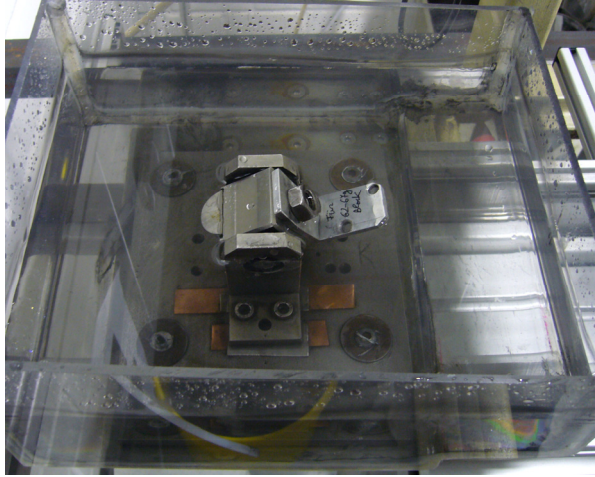
Figure A.3 The water aspect after the sliding wear test of WC-Co-Cr coatings
(the graphite adheres on the specimens surface)
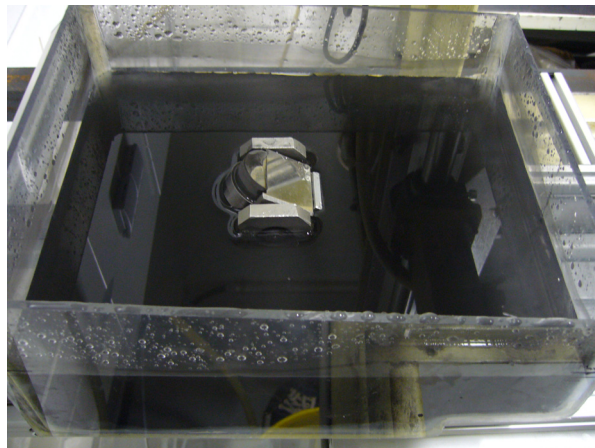
Figure A.4 The water aspect after the sliding wear test of WC-Cr$_3$C$_2$-Ni coatings
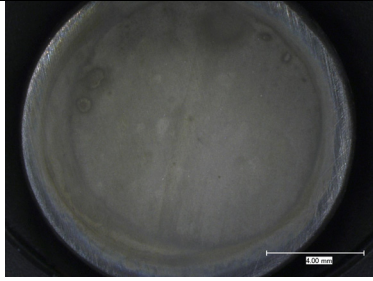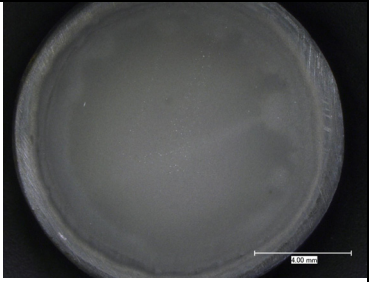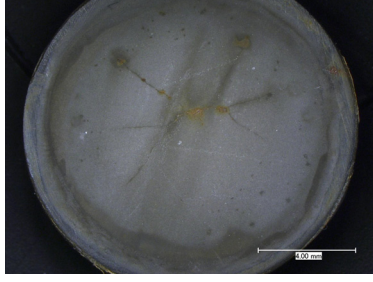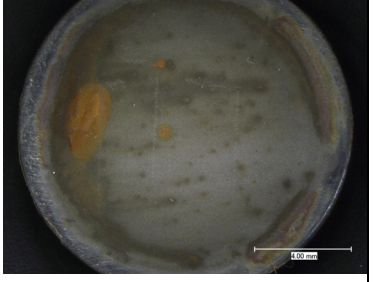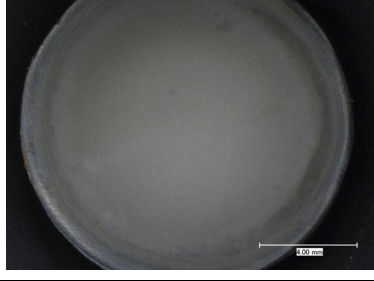(the graphite does not adhere on the specimens surface)

Figure A.5 An visual aspect of the water resulted after electrochemical corrosion tests
(WC-Co-Cr coatings: S1M-3 fine*; S2M-2 medium*; S1-1 and S1-2 coarse*)
(WC-Cr$_3$C$_2$-Ni coatings: S3M1 and S3M2 fine*; S4M-1 and S4M-2 medium*; S2-1 and S2-2 coarse*)
* the type of powder used for the corresponding coating

Table A.8 The wear degree of the stationary specimen (WC-Co ball) after the pin on ring test

Pin on disc test		
Test Parameters	Whithout compress air	With compress air
40 N; 200min⁻¹; 5000m (12570 laps) **Year 2008**		
80N; 475 min⁻¹; 10000m (25000laps)		
40N; 475 min⁻¹; 10000m (25000laps)		
40N; 200 min⁻¹; 10000m (25000laps) (a) **40N; 200 min⁻¹; STOP CONDITION ~3000m (8000laps) (b)**	(a)	(b)
80N; 200 min⁻¹; 10000m (25000laps) (a) **80N; 200 min⁻¹; STOP CONDITION ~1200m (3000laps) (b)**	(a)	(b)

Table A.9 The corroded surfaces of the specimens after the electrochemical tests

Surface before			
surface after			
Powder size [µm]	WC-Co-Cr	Powder size [µm]	WC-Cr$_3$C$_2$-Ni
-10+2		-10+2	
-25+5		-22+5	
-45+20		-30+5	